UNIVERSITAT DE BARCELONA

Regulation of tissue growth: a molecular bridge between extrinsic and intrinsic mechanisms

Regulación del crecimiento tisular: un puente molecular entre los mecanismos extrínsecos e intrínsecos

Ana Patricia de Almeida Ferreira

Programa de Doctorado del Departamento de Genética
Facultad de Biología
Universidad de Barcelona

Regulation of tissue growth: a molecular bridge between extrinsic and intrinsic mechanisms

Regulación del crecimiento tisular: un puente molecular entre los mecanismos extrínsecos e intrínsecos

Memoria presentada por
Ana Patricia de Almeida Ferreira
para optar al grado de Doctor por la Universidad de Barcelona

Development and growth control laboratory
ICREA and Institute for Research in Biomedicine (IRB)
Parc Científic de Barcelona

Barcelona, December 2015

Marco Milán (Director) | Ana Ferreira (Alumna) | Florenci Serras (Tutor)

Agradecimientos

Muchas gracias a todas las personas que, de una manera u otra, han contribuido durante estos años y han hecho posible que llegara hasta aquí. Y si me olvido de alguien, gracias también!

Marco, no hay palabras suficientes para agradecerte! Gracias por acogerme dos veces en el laboratorio. ¡Me lo pasé tan bien la primera vez que quise volver! Y volví a pasármelo muy bien. Gracias por ser tan buena persona y tan buen jefe, haces que sea muy fácil trabajar y hablar contigo. Por la pasión que transmites por la ciencia que nos contagia. Por ser siempre tan positivo y conseguir levantar el ánimo cuando estamos más negativos, y por el apoyo y ayuda durante toda la tesis, y sobre todo durante la dura revisión que nos ha tocado! Por los cafés, por las conversaciones en los pasillos, por las discusiones, no solo las científicas, pero también las del Madrid-Barça, de política y por todo lo demás ¡¡Muchas gracias jefe!!

Larita, *bestie*, nó sé ni por dónde empezar! Como te eche de menos los meses que estuviste por las américas… y cuanto me alegro de que hayas vuelto!!! Además porque sin ti esta tesis no hubiera sido posible. Gracias por la ayuda con el Word, Photoshop, etc. Y sobre todo gracias por todo lo demás, por ser tan buena persona (demasiada a veces ya lo sabes ;)), por el apoyo, las risas, las borracheras, las lágrimas, los viajes y por siempre estar disponible para ayudar. Te echaré muchísimo de menos pero estoy segura que es una amistad para toda la vida, para lo que sea y cuando sea sabes que puedes contar conmigo! Sólo tengo una cosa a apuntar, aparte de que estás un poco sorda: el hecho de que nunca has podido hablar conmigo en catalán (jaja). Estoy segura que te espera un futuro brillante, sea lo que sea que decidas, sé que puedes hacerlo perfecto!

Laurita, como hemos sufrido con Brat!!! Gracias por hacer posible que el proyecto interminable se terminara, ¡qué alivio fue! No se me olvidará nunca la gráfica esa que hemos hecho del timeline de la "motivation over time" del Brat Project! Y te tengo que agradecer por muchas otras cosas, por la amistad, por las discusiones (no solo científicas), por las noches de copas, por enseñarnos Paris (¡que guay fue ese viaje con la Larita!). Merci beaucoup por tout!!! Te he hechado mucho de menos por aquí!

Andrés, boludo, ¡muchas gracias por todo! Por las discusiones científicas que tanto nos ayudaron y enseñaron. Tengo que decir que te admiro mucho por la manera que tienes de ver la vida y de hacerlo parecer todo tan sencillo. Y por el crack que eres. ¡Que falta hiciste por aquí en los últimos años de mi tesis!

Juanchi, ¡cómo te he echado de menos en estos últimos meses! Llegaste al laboratorio como el mejicano muy tímido, que poco hablaba pero que siempre estaba ahí, compañero de office y de las noches en la *fly room*. Me alegro mucho que todo te ha ido bien en tu regreso a Méjico. Ahora solo falta ir a visitarte a Cuernavaca para comer fajitas y beber tequila, ya que la que dejaste aquí sigue intacta!!! (..muy mal, te has ido y ¡¡no hemos abierto la botella!!). ¡Gracias por todo!

Lídia, gracias por hacer que este laboratorio funcione, ¡sin ti no funcionaría! Gracias por ayudar tanto a la gente cuando necesita y por saber tanto de molecular!! Y gracias por ayudarme a mejorar mi castellano, principalmente al principio, y por las barbacoas/paellas/calçotadas en tu casa! No sé cómo haré cuando tenga que hacer un clonaje y no te tenga a ti para pedir ayuda!

Marta, ¡nuestra andaluza! Gracias por habernos enseñado la bella Sevilla, me entraron ganas de ir a vivir allí. Que sigas disfrutando del lab, de Barcelona y ahora del nuevo miembro de la familia, Julia.

Mariana, te has vuelto una verdadera *motard*!! Al principio con la moto azul de 50, pero ahora tienes una moto de verdad! Jaja Gracias por estar siempre ahí y por las sugerencias de sitios para comer. Espero que todo te vaya bien tanto en el lab como a nivel personal.

Najate, *merci* por haberme enseñado tanto sobre Notch (jaja)!!! Es broma, ahora en serio, sin ti esta tesis no tendría los modelitos esos guapos del *illustrator*, ¡gracias! Me encantan tus fotos de *migration* tan guapas que sacas en el confo! *Merci beaucoup* por ayudarme siempre que necesité y te deseo lo mejor! Tenemos que volver al *bowling* porque quiero la revancha! jaja

Terriente, la portada te la dedico a ti por haberme pasado el stock cuando estaba en apuros con la revisión del paper, ¡gracias! Y gracias por la alegría que traes al lab cada día y por haber sido compañera del turno nocturno! Suerte con las *lymph glands* y con ese paper!

Lada, seguirá vivo el legado de los fenotipos no autónomos!!! Me alegro de que así sea porque son muy guapos! ¡Seguro que lograrás una buena tesis! ¡Ánimos!

Célia, ai el p53 sensor... no es fácil trabajar con él pero ya le has pillado el truco! Estoy segura que te irá bien el PhD porque en este laboratorio no hay otra manera. ¡Ánimos con la tesis!

Mercedes, gracias por la alegría diaria y por cuidar de nuestras mosquitas!

Jery, we haven't overlap much in the lab but I'm sure everything will go very good during your PhD. Enjoy Barcelona and good luck in the future!

Héctor, fue un placer trabajar contigo, ¡de verdad! A ti te tengo que agradecer por enseñarme moscas y por trasmitirme de alguna manera la pasión por ellas, por la

paciencia de ensenarme a diseccionar y a montar (ya sé que al principio era muy mala!!), por ser como eres, me encanta como llevas la vida y que seas tan buena persona! Qué pena no haber compartido contigo mis años de PhD!

Duarte, nunca me vou esquecer daquela "entrevista" no "Mocho" e tenho que confessar que estava nervosa…! Mas no final de contas tenho que te agradecer (e muito!) porque foi graças a ti que vim aqui parar! Não sei o que dizeste ao Marco quando voltaste de Lisboa, mas obrigada!!! E obrigada por tudo, por ensinar-me a trabalhar com moscas, por ajudar-me sempre que precisei e pela alegria que trazias todos os días ao laboratorio. Sentiu-se muito a tua falta por aqui desde que te foste embora.

Isabelle, aunque dejaste un vacío en el laboratorio al irte a Paris, me alegro muchísimo de que todo te haya ido bien por ahí. Confeso que al principio me costaba mucho entender tu "french accent" pero era lo que te hacia ser nuestra Isa!!! Gracias por alegrar mis días al entrar en el lab y verte ahí sentada en tu sitio.

Neus, aún me recuerdo de tu ultimo día en el laboratorio, que al salir te quedaste un rato mirando la puerta… pronto me pasara lo mismo! supongo que te has vuelto una verdadera New Yorker con los años que llevas ahí, no? Me alegro que te haya ido bien esa aventura por la Big Apple!!

A todos las personas que pasaran por el laboratorio durante estos años y en especial a Guillem y a Aleix, "mis" estudiantes de máster. Espero haber sido una buena "jefa"¡Gracias!

A Florenci, por ser un tutor tan positivo, por las discusiones científicas y por la ayuda en esta fase final de la entrega de la tesis. Moltes gràcies!

A los miembros de mi TAC, Ángel Nebreda, Jordi Casanova y Florenci Serras por vuestra importante ayuda y vuestros consejos anuales.

A la Microscopy Facility del IRB por la ayuda con los microscopios y procesamiento de imágenes, y sobre todo por los ***Plugins*** del ImageJ que nos facilitan mucho la vida, gracias!

A Pere Martínez, por la disponibilidad y ayuda en la fase final de la entrega de esta tesis, ¡gracias!

A recursos humanos del IRB que siempre que necesité han sido muy rápidos y eficientes, ¡gracias!

A toda la gente del IRB/PCB con quién me cruce a lo largo de estos años.

Obrigada a todos os meus amigos por fazerem com que tudo seja mais fácil (ainda que para muitos deles a mosca era motivo de gozo) e pelos cafés/jantares/copos muitas vezes de última hora.

Obrigada Pai e Mãe! Sem vocês nada disto seria possível, o orgulho que tenho de vocês é enorme e é também a minha inspiração! Obrigada pelo apoio incondicional e constante que, apesar da distância, sempre me fizeram sentir! Obrigada pelas várias e longas viagens de carro com o carro cheio de coisas, pelas encomendas que me enviaram, pelos menús à minha descrição sempre que ia a Lisboa. Enfim, não há outra palavra que um grande e muito obrigada do coração!!

Obrigada Marta, por seres a melhor irmã que alguém poderia ter (e a sério que não digo isto por seres a única!). Obrigada por apoiar-me sempre, pelas visitas a Barcelona (a ida ao Puerto Aventura tem que ser repetida já que tu não andaste em todas!), pelas horas a trocar mensagens e por me aguentares!! Não sabes o quanto me faz feliz ver que tudo te corre tão bem, mas para teres uma noção que saibas que a ti te desejo melhor que a mim própria! Obrigada por tudo!

Obrigada Diogo, que não me esqueço de ti e das tuas piadas sobre as moscas que também têm a sua importância (jaja)!

Carles, a ti te tengo que agradecer más que a nadie y me temo que para eso necesitaría otras 200 páginas! Podría decirte muchísimas cosas, pero simplemente te diré muchas gracias por ser como eres, por apoyarme incondicionalmente en todo y por haber hecho que esta tesis fuera posible.

Table of Contents

Table of Contents

Abstract

The final size of a developing organ is finely modulated by nutrient conditions through the activity of nutrient sensing pathways, such as Insulin and TOR signaling pathways. In addition, patterning signals operate in an autonomous way to control the growth of an organ. How cells integrate distinct inputs (extrinsic and intrinsic signals) to generate organs of appropriate size and shape remains an open question.

The phosphatidylinositol 3-kinase (PI3K)–phosphatase with tensin homology (PTEN) and tuberous sclerosis complex (TSC)–target of rapamycin (TOR) pathways are frequently activated in human cancer, and this activation is often causative of tumorigenesis. How cells acquiring mutations in tumor suppressor genes outcompete neighboring wild type cells is poorly understood.

We utilized the Gal4-UAS system in *Drosophila* imaginal primordia, highly proliferative and growing tissues, to analyze the impact of restricted activation of these pathways on neighboring wild type cell populations. The results presented in this thesis show that activation of these pathways leads to an autonomous induction of tissue overgrowth and to a remarkable non-autonomous reduction in growth and proliferation rates of adjacent cell populations. We show that this non-autonomous response occurs independently of where these pathways are activated, is functional all throughout development, takes place across compartments, and is distinct from cell competition.

We present evidence that the observed autonomous and non-autonomous effects on tissue growth rely on the up-regulation of the proteoglycan Dally, a major element involved in modulating the spreading, stability, and activity of the growth promoting Decapentaplegic (Dpp)/transforming growth factor β (TGF-β) signaling molecule. Our data indicate that a reduction in the amount of available growth factors contributes to the out-competition of wild type cells by overgrowing cell populations.

Whereas nutrient-sensing pathways modulate the final size of the adult structure according to nutrient availability to the feeding animal, Dpp plays an organ-intrinsic role in the coordination of growth and patterning. Our results also unravel a role of Dally as a molecular bridge between the organ-intrinsic and organ-extrinsic mechanisms that regulate organ size. As such, it contributes to integrate nutrient sensing and organ scaling, the fitting of pattern to size.

Introduction

Introduction

Development and Growth Control: General notions

How organs get to their appropriate size?

Control of organ size is a fundamental aspect of biology and it is crucial for organism fitness. During development, organs must grow to the appropriate size, whereas many organs of adult organisms also display homeostatic size-control mechanisms. In general, the final size of an organ or an animal is determined by the number and size of the cells it contains. Therefore, differences in organ or organism size between animals of the same or different species reflect changes in cell number, cell size, or both.

Decades of experimentation have identified multiple regulators of organ size. Broadly, these can be grouped into organ-extrinsic and -intrinsic regulators of size. Organ-extrinsic regulators act in a humoral fashion to scale the size of multiple organs within an organism. They provide systemic information about the organismal status, such as nutrition and developmental stage, and hormones, such as insulin and steroids, are the main players. Organ-intrinsic regulators act in a local fashion to modulate the size and shape of individual organs. They provide information about the local cellular environment, including position within an organ and cell–cell contacts. The idea of growth being controlled in an autonomous manner was initially suggested by transplantation and regeneration experiments and later identified and characterized through genetic studies. However, elucidating mechanisms by which organ-intrinsic cues interface with extrinsic cues to control organ size remains unresolved.

Drosophila as a model organism to study growth control

Since 1900, when Charles Woodworth and Thomas Hunt Morgan started to breed and work with the fruit fly *Drosophila melanogaster* in the laboratory, this tiny fly became one of the most widely used model systems in biological research. Due to its long tradition and well-established knowledge [in 2000 its genome was completely sequenced (Adams et al., 2000)], *Drosophila* became a very powerful model system with sophisticated genetic and molecular tools. These tools allowed to quickly generate loss-of-function mutant animals to query gene function, and epistasis experiments to question gene relationships. Moreover, techniques based on the alteration of gene expression in a particular tissue or group of cells, like the UAS/Gal4 system (Brand and Perrimon, 1993) or the generation of genetic mosaics, allowed the study of essential genes and in many cases to bypass lethality. This also allowed tissue-specific screens to be performed, which permitted to identify and characterize new genetic loci and signaling networks. The ease of genetic studies is due, in part, to the fact that *Drosophila* is a simple organism with only four pairs of chromosomes (three autosomes and the sex chromosomes). However, about 75% of known human disease genes have a recognizable match in the genetic code of the fruit fly (Reiter and Bier, 2002) and 50% of fly protein sequences have mammalian homologues, which makes the fly an important model organism to help us to understand human biology. Another aspect that makes *Drosophila* such a good model system is its high fecundity rates and the short life generation time, about 10 days at 25°C. The life cycle of the fruit fly is divided into four stages (Figure 1). The embryonic stage, where the body axes are first established, takes about 24h at 25°C ending with the hatching of the larva. During the larval stage, the feeding and growing period, animals go through three different larval instars before metamorphosis. The larvae are composed of two types of tissues: the endo-replicative and the proliferative/imaginal tissues. While the first ones go through successive rounds of genome duplication leading

to an increase in cell size without cell division, the second ones are proliferative tissues that will form the adult epidermal structures of the body called imaginal discs (Figure 2). At the end of the third instar larva, animals enter into pupariation, which marks the beginning of metamorphosis. During this pupal stage, there is an intensive tissue remodeling in which larval tissues are histolyzed, while imaginal tissues metamorphose to form the adult structures, and the rigid exoskeleton constrains any future increase in the body dimension. Consequently, body growth is restricted to the feeding period of larval development, and the transition from larva to pupa fixes the future adult size.

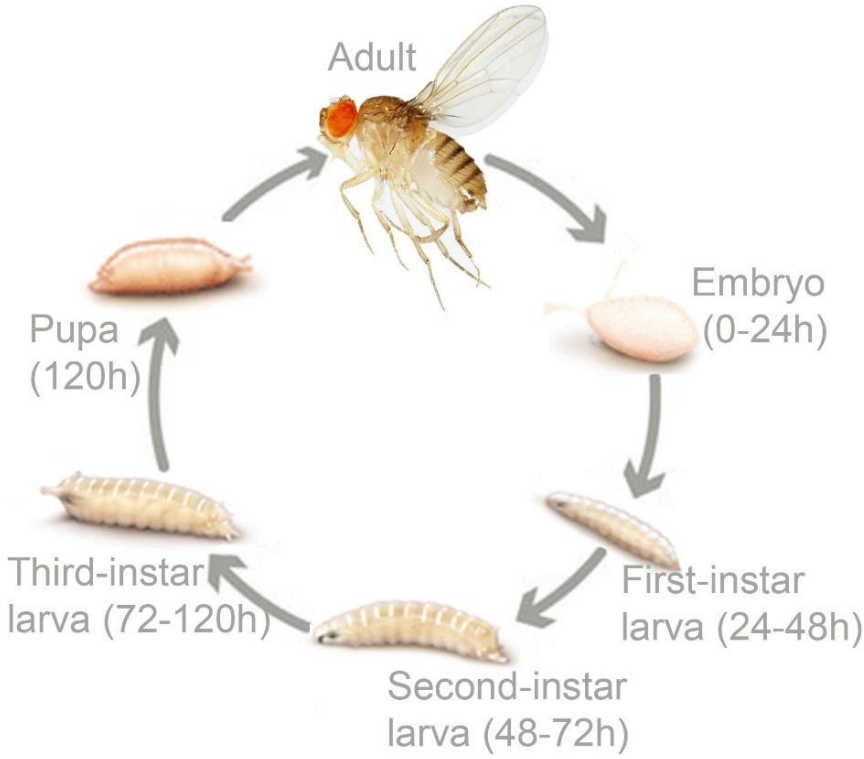

Figure 1. The life cycle of *Drosophila melanogaster*. *Drosophila melanogaster* produces new adults in 10 days at 25°C. Twenty-four hours after the egg is laid, the larva hatches. The fruit fly has three larval instars: first-instar larva (L1) that longs about 24h; afterwards the second-instar larva (L2) hatches and will take also 24h; finally, the third-instar larva (L3) stage will close the larval stage and finish with the encapsulation in the puparium. The puparium is where metamorphosis takes place, after which the adults eclose.

In this thesis, we mainly used the wing imaginal disc of *Drosophila melanogaster* as a model tissue to analyze the effects of targeted activation of growth signaling pathways in specific territories of an organ.

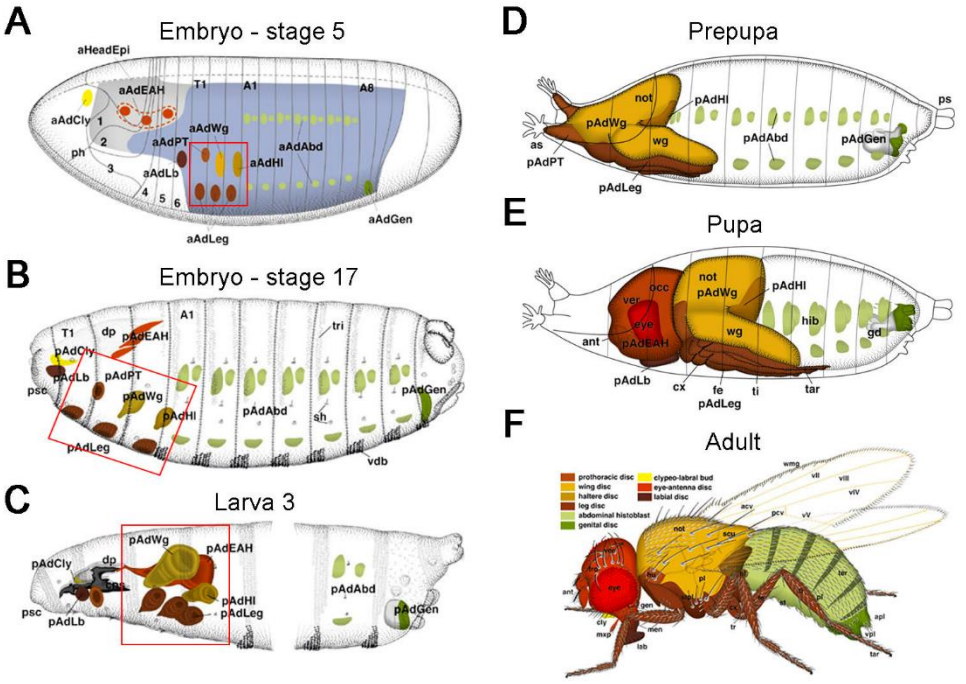

Figure 2. *Drosophila melanogaster* imaginal discs origin and their respective adult organs. The imaginal discs originate early in development as clusters of 5 to 50 undifferentiated groups of cells in the embryonic ectoderm (A). These cells start to develop inside the embryo and are segregated from their neighbors by invagination from the ectoderm (B). During larval development, these groups of cells start to proliferate to give rise to a sac-like structure (C). After the fly has passed through the larval stages, it undergoes metamorphosis. During this process, the imaginal disc extends along its proximal-distal axis by turning inside out in a process called eversion (D, E). Each imaginal disc gives rise to a specific adult structure, such as legs or wings, the body wall, eyes and head cuticle, halteres, antennae or genitalia, and each of them depends on its own genetic cues (F). Adapted from the Atlas of *Drosophila* Development by Volker Hartenstein.

Patterning and Growth of the Wing Imaginal Disc

How is the wing established and develops?

The wing imaginal disc is a sac-like structure composed of a continuous epithelial monolayer that forms a two-sided epithelial sac, which surrounds the disc lumen: on one side of the disc lumen the pseudostratified epithelium – columnar epithelium (ce) – and on the other side the peripodial membrane (pm), a squamous epithelium formed by flat cells (Figure 3). The wing imaginal disc arises from the embryo as a cluster of around 40 cells that proliferate exponentially during the larval period to reach about 33 000 cells. There are about 10-11 divisions in the progeny of each initial cell, each of which takes around 10 hours (Garcia-Bellido and Merriam, 1971; Martín et al., 2009). Shortly after the beginning of pupariation, cell divisions cease and the differentiation of the adult structures begins (Milán et al., 1996). During development, the primordia receives patterning cues to establish the anterior-posterior (AP), dorsal-ventral (DV) and proximal-distal axes. The AP and the DV subdivisions constitute developmental compartments, that had been defined as groups of cells that do not mix with those cells of adjacent compartments (Garcia-Bellido et al., 1973), most probably as a consequence of the compartment specific expression of adhesion molecules (Milán et al., 2001).

During embryogenesis, the wing primordium is first subdivided into anterior and posterior compartments by the activity of the homeodomain transcription factors Engrailed/Invected in posterior cells (Kornberg et al., 1985). Engrailed generates an asymmetry by repressing the expression of the transcription factor Cubitus interruptus (Ci) in posterior cells, and so, Ci is not able to repress the expression of the diffusible protein Hedgehog (Hh). Hh coming from the posterior cells signals to cells in the anterior compartment to induce several target genes like the secreted molecule Decapentaplegic (Dpp) (Zecca et al., 1995), which in turn

organizes pattern and controls growth symmetrically in both compartments (Figure 4).

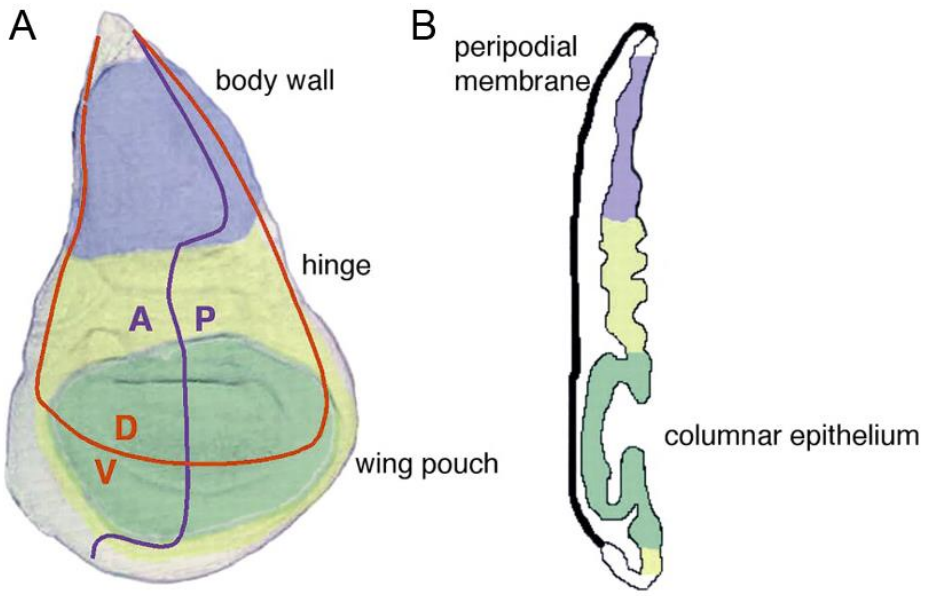

Figure 3. The wing imaginal disc: specification of territories and cellular organization. (A) Cartoon depicting the wing imaginal disc. The horizontal red line corresponds to the dorsal-ventral boundary (DV), and the perpendicular purple line to the anterior-posterior boundary (AP). The notum (body wall) region is in blue, the hinge region in yellow and the wing blade in green. (B) Cartoon depicting a cross-section of the wing imaginal disc. The wing primordium is a cellular monolayer that forms a two-sided epithelial sac. One side of the sac forms a thin squamous sheet, the peripodial membrane, whereas the opposed epithelial surface, the columnar epithelium adopts a pseudostratified columnar morphology. The apical side of both epithelia is oriented towards the lumen of the sac, while the basal side is the external surface. Adapted from (Butler et al., 2003).

The wing primordium contains the progenitors of both the adult body wall (notum) and the wing (Figure 3). This developmental decision, which takes place in second instar stage, is carried out by the opposing activities of two secreted signaling molecules, Wingless (Wg) and the EGFR ligand Vein (Vn), in the most distal and proximal regions of the primordium, respectively (Wang et al., 2000). Hh induces Wg in the ventral-anterior domain where it is required to specify the primordium of the wing blade by activating transcription of *nubbin* (*nub*) and *vestigial* (*vg*) in the wing field and restricting the expression of *homothorax* (*hth*),

teashirt (*tsh*) and *vein* (*vn*) to the proximal region of the wing disc (Ng et al., 1996; Wu and Cohen, 2002). In the other hand, Vn has a dual role in early wing disc development. First, it instructs cells to adopt body wall fate by antagonizing wing fate and activating notum-specifying genes (Diez Del Corral et al., 1999; Wang et al., 2000; Zecca and Struhl, 2002a; Zecca and Struhl, 2002b). Second, EGFR signaling triggers the establishment of a dorsal-ventral axis by inducing the expression of the transcription factor and selector gene Apterous in dorsal cells (Wang et al., 2000; Zecca and Struhl, 2002a; Zecca and Struhl, 2002b). Apterous activates the expression of a Notch ligand, Serrate, in dorsal cells and restricts the expression of another ligand, Delta, in ventral cells (Diaz-Benjumea and Cohen, 1993; Doherty et al., 1996; Irvine and Vogt, 1997). This leads to the symmetric activation of Notch on both sides of the DV boundary. Notch activation leads to expression of Wg at the DV boundary that plays a fundamental role in patterning and growth along de DV axis (Diaz-Benjumea and Cohen, 1995) (Figure 4).

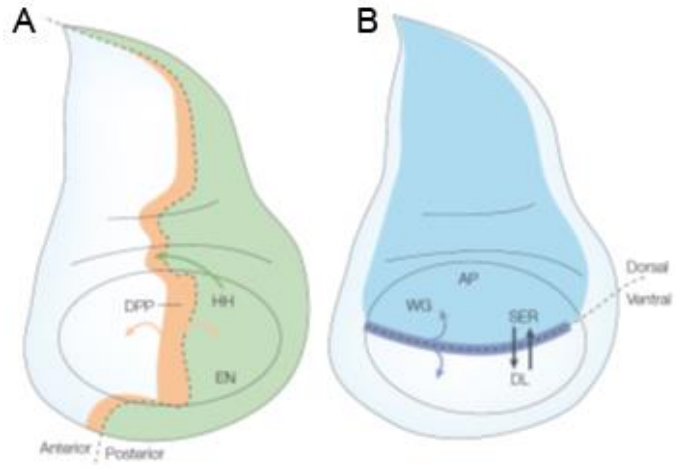

Figure 4. Compartment boundaries and local signaling centers in the developing fly wing. (A) The *Drosophila* wing is subdivided into anterior and posterior cells by a cell lineage restriction boundary that expresses the morphogen Decapentaplegic (DPP, orange). The posterior compartment expresses Hedgehog (HH, green), the expression of which depends on Engrailed (EN). (B) The dorsal compartment of the wing disc expresses the transcription factor Apterous (AP), which results in activation of the Notch ligands Delta (DL) and Serrate (SER) at the dorsal-ventral compartment boundary (dark blue). Once the boundary has been established, it expresses Wingless (WG), which regulates patterning along the DV axis.

Regulation of organ growth

Organ growth is the consequence of an increase in cell number, cell size or both. The balance between cell proliferation and cell death determines cell number, while cell size depends on cell growth (accumulation of mass). During development, mitogens stimulate cell proliferation whereby cell division is driven by the replication of the DNA content and progression of the cell cycle. In the other hand, cell death is a genetically programmed process in which cells commit suicide by inducing DNA fragmentation and protein degradation. Both developmental cues and lack of survival factors can trigger cell death. Cell growth, which is also regulated by extracellular growth factors, entails protein synthesis and organelle biogenesis, leading to an increase in cell mass and size. Thus, size is regulated by extracellular factors that impinge on these three main aspects occurring at the cellular, organ and organismal levels. Since the number of apoptotic cells during normal development of the wing disc is very low, its final size relies on cell growth and cell proliferation.

Proliferation/Cell Cycle

The cell cycle or the cell-division cycle is the sum of events that leads to cell division, producing two daughter cells. The cell cycle of eukaryotes is divided into four distinct phases: G1 phase (GAP1, cell increases size), S phase (DNA replication), G2 phase (GAP2, cell increases size) and M phase (mitosis, cell division) (Figure 5). Entry into each of these phases is dependent on the proper progression and completion of the previous one.

In *Drosophila*, different types of regulators drive cell cycle progression. One of the most important groups of cell cycle regulators is the family of serine-threonine protein kinases, the Cyclin Dependent Kinases (CDK), that are activated in a sequential fashion. The timing of their activation is defined by their post-translational modifications (phosphorylations/ dephosphorylations), and by the

association with proteins called Cyclins (Cyc), which act as the regulatory subunits of the kinase complex. The Cyclin family is divided into two main classes: the 'G1 cyclins' which comprise Cyclin D and Cyclin E, and their accumulation is rate-limiting for progression from the G1 to S phase; and the 'mitotic or G2 cyclins' which include Cyclin A and Cyclin B and are involved in the control of G2 to M transition and mitosis. Cyclins bind to and activate the CDKs, which lead to phosphorylation and inhibition of different cell cycle inhibitors.

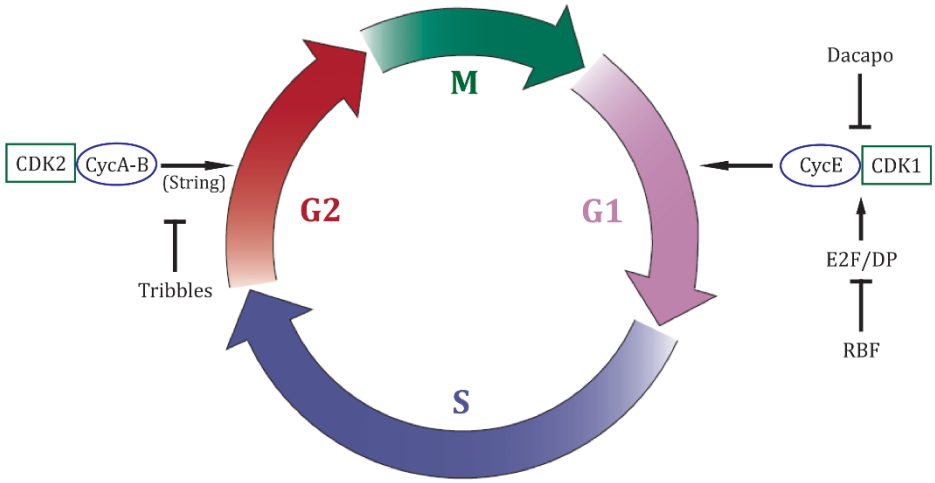

Figure 5. Cell cycle of *Drosophila melanogaster*. The cell cycle is subdivided into four phases: G1, S, G2 and M phases. Two key regulatory checkpoints are represented. In G1, CyclinE limits S phase initiation by binding to CDK1. CycE is regulated by Dacapo/p21 and by E2F which is repressed by the retinoblastoma-like protein RBF. In G2, CyclinA-B bind and activate CDK2 which induce String/Cdc25 thus allowing mitosis initiation. Tribbles functions as a negative regulator of this process.

There are also several transcription factors known to have a role on cell cycle regulation. One example is the E2F transcription factor that, together with its co-factor DP, forms a protein complex that acts as transcription activator promoting Cyclin E (CycE) expression and thus transition from G1 to S phase [(Dynlacht et al., 1994), see Figure 5]. The activity of *String/Cdc25*, a critical regulator of the

activity of the CycA-B/CDK2 complex, is rate limiting for entry into mitosis [Edgar and O'Farrell, 1989), see Figure 5].

The cell cycle regulators presented above induce and allow cell cycle progression. However, different checkpoint mechanisms ensure that cells do not progress through the cell cycle when defects occur. As expected, one of the ways to repress cell cycle progression is through the inhibition of the Cyclins. The *Drosophila* gene *dacapo* (*dap*), which is a member of the p21/p27 family of CDK inhibitors, inhibits CycE/CDK2 activity therefore blocking G1 to S transition (De Nooij et al., 1996; Lane et al., 1996). The *Retinoblastoma-family protein* (RBF) is a family of tumor suppressor proteins known to be able to bind to E2F, thus preventing CycE activation and, as a consequence, G1 to S transition is compromised (Du et al., 1996). *tribbles* is another cell cycle progression repressor that specifically induces degradation of String protein and consequently inhibits G2 to M transition (Mata et al., 2000).

Despite manipulation of cell proliferation in the wing imaginal disc, the resulting wings often attain the normal size. It seems that there is a defined adult size and that either the wing is formed by fewer but larger cells (if cell cycle is blocked), or more but smaller cells (if cell cycle is induced) (Neufeld et al., 1998; Weigmann et al., 1997). Therefore, despite the close relationship between cell proliferation and cell growth, they are independently controlled.

Growth Signaling Pathways

Organ-Extrinsic Signals:

The Insulin/IGF signaling (IIS) and the TOR signaling pathways are two highly conserved pathways that sense energetic and nutrient status in animals from flies to humans. These pathways are the main players in sensing nutritional information in order to coordinate growth and metabolism with nutrient availability. Information about the nutritional status is directly sensed at the level

of individual cells via the TOR pathway, while the systemic response is carried out by the hormonal action of insulin.

Insulin Signaling Pathway

The insulin signaling pathway is highly conserved from *Drosophila* to mammals. In the fly, as in mammals, insulin signaling regulates a number of physiological functions, such as metabolism, tissue growth and longevity. In the past decade, studies in *Drosophila* allowed to identify important conserved components of the signaling pathway. Flies and humans indeed show a surprising amount of conservation and parallelism at the level of the molecular components of the insulin signaling pathway, but also at the level of the physiological outputs of the pathway.

In vertebrates, the metabolic functions of the pathway are mediated by insulin, whereas growth is promoted by the activity of IGFs (Nakae et al., 2001). These different biological functions can be attributed, at least in part, to their binding to different receptors, the insulin receptor (IR) and the IGF-1 receptor (IGF-1R). Given the fact that insects possess a single insulin-like system, they might represent a possible ancestor of the IIS (Wu and Brown, 2006). *Drosophila* insulin-like peptides (Dilps) indeed carry both the metabolic functions of mammalian insulins and the growth-promoting functions of IGFs (Garofalo, 2002), and act through a very well conserved signaling pathway.

To date, eight insulin-like peptides (Dilps1-8) have been identified in *Drosophila*. With the exception of the recently discovered Dilp8 (Colombani et al., 2012; Garelli et al., 2012), which does not signal through the known Insulin-like Receptor [InR, see (Colombani et al., 2015; Vallejo et al., 2015)], Dilps activate a canonical pathway that regulates cell growth and metabolism. Circulating Dilps act systemically on remote target tissues by binding to a receptor tyrosine kinase at the cell surface. Activation of the single *Drosophila* InR by the ligand triggers a

downstream signaling cascade that is strongly conserved between vertebrates and invertebrates (Figure 6).

The first event upon activation of InR is the recruitment of the adaptor protein Insulin receptor substrate (IRS), named Chico in *Drosophila*, as well as the regulatory (p60) and catalytic (Dp110) subunits of the phosphoinositide 3-kinase (PI3K, also called Dp110) to the receptor, which leads to the activation of the catalytic subunit (Engelman et al., 2006). Activated PI3K phosphorylates phosphatidylinositol-4,5-diphosphate (PIP2) on the plasma membrane to produce phosphatidylinositol-triphosphate (PIP3). This stimulation is reversed by the action of PTEN (phosphatase and tensin homolog), a negative regulator of the PI3K pathway (Goberdhan et al., 1999) that has been identified as a tumor suppressor gene in mammals. PIP3 recruits Akt (a proto-oncogene also known as PKB, protein kinase B) to the plasma membrane and its subsequent phosphorylation. The protein kinase Akt has several distinct effectors and functions that I will briefly described. In one hand, Akt activation promotes the uptake of glucose through the insertion of glucose transporters into the membrane and glycogen synthesis. In this way it increases the energy supply of the cell by inducing glucose storage (Taniguchi et al., 2006). Moreover, Akt is involved in growth regulation and has as main effectors TOR (described below) and the Forkhead Box O (FOXO) transcription factor (Figure 6). Phosphorylation of FOXO by AKT promotes growth by preventing FOXO of entering into the nucleus where it acts as a transcriptional repressor and a negative regulator of growth. FOXO is activated only when insulin signaling is low and although FoxO mutants do not show tissue overgrowth under normal conditions, FoxO limits growth in adverse conditions such as poor nutrition thus mediating the response to starvation (Jünger et al., 2003; Kramer et al., 2003; Puig et al., 2003). Overexpression of *Drosophila* FOXO (dFOXO) can inhibit cell proliferation and leads to reduced organ size by reducing cell number (Puig et al., 2003). FOXO is known to negatively regulate growth by targeting different pathways. In response to cellular stresses, such as nutrient deprivation or increased levels of reactive

oxygen species, dFOXO is activated and inhibits growth through the action of target genes such as the eukaryotic initiation factor 4E binding protein 4EBP (Jünger et al., 2003). 4EBP, in its non-phosphorylated form, is normally bound to the Eukaryotic translation initiation factor 4E (eIF4E) inhibiting translation initiation. When phosphorylated, 4EBP is unable to bind to the eIF4E thus allowing protein translation to occur (Jastrzebski et al., 2007). The transcription factor dMyc is another known target of the PI3K pathway via direct binding of FOXO to the *Drosophila myc* promoter (Teleman et al., 2008). dMyc is known to have a role in promoting ribosome biogenesis (Grewal et al., 2005). The role of PI3K pathway in size and growth control emerged from studies in *Drosophila*, where loss-of-function mutants of components of the pathway were found to display reduction of tissue growth associated with either lethality or severely reduced body size. For example, viable mutants of *chico*, the *Drosophila* ortholog of IRS, are smaller than wild type flies as a consequence of smaller and fewer cells (Böhni et al., 1999). A similar outcome is observed by mutations in the *insulin receptor* gene or by severe nutrient deprivation. On the contrary, *PTEN* mutants show dramatic tissue overgrowth. Similarly, flies in which other positively regulators of the pathway, such as PI3K, are activated also show overgrown phenotypes (Leevers et al., 1996).

Consistent with the role in tissue growth, hyperactivation of PI3K signaling is commonly observed in various types of human cancer (Yuan and Cantley, 2008). Deletion of *PTEN* is associated with aggressive metastatic potential and poor prognosis (Cully et al., 2006), and targeted depletion of *PTEN* in epithelial cells leads to rapid development of endometrial, prostate, and thyroid neoplasias in mouse models (Mirantes et al., 2013). Interestingly, even malignant growth can be promoted by systemic nutritional signaling. Caloric restriction, which lowers levels of circulating IGF-1 and insulin, can reduce growth of several types of tumors. The sensitivity of tumors to caloric restriction depends on the status of PI3K signaling: constitutive activation of the PI3K, e.g., by loss of *PTEN*, renders the tumors insensitive to caloric restriction (Kalaany and Sabatini, 2009). In

contrast, PTEN mutant cells in *Drosophila* tissues become more aggressive upon nutrient restriction (Nowak et al., 2013).

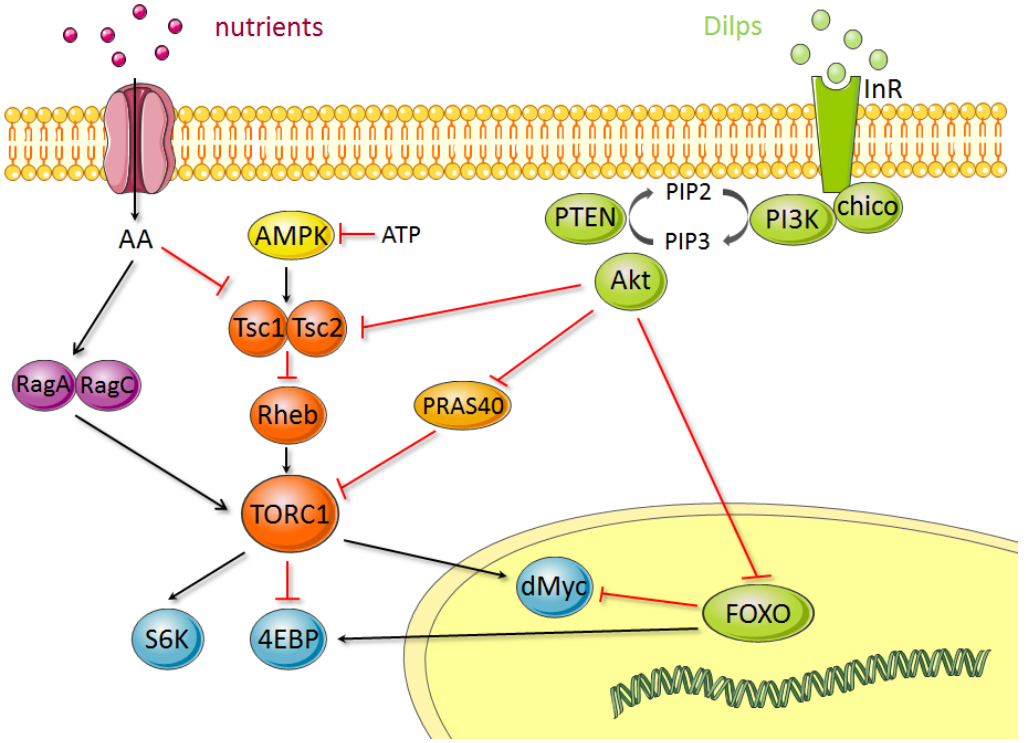

Figure 6. Diagram showing the IIS and TOR signaling pathways. The main elements of the conserved IIS and TOR signaling pathways are shown in green and orange, respectively. Another input signals controlling this nutrient sensing pathway are also depicted. In blue are some of the most important downstream effectors of these pathways. Black arrows represent positive regulation and red bar-ended lines indicate inhibitory interactions. Details of each interaction are described in the main text.

TOR Signaling Pathway

The protein kinase TOR (target of rapamycin) is the main mediator of cellular nutrient sensing, role that is conserved from yeast to mammals. TOR complex 1 (TORC1) is the major rapamycin sensitive form of TOR, and it is the primary mediator of energy and amino acid sensing for growth control. TOR complex 2 (TORC2) is insensitive to the inhibitory effects of rapamycin, and it phosphorylates substrates distinct from those phosphorylated by TORC1 (review in Hietakangas & Cohen 2009). The main mechanism by which TORC1 regulates

tissue growth is by adjusting protein biosynthesis in response to nutrient levels, which is a rate limiting process in cell growth. It does so mainly by regulating two translational regulators: ribosomal protein S6 kinase (S6K) and eukaryotic initiation factor 4E binding protein (4EBP) (Figure 6). TOR allows the assembly of the translation preinitiation complex and stimulates peptide chain elongation by inhibition of 4EBP and activation of S6K respectively (Holz et al., 2005; Wang et al., 2001). In *Drosophila,* inhibition of *dTOR* has been shown to reduce body growth and cause larval lethality (Zhang et al., 2000). Moreover, TORC1-depentent transcriptional regulation of genes involved in ribosome assembly was shown to be in part through the transcriptional activation of dMyc transcription factor (Teleman et al., 2008). As stated above, dMyc promotes ribosome biogenesis (Grewal et al., 2005). In this way, TORC1 allows the rate of translation to be coupled with the amount of ribosomes. It has been recently shown that most of the transcriptional output downstream of TORC1 is controlled by two transcription factors REPTOR and REPTOR-BP in *Drosophila* (Tiebe et al., 2015).
The small GTPase Rheb (Ras homologue enriched in brain) controls the activity of TORC1, although the mechanism by which Rheb activates TORC1 is still a matter of discussion. *Rheb* mutant flies show severe undergrowth as a consequence of reduced cell size and cell number (Saucedo et al. 2003; Stocker et al. 2003), and Rheb overexpression gives rise to overgrowth phenotypes (Saucedo et al. 2003). The tumor suppressors TSC1 and TSC2 (Tuberous Sclerosis Complex genes 1 and 2) regulate Rheb activity. As a complex, they act as a Rheb-GTPase activating protein (Rheb-GAP), promoting GTP hydrolysis and driving Rheb to the inactive GDP-bound state (Inoki et al., 2003a; Tee et al., 2003; Zhang et al., 2003). Mutations in TSC1 and TSC2, that lead to hyperactivation of the target of rapamycin (TOR) pathway, are causative of tuberous sclerosis, a hamartoma syndrome associated with a predisposition to malignancy (Inoki et al., 2005). Likewise, heterozygous Tsc1 or Tsc2 mutant mice have been shown to develop renal and extrarenal tumors such as hepatic hemangiomas (Kobayashi et al., 2001). In *Drosophila*, TSC1 and TSC2 mutants are lethal, but clones of cells lacking

TSC1/2 activity show strong overgrowth as a result of an increase in cell size and number (Potter et al., 2001; Tapon et al., 2001).

TORC1 activity is regulated by the amount of cellular amino acids, thus linking the nutritional status of the cell with the rate of protein synthesis (Avruch et al., 2009). This regulation occurs downstream of the TSC1/2 complex (Smith et al., 2005) but Rheb function is essential for TORC1 to be active by amino acids (Kim et al., 2008; Sancak et al., 2008). TORC1 activation by amino acids also requires another group of small GTPases, the Rag proteins (Kim et al., 2008; Sancak et al., 2008) (Figure 6). The mechanism by which amino acids regulate Rag complex activity is still unknown. Expression of a constitutively active form of RagA promotes tissue growth in the *Drosophila* wing, whereas expression of dominant negative form of RagA inhibits it, as expected by its ability to activate TORC1 (Kim et al., 2008).

TORC1-mediated cell growth is also under control of an energy sensing-mechanism that depends on AMPK (AMP-activated protein kinase). AMPK activity monitors the immediately available energy by measuring the cellular ATP levels (Hardie, 2007) as well as energy stores in form of glycogen (McBride et al., 2009). AMPK signaling, when ATP levels are low, regulates growth by phosphorylating and activating TSC2, which results in TORC1 inhibition (Inoki et al., 2003b) (Figure 6).

Crosstalk between Insulin and TOR pathways

As stated above, one effector of Akt in growth regulation is TOR (Figure 6). Such regulation allows the link between the systemic nutrient sensing and the cell-intrinsic nutrient sensing components. However, in the last years this connection has been under debate. Studies in *Drosophila* showed *in vitro* that Akt phosphorylates and inhibits TSC2 activity, which leads to TORC1 activation (Potter et al., 2002). However, two distinct studies *in vivo* showed that mutant forms of TSC1 and TSC2 lacking the Akt phosphorylation sites do not present defects in TOR activity (Dong and Pan, 2004; Schleich and Teleman, 2009) thus

challenging the idea that this link is functionally relevant under physiological conditions. Recently, the protein PRAS40 (Proline-rich AKT substrate 40) has been shown to directly interact with TORC1 and inhibits its interaction with substrates (Figure 6). PRAS40 is phosphorylated by Akt on a single site, thus relieving TORC1 inhibition (Sancak et al., 2007; Vander Haar et al., 2007). This phosphorylation event is then necessary for insulin-induced TORC1 activation. In *Drosophila*, overexpression of dPRAS40 reduces tissue growth in an autonomous manner by reducing cell size, which is consistent with an inhibition of TORC1. However, while changes in TORC1 activity strongly affect body size, *PRAS40* mutant flies are viable and present no obvious changes in body growth, which suggests that *PRAS40* does not regulate TORC1 activity during the growth period. Nevertheless, in *PRAS40* mutant females TORC1 canonical targets are upregulated specifically in the ovaries, revealing that PRAS40 represses TORC1 specifically in this tissue. Ubiquitous reduction of insulin signaling decreases TORC1 activity in a PRAS40-dependent manner only in the ovary and not in the rest of the body probably due to PRAS40 being maintained inactive in those tissues. Consistently, removal of *PRAS40* in *chico* mutants rescues female fertility bur not body undergrowth. These results show that Insulin and TOR signaling are linked only in specific tissues and that PRAS40 mediates this crosstalk (Pallares-Cartes et al., 2012).

Organ-Intrinsic Signals:

Even though environmental conditions have an important role in organ growth, size, shape or pattern of every *Drosophila* adult structure is genetically determined in an autonomous manner by each imaginal disc through the action of several signalling pathways. This idea comes from transplantation experiments in which young wing discs when transplanted into the abdomen of adult flies grow fine until they achieve the normal size of a mature wing disc (Bryant and Simpson, 1984).

Hippo Signaling Pathway

The Hippo signaling pathway has been implicated in the regulation of organ size due to its fundamental roles in promoting cell proliferation and in inhibiting apoptosis. This pathway was first discovered in *Drosophila* by means of genetic screens and its evolutionary conservation is certainly extensive. Actually, mutations in the Hippo pathway induce tumors in mouse models and occur in a broad range of human carcinomas, including lung, colorectal, ovarian, and liver cancers [reviewed in (Harvey et al., 2013)].

The Hippo pathway consists of three major modules: a core kinase cassette, downstream transcriptional regulatory proteins, and multiple upstream regulatory proteins (Figure 7). The core kinase cassette is composed of two kinases, Hippo (Hpo) and Warts (Wts), and two adaptor proteins, Salvador (Sav) and Mob as tumor suppressor (Mats). Hpo together with the scaffold protein Salvador (Sav) mediates Wts activation. Wts together with the other scaffold protein, Mats, phosphorylates the transcriptional co-activator Yki. This phosphorylation event causes Yki retention in the cytosol and its repression, leading to cell cycle exit, apoptosis and growth inhibition (Huang et al., 2005; Udan et al., 2003). Yki promotes tissue growth and survival in conjunction with several transcription factors, including Scalloped (Sd), Homothorax (Hth), Teashirt (Tsh) and Mothers against decapentaplegic (Mad). Yki has as transcriptional targets many genes involved in growth, proliferation and apoptosis (Figure 7). The *bantam* microRNA is a well-known target of Yki that promotes cell survival and proliferation (Nolo et al., 2006; Thompson and Cohen, 2006). *cycE*, which regulates the G1 to S transition during the cell cycle, is also induced by Yki (Tapon et al., 2002). Another known target of the Hippo pathway is the *Drosophila Inhibitor of Apoptosis* (DIAP-1), a fundamental gene involved in promoting cell survival (Tapon et al., 2002; Wu et al., 2003). Imaginal discs with clones of cells mutant for Hpo, Sav, Wts or Mats show outgrowths with extra folding of the tissue but preserve their epithelial nature (Wu et al., 2003). More recently, it has been

shown that the expression of the *Drosophila* dMyc protein (dMyc) is also regulated by the Hippo pathway and that it functions as an essential cellular growth effector of the pathway (Neto-Silva et al., 2010).

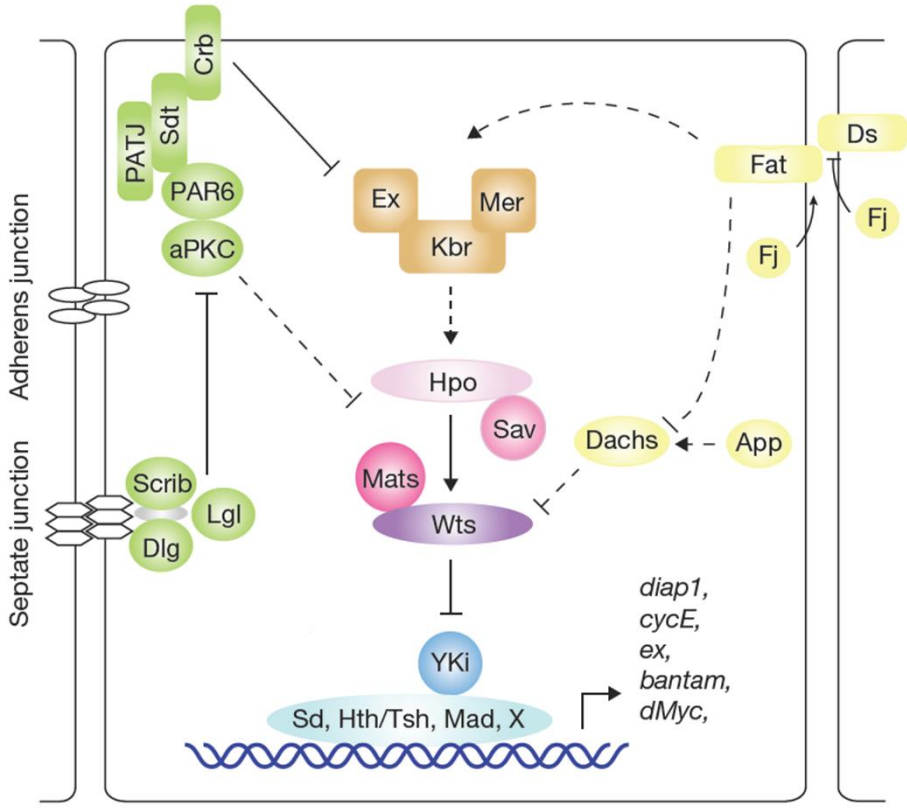

Figure 7. Diagram showing the Hippo signaling pathway in *Drosophila*. The main elements of the conserved Hippo signaling pathway are shown. Black arrows represent positive regulation and black bar-ended lines indicate inhibitory interactions. Dashed lines indicate unknown mechanisms. Details of each interaction are described in the main text. Adapted from (Zhao et al., 2011).

The upstream branches of the Hippo pathway are complex since they involve multiple regulatory proteins and their mode of action is not yet fully understood. Nevertheless, it seems clear that many of these upstream regulatory proteins concentrate at cell junctions and they allow the Hippo pathway to be regulated by cell-cell contact, cell polarity, and the actin cytoskeleton, thereby enabling the

activity of the pathway to respond to tissue organization and integrity. Once the cadherin Dachsous (Ds) forms an heterodimeric bridge with the cadherin Fat of an adjacent cell, Fat activates both kinases, Hpo and Wts (Bennett and Harvey, 2006; Cho et al., 2006). Three membrane-associated proteins, Kibra, Expanded (Ex) and Merlin (Mer) work as adaptor proteins and it was reported that they have redundant and overlapping roles in activating the Hippo pathway. These proteins can interact with each other and they have similar loss-of-function overgrowth phenotypes (Baumgartner et al., 2010; Genevet et al., 2010; McCartney et al., 2000; Yu et al., 2010). Despite the fact that it is not entirely clear how they influence the activity of the Hippo core kinase cassette, overexpression of Kibra, Ex and Mer was shown to stimulate activity of Hpo and Wts, whereas its knockdown reduced apical membrane localization of Hpo (Baumgartner et al., 2010; Genevet et al., 2010; Yu et al., 2010). The apicobasal polarity proteins Discs large (Dlg), Lethal giant larvae (Lgl) and Scribble (Scrib) form a complex that localizes to the basolateral membrane of epithelial cells. Mutations in these three genes and also in the apicobasal polarity protein Crumbs (Crb) caused translocation of Yki into the nucleus and the consequent upregulation of the Hippo pathway target genes (Chen et al., 2010; Grzeschik et al., 2010a; Ling et al., 2010; Robinson et al., 2010; Zhao et al., 2008). The mechanism by which these proteins control Hippo pathway activity is not completely clear. The regulation of the Hippo pathway by cadherin-mediated cell-cell interactions makes it likely that it is influenced by many developmental signaling pathways and thus plays a key role in defining organ size and shape.

Morphogens

Classically, a morphogen is defined as a molecule that spreads from a localized source such that its concentration declines in a continuous and predictable fashion, providing a series of concentration thresholds, and thus, controlling the

behavior of surrounding cells as a function of their distance from the source. In this way, they specify distinct cell fates in a concentration-dependent manner.

In particular, Hedgehog (Hh), Wingless (Wg) and Decapentaplegic (Dpp) have been shown to act directly at a distance and in a concentration-dependent manner in the fly limbs (Lecuit et al., 1996; Nellen et al., 1996; Neumann and Cohen, 1997; Strigini and Cohen, 1997; Zecca et al., 1996). Hedgehog is expressed in the posterior compartment and signals to the anterior compartment in order to activate its target genes (Figure 8). Dpp is a target of Hh signaling and is induced in a stripe of cells adjacent to the AP boundary of the wing disc (Zecca et al., 1995) (Figure 8). Dpp spreads towards both anterior and posterior cells to act as a long-range morphogen by inducing expression of its target genes (in detail below). Wg is secreted from the DV border of the wing disc and acts as a long-range morphogen (Figure 8) by inducing the expression of Wg target genes, including *senseless* (*sens*), *distalless* (*dll*), and *vestigial* (*vg*) (Neumann and Cohen, 1997; Zecca et al., 1996). When Wg and/or Dpp were ectopically expressed in clones of cells, it was observed that they were capable of organizing supernumerary limbs (Struhl and Basler, 1993; Zecca et al., 1995). Although morphogens were first presented as the master regulators of tissue patterning, several genetic experiments have shown that Dpp and Wg also have a role in growth, survival and proliferation of the cells. It was shown that loss of Dpp or Wg activity in the developing wing leads to growth defects and loss of wing tissue (Zecca et al., 1995; Zecca et al., 1996). In the opposite direction, Wg or Dpp can promote growth when ectopically activated within the wing disc indicating again that there is a strict correlation between patterning and growth (Basler and Struhl, 1994; Johnston and Schubiger, 1996). However, a recent study points out that the graded distribution of Wg is not required to stimulate cell proliferation at least during the later stages of wing development (Baena-Lopez et al., 2009). As organ-intrinsic regulators of growth, these molecules likely account for the autonomous control of organ size.

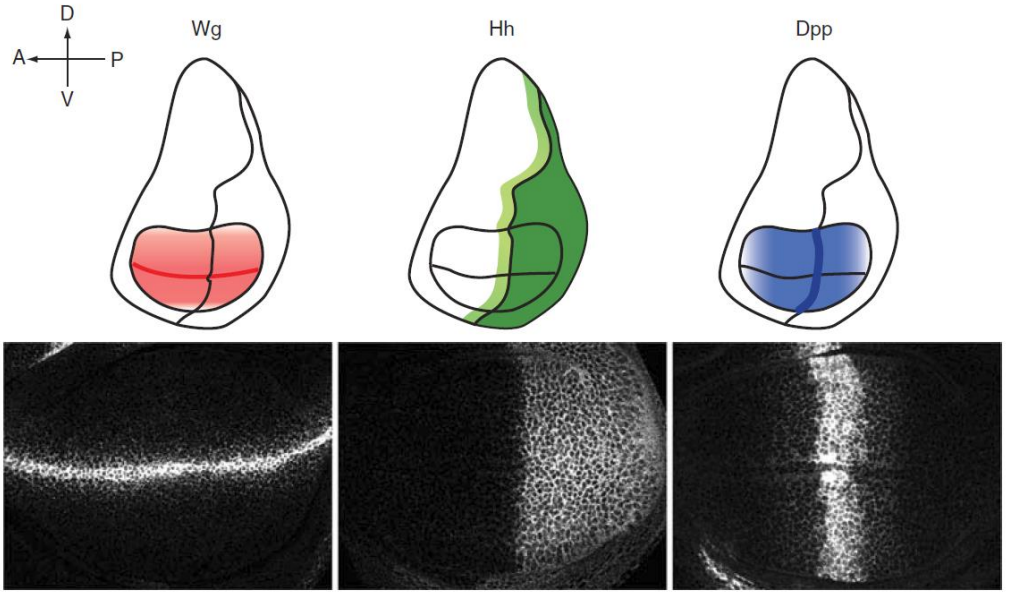

Figure 8. Distribution of Wg, Hh and Dpp morphogens in the *Drosophila* wing imaginal disc. In third instar larvae wing discs, Wg is expressed at the DV boundary and (red) acts as a long-range morphogen to organize patterning along the DV axis (light red). Hh is expressed in the P compartment (green) and moves into the A compartment to activate gene expression in a stripe of cells adjacent to the AP boundary (light green). Dpp is produced at the AP boundary (blue) and acts as a long-range morphogen that controls growth and patterning of wing cells along the AP axis (light blue). Adapted from (Yan and Lin, 2009).

The Dpp morphogen gradient

Decapentaplegic (Dpp), the fly homologue of vertebrate bone morphogenetic proteins BMP2 and BMP4, belongs to the transforming growth factor-β (TGF-β) family and functions directly at a distance to specify gene expression patterns in a concentration-dependent manner. Dpp, induced by Hh signaling coming from posterior cells (Zecca et al., 1995), is expressed along the boundary between the anterior and posterior compartments of the wing imaginal disc, and forms a concentration gradient along the AP axis of the wing primordium (Lecuit et al., 1996; Nellen et al., 1996). The local synthesis of the ligand and its action at a distance indicated that Dpp forms a protein gradient, with its highest level at the center of the wing along the AP compartment boundary, with levels declining as

the distance from this boundary increases. Different scenarios have been proposed to participate in or regulate gradient formation and interpretation which I will describe bellow in detail.

Upon binding to the type I-type II/Thick veins (Tkv)-Punt receptor complex, the intracellular signal transducer and transcription factor Mothers against Dpp (Mad) becomes phosphorylated and activated (Kim et al., 1997; Ruberte et al., 1995). Activated Mad forms a complex with Medea and enters the nucleus to inhibit the expression of the transcriptional repressor Brinker (Brk) (Figure 9). These events convert the Dpp morphogen gradient into an inverse gradient of Brk repressor activity that mediates many of the patterning and growth functions of Dpp (Martín et al., 2004; Müller et al., 2003; Pyrowolakis et al., 2004; Schwank et al., 2008). When *brk* is ectopically expressed, cells that normally respond to Dpp become refractory to it. Therefore, in order to activate target genes, the Dpp signaling pathway must remove Brk. This downregulation of *brk* occurs at the transcriptional level. Both Brk and P-Mad regulate Dpp target genes, such as *daughters against dpp* (*dad*), *spalt* (*sal*) and *optomotor-blind* (*omb*) (Figure 9). Dad is an inhibitory SMAD that downregulates Dpp signaling in the wing primordium (Tsuneizumi et al., 1997). As it is induced by Dpp, its inhibitory function is highest in regions of high Dpp activity. This negative feedback loop might modulate the duration and intensity of the signal. The Spalt and Omb target genes are activated by P-Mad in a concentration-dependent manner, and the inverse gradient of Brk repressor is fundamental to control the expression state of these Dpp-induced genes along the AP axis (Moser and Campbell, 2005; Müller et al., 2003; Winter and Campbell, 2004). Expression boundaries of both *sal* and *omb* are set by Brk (Campbell and Tomlinson, 1999; Jaźwińska et al., 1999); *omb* is less sensitive to Brk than *sal* and as such its domain of expression is broader. Although it is still unclear how *sal* and *omb* are repressed at different concentrations of Brk, one study suggests that different repression domains of Brk are sufficient to repress *omb* but not *sal* (Kirkpatrick et al., 2001).

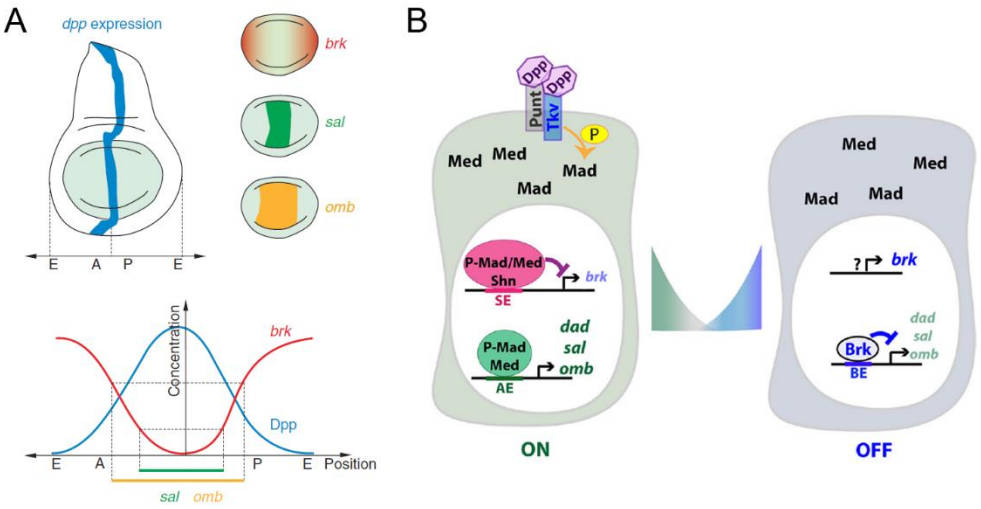

Figure 9. Dpp morphogen signaling cascade in the *Drosophila* wing imaginal disc. (A) In the upper panel representation of the expression patterns of *dpp* (in blue), *brk* (in red), *sal* (in green) and *omb* (in yellow). Dpp is secreted from its site of production at the center of the disc and spreads into the A and P compartments, establishing a gradient with highest levels in the center and lowest in the lateral regions. Brk forms an inverse gradient to the Dpp gradient. Brk levels are important, together with Dpp activity levels, to set the expression boundaries of sal and omb. As omb is repressed by high levels of Brk and sal by lower levels, omb is expressed in a broader domain than sal (lower panel). (B) Representation of the transcriptional activity of the Dpp signaling cascade in cells with two extreme levels of Dpp: a medial cell with high Dpp activity levels in green and a lateral cell with low Dpp activity levels in blue. The question mark highlights the unknown transcriptional activator of *brk* and pent. SE: Silencer Element, AE: Activating Element, BE: Brinker Element. Details are described in the main text. Adapted from (Hamaratoglu et al., 2014; Schwank and Basler, 2010).

Dpp functions: from patterning to growth

Ectopic expression of Dpp in clones of cells both in the anterior or posterior compartments caused reorganizations of the wing pattern suggestive of a long-range activity of this morphogen (Capdevila and Guerrero, 1994; Zecca et al., 1995). In addition, these clones induce over-proliferation of surrounding cells and sometimes lead to organ duplications (Zecca et al., 1995). Hence, ectopic Dpp can induce proliferation of an extra tissue and, at the same time, patterns it in the same way as the wild type tissue. How the growth and patterning of developing tissues are controlled and coordinated has been a long-standing question in

developmental biology. The Dpp morphogen, that plays a role in both of these processes by providing positional information to the cells in the tissue and by acting as a trigger for tissue growth, is of crucial importance in the coordination of growth and patterning of the wing imaginal disc.

In the mature wing of the fly, the positioning of the veins along the anteroposterior axis are manifestations of different Dpp patterning outputs. Together with Brk, Sal and Omb, encoding transcriptional regulators, Dpp is involved in the vein positioning of the adult wing. Sal and Brk are required for the specification of the longitudinal vein 2 in the anterior compartment, while Omb and Brk are important in the establishment of the vein 5 in the posterior compartment (reviewed in De Celis, 2003).

The conclusion that Dpp is critical for growth of the wing imaginal disc comes from the observation that mutant flies lacking Dpp expression in the wing imaginal disc fail to form wings (Zecca et al., 1995) and clones of cells unable to transduce Dpp are eliminated from the wing blade (Burke and Basler, 1996). In an opposite way, overexpression of Dpp in its own domain causes overgrown wing imaginal discs (Burke and Basler, 1996). Since Dpp is a potent growth promoter, one would expect that growth takes place where Dpp activity is highest. But actually, proliferation is uniform across the wing disc (Milán et al., 1996), while Dpp activity is graded. This morphogen gradient is required for uniform proliferation since uniform Dpp signaling, by overexpression of Dpp throughout the wing disc, causes lateral cells to proliferate more (Schwank et al., 2008). Several models have been proposed in order to explain how the gradient of Dpp activity drives uniform proliferation in the wing imaginal disc. Some of these models propose an instructive role of Dpp in growth, while others suggest a permissive one.

1. The Memory Model

According to this model, the Dpp gradient at the onset of wing disc development programs the cells of the disc along the AP axis to acquire different sensitivities towards a mitogenic activity of Dpp—such that lateral cells become more sensitive relative to medial cells. Thus, during the growth period of the disc, the Dpp morphogen gradient would lead to uniform proliferation despite elevated Dpp activity in medial compared with lateral regions. If this model is correct, an early exposure to equal levels of Dpp activity throughout the wing disc would make the sensitivity to the mitogenic action of Dpp the same in all the cells. However, by doing so lateral cells still proliferate faster than medial cells (Schwank et al., 2008), indicating that the different sensitivities according to the position in the disc are not due to an early exposure to a gradient of Dpp.

2. The Threshold Model

This model states that Dpp would drive uniform proliferation because its activity exceeds a certain minimal level throughout the disc. It would then predict that once the minimal value is exceeded, differences in Dpp levels should no longer matter. A couple of experimental data contradicts this model: (1) ectopic activation of Dpp leads to overgrown discs (Burke and Basler, 1996; Capdevila and Guerrero, 1994); and (2) lateral clones with constitutively active Dpp signaling grow faster than wild type clones (Martín-Castellanos and Edgar, 2002).

3. The Gradient Models

This model predicts that cells compare the levels of Dpp they are exposed to with those of their neighbors. When the differences between these levels are sufficiently high (the gradient of Dpp is sufficiently steep) cells proliferate (Day and Lawrence, 2000). According to this model, one would expect proliferation to stop where these differences are zero, such as in discs with ubiquitous Dpp expression, and this is not the case. This discrepancy led to a refinement of the model (Rogulja and Irvine, 2005). During early wing disc development, lateral cells may become differently programmed, such that they not only react to the

steepness of the gradient, like medial cells, but also to the absolute levels of local Dpp - even when these are uniform. The observation that juxtaposition of cells with distinct Dpp signaling levels does not drive proliferation (eg. expression of a constitutively active form of the Tkv receptor exclusively in the medial region leads to normal growth within the whole disc (Schwank et al., 2008)) challenges the legitimacy of this model.

4. The Inhibitor Model

This model postulates that a growth inhibitor forms an opposite gradient to the one generated by Dpp and by doing so, this inhibitor guides the near-uniform activation of the Dpp pathway and the corresponding un-patterned cell proliferation (Serrano and O'Farrell, 1997). Two scenarios might be possible: either the expression of the growth inhibitor is controlled by Dpp or arises in an independent way. If the first situation is correct, then homogeneous activation of Dpp would lead to homogenous growth and, as described above, this is not the case. For the second scenario, one could speculate that Hh signaling could control, as it regulates all known AP patterning genes such as Dpp itself, the expression of such putative inhibitor. However, uniform activation of Hh signaling in the anterior half of the wing disc shows overgrowth and high proliferative rates in the anterior lateral region (Basler and Struhl, 1994). These observations, together with the fact that no such inhibitor has been identified so far, make this model quite speculative.

5. The Steamroller Model / Growth Equalization Model

This model, as the previous one, is based on multiple growth inputs. Dpp levels along the AP axis set different Brk expression levels: high laterally and low medially. This model postulates that lateral cells have a growth advantage compared with medial cells, and that the Dpp/Brk system is necessary to restrict lateral proliferation. The high lateral Brk levels are required to restrict the over-proliferation that would otherwise occur in this region (Martín et al., 2004; Schwank et al., 2008). This idea comes from the observation that wing discs

lacking both Dpp and Brk resulted in a non-uniform proliferation pattern with increased growth laterally and decreased growth medially (Schwank et al., 2008). In the absence of the Dpp/Brk system, lateral over-proliferation inhibits growth in the medial area by an unknown mechanism. Another recent piece of evidence that supports this model is that in the absence of Dpp spreading, by trapping Dpp at its source, lateral cells still divide at normal rates, while medial cells divide at a lower rate (Harmansa et al., 2015).

6. Opposing growth-pathways Model

In this model, the distinct activities of Dpp and Fat signaling complement each other and provide the basis for a relatively even proliferation pattern along the AP axis of the wing primordium. Fat signaling pathway is regulated in a Dpp-independent manner. In medial cells, Dpp activity inhibits Brk and thus allowing cells to proliferate. In contrast, Fat activity in medial cells represses growth via the Hippo signaling pathway. In lateral cells, Brk is expressed and is responsible to repress growth, while the absence of Fat activity allows cells to proliferate. *fat* mutant wing discs show higher proliferation rates in the medial region (Schwank et al., 2011). Uniform Dpp gives rise to hyper-proliferation specifically of lateral cells. However, simultaneous depletion of Fat and Dpp signaling leads to high proliferation levels both in medial and lateral regions of the wing primordium (Schwank et al., 2011). Inhibition of the Dpp pathway fully counteracted the increased proliferation rates occurring in the medial region of *fat* mutant discs.

<u>How Dpp regulates organ growth?</u>

The observation that there are no changes in cell size when Dpp levels are altered indicates that Dpp does not regulate organ growth by affecting cell size (Martín-Castellanos and Edgar, 2002). Evidence for an existing relationship between Dpp signaling and proliferation rates comes from different studies. It was first shown that ectopic activation of Dpp signaling in the lateral regions of the wing disc, where endogenous levels are very low, causes an increase in proliferation rates

(Martín et al., 2004; Martín-Castellanos and Edgar, 2002; Rogulja and Irvine, 2005; Schwank et al., 2008).

dpp loss-of-function and *brk* gain-of-function clones are eliminated from the wing disc (Adachi-Yamada et al., 1999; Burke and Basler, 1996; Moreno et al., 2002) which supports the idea that Dpp has a role in cell survival. Moreover, *brk* gain-of-function clones are eliminated by apoptosis which is prevented by blocking apoptosis (Moreno et al., 2002). In this sense, Dpp acts as a survival factor.

Despite the above-mentioned evidences, the molecular components linking Dpp signaling activity to the cell cycle or to the apoptotic machinery are still unknown. What is demonstrated so far is that Dpp uses the transcriptional repressor Brk to regulate tissue growth (Jaźwińska et al., 1999; Martín et al., 2004; Schwank et al., 2008). Several observations coming from genetic interactions corroborate this conclusion. Mutants for *dpp* present rudimentary wings. However, *brk* mutant clones induced in this genetic background are able to induce outgrowths of wing material (Jaźwińska et al., 1999). As stated before, ubiquitous activation of Dpp signaling causes over-proliferation of the lateral region of the wing disc and a decrease in the proliferation rates in the most medial part of the primordium (Schwank et al., 2008). The same effect on proliferation rates along the AP axis of the wing in observed in wing discs that lack Brk (Schwank et al., 2008). Moreover, the dramatic reduction in size of wing imaginal discs observed in *dpp* mutants is completely rescued by the removal of *brk*. In fact, wing discs of double mutants (*dpp* and *brk*) present the same phenotype as the *brk* mutant alone, which indicates that Dpp induces growth via Brk repression. Moreover, this observation also supports the idea that the graded distribution of neither Dpp nor Brk is a prerequisite for proliferation (Schwank et al., 2008). However, it remains obscure the downstream machinery linking Brk to cell proliferation or/and survival. One known transcriptional target of Dpp is Vestigial (Vg). Cells in the wing disc lacking *vg* function undergo cell death, causing a loss of the corresponding structures in the adult (Agrawal et al., 1995). However, ubiquitous expression of *vg* does not lead to larger wing discs (Baena-Lopez and García-Bellido, 2006). Two different

studies suggest that the Hippo pathway might be important for the regulatory activity of Dpp. One of them shows that Brk has an effect on the expression levels of the microRNA *bantam* (Martín et al., 2004), a known Hippo target able to promote cell survival and proliferation (Nolo et al., 2006; Thompson and Cohen, 2006). The other study shows that the Dpp gradient controls the expression of the *four-jointed* (*fj*) and *dachsous* (*ds*) genes. Graded Fj and Ds levels lead to partial inactivation of Fat and hence decreased Hippo pathway activity (Rogulja et al., 2008). However, *fj* and *ds* expression is also influenced by Vg (Baena-Lopez and García-Bellido, 2006), and it is possible that Dpp affects its expression only indirectly via *vg*. dMyc, which drives cellular growth by promoting ribosome biogenesis, has also been shown to be a direct target of Brk (Doumpas et al., 2013).

Dpp gradient formation

The mechanism by which Dpp disperses in a long-range fashion has been a matter of debate since the first studies of Dpp gradient formation were published. A gradient is generated because the morphogen is not able to accumulate indefinitely but rather is cleared either by receptor-mediated uptake or by degradation (Müller et al., 2013). Several models have been proposed to explain how Dpp diffuses away from the source (Figure 10). The simplest explanation would be that morphogens diffuse through the extracellular matrix. However, the reliability of the capacity of morphogens to diffuse over long morphogenetic fields lead to the proposition of cell-based models of transport. In this way, the proposed models for explaining the Dpp gradient formation can be divided into two categories: one that comprises cell-based models of active morphogen transport (transcytosis and cytonemes) and the other one that is based on the diffusion through the extracellular space (free diffusion and hindered diffusion). Of course, the models described above are not exclusive; they may work together in order to fine tune the amplitude and range of morphogen gradient.

1. Transcytosis

Transcytosis is a mode of transport by which morphogens are shuttled across cells through repeated cycles of endocytosis and exocytosis (Figure 10A). Signaling molecules bind to the cell surface, resulting in their cellular uptake by endocytosis. Upon exocytosis, the signal is released again from the cell. By undergoing multiple rounds of cellular uptake and release, the molecules become dispersed in the target tissue. Some observations have linked receptor-mediated endocytosis to Dpp dispersal through transcytosis [for example, the restricted range of Dpp signaling when endocytosis is prevented (González-Gaitán and Jäckle, 1999)]. Also, in clones of cells in which Dpp uptake was prevented, Dpp accumulates in wild type cells on the edge of the clones, closer to its source, while cells situated behind the clone, that is farther away from the morphogen source, show reduced amounts of Dpp signaling (Entchev et al., 2000). However, another study has shown that transcytosis is not essential for Dpp transport (Belenkaya et al., 2004).

2. Cytonemes

This model proposes that long cytoplasmic processes called cytonemes extend from target cells towards the source of morphogens to shuttle the morphogen bound to its receptor back to target cell bodies (Figure 10B). Cytonemes are apical actin-based filopodia, and, by extending these structures ,cells can directly contact with the morphogen-producing cells regardless of their distance from the source. It has been reported that cytonemes contain punctae of the Dpp ligand and its receptor Tkv (Hsiung et al., 2005; Roy et al., 2011). However, due to lack of tools to abolish cytoneme function and to the difficulty to observe them, it is not clear yet if they play any role in generating the Dpp morphogen gradient.

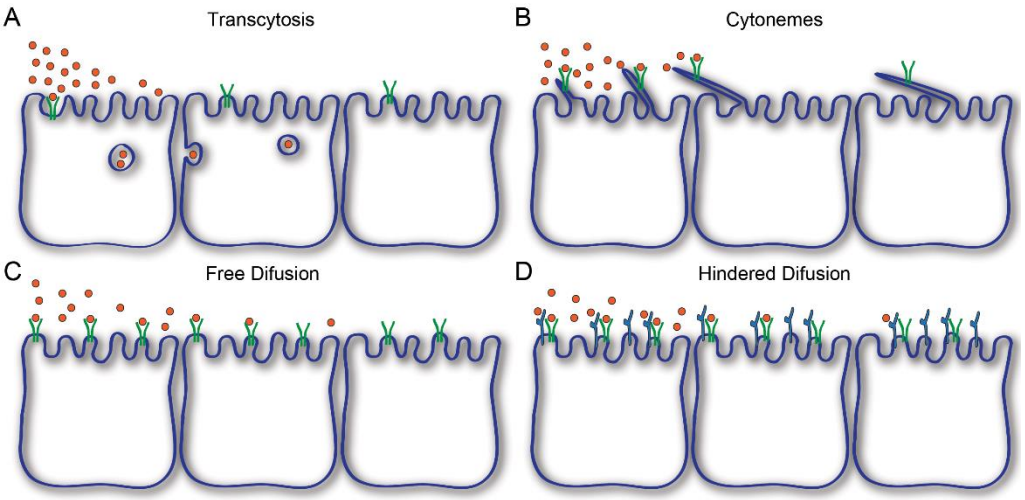

Figure 10. Models of Dpp gradient formation. (A) Transcytosis: following this hypothesis, Dpp is shuttled from cell to cell along the AP axis inside of endosomes. (B) Cytonemes: in this scenario, Dpp is transported on long cell extensions that contact the zone of Dpp production. (C) Free diffusion: in this model, the Dpp simply diffuses in the extracellular fluid. (D) Hindered diffusion: this model proposes that Dpp diffuses through the extracellular matrix and interacts with local proteins that help to its diffusion.

3. Free Diffusion

In the simplest case of morphogen dispersal, Dpp molecules move by free diffusion from the source to the target tissue (Figure 10C). This implies that morphogen molecules are not significantly affected either by the tortuosity of the extracellular space, or by transient binding interactions with other proteins, such as receptors or components of the extracellular matrix. Some FRAP (Fluorescence Recovery After Photobleaching) experiments, using a Dpp-GFP transgene, revealed a fraction of Dpp moving at speeds that would resemble those expected if Dpp was dispersing by free diffusion (Zhou et al., 2012). However, it was shown in wing imaginal discs that a secreted form of green fluorescence protein (GFP) fails to form a concentration gradient, indicating that simple diffusion alone cannot explain the graded distribution of the Dpp morphogen (Entchev et al., 2000).

4. Hindered diffusion

This model considers that both sinuosity and binding interactions slow down the dispersion speed of a morphogen across the field and that it might even be required for proper morphogen gradient formation (Figure 10D). Interactions of morphogens with their receptors and extracellular matrix (ECM) proteins can help to shape their gradients. Recent experimental data unraveled an important role of interactions between the morphogens and the heparan sulfate proteoglycans (HPSGs) in the regulation of morphogen gradients. Furthermore, since HPSGs can bind to many cell surface co-receptors and secreted proteins, they can offer a platform to morphogens to interact with other important components.

Given the fact that the largest fraction of the Dpp ligand is extracellular and that it seems to correspond to the signaling pool, nowadays the view that the Dpp gradient is established by a diffusion-based mechanism is gaining weight. In that sense, from now on we will assume that Dpp disperses by diffusion.

An important role of HSPGs in Dpp gradient formation

Heparan sulfate proteoglycans (HPSGs) have been shown to play an important role in the regulation of the Dpp gradient formation. HSPGs are cell-surface or extracellular matrix (ECM) macromolecules that comprise a protein core to which heparan sulfate (HS) glycosaminoglycan (GAG) chains are attached (Bernfield et al., 1999). They can be classified into three families based on their core protein structure: syndecans, glypicans and perlecans. Glypicans and syndecans are cell surface HSPGs and are linked to the plasma membrane by a glycosylphosphatidyl inositol (GPI) anchor or a transmembrane domain, respectively. Perlecans are secreted HSPGs that are mainly distributed in the ECM. All these three families are evolutionary conserved from vertebrates to *Drosophila* (Yan and Lin, 2009). The *Drosophila* genome encodes for two glypicans – Division abnormally delayed (Dally) and Dally-like (Dlp)-, a single syndecan (sdc), and a single perlecan -

terrible reduced optic lobes (trol). Considerable evidence suggests that the glypicans Dally and Dally-like play major roles in regulating the Dpp gradient formation. Biochemical studies have shown that Dpp is an heparin-binding protein (Groppe et al., 1998). In fact, both Dpp activity and extracellular levels of Dpp-GFP have been reported to be reduced in clones of cells that lack one of the enzymes required for the biosynthesis of proteoglycans, Sulfateless (sfl) (Belenkaya et al., 2004). In addition, in these *sfl* mutant clones Dpp-GFP movement is blocked, which favors that Dpp moves from cell to cell by a hindered diffusion mechanism (Belenkaya et al., 2004). Animals mutant for *Dally* show Dpp-like patterning defects in the wing and genetically interact with the Dpp signaling pathway (Jackson et al., 1997). In addition, ectopic expression of Dally results in enhanced Dpp signaling in the wing disc (Fujise et al., 2003). Altogether, these results strongly suggest that Dally has a positive impact in Dpp signaling. *In vivo* experiments using a Dpp-GFP fusion protein that lacks a domain essential for its interaction with Dally showed a shorter half-life when compared to a wild type Dpp-GFP, suggesting that Dally stabilizes Dpp in the ECM (Akiyama et al., 2008). Genetic interaction experiments revealed that *dally* suppresses the effect of *tkv* on the Dpp gradient formation. The receptor Tkv can downregulate Dpp signaling by receptor-mediated endocytosis of Dpp. Since Dally is able to antagonize Tkv, probably by inhibiting this process, it regulates Dpp distribution and signaling by interfering with receptor-mediated internalization and degradation of the Dpp–receptor complex (Akiyama et al., 2008). Both in haltere and wing imaginal discs, Dpp mobility is biased towards cells with higher levels of Dally (Akiyama et al., 2008; Crickmore and Mann, 2007). Removal of Dally and Dlp show stronger defects in both Dpp signaling and extracellular levels of Dpp when compared to single depletion of these proteins, suggesting that Dally and Dlp are partially redundant in Dpp gradient formation (Belenkaya et al., 2004).

Despite the above implications of the glypicans Dally and Dlp in Dpp gradient formation, they have also been associated with other morphogens. They were shown to be essential for Wg gradient formation (Han et al., 2005; Lin and

Perrimon, 1999; Tsuda et al., 1999). Both Dally and Dally-like are involved and are functionally redundant in Hh movement during wing development (Han et al., 2004). Similarly, the distribution of the Unpaired morphogen in the ovary as well as in the eye imaginal disc also depends on Dally and Dlp (Hayashi et al., 2012; Zhang et al., 2013).

Since HSPGs are major regulators of morphogen gradient formation, their expression has to be tightly controlled during development. The expression of both *dally* and *dlp* is regulated by Wg and Hh signaling, forming a feedback loop to fine tune their morphogen gradients (Fujise et al., 2001). Recent studies also showed that the Hox selector gene, Ultrabithorax (Ubx), can modulate Dpp signaling and tissue growth through transcriptional regulation of *dally* (Crickmore and Mann, 2007). In the haltere disc, Ubx represses *dally* expression and this is one of the reasons for the low Dpp activity in the posterior compartment of the haltere and its reduced size (Crickmore and Mann, 2007). Interestingly, the Hippo signaling pathway also modulates different morphogen signaling through transcriptional control of *dally* and *dlp* (Baena-Lopez et al., 2008).

Scaling of the Dpp gradient during growth

A universal property of animal development is the capacity to scale body size and pattern in response to environmental conditions as well as during evolution. For instance, nutrient deprivation leads to formation of smaller adults with proportionally smaller parts. This invariance in proportions, despite the change in absolute organ and body size, is called scaling. The relative position of the wing veins of the adult wing is a natural benchmark to measure the degree of anatomical scaling. Remarkably, starved larvae result in diminutive adults with wings perfectly patterned and proportional to the body size (reviewed in Parker 2011). Therefore, we can conclude that pattern scales with tissue size. The specific position of the different veins of the adult wing along the AP axis depends on the

activity of Dpp. Thus, it is legitimate to say that in starved animals the Dpp activity gradient scales down with tissue size in order to maintain correctly proportioned and fully functional wings (Figure 11).

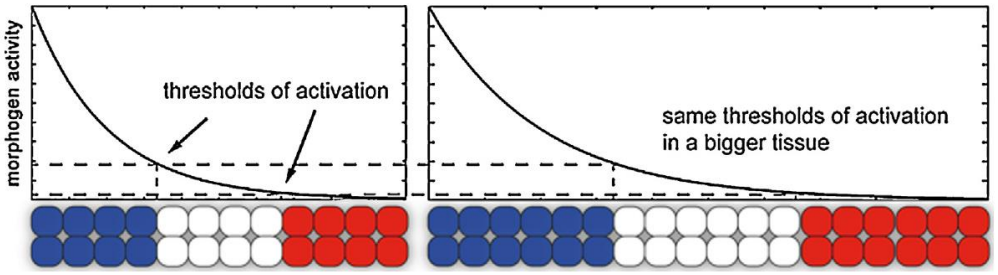

Figure 11. Scaling of Dpp activity gradient. A morphogen or activity gradient is read out in the target field, establishing a pattern. In a bigger tissue where Dpp expands and the gradient scales, the resulting pattern keeps the same proportions (1/3 of blue, red and white) and thus scales perfectly, provided that the boundaries are defined at the same threshold concentrations.

The first evidence for the scaling ability of Dpp comes from the observation that the *spalt* expression domain scaled when the size of the posterior compartment was experimentally altered (Teleman and Cohen, 2000). Three different studies showed that both the Dpp morphogen (visualized by a Dpp-GFP fusion protein expressed in the Dpp stripe) as well as the cellular response to the Dpp gradient (visualized by P-Mad antibody and a GFP driven by a Dpp responsive *dad* enhancer) expand and adjust to the growing tissue size throughout development (Ben-Zvi et al., 2011; Hamaratoglu et al., 2011; Wartlick et al., 2011b). In this sense, the Dpp gradient scales with tissue size as the wing imaginal disc grows. It is interesting to note that it is not so clear whether this hypothesis is correct for later stages of development, since late third instar wing discs showed less robust scaling (Wartlick et al., 2011a). Moreover, scaling of the downstream targets of Dpp, such as the genes *sal* and *omb*, is not equally good at all positions of the field. While the Sal domain scaled extremely well in the anterior compartment, it does not in the posterior compartment. On the contrary, the Omb domain scaled very well in the posterior compartment but not in the anterior compartment

(Hamaratoglu et al., 2011). Remarkably, this is consistent with the fact that Sal is required for the positioning of the vein 2 in the anterior compartment, while Omb is responsible for the positioning of the vein 5 in the posterior compartment (De Celis, 2003).

Two models have been proposed to explain how scaling of the Dpp gradient is obtained, one based on the decrease of Dpp degradation and the other on the increase of Dpp diffusion.

1. Expansion by dilution mechanism

In this model, a long-lived secreted expander molecule promotes Dpp degradation. In the other hand, tissue growth stabilizes Dpp by diluting this antagonist. The reduction in the Dpp degradation rate occurs in response to cell division events, so that the degradation rate is inversely proportional to the number of cells (Wartlick et al., 2011a). Analysis of Dpp gradient scaling in anisotropic (directional) growth conditions showed that the gradient scales better with area than with length which suggests that Dpp scales due to a dilution-type mechanism (Wartlick et al., 2011a).

2. Expansion-repression mechanism

This model suggests that scaling arises because of a feedback loop comprised by the morphogen itself and a hypothetical expander molecule (Ben-Zvi and Barkai, 2010; Ben-Zvi et al., 2011; Hamaratoglu et al., 2011). The expander molecule diffuses from the lateral part of the wing disc and helps the morphogen to spread. Its expression is repressed in the medial region by Dpp itself (Ben-Zvi and Barkai, 2010). One prediction of this model is that the expander is a stable molecule and consequently it accumulates in the tissue, keeping the gradient extended. Eventually, the morphogen reaches the most lateral region of the disc and the expander production is shut off. As the disc grows, the lateral areas can again transcribe the expander and as such, the morphogen gradient spreads.

Consistent with this model, the secreted molecule Pentagone (Pent) has been identified as an expander of the Dpp morphogen in the wing disc. Absence of *pent* in the wing imaginal disc causes a severe contraction of the Dpp activity gradient resulting in patterning and growth defects (Vuilleumier et al., 2010). In these mutant wing discs, the P-Mad gradient does not scale with tissue size throughout development (Ben-Zvi et al., 2011; Hamaratoglu et al., 2011) and neither the expression domains of most of Dpp target genes (Hamaratoglu et al., 2011). In an inverse way, when *pent* is ubiquitously expressed in the posterior compartment causes an overexpansion of the P-Mad gradient (Ben-Zvi et al., 2011). Overall, these results demonstrate that Pent is required for the adjustment of the Dpp activity gradient to tissue size. Secreted Pent molecules move towards the center of the disc and help Dpp to reach further away. This expansion of Dpp gradient narrows the lateral domain of Pent-producing cells. However, high enough concentrations of Dpp never reach the most lateral regions of the disc and therefore Pent expression is never completely shut off (Hamaratoglu et al., 2011). Since Pentagone does not seem to directly interact with Dpp, it has been proposed that it may do so indirectly via binding the glypican Dally (Vuilleumier et al., 2010). Dally binds and enriches extracellular Dpp at the cell surface of wing imaginal cells. Glypican-bound ligand is then passed either to receptors for endocytosis and signaling (co-receptor activity of glypicans) or to glypicans of neighboring cells for further lateral movement (facilitated transport activity – see Hindered Diffusion Model) (Belenkaya et al., 2004; Fujise et al., 2003). Somehow, Pent is involved in keeping the balance between these two activities maybe by distracting a fraction of the ligand from local signaling to lateral movement through its interaction with Dally. This could be achieved by having an active role, acting on glypicans to promote the lateral movement of the ligand, or a more indirect role, antagonizing the co-receptor function of glypicans. In an alternative view, instead of interacting with Dally, Pent might regulate the interaction of glypicans with Dpp. A similar activity has been assigned to Shifted, who has been proposed to mediate the interaction of Dally with Hedgehog and is required for its

proper activity and movement in the wing imaginal disc (Glise et al., 2005; Gorfinkiel et al., 2005).

In agreement with the fact that *pent* mutants have their name due to the lack of the longitudinal vein 5 in the adult wing, the scaling of the posterior Omb domain is diminished in these mutants. However, the anterior Sal domain still exhibits good scaling and as such the specification of vein 2 is not affected (Hamaratoglu et al., 2011). This suggests that, although Pent is clearly required for expansion of the Dpp gradient, it may not be the only expander at work to ensure proper scaling of some downstream targets of Dpp.

Cell Interactions and Tissue Homeostasis

Maintenance of tissue homeostasis is vital for the survival of multicellular organisms. Interestingly, even unicellular organisms, like the social amoebae *Dictyostelium discoideum,* take advantage of cell-cell interactions to cooperate and build multicellular structures such as the stalk for sporulation. Cell-cell interactions within a tissue allow cells to communicate with each other in response to changes in their microenvironment. As such, the ability of cells to send and receive signals plays a crucial role in the development and function of multicellular organisms, as it is essential for the survival of the cell.

Cell Competition

Cell competition is a homeostatic mechanism evolved to identify and subsequently eliminate cells that are poorly adapted to their developmental environment and may compromise the overall fitness of animal tissues. The concept of competition for survival has been intensively studied by microbiologists [the microbial antagonism induced by bacteriocin of *Escherichia coli* is a representative example (reviewed by Riley and Wertz, 2002)]. By contrast, biologists studying multicellular systems had barely considered the concept of competition between cells of the same species in a tissue until 1975 when Morata and Ripoll discovered the phenomenon of cell competition in *Drosophila* (Morata and Ripoll, 1975). They used the wing imaginal disc to study the behavior of a class of dominant mutations called *Minutes* that encode for ribosomal proteins and that reduce the rate of cell division in a cell-autonomous manner. *Minute* heterozygous (*Minute*$^{+/-}$) flies develop more slowly than wild type flies but are viable and show normal body size (Morata and Ripoll, 1975). However, when mitotic wild type clones were generated in a slower-growing *Minute*$^{+/-}$ field, they found that the wild type clones occupied most areas of the

adult wing, and at the same time, *Minute*$^{+/-}$ cells were eliminated from the tissue. Later on, it was shown that wild type cells adjacent to *Minute*$^{+/-}$ cells tended to divide more often than those positioned in the center of the clone and that *Minute*$^{+/-}$ cells not in contact with wild type cells were not eliminated (Simpson and Morata, 1981). Therefore, the phenomenon of cell competition, defined by the elimination of slow-dividing cells (losers) when confronted with a faster growing population (winners), depends on short-range cell-cell interactions (Figure 12). The recovery of *Minute*$^{+/-}$ tissue increased when induced late or upon larvae starvation, which suggested that elimination required a differential growth rate (Simpson, 1979). Interestingly, the final size of the wings was unaffected by competition, which suggests that wild type cells grow at the expense of *Minute*$^{+/-}$ cells, and this phenomenon is ineffective across compartments (Simpson and Morata, 1981). Elimination of loser cells was shown to require an active induction of apoptosis in *Minute*$^{+/-}$ cells by the surrounding wild type (*Minute*$^{+}$) cells (Abrams, 2002; Milán, 2002; Moreno et al., 2002). Thus, cell competition could work as a quality control mechanism that maximizes tissue fitness by eliminating suboptimal cells. Several reports have shown that cell competition also occurs in the mammalian system. Interestingly, a mutation in a ribosomal protein led to competitive interactions in mouse blastocysts (Oliver et al., 2004). Furthermore, cell competition was shown to occur in mammalian culture cells (Norman et al., 2012).

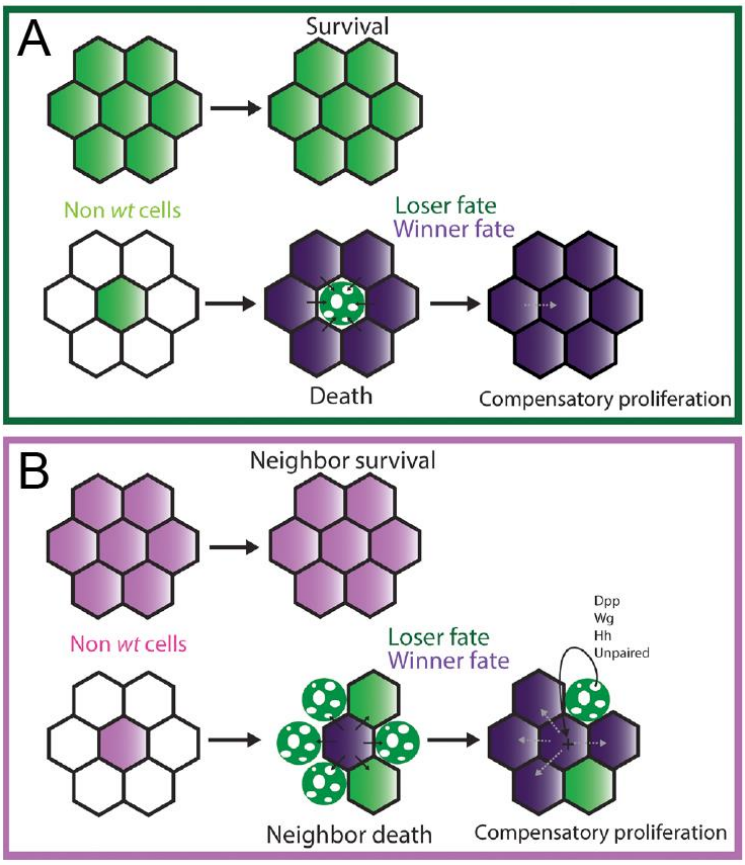

Figure 12. The phenomenon of cell competition. (A) In "classical" cell competition, mutant cells (green) surrounded by cells of the same genotype do survive (top). However, when surrounded by wild type cells (white cells) they are eliminated from the epithelia (bottom). Due to a growth advantage over the mutant cells, the wild type cells become winners (dark purple) and replenish the tissue by compensatory proliferation. (B) Supercompetitors cells (light purple) do not induce apoptosis when surrounded by cells with the same genotype (top). Nevertheless, they can grow at the expense of the surrounding wild type cells (white) by inducing their death (bottom). The compensatory proliferation of the winner cells is due to the secretion of mitogens, such as Dpp, Wg, Hh and Upd by the dying cells (black arrow). The loser fate and the winner fate are depicted in green and dark purple respectively. Adapted from (Levayer and Moreno, 2013).

Relevant to the cancer field was the discovery of super-competitors. In a similar fashion as the first steps of cancer progression, mutations that lead to increased cell fitness lead to clonal invasion of the tissue at expense of wild type surrounding cells (Figure 12). The first candidate to fit in this super-competitor definition was the proto-oncogene dMyc, since clones expressing high levels of dMyc overgrew

at the expense of the surrounding tissue until they filled the compartment (De La Cova et al., 2004; Moreno and Basler, 2004). Clone expansion required the elimination of the surrounding cells by apoptosis, which was induced through JNK activation (Moreno and Basler, 2004), and induction of the apoptotic gene Hid in the loser cells (De La Cova et al., 2004). In an opposite manner, downregulation of *dmyc* in clones led to their elimination (Johnston et al., 1999). Remarkably, cells with two additional copies of *dmyc* behaved as super-competitors or losers when confronted with wild type cells or cells with four copies of *dmyc*, respectively (Moreno and Basler, 2004), which demonstrates that competition is based on relative and not absolute levels of *dmyc*. The *Minute* mutation suppressed the super-competitor phenotype of *dmyc* overexpression (Moreno and Basler, 2004), which suggests that *dmyc* competition could be genetically related to *Minute*. Interestingly, in the mouse embryo, cells with lower levels of Myc are eliminated (Clavería et al., 2013; Sancho et al., 2013).

The Hippo pathway was also demonstrated to be involved in cell competition. Resembling *dmyc* overexpression, mutations in components of the Hippo pathway produced super-competitive clones of cells, which invade the whole compartment (Tyler et al., 2007). This is probably driven by the upregulation of *dmyc* by Yki, as dMyc downregulation was enough to abolish the super-competitive status of activated Yki clones (Ziosi et al., 2010).

Defects in polarity genes also induce cell competition. It was extensively shown that clones of cells mutant for *lgl/dlg/scrib*, when surrounded by wild type cells, are eliminated by a JNK-dependent apoptosis due to loss of apico-basal polarity (Froldi et al., 2010; Grzeschik et al., 2010b; Menéndez et al., 2010; Tamori et al., 2010). The close relationship between the Hippo pathway and apico-basal polarity cues (described earlier in the introduction), in addition to several epistatic experiments suggest that the Hippo pathway is the major inducer of cell competition downstream of polarity defects.

Since the discovery of the *Minute*- and dMyc-driven cell competition, the collection of pathways that induce competitive interactions has been continuously growing

and many of them depend, at the end, on *Minute* or dMyc. However, this is not true for all the cases. Some of the exceptions include modulations of Wg and JAK-STAT signaling pathways. Local downregulation of Wg signaling lead to clone elimination, while its hyper-activation generated super-competitive interactions (Giraldez and Cohen, 2003; Johnston and Sanders, 2003). Similarly, downregulation of JAK-STAT signaling in a group of cells lead to their elimination by apoptosis, whereas STAT hyper-activation produced super-competitors that grow at the expense of the surrounding wild type cells (Rodrigues et al., 2012). Cell competition induced by both Wg and JAK-STAT signaling has been shown to be independent of dMyc (Amoyel and Bach, 2014; Giraldez and Cohen, 2003; Johnston and Sanders, 2003; Rodrigues et al., 2012). Yet, super-competition is not a general feature induced by any hyper-proliferative clone, as overexpression of the PI3K/Dp110 or the cell cycle regulators Cyclin D and Cdk4 both generated large clones, but no elimination of the surrounding cells was observed (De La Cova et al., 2004; Moreno and Basler, 2004). These observations suggest that a difference in growth rates alone does not always trigger cell competition.

Hallmarks of cell competition

The first trademark is the survival defect of loser cells. Outcompeted cells undergo apoptosis and are eventually eliminated from the tissue. Most of this apoptosis is observed at the boundary between the two confronting cell populations, the winners and the losers, since cell competition is based on direct cell-cell interactions between two different types of clones.

The second hallmark is that loser cells remain viable in a homotypic environment, when surrounded by cells with the same genetic background. In fact, in a group of loser cells, the cells in the center of the clone do not undergo apoptosis since they are surrounded by cells with the same fitness.

When a *Minute* background is able to both rescue the elimination of mutant cells and the competition-dependent cell death observed at a boundary with wild type cells, one can say that the mutant cells fulfill the third hallmark of cell competition.

What are the cells competing for?

One intriguing question in the field is what could be the limiting factors for which cells are competing. The ligand capture hypothesis proposes that cells compete for extracellular survival and growth factors (Moreno, 2008). This was suggested based on the observation that the elimination of *Minute* clones was driven by a relative deficit of Dpp activation, leading to ectopic upregulation of its negative downstream target Brinker (Moreno et al., 2002). Therefore, cells compete for the uptake of limiting growth and survival factors, such as Dpp, so that any cell showing a relative fitness disadvantage might result in reduction of Dpp uptake, which is translated into a low survival signaling and their consequent elimination (Figure 13). It remains to be understood how less fits cells end up with a lower Dpp uptake.

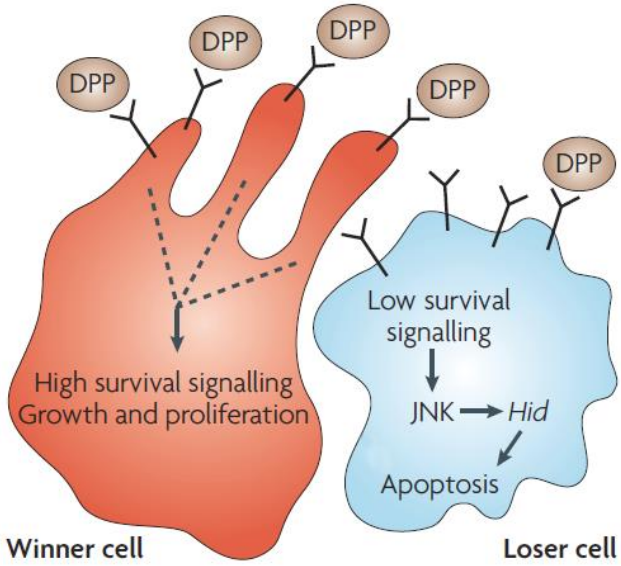

Figure 13. The ligand-capture hypothesis. Cells compete for extracellular survival and growth factors such as Dpp. Somehow, winner cells (in red) are able to obtain more Dpp growth and survival factor. Consequently, the nearby loser cells (in blue) have a lower survival signaling, activate the JNK signaling and/or Hid transcription, which leads to apoptosis. Cells compare Dpp signaling levels between them, which leads to the definition of which become the losers. Adapted from (Moreno, 2008).

Another possibility could be that cell competition occurs because of limited space and mechanical constraints. Despite of events of cell competition, the final wing and compartment size is largely unaffected compared to wild type wings. Growth in a limited space could be a key factor to drive cell competition. Differential growth rates between neighboring cells could induce mechanical stress and feedback on the rate of cell division and apoptosis (Shraiman, 2005). In this sense, elimination of the loser cells could be due to mechanical constraints induced by fast-growing cells.

The function of cell competition

The conservation of cell competition from invertebrates to mammals suggests that this phenomenon has important evolutionary purposes. The elimination of less fit cells suggests that cell competition is a mechanism by which tissues maximize their fitness and buffer potential genetic fluctuations at the cellular level.

Since elimination of suboptimal loser cells is accompanied by compensatory proliferation of optimal winner cells, resulting in organs with the normal final size and shape, cell competition has been proposed to be a size-control mechanism. Moreover, adult organ size becomes more variable when cell competition is blocked in developing tissues, suggesting that it is also important to reduce size variability (De La Cova et al., 2004).

In addition, the observation that discontinuities in the Dpp gradient in imaginal discs generate local apoptosis mediated by the activation of the JNK pathway suggested that there is a mechanism by which incorrectly specified cells are identified and removed (Adachi-Yamada and O'Connor, 2002). This process was called morphogenetic apoptosis and is likely related to cell competition since apoptosis is triggered in the loser cells between 24-48 hours after the onset of the cell interactions (Adachi-Yamada and O'Connor, 2002). It has also been shown that clones of cells overexpressing *spalt*, which is normally expressed in the medial part of the wing disc, are eliminated in the lateral regions where *spalt* is

not normally expressed but they do survive in medial region (Milan et al., 2002). Ectopic Spalt activity in the lateral region leads cells to acquire an incorrect medial identity that is recognized as aberrant by the neighboring cells thus triggering cell competition.

The universal proposition is that cell competition fulfills a general surveillance role to recognize and eliminate cells with developmental/metabolic features different from those of normal cells of the same population. Interestingly, the elimination of less fit cells has been shown to delay aging and prolong lifespan in *Drosophila* (Merino et al., 2015).

Tumor suppressor or pro-tumoral role

Tumors are caused by uncontrolled proliferation of transformed mutant cells with either activated oncogenes or inactivated tumor suppressors, and malignant neoplasias arise from tumor cells that have lost the ability to assemble and create tissues of normal form and function. In other words, cancer can be seen as a disease that arises when mutant cells fail to obey the intrinsic tissue-integrity and organ-size control systems. Since the process of cell competition is deeply involved in the maintenance of tissue integrity and regulation of organ size, the relationship between cell competition and cancer progression is currently an issue of interest. Actually, there is now evidence that cell competition can function as both a tumor promoter as well as a tumor suppressor. Deriving from the general surveillance function described above it comes the idea of cell competition as a tumor suppressor mechanism. It assures elimination of potentially deleterious (precancerous) cells and promotes epithelial integration. This idea comes from the studies revealing that epithelial cells mutant for tumor suppressor genes, such as *lgl*, *dlg* and *scrib*, which show overgrowth and tumorigenesis in a homotypic situation, are frequently eliminated through cell competition when surrounded by wild type cells (Froldi et al., 2010; Grzeschik et al., 2010b; Menéndez et al., 2010; Tamori et al., 2010). Elimination of abnormal cells that

would otherwise over-proliferate could mitigate the appearance of the fast-growing clonal population and the expansion of a precancerous field.

However, it was demonstrated that the surveillance role of cell competition can sometimes be evaded since induction of *lgl* and *scrib* mutant clones can eventually generate tumors. Clones of cells mutant for *lgl* or *scrib* in which either the Ras signaling pathway is constitutively active or Yki is overexpressed are frequently not eliminated and can develop overgrowing tumors colonizing the entire disc (Menéndez et al., 2010). By acquiring a higher proliferation rate, *lgl* or *scrib* mutant cells become super-competitors and eliminate the surrounding non-tumor cells. This would be a reversion of the normal process and now cell competition behaves as a tumor promoting mechanism. So, tumor cells by creating a protective microenvironment, evade cell competition and become tumorigenic. Another example is the observation that, while individual endocytosis defective *Rab5* mutant cells are eliminated by cell competition, if a group of about 400-500 cells, also surrounded by normal cells, are simultaneously made defective for *Rab5* activity they do survive and form an invasive tumor (Ballesteros-Arias et al., 2013). It is worth to note that these *Rab5* defective cells do not have a proliferative advantage. They continue proliferating while the rest of the disc grows at a lower rate.

Super-competitive interactions could be exploited by the early tumor in order to kill neighboring normal cells and accelerate its expansion. The observation that cells with high dMyc levels, and as such higher proliferation rates, are able to eliminate the wild type cells that surround them, indicates that cell competition favors cells with high dMyc activity. In fact, higher Myc activity is a characteristic feature of many tumor cells (Gabay et al., 2014).

Another possibility is that the tumorigenic potential of cell competition is a side effect of the mechanism of cell removal by apoptosis. This is because it is well known that cells that enter the apoptotic program not only activate the caspases for self-destruction but they also secrete mitogenic signals that induce proliferation of neighboring cells (Pérez-Garijo et al., 2004; Ryoo et al., 2004). In

cases of large-scale cell competition, the amount of proliferative signaling emanating from the dying cells may be sufficient to stimulate growth of the tissue close by and outside the range of cell competition, becoming tumorigenic.

In the example above mentioned concerning simultaneous generation of cells defective for *Rab5*, the interface between normal and *Rab5* mutant cells has been shown to be highly proliferative and the dividing cells are often very close to those dying by apoptosis (Ballesteros-Arias et al., 2013). This suggests that the proliferative signaling from apoptotic cells may contribute to the growth of the tumor. In fact, suppression of apoptosis in the *Rab5* mutant domain strongly inhibits the overgrowth of the tumor (Ballesteros-Arias et al., 2013). Thus, under these circumstances cell competition reverses its normal anti-tumoral role and stimulates growth through proliferative signals from apoptotic cells.

Genetic mosaic analysis also revealed an unusual tumor-promoting cell population called "oncogenic niche cells" (ONCs). Oncogenic niche cells drive non-autonomous tumor progression through cellular competition and cooperation with surrounding cells (reviewed in Enomoto et al., 2015). Clones of cells that overexpress *Src* in the *Drosophila* wing imaginal disc are eliminated by cell competition (Vidal et al., 2006). However, these clones also function as ONCs causing non-autonomous overgrowth of surrounding tissue (Enomoto and Igaki, 2012). Similarly, cell mutants for *Rab5* are able to form ONCs that, through the secretion of the growth factor Unpaired, causes overgrowth of the nearby cells (Takino et al., 2014). In a similar phenomenon, when cell death is induced but not executed, typically through expression of the caspase inhibitor *p35*, persistent "undead" cells become ONCs and trigger non-autonomous overgrowth through the secretion of the growth factors Dpp and Wg (Huh et al., 2004; Pérez-Garijo et al., 2004; Ryoo et al., 2004). Aneuploid cells when maintained in the tissue also trigger non-autonomous hyperplasia by secreting Wg (Dekanty et al., 2012). Intriguingly, undead cells can also cause non-autonomous apoptosis (Pérez-Garijo et al., 2013). Overall, dying ONCs may unleash an autocatalytic wave of death, growth factor secretion and proliferation.

In vertebrates, it has been shown that cell competition has an important anti-tumoral role in the mouse thymus (Martins et al., 2014). Finally, cell competition may also have a tumor-stimulating role in mammalian tissues. It was shown that apoptotic cells release a growth factor and in this way stimulate the growth of surrounding cells (Huang et al., 2011).

Metabolic Competition

Nutrient competition between cells can influence cell growth, survival, and function. Tumor cells are metabolically more active than normal cells and one can expect higher demand of glucose, sugars and nutrients by these cells. Thus, a fierce competition likely exists between cells in the tumor microenvironment.

Studies in *Drosophila* imaginal primordia has shown that competition for nutrients contributes to the growth of *PTEN* mutant cells and the out-competition of wild type surrounding cells (Nowak et al., 2013). *PTEN* mutant clones do normally overgrow in well fed larvae (Goberdhan et al., 1999). Upon nutrient restriction, clones of cells lacking *PTEN* are further increased in size due to hyper-proliferation (Nowak et al., 2013) so switching from hypertrophic growth to hyperplastic growth (Figure 14). Interestingly, this occurs at the expense of neighboring wild type cells. Arguing against a major role of "classical" cell competition described above in the overgrowth phenotype is the fact that apoptosis was only observed in the mutant tissue and not in the surrounding wild type cells. Moreover, blocking apoptosis was not able to rescue the loss of the surrounding tissue (Nowak et al., 2013). It was also observed that reduction in amino acid uptake by reducing the levels of the amino acid transporter Slimfast caused clones of *PTEN* mutant cells to collapse (Nowak et al., 2013). Overall, *PTEN* mutant clones are proposed to eliminate the neighboring tissue by competition for local and systemic pools of nutrients and other growth-promoting factors. Interestingly, this non-autonomous phenomenon not only affects closely neighboring tissues but also acts at a longer range since the size of other

structures of the fly was also reduced (Nowak et al., 2013). This suggests that the *PTEN* mutant tissue efficiently competes with other larval tissues for common resources to support their massive growth, thereby launching a vicious cycle in the neighboring tissue that is further starved and reduced. Remarkably, it was demonstrated that human cancer cell lines lacking *PTEN* or with increased *PI3K* activity are more resistant to dietary restriction (Kalaany and Sabatini, 2009).

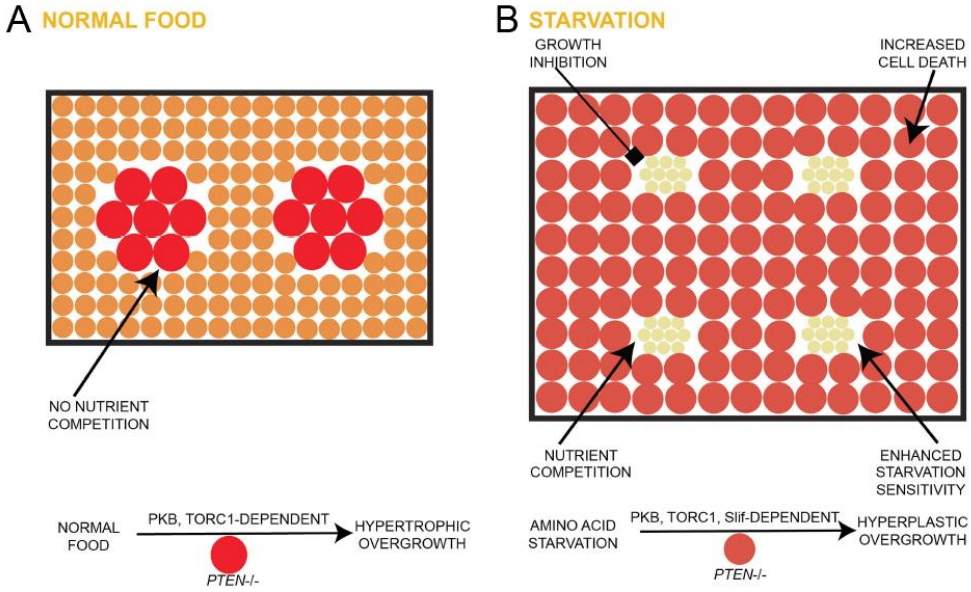

Figure 14. Metabolic competition upon nutrient challenge. (A) Under standard food conditions, *PTEN* mutant tissue overgrows in a hypertrophic manner, giving rise to bigger structures. (B) Upon nutrient restriction, the *PTEN* mutant tissue is metabolically more active and outcompetes the surrounding wild type tissue, resulting in a hyperplastic overgrowth. The size of the tissue is further increased because of more *PTEN* mutant cells. The *PTEN* mutant tissue is susceptible to apoptosis, and it depends on the function of the amino acid transporter Slimfast. Under both conditions, the *PTEN* mutant tissue exhibits high insulin signaling activity and is dependent on the functions of PKB and TORC1. Adapted from (Nowak et al., 2013).

Glucose competition in the tumor microenvironment was also demonstrated to influence cancer progression. In a mouse model it was shown that tumor cells can metabolically restrict immune cells and, and as such, affect their functionality which can thus influence cancer progression (Chang et al., 2015).

Coordination of growth

In order to give rise to a fully functional organism, growth has to be coordinated between and within the different structures of an animal. Therefore, organ-autonomous signals must assure that growth is coordinated within the organs, namely between its different cell populations such as the compartments of the wing imaginal disc. The observation that cell competition does not cross the boundaries between adjacent compartments led to the hypothesis that compartments might be independent units of growth, providing evolution with building blocks that could be changed while insulating the rest of the animal (Crick and Lawrence, 1975). Consistent with this view is the observation that compartments with different growth rates behave as independent developmental units. The generation of fast-growing (M+) compartments in slow developing larvae (M/+) showed that each compartment grows at its own rate and manifests autonomous regulation in the expression of the developmental genes *wingless* and *vestigial* (Martín and Morata, 2006). In spite of these differences, they differentiate into adult wings of the correct size and shape.

However, there are also evidences that support the idea that adjacent compartments can adjust their growth rates in a coordinated manner. In *Contrabithorax* mutant wings, in which one compartment is reduced in size due to the transformation to haltere by the ectopic expression of Ubx, the adjacent compartment adjust its final size resulting in smaller but proportional adult wings (Gonzalez-Gaitan et al., 1990). Similarly, when the number of cells in one compartment is reduced, cells in the adjacent compartment reduce proliferation and enter apoptosis (Milán et al., 1997). Moreover, when growth rates are reduced in one defined territory within the developing wing primordia, adjacent cell populations respond as a whole by decreasing their growth and proliferation rates (Mesquita et al., 2010). In the latter case, the non-autonomous response depends on the activation of *dp53* in the affected territory, which mediates the regulation of growth and proliferation rates in the neighboring domain. Downstream of *dp53*,

the effector caspases have an important role in reducing the proliferation rates of the adjacent territories (Mesquita et al., 2010).

Although stated that compartments are independent developmental units, it is clear that upon insults affecting growth/proliferation rates of a specific territory, the adjacent cell population is able to respond in a coordinated manner in order to maintain tissue homeostasis and achieve a fully functional adult structure.

Project and Objectives

The nutrient sensing pathways, such as the PI3K/PTEN and TSC/TOR pathways, play a fundamental role in modulating the final size of an organ according to the nutritional state of the animal. Growth of a particular organ is independently controlled in an autonomous fashion by the activity of patterning signals. How cells integrate distinct inputs (extrinsic and intrinsic signals) to generate organs of appropriate size and shape remains unknown.
On the other hand, mutations that cause activation of either the PI3K/PTEN or TSC/TOR signaling pathways are causative of tumorigenesis and often found in human tumors. How cells depleted of tumor suppressor genes outcompete neighboring wild type cells, especially during the early stages of tumorigenesis after initial mutagenesis and transformation, remain largely unknown.

In order to tackle these two distinct issues, we have used the *Drosophila* wing primordium as a model system and addressed the following main objectives:

- Characterization of the autonomous and non-autonomous effects on tissue growth caused by restricted activation of the PI3K/PTEN and TSC/TOR signaling pathways in defined cell populations of the developing wing.

- Identification of the molecular mechanisms mediating the autonomous and non-autonomous effects on tissue growth caused by restricted activation of the PI3K/PTEN and TSC/TOR signaling pathways.

- Identification of the molecular mechanisms underlying the integration of nutrient sensing pathways and organ-intrinsic mechanisms in order to give rise to well-proportioned organs.

Results

Results

Effects of Targeted Activation of Growth in Epithelial Cells

In order to address whether activation of growth promoting pathways in specific cell populations has any effect on the surrounding cell populations, we made use of the Gal4/UAS system (Brand and Perrimon, 1993) to drive expression of different transgenes in specific territories of the wing imaginal disc. To promote growth, we activated the PI3K/PTEN and TSC/TOR pathways, which are known to induce tissue growth in the developing imaginal primordia and to give rise to overgrown adult structures (Gao and Pan, 2001; Goberdhan et al., 1999; Huang et al., 1999; Ito and Rubin, 1999; Tapon et al., 2001). To activate the PI3K/PTEN pathway, we made use of two different transgenes: UAS-PI3K-92E (also termed *Drosophila* p110 or Dp110); and a double stranded RNA (dsRNA) form of PTEN (a negative regulator of PI3K/Dp110), a tumor suppressor gene that acts negatively on the insulin pathway in invertebrate and mammalian systems (Goberdhan et al., 1999). To activate the TSC/TOR pathway we used a UAS-Rheb transgene, to express the guanosine-5'-triphosphate (GTP)-binding protein Rheb, which binds and activates TOR (Stocker et al., 2003; Zhang et al., 2003). Larvae containing the *Gal4* driver and the *UAS* transgene were grown at 25°C until eclosion of the adult flies in order to analyse the resulting adult wings in what concerns size. Larvae expressing an *UAS-GFP* transgene and the corresponding *Gal4* driver were subjected to the same temperature schemes and used as controls.

Activation of PI3K/PTEN and TSC/TOR signaling pathways cause tissue overgrowth in the wing primordia

The activation of the PI3K/PTEN pathway in the whole wing blade (with the *nubbin-gal4* driver, Figure 15), either by expression of Dp110/PI3K or a double

stranded RNA (dsRNA) form of PTEN, gave rise to larger wings than those of control flies expressing green fluorescent protein (GFP) (Figure 15A and 15B). The increase in tissue size was a consequence of both an increase in cell size (reflected by a reduction in cell densities in the adult wing, Figure 15D) and in cell number, as the increase in tissue size (Figures 15B and 15C) was much larger than the reduction in cell densities (Figure 15D). Cell density was measured as the number of hairs (each wing cell differentiates a hair) per defined area.

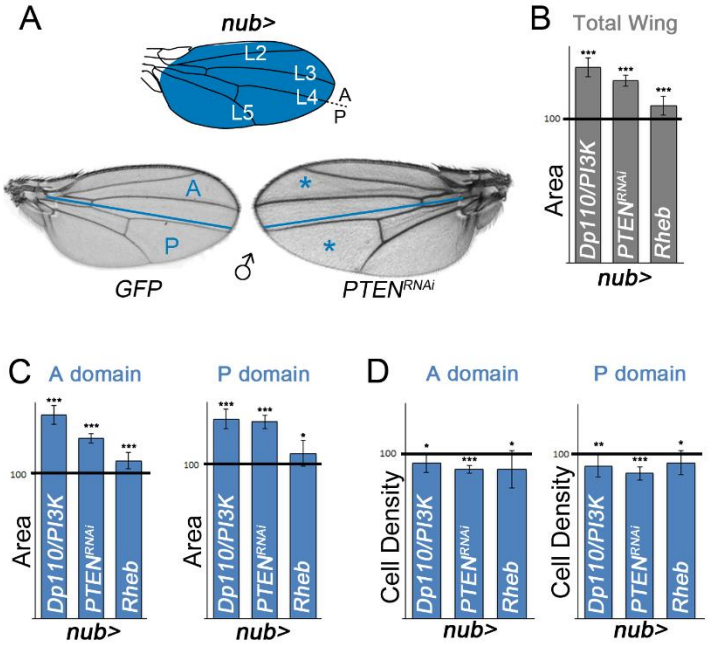

Figure 15. Activation of PI3K/PTEN and TSC/TOR pathways in the wing imaginal disc. (A) Schemes of adult wing with the *nub* expression domain marked in blue and cuticle preparations of male adult wings expressing *GFP* or *PTEN*^{RNAi} under the control of the *nub-gal4* driver. The blue line marks the boundary between anterior (A) and posterior (P) compartments. The wing is decorated with four longitudinal veins (L2–L5), and the anterior side of L4 corresponds to the AP compartment boundary. (B–D) Histograms plotting tissue size (B-C) and cell density (D) of the whole wing (B), or the A and P compartments (C-D) of adult wings expressing the indicated transgenes in the *nub* domain normalized as a percent of the control wings. Error bars show the standard deviation. Number of wings analyzed per genotype ≥ 10. ***p < 0.001;**p < 0.01; *p < 0.05. See also Table 1.

Activation of the TOR pathway, by depletion of TSC1 or TSC2, leads to strongly overgrown tissues and larval lethality (Zhang et al., 2003). In order to reduce larval lethality and be able to analyze the resulting adult wings, we induced mild activation of the TOR pathway by overexpressing Rheb. Rheb overexpression gives rise to overgrown adult wings (Figure 15B). The observed increase in tissue size is mainly a consequence of an increase in cell size (Figure 15D), as the reduction in cell densities is to a similar extent as the increase in tissue size (Figures 15B and 14C). We observed that activation of either the PI3K/PTEN and TSC/TOR pathways in all the wing blade gives rise to an increase in tissue size and that that these pathways exert this action by affecting cell size and cell proliferation in different manners.

The adult wing is subdivided into an anterior (A) and a posterior (P) compartment, and the boundary between these two cell populations is easily identified in the adult wing (Figure 15A), as it corresponds to the anterior side of the fourth longitudinal vein (L4, Figure 15A). The observed increase in tissue size upon activation of the PI3K/PTEN or TSC/TOR pathways in the whole wing blade was similar in both compartments (Figure 15C).

Activation of growth in specific territories causes a non-autonomous reduction in tissue size

We wanted to address the potential non-autonomous effects of activation of the PI3K/PTEN or TSC/TOR pathways on neighboring wild type cell populations. Thus, we drove transgene expression in either the anterior (with the *ci-gal4* driver) or posterior (with the *en-gal4* or *hh-gal4* drivers) compartments of the developing *Drosophila* wing and quantified the size of the adjacent compartments in the resulting adult structures (Figures 16-18). The autonomous capacity of these transgenes to induce tissue and/or cell growth and cell proliferation was also observed with these Gal4 drivers (Figures 16A-D, 17A-D and 18A-D; blue bars). Interestingly, the size of neighboring wild type tissues decreased in all cases

(Figures 16A, 16C, 17A, 17C, 18A and 18C; white bars), and this decrease was accompanied by a reduction in cell size (reflected by an increase in cell densities in the adult wing) (Figures 16D, 17D and 18D, white bars). Therefore, activation of growth promoting pathways in specific territories of the wing imaginal disc causes a reduction in tissue and cell size of the neighboring wild type cell population. The total size of the wing is mostly maintained upon targeted activation of these pathways in the anterior or posterior compartments of the wing primordia (Figures 16B, 17B and 18B).

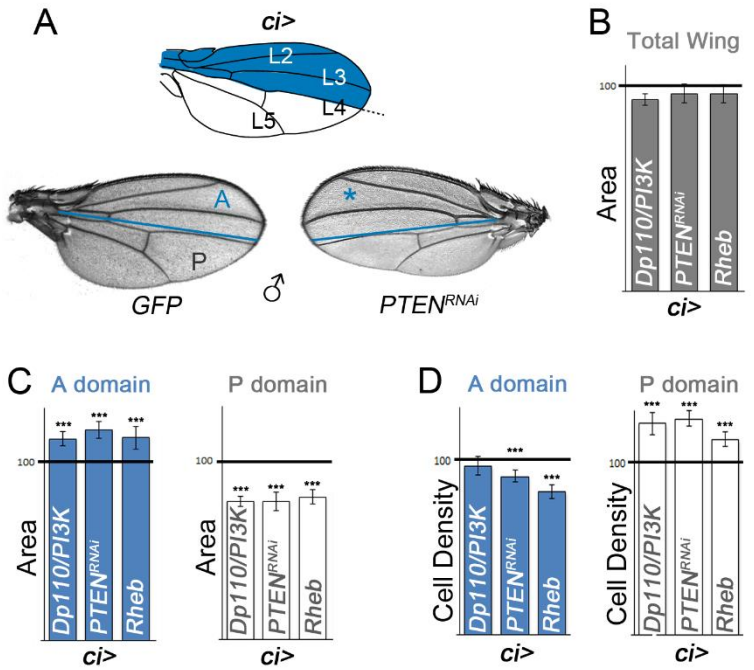

Figure 16. Activation of PI3K/PTEN and TSC/TOR pathways in the anterior compartment. (A) Schemes of adult wing with the *ci* expression domain marked in blue and cuticle preparations of male adult wings expressing *GFP* or *PTEN*^{RNAi} under the control of the *ci-gal4* driver. The blue line marks the boundary between anterior (A) and posterior (P) compartments. The wing is decorated with four longitudinal veins (L2–L5), and the anterior side of L4 corresponds to the AP compartment boundary. The affected territory is marked with a blue asterisk. (B–D) Histograms plotting tissue size (B-C) and cell density (D) of the whole wing (B), or the A (blue bars) and P (white bars) compartments (C-D) of adult wings expressing the indicated transgenes in the *ci* domain normalized as a percent of the control wings. Error bars show the standard deviation. Number of wings analyzed per genotype ≥ 10. ***p < 0.001. See also Table 2.

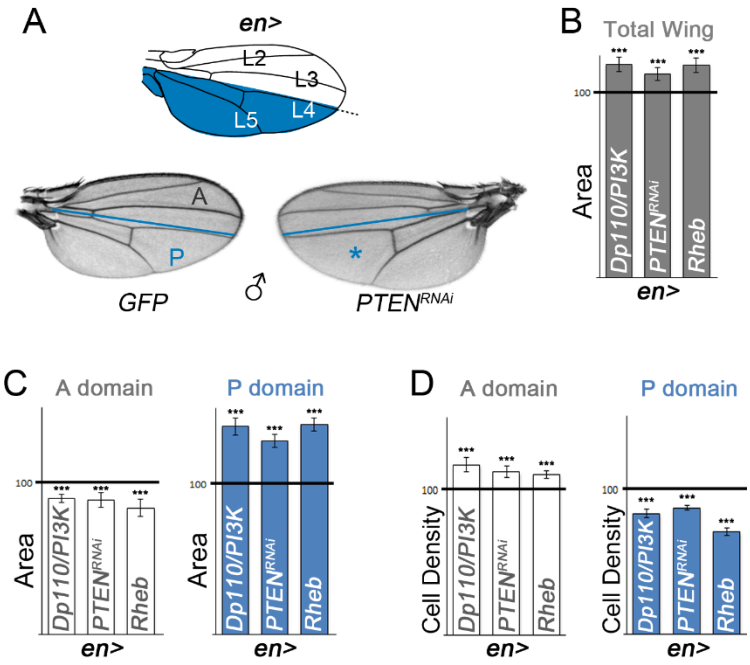

Figure 17. Activation of PI3K/PTEN and TSC/TOR pathways in the posterior compartment. (A) Schemes of adult wing with the *en* expression domain marked in blue and cuticle preparations of male adult wings expressing *GFP* or *PTEN*^{RNAi} under the control of the *en-gal4* driver. The blue line marks the boundary between anterior (A) and posterior (P) compartments. The wing is decorated with four longitudinal veins (L2–L5), and the anterior side of L4 corresponds to the AP compartment boundary. The affected territory is marked with a blue asterisk. (B–D) Histograms plotting tissue size (B-C) and cell density (D) of the whole wing (B), or the A (white bars) and P (blue bars) compartments (C-D) of adult wings expressing the indicated transgenes in the *en* domain normalized as a percent of the control wings. Error bars show the standard deviation. Number of wings analyzed per genotype ≥ 10. ***p < 0.001. See also Table 3.

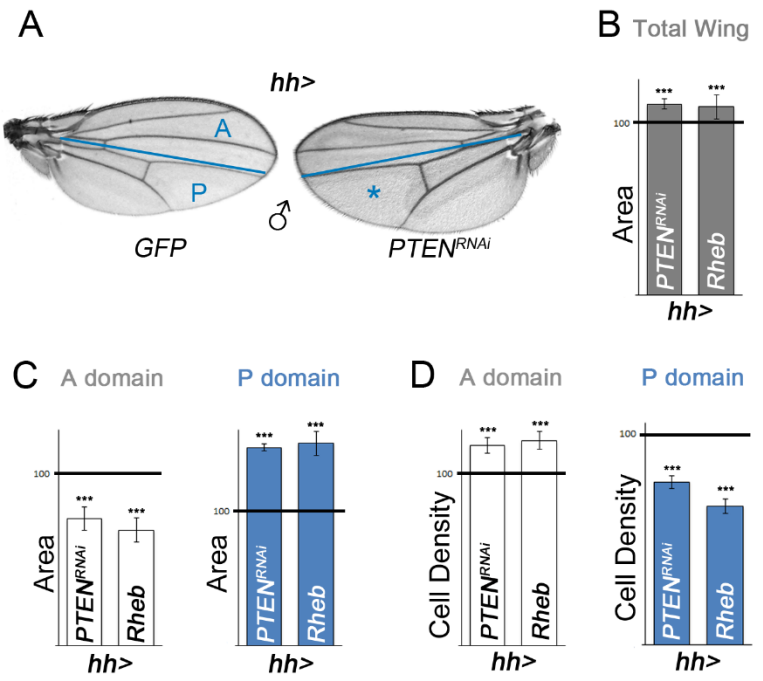

Figure 18. Activation of PI3K/PTEN and TSC/TOR pathways in the posterior compartment. (A) Cuticle preparations of male adult wings expressing *GFP* or *PTEN*^{RNAi} under the control of the *hh-gal4* driver. The blue line marks the boundary between anterior (A) and posterior (P) compartments. The affected territory is marked with a blue asterisk. (B–D) Histograms plotting tissue size (B-C) and cell density (D) of the whole wing (B), or the A (white bars) and P (blue bars) compartments (C-D) of adult wings expressing the indicated transgenes in the *hh* domain normalized as a percent of the control wings. Error bars show the standard deviation. Number of wings analyzed per genotype ≥ 10. ***p < 0.001. See also Table 4.

Whether the reductions in cell and tissue size are two independent processes non-autonomously regulated by the PI3K/PTEN and TSC/TOR pathways or whether there is a causal relationship between them is further analyzed in the following sections. The non-autonomous effects on tissue growth were also obtained with other Gal4 drivers not specific to compartments (Figure 19). Activation of the PI3K/PTEN pathway in the medial region of the wing primordia (in *spalt*^{PE}*-gal4; UAS-PTEN*^{RNAi} individuals) caused a reduction in size of the most lateral regions of the adult wing (Figure 19A and 19B, white bars) and a non-autonomous reduction

in cell size (Figure 19B, white bars). As expected, an autonomous increase in tissue and cell size was observed in the transgene-expressing domain (Figure 19A and 19B, blue bars).

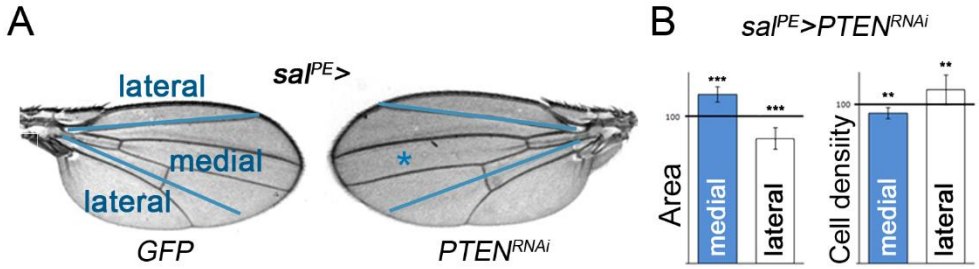

Figure 19. Non-autonomous effect of activation of growth is not specific to compartments. (A) Cuticle preparations of male adult wings expressing *GFP* or *PTEN*^{RNAi} under the control of the *spalt*^{PE}*-gal4* driver. The blue lines mark the borders between the medial and lateral regions of the wing. The affected territory is marked with a blue asterisk. (B) Histograms plotting tissue size (on the left) and cell density (on the right) of the medial (blue bars) and lateral (white bars) regions of adult wings expressing *PTEN*^{RNAi} in the *spalt* domain normalized as a percent of the control wings. Error bars show the standard deviation. Number of wings analyzed per genotype ≥ 10. ***p < 0.001;**p < 0.01. See also Table 5.

Since one of the effects of activation of the PI3K/PTEN signaling pathway is an increase in the cell proliferation rates, we wondered whether driving cell proliferation alone was able to produce a non-autonomous effect on the adjacent cell population. Increased cell proliferation, by means of overexpression of the cell cycle regulators String/Dcdc25 and CycE (which drive G2/M and G1/S transitions, respectively), gave rise to a higher number of cells as a consequence of increased mitotic activity [Figures 20B and 21B, see also (Neufeld et al., 1998)] but was not sufficient to promote tissue growth (Figure 20A and 20B, blue bars). The transgene-expressing compartment was, if anything, slightly smaller (Figure 20B, blue bars), most probably because of the observed increase in the number of apoptotic cells in the tissue [Figure 21A, see also (Neufeld et al., 1998)]. Thus, the capacity of PI3K/PTEN to promote tissue growth does not depend only on increased cell proliferation rates. Driving cell proliferation was not sufficient to exert any non-autonomous effects on tissue or cell growth either (Figure 20A and

20B, white bars). All together, these results indicate that tissue overgrowth, induced by different means and independently of whether it is a consequence of increased cell size and/or cell number, causes a non-autonomous reduction in tissue size of adjacent cell populations.

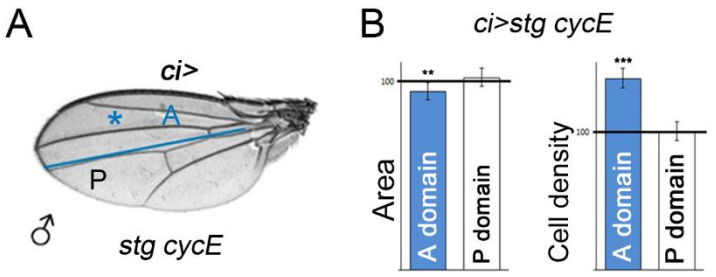

Figure 20. Increased cell proliferation rates does not has an impact in the neighboring domain. (A) Cuticle preparation of male adult wing expressing *stg:cycE* under the control of the *ci-gal4* driver. The blue lines mark the border between the anterior and posterior compartments of the wing. The affected territory is marked with a blue asterisk. (B) Histograms plotting tissue size (on the left) and cell density (on the right) of the anterior (blue bars) and posterior (white bars) compartments of adult wings expressing *stg:cycE* in the *ci* domain normalized as a percent of the control wings. Error bars show the standard deviation. Number of wings analyzed per genotype ≥ 10. ***p < 0.001;**p < 0.01. See also Table 6.

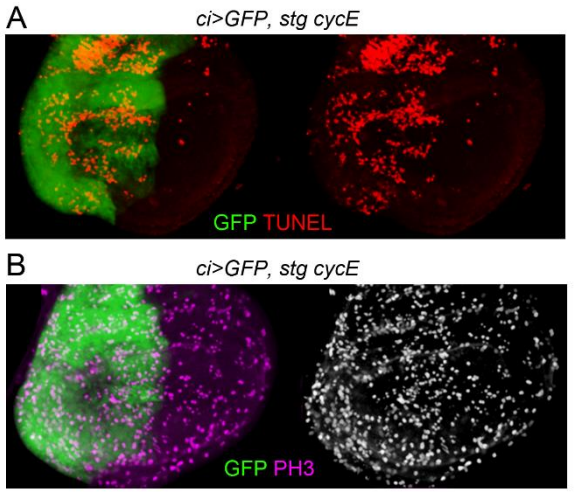

Figure 21. Increased cell proliferation rates does not has an impact in the neighboring domain. (A) *ci>GFP, stg:cycE* wing imaginal discs labelled with TUNEL to visualize apoptotic cells (in red) or with an antibody against phosphorylated histone3 (PH3, in magenta or white) to visualize mitotic cells (B). The *ci* domain is labelled with GFP (in green). Note the higher number of apoptotic cells and increased mitotic activity upon transgene expression.

Targeted Activation of the PI3K/PTEN or TSC/TOR Pathways Induces a Non-autonomous Reduction of Growth Rates in Adjacent Cell Populations

The results presented so far indicate that activation of growth promoting pathways in defined territories of the wing primordia causes a non-autonomous decrease in final tissue size of nearby cell populations. To understand whether this non-autonomous response is an active mechanism that takes place during development, we monitored the size of the A and P compartments throughout development after targeted expression of growth-promoting transgenes in anterior cells. Larvae expressing Dp110/PI3K, Rheb, or GFP in the A compartment (with the *ci-gal4* driver) were grown at 25°C, and the absolute size of the transgene-expressing (A) and non-expressing (P) compartments was quantified at a range of time points of larval development. We focused our attention on third instar wing discs (from 72h to 140h after egg laying [AEL]), as primordia of the future adult wings are specified in late second instar (around 60 h AEL, (Ng et al., 1996)). The autonomous impact of Dp110/PI3K or Rheb on tissue growth was already visible in mid–late third instar wing discs (96–140h AEL), and, most interestingly, this was accompanied by a clear reduction in tissue size of the neighboring P compartment (Figure 22A and 22B). Both the autonomous increase in tissue size as well as the reduction in the size of the adjacent domain was more evident as development proceeds (Figure 22). Thus, activation of growth promoting pathways in one territory causes a non-autonomous reduction in growth rates of the adjacent cell population throughout development.

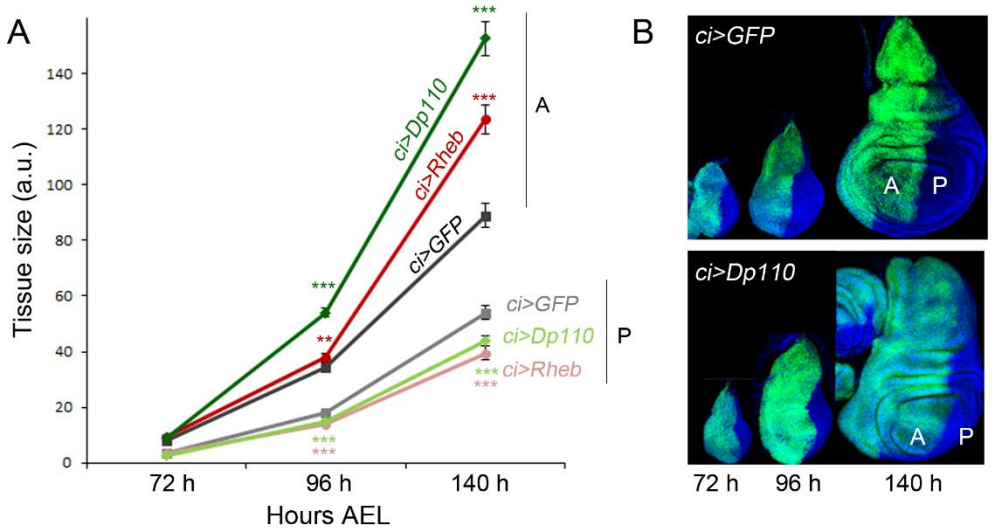

Figure 22. Reduction of growth rates of the neighboring domain. (A) Quantification of tissue size (in arbitrary units [a.u.]) of both anterior (A, dark colors) and posterior (P, light colors) domains of wing imaginal discs where *GFP* (grey curves), *Dp110* (green curves) and *Rheb* (red curves) were expressed in the anterior compartment using the *ci-gal4* driver in three distinct time points during development (in hours [h] AEL). Error bars show the standard deviation. Number of wing discs analyzed per genotype ≥ 15. ***p < 0.001; **p < 0.01. (B). Examples of *ci>2xGFP* (upper panel) and *ci>GFP, Dp110* (lower panel) wing imaginal discs in the developmental time points shown in panel A. The transgene-expressing domain is marked with GFP (in green), and the disc is labelled with DAPI (in blue). The A and P compartments are indicated. See also Table 7.

Targeted Activation of the PI3K/PTEN or TSC/TOR Pathways Induces a Non-autonomous Reduction of Proliferation Rates in Adjacent Cell Populations

In order to investigate whether cell proliferation rates are also regulated in a non-autonomous manner, we induced neutral clones of cells at the beginning of the third instar period (72h AEL) and examined the size of these clones 72h after induction in late third instar wing imaginal discs. Clone size (in arbitrary units [a.u.]) and number of cells per clone were measured in *ci-gal4; UAS-GFP/UAS-Dp110* wing discs and these two measurements were compared to those of control clones induced in *ci-gal4; UAS-GFP/+* wing discs grown in parallel. In Dp110-

expressing wing discs, the size of the clones in the A compartment was, as expected, significantly larger than the size of clones quantified in the A compartment of GFP-expressing discs (Figure 23A and 23B). However, these clones were not composed by a higher number of cells (Figure 23C). Interestingly, the clone size and the number of cells per clone were significantly smaller in the posterior compartment of Dp110-expressing wing discs than in GFP-expressing ones (Figure 23A–23C).

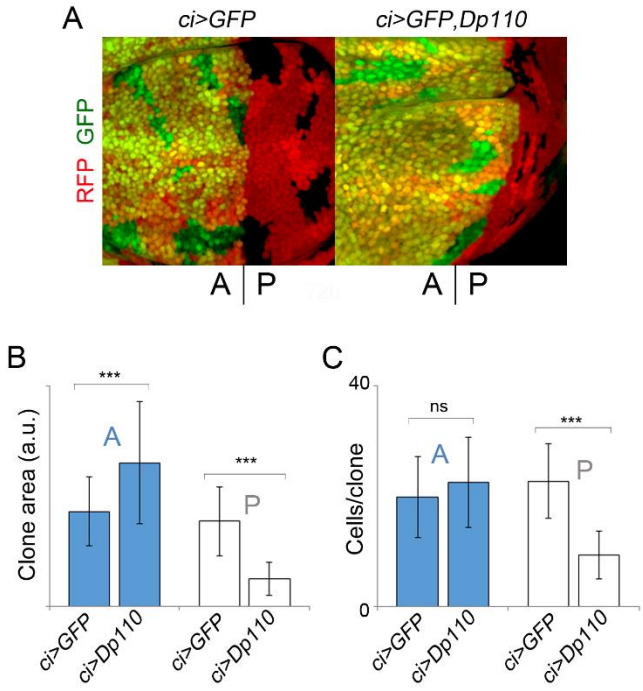

Figure 23. Reduction of proliferation rates in the neighboring territory. (A) Examples of clones of cells in *ci>GFP* (left panel) and *ci>GFP, Dp110* (right panel) wing discs 72h after clone induction. The transgene-expressing domain is marked with GFP (in green), and the clones are labelled by the absence of nuclear red fluorescent protein (RFP, red) expression. The A and P compartments are indicated. (B, C). Histograms plotting the size of clones (in a.u., B) and the number of cells per clone (C) located in the A or P compartment of *ci>GFP* and *ci>GFP, Dp110* wing discs. Error bars indicate the standard deviation. Number of clones analyzed per genotype ≥ 30. ***p < 0.001; ns, not significant. See also Table 8.

From the clonal analysis, we can conclude that activation of growth promoting pathways in one territory of the wing imaginal disc causes a reduction in the proliferation rates of the adjacent cell population, in addition to the already

described reduction in the growth rates. In order to understand if a particular phase of the cell cycle was affected, we carefully monitored the cell cycle profile in those cells. First, we made use of several markers of the different phases of the cell cycle. To analyse S-phase progression, we exposed wing imaginal discs of *ci>GFP* and *ci>GFP, Rheb* larvae to BrdU incorporation for 45 minutes. BrdU is a synthetic nucleoside analogue of thymidine that can be incorporated into the newly synthesized DNA of replicating cells (S phase cells). Using a specific antibody for BrdU to detect the incorporated BrdU, we are able to visualize cells that were actively replicating their DNA. BrdU incorporation levels were similar in the A and P compartments of the Rheb-expressing discs when compared to control GFP-expressing discs (Figure 24A). Next, using *in situ* hybridization, we monitored the expression levels of *Dcyclin E* (*DcycE*) and *Dcdc25/string*, two genes that act in wing disc cells as rate limiting factors of G1/S and G2/M transitions, respectively. The mRNA levels of these two genes were also very similar in A and P compartments of wing discs in which Dp110/PI3K expression was driven in the anterior domain (Figure 24B).

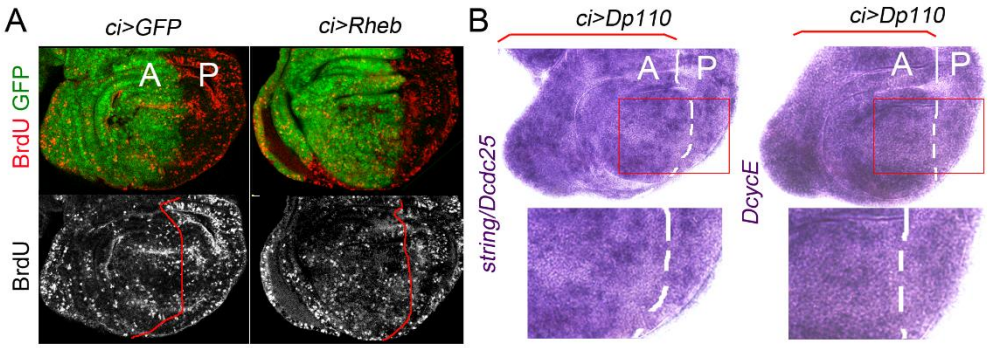

Figure 24. No changes in cell cycle markers. (A) Examples of *ci>GFP* and *ci>GFP, Rheb* wing discs labeled to visualize BrdU (in red or white) with the anterior compartment marked with GFP (in green). (B). Wing imaginal discs of *ci>GFP, Dp110* flies labeled to visualize *string/Dcdc25* (on the left) or *cyclin E* (on the right) mRNA expression. The A and P compartments are indicated and the AP boundary is marked with a red line (A) or a white line (B).

To analyse mitotic activity, we stained third instar wing imaginal discs with an antibody against a phosphorylated form of histone H3 at serine 10 (PH3) that labels mitotic cells. No qualitative difference was observed in PH3 staining in wing imaginal discs where PI3K/PTEN or TSC/TOR signalling pathways were activated in the anterior compartment when compared to control discs (Figure 25A). Quantifying the number of mitotic cells (cells positive for PH3) per area of each compartment showed that no major differences in mitotic activity occur in neither the autonomous and non-autonomous compartments of wing discs where *Rheb* or *Dp110* were overexpressed either in the anterior or posterior compartment when compared to control wing discs (Figure 25B and 25C). Altogether, these observations suggest that the non-autonomous impact on proliferation rates is not due to any obvious arrest in a specific phase of the cell cycle.

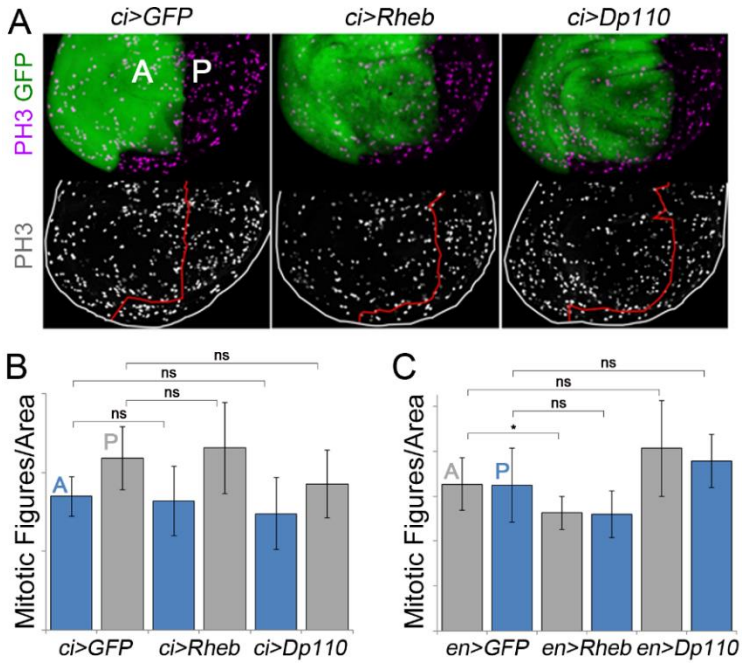

Figure 25. Mitotic activity remains unchanged. (A) Examples of *ci>GFP*, *ci>GFP, Rheb* and *ci>GFP, Dp110* wing discs stained for PH3 (in magenta or white) with the anterior compartment marked with GFP (in green). The A and P compartments are indicated. (B, C). Histograms plotting the number of mitotic figures/area for the anterior and posterior compartments of wing discs of *ci>GFP*, *ci>GFP, Rheb*, *ci>GFP, Dp110* (B) and *en>GFP*, *en>GFP, Rheb* and *en>GFP, Dp110* (C). Error bars indicate the standard deviation. No significant differences where observed. Number of discs analyzed per genotype ≥ 10. *$p < 0.05$; ns, not significant. See also Table 9.

To further confirm this idea we also used a fluorescence-activated cell sorter (FACS) to collect data about the DNA content of dissociated cells from 120h AEL wing discs expressing *Dp110* or *GFP* under the control of the *ci-gal4* driver. We observed that the cell cycle profile of anterior and posterior cells was very similar in the two genotypes analyzed (Figure 26). Taken together, these results indicate that activation of growth promoting pathways causes a non-autonomous reduction in proliferation rates, without any obvious arrest in any particular cell cycle stage, and imply that the non-autonomous reduction in tissue size observed in adult wings is a consequence of not only reduced cell size but also reduced cell number.

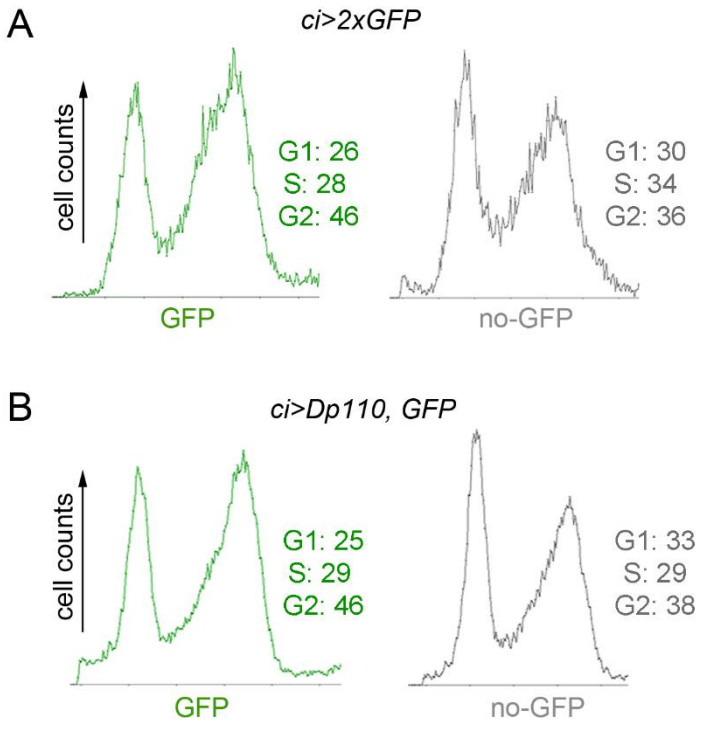

Figure 26. Cell cycle profile upon targeted activation of growth. DNA-content profile of FACS-sorted GFP-expressing and non-expressing cells dissociated from *ci>2xGFP* (A) and *ci>GFP, Dp110* (B) wing imaginal discs. Percentage of cells in G1, G2, and S is indicated. Note that no major differences were seen in the percentage of cells in the different phases of the cell cycle both in the autonomous as in the non-autonomous compartment.

Mechanism of the Non-autonomous Response

The results presented so far point out that when growth-promoting pathways are activated in specific territories of the developing wing, a non-autonomous response is triggered and a reduction in growth and proliferation rates of nearby wild type territories is observed. Next, we wanted to understand the mechanism behind this non-autonomous response.

The non-autonomous response is not due to a systemic effect on growth

In some situations, an insult to the imaginal discs can trigger a systemic response in what concerns its growth rates and developmental timing. For example, abnormally growing imaginal discs present a developmental delay, which is a consequence of secretion of Dilp8 by those cells (Colombani et al., 2012; Garelli et al., 2012). We wondered whether the non-autonomous effects on tissue size that we observed are a local response or a systemic response triggered by the insult given to imaginal cells. Expression of Rheb, Dp110/PI3K or a dsRNA against PTEN under the control of the *ci-gal4* driver did not cause major changes in the final pupal volume when compared to the GFP control animals (Figure 27A). The same was observed in larvae expressing the same transgenes in the *engrailed* expressing domain (Figure 27B). These observations indicate that, targeted activation of growth promoting pathways in specific territories of the wing imaginal disc does not affect final body size.

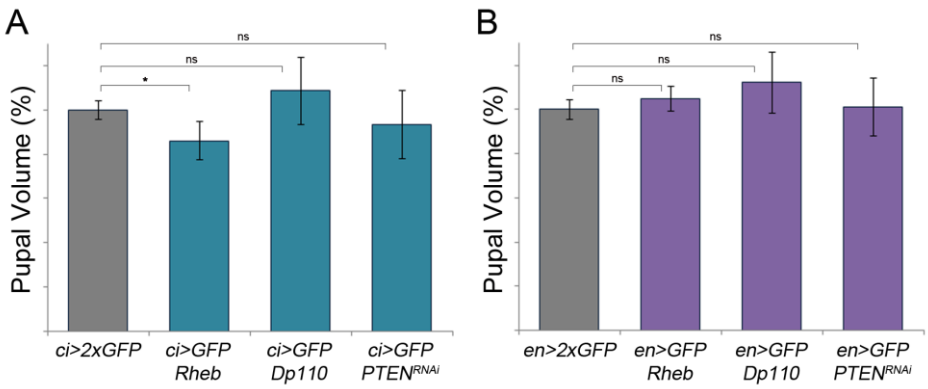

Figure 27. Restricted activation of growth does not affect final body size. Quantification of pupal volume upon expression of *Rheb*, *Dp110* and *PTEN^{RNAi}* under the control of the *ci-gal4* (A) or the *en-gal4* (B) drivers, expressed in percentage of control animals. Error bars represent standard deviation. At least 10 pupas per genotype were measured. *p < 0.05; ns, not significant. See also Table 10.

These results show that no systemic effects in the growth rates and final body size occur upon restricted activation of growth to specific cell populations of the wing imaginal disc. This strongly suggests that the observed non-autonomous effects on growth and proliferation rates are most probably a local response within the wing imaginal disc. These observations also led us to reject the possibility that the non-autonomous effects are due to the expression of the *gal4* driver in other tissues besides the anterior or posterior domains of the wing primordia. Furthermore, when we induced the activation of the growth pathways with the *spalt^{PE}-gal4* driver, which is specific to the wing imaginal disc and is not expressed in any other tissue, we also observed a non-autonomous reduction in tissue size (Figure 19).

The non-autonomous effects on tissue growth are independent of apoptosis and "classic" cell competition

The non-autonomous reduction in growth rates caused by activation of the PI3K/PTEN or TSC/TOR pathways in defined cell populations of the developing

wing primordia is reminiscent of cell competition, a short-range elimination of slow-dividing cells through apoptosis when confronted with a faster-growing cell population. In pursuance of the idea that the compartments could be competing once a growth advantage is given to one territory, we performed a terminal deoxynucleotidyl transferase dUTP nick end labeling (TUNEL) assay to label DNA strand breaks induced by apoptotic cell death and quantified the number of apoptotic cells in the transgene-expressing and non-expressing cell populations. A clear increase in TUNEL-positive cells was observed in those territories expressing Rheb or Dp110/PI3K when compared to GFP-expressing tissues (Figure 28A and 28B, green bars). A similar cell autonomous induction of apoptosis was previously observed in PTEN mutant cells (Nowak et al., 2013), most probably reflecting a deleterious effect of non-physiological activation of these pathways in proliferating cells. However, the number of apoptotic cells in adjacent cell populations was small and very similar to the one found in control tissues expressing GFP [Figure 28A and 28B, grey bars, see also (Milán et al., 1997)].

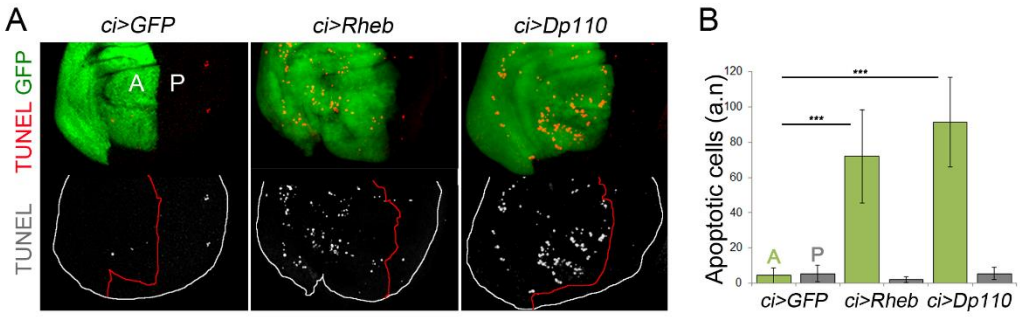

Figure 28. Apoptosis is not observed in the non-autonomous territory. (A) *ci>GFP*, *ci>Rheb*, and *ci>Dp110* wing imaginal discs labelled with TUNEL to visualize apoptotic cells (in red or white). The *ci* domain is labelled with GFP (in green), and the boundary between A and P cells is marked by a red line. (B) Histogram plotting the quantification of the absolute number of TUNEL-positive cells in the A (green bars) and P (grey bars) compartments of the indicated genotypes. Error bars indicate the standard deviation. Number of wing discs analyzed per genotype ≥ 10. ***p < 0.001. See also Table 11.

When apoptosis was reduced in the whole animal by halving the dose of the pro-apoptotic genes hid, grim, and reaper (in Df(H99)/+ larvae), the number of apoptotic cells in the tissue was reduced (Figure 29F, green bars), but the non-autonomous reduction in tissue size was not rescued (Figure 29A, 29B, 29D and 29E, white bars). This reduction in the number of apoptotic cells did not have any impact on cell size (Figure 29C).

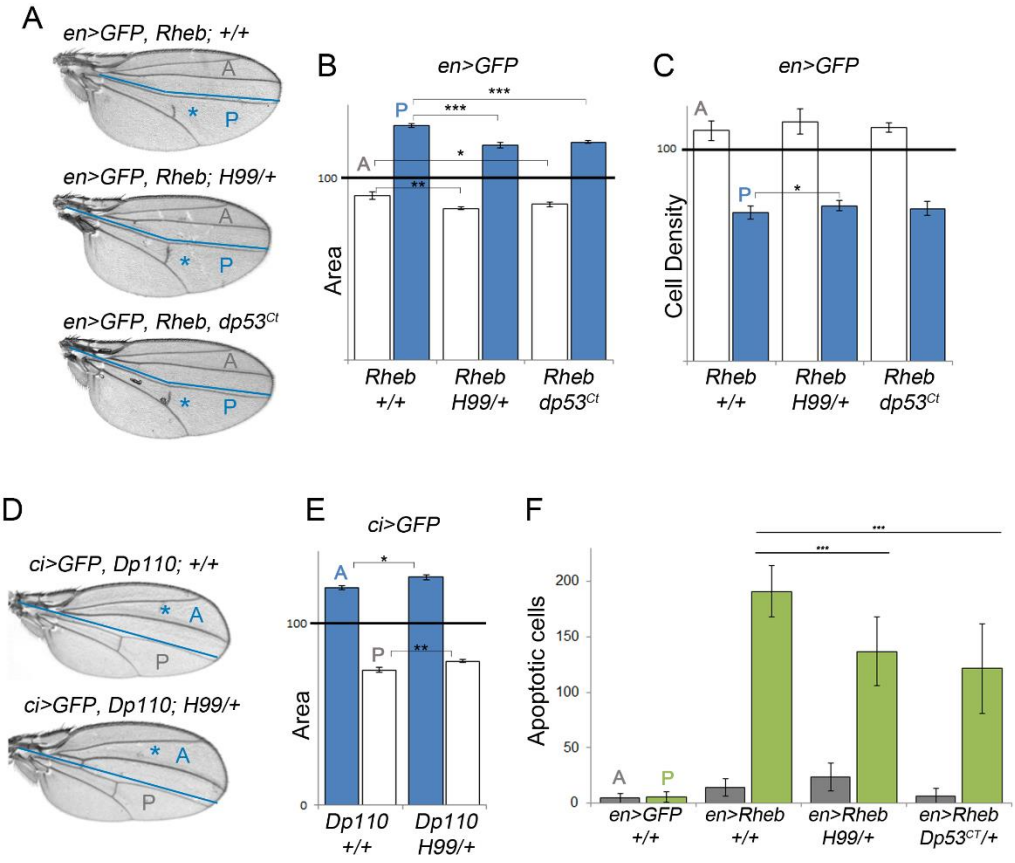

Figure 29. The non-autonomous reduction in tissue size does not rely on Dp53 nor apoptosis. (A, D) Cuticle preparations of *en>GFP, Rheb* (A), and *ci>GFP, Dp110* (D) adult wings either in a wild type background, in a heterozygous background for *H99*, or coexpressing a dominant negative form of Dp53 (*Dp53^{Ct}*). The blue line marks the boundary between the A and P compartments. The domains of transgene expression are marked with a blue asterisk. (B, C, E) Histograms plotting tissue size (B, E) and cell density values (C) of the transgene-expressing compartment (blue bars) and the adjacent cell populations (white bars) of adult wings with the indicated genotypes normalized as a percent of the control wings. (F) Histogram plotting the quantification of the absolute number of TUNEL-positive cells in the P (green bars) and A (grey bars) compartments of the indicated genotypes. Error bars show the standard deviation. Number of wings analyzed per genotype ≥ 10. ***p < 0.001;**p < 0.01; *p < 0.05. See also Table 12.

The transcription factor and tumor suppressor p53, a short-lived, nonabundant protein in healthy cells, plays a fundamental role in regulating the response of mammalian cells to stress, in part through the transcriptional activation of genes involved in apoptosis and cell cycle regulation (Levine, 1997). Impaired protein translation in *Drosophila* tissues has been previously shown to induce Dp53 activation and Dp53-dependent inhibition of growth and proliferation rates in adjacent tissues (Mesquita et al., 2010). Indeed, the apoptosis observed upon overexpression of Rheb was in part due to Dp53 activity since co-expression of a dominant negative form of Dp53 was able to decrease the number of apoptotic cells (*Dp53^{Ct}*, Figure 29F). However, the non-autonomous effects on tissue growth and cell size caused by *Rheb* overexpression were unaffected by expression of a dominant negative version of Dp53 (*Dp53^{Ct}*, Figure 29A, 29B and 29C). Taken together, all these results indicate that Dp53 is not required in the overgrown territory to non-autonomously reduce the growth rates of neighboring cell populations and that the non-autonomous decrease in growth rates is not a consequence of programmed cell death.

Apoptotic cells can produce signals to instruct neighboring cells either to undergo additional proliferation or apoptosis (Huh et al., 2004; Pérez-Garijo et al., 2004; Pérez-Garijo et al., 2013; Ryoo et al., 2004). We thus analyzed whether the apoptotic cells observed in the transgene-expressing compartment exerted any non-autonomous effect on the neighboring compartment. Expression of p35, a baculovirus protein well known to block apoptosis at the level of the effector apoptotic caspases (Hay et al., 1994), was not able to rescue the non-autonomous decrease in tissue growth caused by Rheb overexpression (Figure 30A, white bars). In fact, we find out that expression of p35 slightly reduce the autonomous overgrowth caused by Rheb expression (Figure 30A, blue bars) and further reduced the size of the adjacent territory (Figure 30A, white bars). We found out that p35 expression caused an increase in cell density in both the transgene-expressing compartment (Figure 30B, blue bars) as well as in the neighboring domain (Figure 30B, white bars), most probably reflecting apoptosis-induced cell

proliferation caused by undead cells. Indeed, mitotic activity was both autonomously and non-autonomously increased in the developing primordia expressing p35 (Figure 30C, blue and grey bars). These results indicate that dying cells in the transgene expressing compartment do not contribute to the non-autonomous reduction in tissue and cell size.

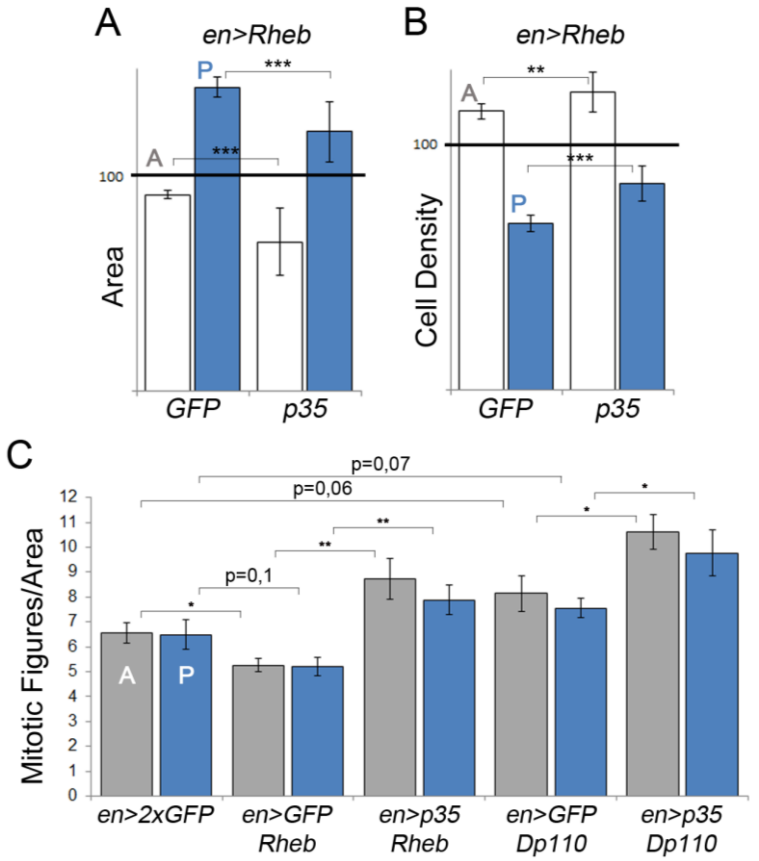

Figure 30. The dying cells do not contribute to the non-autonomous reduction in tissue and cell size. (A, B) Histograms plotting tissue size (A) and cell density (B) values of the transgene-expressing compartment (blue bars) and the adjacent cell populations (white bars) of adult wings of *en>GFP, Rheb* and en>*Rheb, p35* normalized as a percent of the control GFP-expressing wings. (C) Histogram plotting the number of mitotic figures/area for the anterior (grey bars) and posterior (blue bars) compartments of wing discs of *en>2xGFP*; *en>GFP, Rheb*; *en>Rheb, p35; en>GFP, Dp110* and *en>Dp110, p35*. Error bars indicate the standard deviation. Number of wings/discs analyzed per genotype ≥ 10. ***p < 0.001; **p < 0.01; *p < 0.05. See also Table 13.

The non-autonomous effects on tissue growth are not due to competition for nutrients

PTEN mutant cells generated in *Drosophila* tissues have been recently shown to acquire a growth advantage under starvation conditions at the expense of the wild type neighboring cells, and this growth advantage has been proposed to rely on the withdrawal of nutrients from neighboring cells (Nowak et al., 2013). To assess the impact of nutrient availability on the autonomous and non-autonomous effects caused by expression of *Rheb* or $PTEN^{RNAi}$ in defined territories of the wing primordium, larvae expressing these transgenes in either the A or P compartment were reared on food with varying yeast content, the main source of micronutrients and amino acids in fly media. Our standard medium contains 50 g/l yeast. We thus subjected experimental larvae expressing either a dsRNA against *PTEN* or *Rheb* and control larvae expressing GFP to media containing 100 g/l and 20 g/l yeast and analyzed the size of the transgene-expressing and non-expressing cell populations in the resulting adult wings. Despite the expected reduction in the total wing size of animals reared on food containing 20 g/l yeast (Figure 31A), the extent (in percentage) of the non-autonomous decrease in tissue size caused by activation of PI3K/PTEN or TSC/TOR signaling pathways was similar to that observed in animals reared on food containing 100 g/l yeast (Fig 30B and 30C, white bars) when compared to control GFP-expressing wings raised in the same food. Thus, the non-autonomous reduction in growth rates is not affected by starvation and is most probably not a direct consequence of the withdrawal of nutrients from neighboring cells.

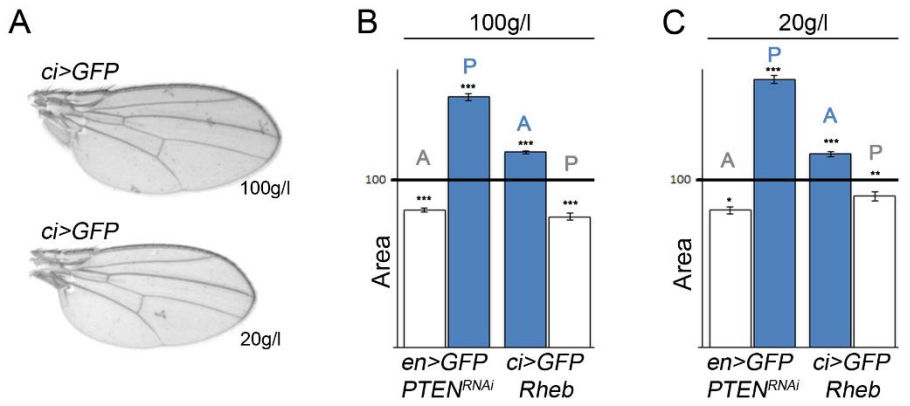

Figure 31. The non-autonomous reduction in tissue size does not rely on competition for nutrients. (A) Cuticle preparations of *ci>GFP* adult wings of well-fed (100 g/L yeast food, top) and starved (20 g/L yeast food, bottom) animals. Note the reduction in wing size caused by starvation. (B, C) Histograms plotting tissue size of the transgene-expressing compartment (blue bars) and the adjacent cell populations (white bars) of adult wings of *en>GFP, PTEN*^{RNAi} and *ci>GFP,Rheb* animals normalized as a percent of the control GFP-expressing flies raised in well-fed (100 g/L yeast food, B) and starved (20 g/L yeast food, C). Error bars show the standard deviation. Number of wings analyzed per genotype ≥ 10. ***p<0.001; **p<0.01; *p<0.05. See also Table 14.

The non-autonomous effects on tissue growth are due to competition for Dpp ligand availability

We noticed that activation of the PI3K/PTEN or TSC/TOR pathways in defined populations of the wing primordium gave rise to larger but well-proportioned adult structures, perceived by the localization of the veins (Figure 32A, blue arrows). The adjacent wild-type territories were reduced in size, but the patterning elements (e.g., longitudinal veins) were also proportionally well located (Figure 32A, grey arrows).

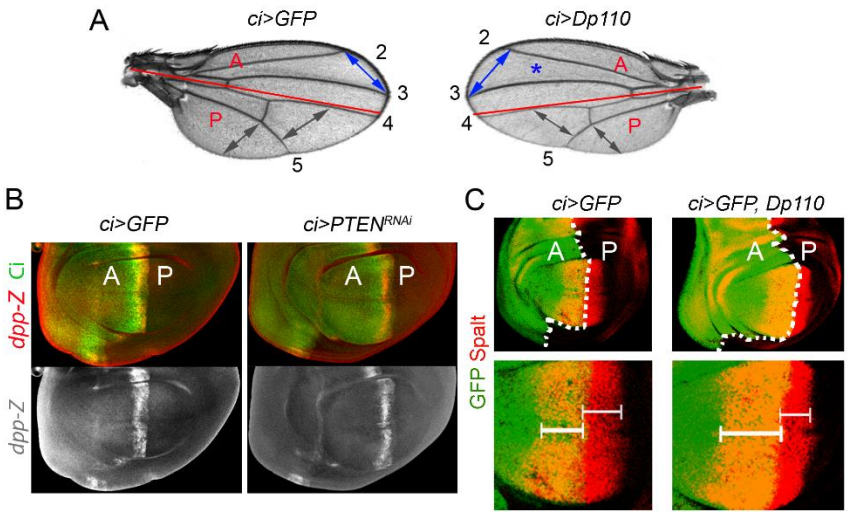

Figure 32. Pattern scales with tissue size upon targeted activation of growth. (A) Cuticle preparation of adult wings expressing *GFP* or *Dp110* under the control of the *ci-gal4* driver, which drives transgene expression in the anterior compartment. Note the expansion of the anterior intervein regions (blue arrows) upon induction of growth and the corresponding reduction of the posterior intervein regions (grey arrows). The anterior and posterior compartments are labelled, and the AP boundary is marked by a red line and the numbers indicate the different veins of the wing. (B) Wing imaginal discs of *ci>GFP* and *ci>PTEN^{RNAi}* larvae labelled to visualized Ci protein (in green) and β-galactosidase (βGal, in red or white) to visualize *dpp* (*dpp-lacZ*) expression. The width of the *dpp-lacZ* stripe (normalized with respect to the width of the wing pouch) was *ci>GFP* = 0.082 ± 0.005; *ci>PTEN^{RNAi}* =0.088 ± 0.003; p = 0.55; n > 6. (C) Wing imaginal discs of *ci>GFP* and *ci>GFP, Dp110* larva labelled to visualize Spalt (in red) and GFP (in green) protein expression. The white dashed line marks the boundary between A and P cells. The lower panels show magnification of the Spalt domain. Note that the anterior Spalt domain is wider upon *Dp110* expression (thick bracket) whereas the posterior Spalt domain (thin brackets) is reduced.

The signaling molecule Dpp, a member of the TGF-β superfamily, is expressed at the boundary between the A and P compartments in the developing wing (Figure 32B) and plays a major role in positioning the wing veins along the anteroposterior axis (see Introduction for details). Interestingly, the Dpp gradient scales with size in order to correctly maintain the wing proportions and, as such, the positioning of the veins. Moreover, Dpp is well known to promote tissue growth making it a good candidate to function as a bridge between growth and patterning. We thus wondered whether the autonomous and non-autonomous effects of *Rheb* or *Dp110/PI3K* overexpression on tissue growth relies on modulating the range of Dpp activity. We first monitored *dpp* expression using a *dpp-lacZ* reporter. No major changes were observed upon activation of

PI3K/PTEN signaling pathway in the anterior compartment of the wing discs when compared to control wing discs (Figure 32B). Since *dpp* production was not affected, we next monitored the range of the Dpp activity gradient visualized by the expression of the Dpp target gene Spalt and with an antibody against the phosphorylated form of the Dpp transducer Mothers Against Dpp (pMAD). As expected, and as a result of the capacity of Dpp gradient to scale with tissue size, we noticed that the Spalt domain was wider upon *Dp110* expression whereas the domain of Spalt expression in the neighboring territory was reduced (Figure 32C, white brackets). The activity of the pathway, which can be visualized with the pMAD antibody, also expanded in the overgrowing transgene-expressing compartment (Figure 33A). In order to quantify the autonomous and non-autonomous impact of tissue growth on the Dpp activity gradient, we extracted the pMAD profiles along four lines perpendicular to the *dpp* expression domain (yellow lines in Figure 33A) and plotted the average pMAD values along the AP axis in experimental (blue in Figure 33B, 33C, 33E and 33G) and control (red in Figure 33B, 33C, 33E and 33G) wing discs. The control and the experimental larvae were raised in the same conditions and immunolabelled in the same tube. Since the boundary between A and P cells is out of phase in control and Dp110-expressing wing discs (Figure 33B), the pMAD profiles were aligned with respect to the AP boundary to better visualize the autonomous and non-autonomous effects on the Dpp activity gradient (Figure 33C, 33E and 33G). We observed a visible expansion along the AP axis of the pMAD gradient towards the overgrowing compartment, either by promoting growth in the anterior or in the posterior territory of the wing primordium (black asterisk in Figure 33C, 33E and 33G). Despite of that, the total amount of pMAD, quantified as total pixel intensity within each compartment (see Materials and Methods), was comparable in overgrowing and control compartments in the three experimental setups (Figure 33D, 33F and 33H, blue bars).

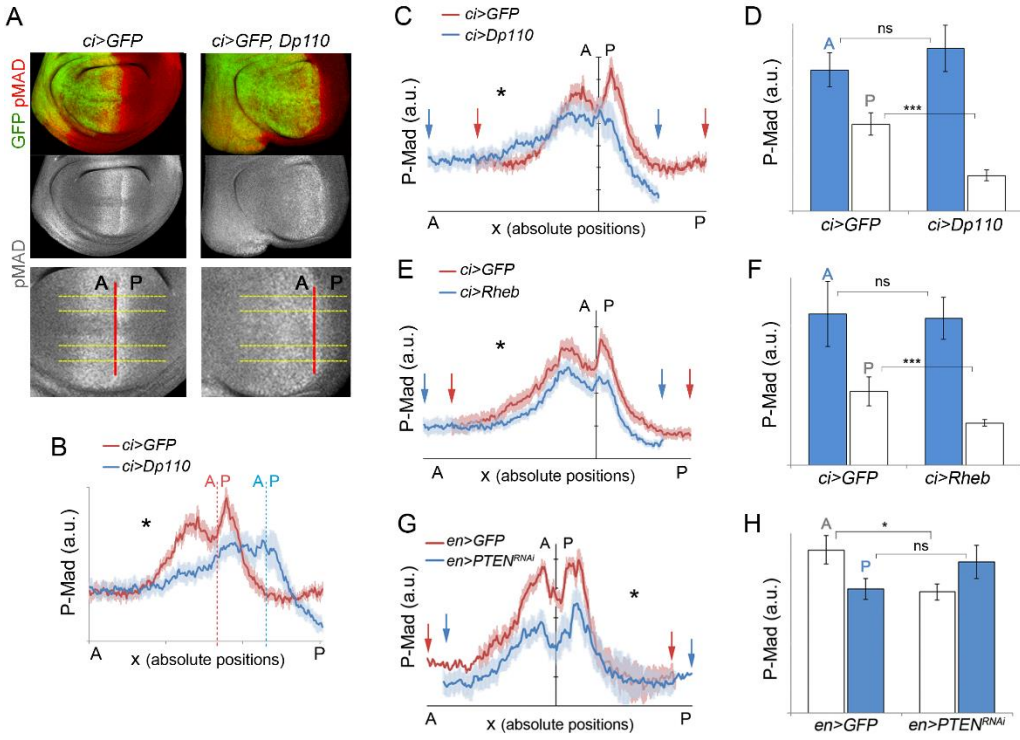

Figure 33. Autonomous and non-autonomous effects on the Dpp activity gradient. (A) Wing imaginal discs of *ci>GFP* and *ci>GFP, Dp110* larva labelled to visualize pMAD protein (in red or white) and GFP (in green). Lower panels show magnifications of the pMAD domains with a red line marking the boundary between the A and P compartments. Horizontal yellow lines were used to generate the pMAD profiles. (B, C, E, G) Average pMAD profiles of wing discs expressing *GFP* (red line) or *GFP* and the corresponding transgenes (blue line) under the control of the *ci-gal4* (B, C, E) or the *en-gal4* (G) drivers. Profiles were taken along the AP axis and plotted in absolute positions. The standard error to the mean is shown in the corresponding color for each genotype. In B, the AP boundary of each experiment is marked by a dashed line of the corresponding color. In C, E and G, the AP boundary of both experiments was aligned to allow comparison of the profile in each compartment. The domains of transgene expression are marked with a black asterisk. Arrows mark the limits of the Dpp activity gradients. (D, F, H) Histograms plotting the total intensity of the pMAD signal in a.u. of the autonomous (blue bars) and non-autonomous (white bars) territories of *ci>GFP* and *ci>Dp110* (D) or *ci>Rheb* (F) and of *en>GFP* and *en>PTEN^{RNAi}* wing discs (H). Error bars indicate the standard deviation. Number of wing discs analyzed per genotype ≥ 5. ***$p < 0.001$; *$p < 0.05$; ns, not significant. See also Table 15.

To further demonstrate that activation of growth promoting pathways does not have any impact in the Dpp signaling levels per se, we drove Dp110/PI3K overexpression in the whole wing primordium using the *nub-gal4* driver and extracted the pMAD gradient profile in those wing discs (Figure 34A). We observed a clear change in the slope of the pMAD gradient due to the bigger size of the tissue (Figure 34B). However, no changes in the total amount of pMAD were observed (Figure 34C). These results indicate that tissue growth has a major impact in Dpp spreading but not signaling/activity levels.

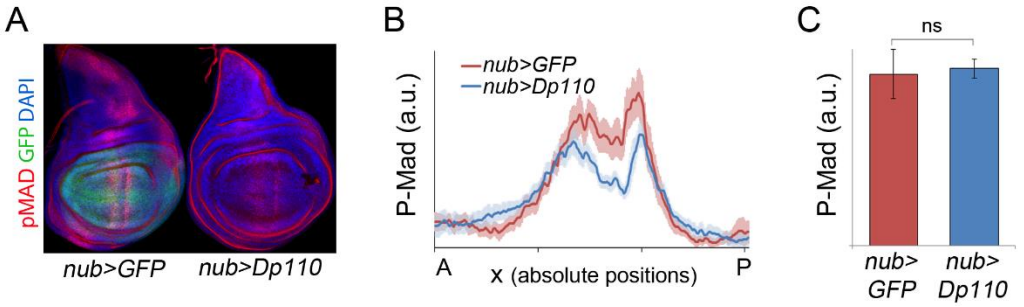

Figure 34. Dpp activity levels are unaffected in overgrown tissues. (A) Wing imaginal discs of *nub>GFP* and *nub>Dp110* larvae labelled to visualize pMAD protein (in red), GFP (in green), and DAPI (in blue, to visualize nuclei). (B) Average pMAD profile of wing discs expressing *GFP* (red line) or *Dp110* (blue line) in the *nubbin* domain. Profiles were taken along the AP axis and plotted in absolute positions. The standard error to the mean is shown in the corresponding color for each genotype. Number of wing discs analyzed per genotype ≥ 7. (C) Histogram plotting the total intensity of the pMAD signal in a.u. of the *nubbin* domain of *nub>GFP* (red bar) and *nub>Dp110* (blue bar) wing discs. Error bars indicate the standard deviation. Number of wing discs analyzed per genotype ≥ 5. ns, not significant. See also Table 16.

Two observations suggest that the tissue autonomous expansion of the pMAD gradient was a consequence of increased tissue size and not cell number. First, Rheb overexpression increased tissue and cell size, but not cell number, and lead to the expansion of the gradient (Figure 33E, black asterisk). Second, increased cell number without affecting tissue size, by means of expression of the cell cycle regulators CycE and String/Dcdc25, did not have any impact on the pMAD gradient (Figure 35, black asterisk).

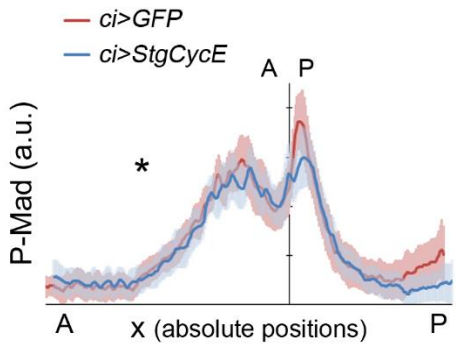

Figure 35. Increased cell number does not change the Dpp activity gradient. Average pMAD profile of wing discs expressing *GFP* (red line) or *Stg,CycE* (blue line) in the *ci* domain. Profiles were taken along the AP axis and plotted in absolute positions. The standard error to the mean is shown in the corresponding color for each genotype. The AP boundary of both experiments was aligned to allow comparison of the profile in each compartment. The domain of transgene expression are marked with a black asterisk. Number of wing discs analyzed per genotype ≥ 5.

Interestingly, we noticed that the width of the Dpp activity gradient, monitored by the expression of Spalt (Figure 32C) and pMAD (Figure 33A, 33B, 33C, 33E and 33G), was non-autonomously reduced upon activation of the PI3K/PTEN and TSC/TOR pathways. Furthermore, the total amount of pMAD signaling was lower in the adjacent wild type territories (Figure 33D, 33F and 33H, white bars). This non-autonomous effect was not observed upon expression of cell cycle regulators CycE and String/Dcdc25 (Figure 35). This led us to propose that the non-autonomous reduction in tissue size is due to competition for the Dpp ligand triggered by the activation of PI3K/PTEN and TSC/TOR signaling in distinct cell populations. To test this hypothesis, we compared the size of the Dp110/PI3K-expressing territory and the corresponding adjacent compartment upon depletion of Dpp, by means of expression of a dsRNA against *dpp* in the anterior compartment (Figure 36). Since depletion of *dpp* with *ci-gal4* caused pupal lethality, we measured third instar wing imaginal discs. Overexpression of Dp110/PI3K in a wild type background caused, as extensively shown above, a reduction in tissue size of the adjacent territory (Figure 36A, white bars). Expression of a dsRNA against *dpp* in A cells gave rise to a strong reduction in tissue size (Figure 36B and 36C), comparable to those of wing discs mutant for

dpp [dpp^{d12}/dpp^{d14}, see (Schwank et al., 2008)]. Whereas Dp110/PI3K was still able to induce overgrowth of the dpp^{RNAi} expressing territory (Figure 36B, blue bars), the non-autonomous reduction in tissue size was largely rescued (compare Figure 36A and 36B, white bars). These results indicate that tissue growth has a major impact in Dpp spreading, but not signaling, and that the non-autonomous reduction in tissue size is most probably a consequence of reduced Dpp signaling. We propose that the reduction in Dpp signaling is due to a higher efficiency in the trapping of the Dpp ligand by the overgrowing cell population.

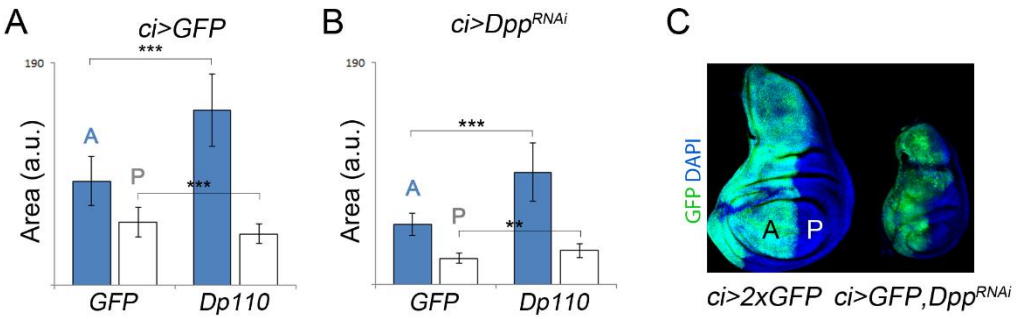

Figure 36. Non-autonomous reduction in tissue size rescued by Dpp depletion. (A) Histogram plotting the area (in a.u.) of anterior (blue) and posterior (white) domains of wing discs expressing *GFP* or *GFP* and *Dp110* in the *ci* domain. Error bars show the standard deviation. Number of wing discs analyzed per genotype ≥ 15. ***p < 0.001. (B) Histogram plotting the area (in a.u.) of anterior (blue) and posterior (white) domains of wing discs expressing either *GFP* or *Dp110* in the *ci* domain together with a dsRNA against *dpp*. Error bars show the standard deviation. Number of wing discs analyzed per genotype ≥ 15. ***p < 0.001; **p < 0.01. (C) Wing imaginal discs of *ci>2xGFP* and *ci>GFP, dpp^{RNAi}* larvae labelled to visualize GFP (in green) and DAPI (in blue, to visualize nuclei). See also Table 17.

A New Role for the Dally Proteoglycan

As described above we observed an impact of PI3K/PTEN and TSC/TOR signaling in Dpp spreading, which suggests that diffusion of Dpp is affected. So, both PI3K/PTEN and TSC/TOR pathways might have an impact on the expression of genes important for Dpp diffusion.

Expression of the Thickveins receptor is not regulated by targeted activation of the PTEN/PI3K and TSC/TOR pathways

The Dpp type I receptor Thickveins (Tkv) has been shown to trap the Dpp ligand and limit its spreading. Clones of cells overexpressing Tkv located in a region where the level of Dpp activity falls below the normally required to induce Spalt, show high Spalt expression on the side of the clone facing the source of Dpp and its decreases across the clone. (Lecuit and Cohen, 1998).
To discard the possibility of the contribution of Tkv to the non-autonomous effects on tissue size upon targeted deregulation of the PI3K/PTEN pathway, we checked Tkv expression upon depletion of PTEN. When PTEN was depleted in the anterior compartment of the wing disc, Tkv expression levels were unaffected, visualized with both an enhancer and a protein trap (Figure 37). Despite the fact that higher levels of the Tkv receptor are able to trap Dpp, our results indicate that Tkv does not appear to be a good candidate to be mediating the non-autonomous effects on tissue growth caused by activation of the PI3K/PTEN and TSC/TOR signaling pathways.

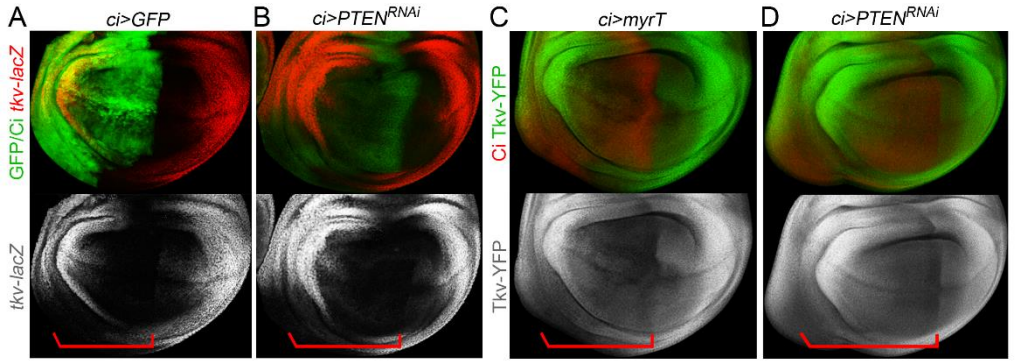

Figure 37. Thickveins expression is unaffected by depletion of PTEN. (A, B) Wing imaginal discs of *ci>GFP* and *ci>PTEN^{RNAi}* labelled to visualize *thickveins* expression with a *tkv-lacZ* reporter (antibody to β-Gal, green or white) and GFP (A) or Ci (B) expression (in green) to mark the transgene-expressing domain. (C, D) Wing imaginal discs of *ci>myrT* (C) and *ci>PTEN^{RNAi}* (D) labelled to visualize Thickveins protein levels using a Tkv-YFP reporter (in green or white) and Ci expression (in red) to mark the transgene-expressing territory. Note that no changes in Tkv expression were observed upon targeted activation of PI3K/PTEN signaling pathway (red brackets).

Dally glypican is upregulated upon activation of the PI3K/PTEN and TSC/TOR signaling pathways

Heparan sulfate proteoglycans (HSPGs) of the glypican family play key roles in the regulation of morphogen signaling and distribution. Glypicans are glycosylphosphatidylinositol (GPI)-anchored HSPGs that have a protein core to which heparan sulfate (HS) chains are covalently attached. HS chains provide binding sites for many growth factors, and the glypicans Dally and Dally-like contribute to the spreading of the Dpp ligand (see Introduction for details). We wondered whether the impact of PI3K/PTEN and TSC/TOR pathways on Dpp spreading are mediated by one or both of these glypicans. Dally-like protein levels were largely unaffected upon targeted activation of PI3K/PTEN and TSC/TOR signaling pathways in one compartment of the wing (Figure 38). By contrast, the expression levels of Dally, visualized with two distinct reporters, an enhancer-trap and a protein trap, were clearly increased upon activation of the PI3K/PTEN or TSC/TOR pathways (Figure 39).

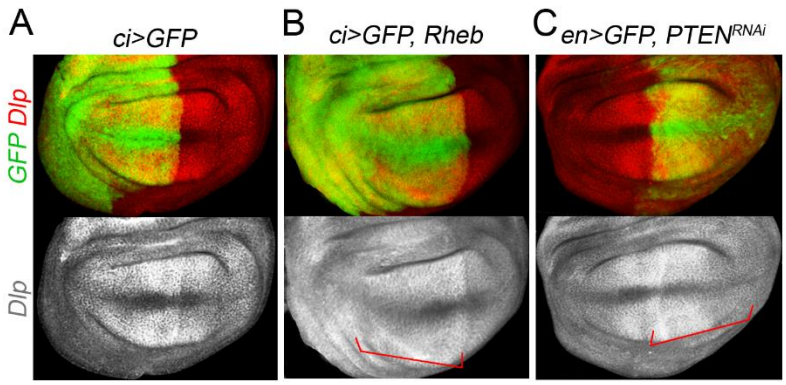

Figure 38. Dally-like levels are not modulated by activation of the PI3K/PTEN and TSC/TOR signaling pathways. (A, C) Wing imaginal discs of *ci>GFP* (A), *ci>GFP, Rheb* (B) and *en>GFP, PTEN*^{RNAi} labelled to visualize Dally-like protein (in red or white) and GFP expression to mark the transgene-expressing domain. Note unchanged levels of Dlp in *Rheb* and *PTEN*^{RNAi} expressing cells (red brackets).

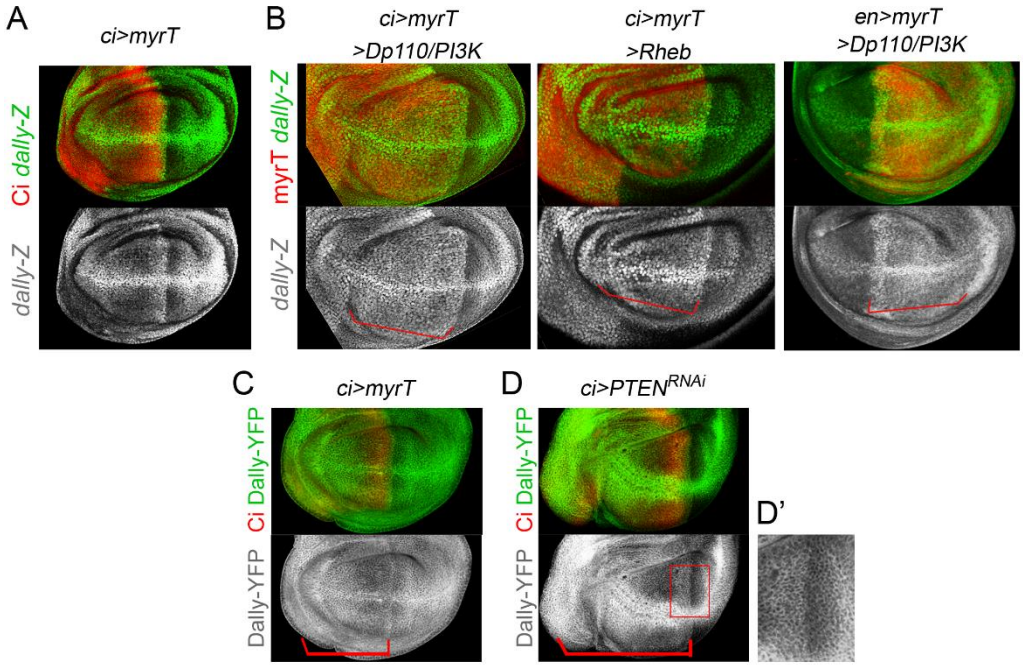

Figure 39. Dally upregulation upon activation of PI3K/PTEN and TSC/TOR pathways. (A, B) Representative wing discs of the indicated genotypes labelled to visualize *dally-lacZ* (antibody to β-Gal, green or white) and myrTomato (myrT, in red) expression to mark the transgene-expressing domain. Note stronger expression of *dally-lacZ* upon activation of the PI3K/PTEN and TSC/TOR pathways (red brackets). (C, D) Wing imaginal discs of *ci>myrT* (C) and *ci>PTEN*^{RNAi} (D) labelled to visualize Dally expression by means of a Dally-YFP reporter. Red brackets indicate the domain of transgene expression. High magnification of the squared region is shown in the right panel (D').

Dally overexpression is able to phenocopy targeted activation of growth

We next checked the capacity of targeted overexpression of Dally to phenocopy the autonomous and non-autonomous effects on tissue growth, proliferation rates and Dpp gradient formation caused by targeted activation of the PI3K/PTEN or TSC/TOR signaling pathways. Overexpression of Dally in the anterior or posterior compartments of the developing wing resulted in a tissue-autonomous increase in size (Figure 40A-D, blue bars) and, most importantly, a non-autonomous reduction in the size of the adjacent wild type territories (Figure 40A-D, white bars). In contrast to what happened when the PI3K/PTEN or TSC/TOR pathways were activated, the increase in tissue size was accompanied by an increase in cell number, observed by an increase in cell density of the transgene expressing compartment (Figure 40B and 40D, blue bars). Moreover, the non-autonomous reduction in tissue size caused by Dally overexpression was not accompanied by a decrease in cell size as cell densities, if anything, decreased (Figure 40B and 40D, white bars). Thus, other elements regulated by the PI3K/PTEN and TSC/TOR growth-promoting pathways, besides Dally, might have a non-autonomous impact on cell size. These results reinforce our previous observations that the non-autonomous reduction in cell size are observed in adult wings and not in wing primordia.

With the aim of addressing whether growth and proliferation rates are also regulated in a non-autonomous manner by the overexpression of Dally, we induced wild type clones at the beginning of the third instar larval period (72h AEL) and examined the size of these clones 72h later in late third instar wing discs. Clone size and number of cells per clone were measured both in the anterior and posterior compartments of *ci-gal4; UAS-GFP/UAS-Dally* wing discs, and these two measurements were compared to those of control clones induced in *ci-gal4; UAS-GFP/+* wing discs and grown in parallel. In Dally-overexpressing wing discs, the size of the clones and the number of cells per clone in the anterior compartment

were significantly bigger than the size of clones quantified in the anterior compartment of GFP-expressing discs (Figure 40E and 40F, blue bars). Interestingly, clone size and number of cells per clone were significantly smaller in the posterior compartment of Dally-expressing wing discs than in GFP-expressing discs (Figure 40E and 40F, white bars). These results indicate that overexpression of Dally causes a non-autonomous reduction in proliferation rates and imply that the non-autonomous reduction in tissue size observed in adult wings is a consequence of reduced cell number.

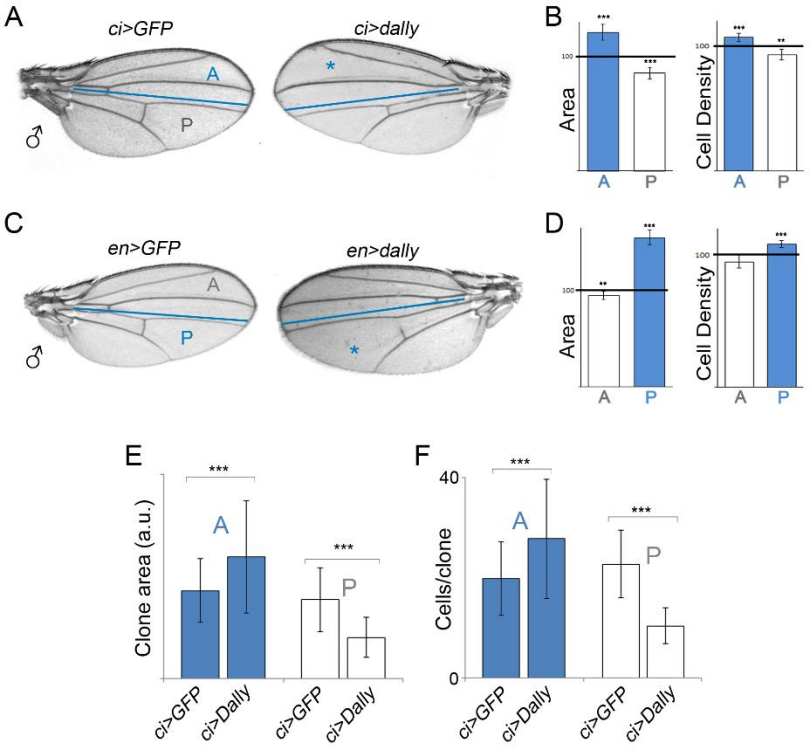

Figure 40. Dally overexpression phenocopies the autonomous and non-autonomous effects of activation of PI3K/PTEN and TSC/TOR pathways. (A, C) Cuticle preparations of male adult wings expressing *GFP* or *Dally* under the control of the *ci-gal4* (A) or *en-gal4* (C) drivers. The blue line marks the boundary between the anterior (A) and posterior (P) compartments, and the domains of Dally overexpression are marked with a blue asterisk. (B, D). Histograms plotting tissue size (left) and cell density values (right) of the Dally-expressing domains (blue bars) and the adjacent compartments (white bars) of adult wings overexpressing *Dally* under the control of the *ci-gal4* (B) or *en-gal4* (D) drivers. Values are normalized as a percent of the control GFP-expressing wings. Error bars show the standard deviation. Number of wings analyzed per genotype ≥ 10. (E, F) Histograms plotting the size of clones (in a.u., E) and the number of cells per clone (F) located in the A or P compartment of *ci-gal4, UAS-GFP/+* and *ci-gal4, UAS-GFP/UAS-dally* wing discs. Error bars indicate the standard deviation. Number of clones analyzed per genotype ≥ 30. ***p < 0.001; **p < 0.01. See also Table 18.

Dally overexpression has an impact specifically in Dpp morphogen

Dally is known to have a role in Dpp gradient formation. Accordingly, targeted overexpression of Dally also gave rise to a tissue-autonomous increase in the width of the pMAD signaling gradient and to a remarkable reduction in pMAD signaling in nearby territories (Figure 41A and 41B). In this case, the total amount of pMAD was higher in Dally overexpressing territories than in the control one (Figure 41C, blue bars) and reduced in the neighboring territory when compared to GFP-expressing discs (Figure 41C, white bars).

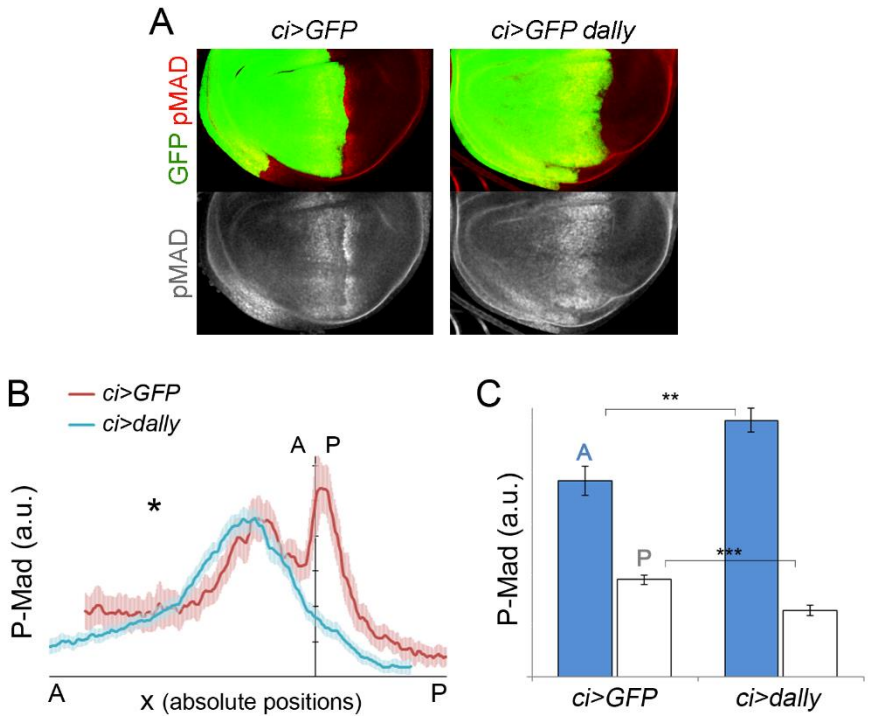

Figure 41. Impact of Dally overexpression on the Dpp gradient. (A) Wing imaginal discs of *ci>GFP* and *ci>GFP, dally* larvae labelled to visualize pMAD protein (in red or white) and GFP (in green) to mark the anterior compartment. (B) Average pMAD profiles of wing discs expressing *GFP* (red line) or *GFP* and *Dally* (blue line) under the control of the *ci-gal4* driver. Profiles were taken along the AP axis and plotted in absolute positions. The standard error to the mean is shown in the corresponding color for each genotype. The AP boundary of both experiments was aligned to allow comparison of the profile in each compartment. The domain of transgene expression are marked with a black asterisk. Number of wing discs analyzed per genotype ≥ 5. (C) Histogram plotting the total intensity of the pMAD signal (in a.u.) of the anterior (blue bars) and posterior (white bars) compartments of *ci>GFP* and *ci>GFP, dally* wing discs. Error bars indicate the standard deviation. Number of wing discs analyzed per genotype ≥ 5. ***p < 0.001; **p < 0.01. See also Table 19.

We noticed that the patterning elements, including wing veins and the wing margin, were well located and formed, thus indicating that Dally overexpression exerts a specific role on Dpp gradient formation and a minor role on the other secreted signaling molecules involved in wing growth and patterning. It was previously shown that Dally is essential for Wg gradient formation (Han et al., 2005) and also to Hh movement (Han et al., 2004) in wing disc cells. We checked whether Dally affects Hh and Wg signaling in the wing imaginal disc.

In wild type wing discs, Hh stabilizes Cubitus interruptus (Ci) protein as far as 8–10 cells away from the AP boundary (Strigini and Cohen, 1997). Patched (Ptc), another target that requires higher levels of Hh, can be detected as far as five cells away from the boundary in the wild type wing disc (Alexandre et al., 1996). Neither the Ci nor the Ptc expression domains were extended upon overexpression of Dally in either the anterior or posterior compartments of the wing disc (Figure 42A and 42B). Wg is expressed along the DV boundary and activates its targets genes, such as Distalless (Dll), in a concentration-dependent manner. Overexpression of Dally either in the posterior or in the anterior compartment of the wing primordium did not affect Wg expression nor spreading (Figure 42B). In addition, the expression domain of one of its target genes Dll remained unchanged (Figure 42C). These results indicate that Dally does not appear to have a major influence on Hh and Wg morphogen movement.

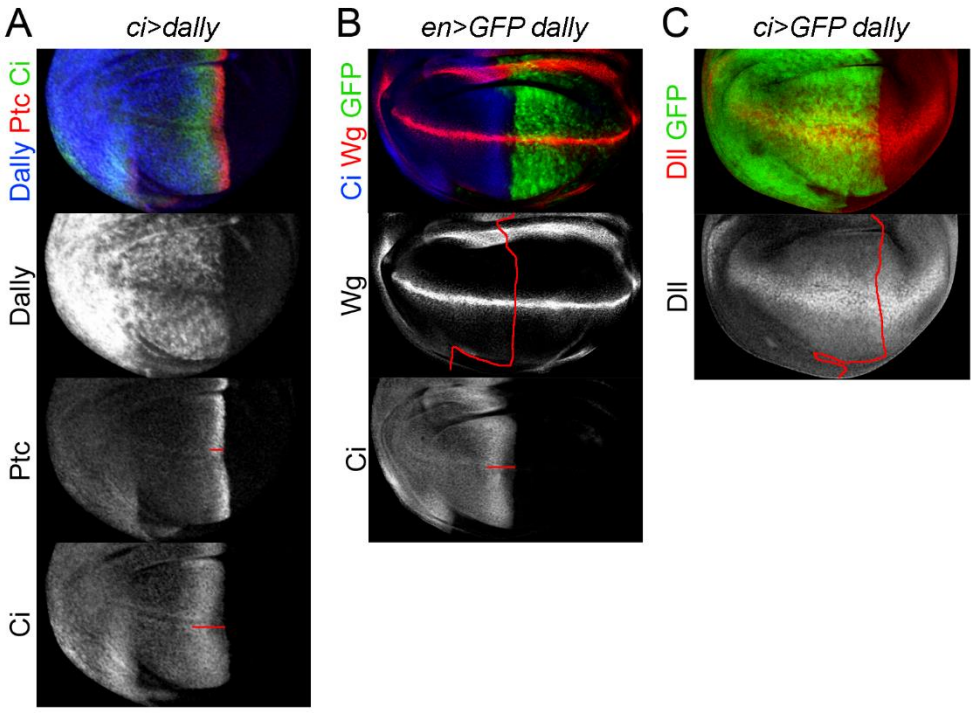

Figure 42. Impact of Dally overexpression on Hh and Wg signaling. (A) Wing imaginal disc of *ci>dally* larvae labelled to visualize Dally (in blue or white), Ptc (in red or white) and Ci (in green or white) proteins. (B) Wing imaginal disc of *en>GFP, dally* larvae labelled to visualize Wg (in red or white), Ci (in blue or white) and GFP (in green) proteins. (C) Wing imaginal disc of *ci>GFP, dally* larvae labelled to visualize Dll (in red or white), and GFP (in green) proteins. The red line marks the boundary between the A and P compartments (in B and C). The horizontal red lines highlight the unchanged width of Ci and Ptc expression domains upon Dally overexpression (in A and B).

By overexpressing Dally we were able to further enhance the phenotype of targeted activation of growth in specific territories of the wing imaginal discs. Activation of PI3K/PTEN signaling in the anterior domain, either with expression of Dp110 or a dsRNA against PTEN, together with overexpression of Dally gave rise to an autonomous increase in size (Figure 43B and 43E, blue bars) and a further non-autonomous reduction in tissue size (Figure 43B and 43E, white bars) when compared to expression of growth promoting transgenes alone. No changes in the autonomous nor in the non-autonomous territories in what concerns cell size were observed (Figure 43C and 43F).

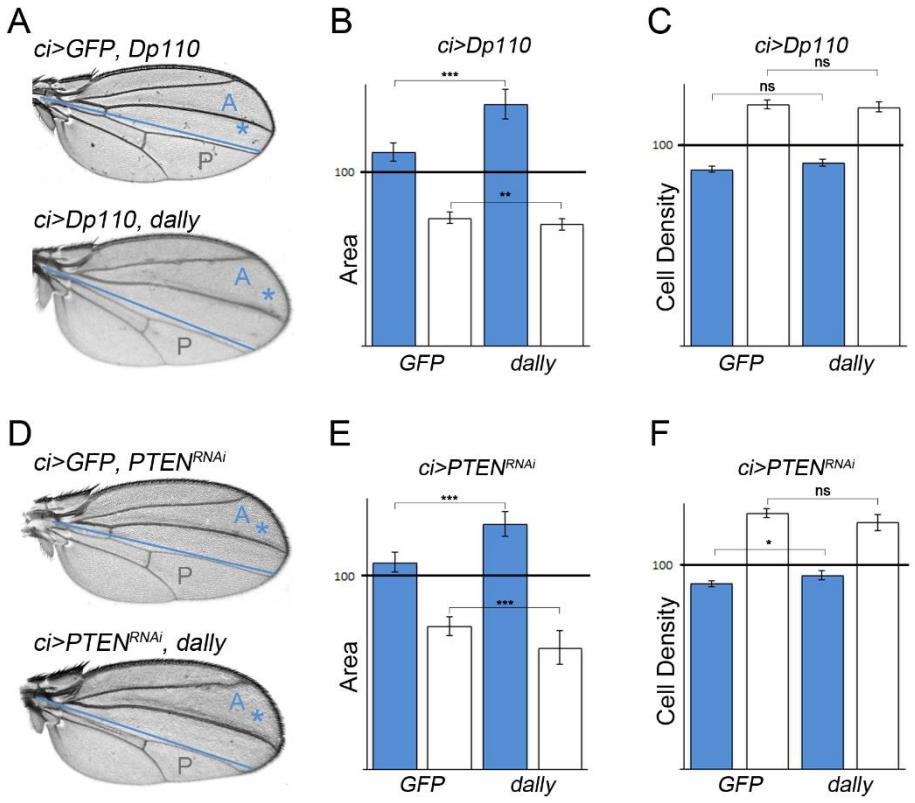

Figure 43. Dally co-expression further enhances the autonomous and non-autonomous effects in tissue size of targeted activation of growth. (A, D) Cuticle preparations of male adult wings of *ci>GFP, Dp110* and *ci>Dp110, dally* (A), *ci>GFP, PTEN^{RNAi}* and *ci>PTEN^{RNAi}, dally* (D). The blue line marks the boundary between the anterior (A) and posterior (P) compartments, and the domains of transgene expression are marked with a blue asterisk. (B-F). Histograms plotting tissue size (B, E) and cell density values (C, F) of the transgene expressing domains (blue bars) and the adjacent compartments (white bars) of adult wings of the indicated genotypes. Values are normalized as a percent of the control GFP-expressing wings. Error bars show the standard deviation. Number of wings analyzed per genotype ≥ 10. ***$p < 0.001$; **$p < 0.01$; *$p < 0.05$; ns, not significant. See also Table 20.

Dally contributes to the autonomous and non-autonomous effects on tissue growth upon targeted activation of PI3K/PTEN and TSC/TOR signaling pathways

Since targeted activation of PI3K/PTEN and TSC/TOR signaling pathways upregulates Dally expression levels and its overexpression is able to phenocopy the effects on tissue growth, we next addressed whether Dally contributes to the autonomous and non-autonomous effects on tissue growth caused by targeted deregulation of the PI3K/PTEN and TSC/TOR signaling pathways. We thus depleted Dally in a condition where we drove Dp110 or Rheb expression in one compartment of the wing disc. For this purpose, we made use of a dsRNA against Dally. Expression of *dally*^{RNAi} in either the anterior or the posterior compartment of the wing, in an otherwise wild type background, caused a mild tissue-autonomous size reduction (Figure 44A and 44B, blue bars), but no visible size effects were observed in adjacent compartments (Figure 44A and 44B, white bars). The width of the Dpp activity gradient, monitored by the profile of pMAD expression, was mildly reduced in the transgene-expressing compartment (Figure 44E and 44F).

Interestingly, depletion of Dally was able to largely rescue not only the autonomous but also the non-autonomous effects on tissue growth caused by Rheb or Dp110/PI3K expression (Figure 45). The autonomous tissue overgrowth caused by Rheb expression in either the anterior or the posterior compartment of the wing was rescued when *dally* was depleted in those cells (Figure 45A, 45B, 45D and 45E, blue bars). The non-autonomous reduction in tissue size was completely rescued upon Dally depletion (Figure 45A, 45B, 45D and 45E, white bars). However, the non-autonomous reduction in cell size upon Rheb expression was not rescued upon *dally*^{RNAi} co-expression (Figure 45C and 45F, white bars). We observed similar autonomous and non-autonomous effects on tissue and cell size by depleting Dally upon Dp110/PI3K expression in the anterior domain (Figure 45G, 45H and 45I).

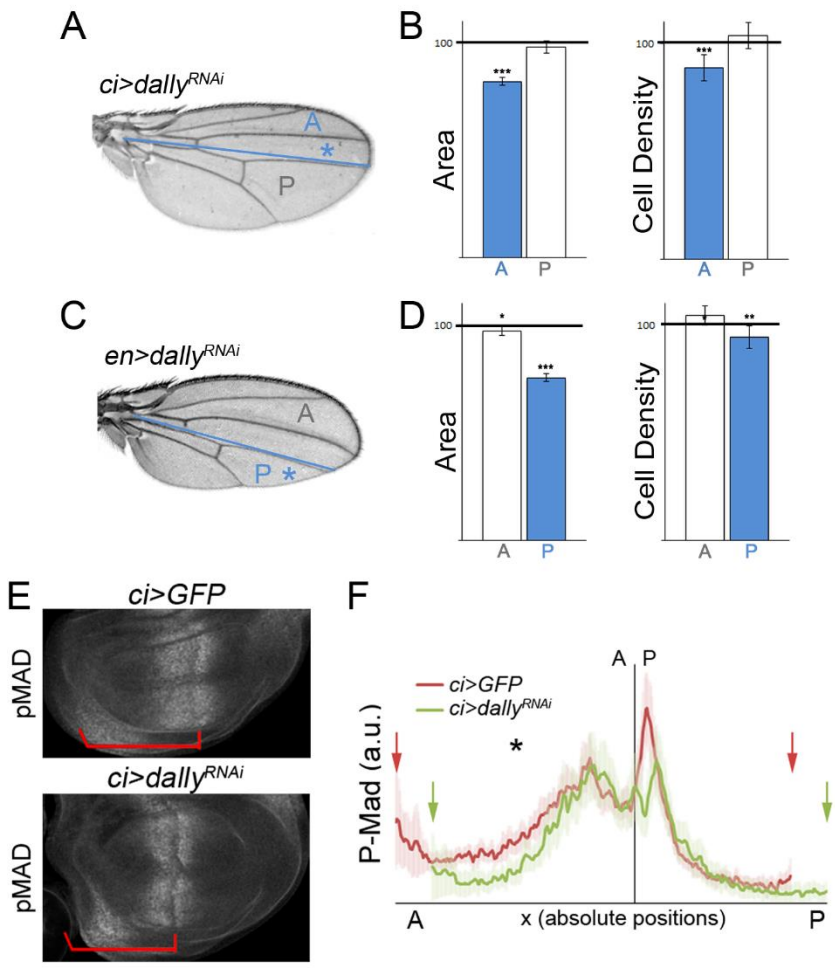

Figure 44. Dally depletion has little impact on tissue growth. (A, C) Cuticle preparations of male adult wings of *ci>dally*^{RNAi} (A) and *en>dally*^{RNAi} (C). The blue line marks the boundary between the anterior (A) and posterior (P) compartments, and the domains of transgene expression are marked with a blue asterisk. (B, D) Histograms plotting tissue size (on the left) and cell density values (on the right) of the transgene expressing domains (blue bars) and the adjacent compartments (white bars) of adult wings of *ci>dally*^{RNAi} (B) and *en>dally*^{RNAi} (D) animals. Values are normalized as a percent of the control GFP-expressing wings. Error bars show the standard deviation. Number of wings analyzed per genotype ≥ 10. ***p < 0.001; **p < 0.01; *p < 0.05; ns, not significant. (E) Wing imaginal discs of *ci>GFP* and *ci>dally*^{RNAi} larvae labelled to visualize pMAD protein (in white). Red brackets show the transgene-expressing compartment. (F) Average pMAD profiles of wing discs expressing GFP (red line) or dally^{RNAi} (green line) in the *ci* domain. Profiles were taken along the AP axis and plotted in absolute positions. The standard error to the mean is shown in the corresponding color for each genotype. The AP boundary of both experiments was aligned to allow comparison of the profile in each compartment. Number of wing discs analyzed per genotype ≥ 7. The domains of transgene expression are marked with a black asterisk. Arrows mark the limits of the Dpp activity gradients. See also Table 21.

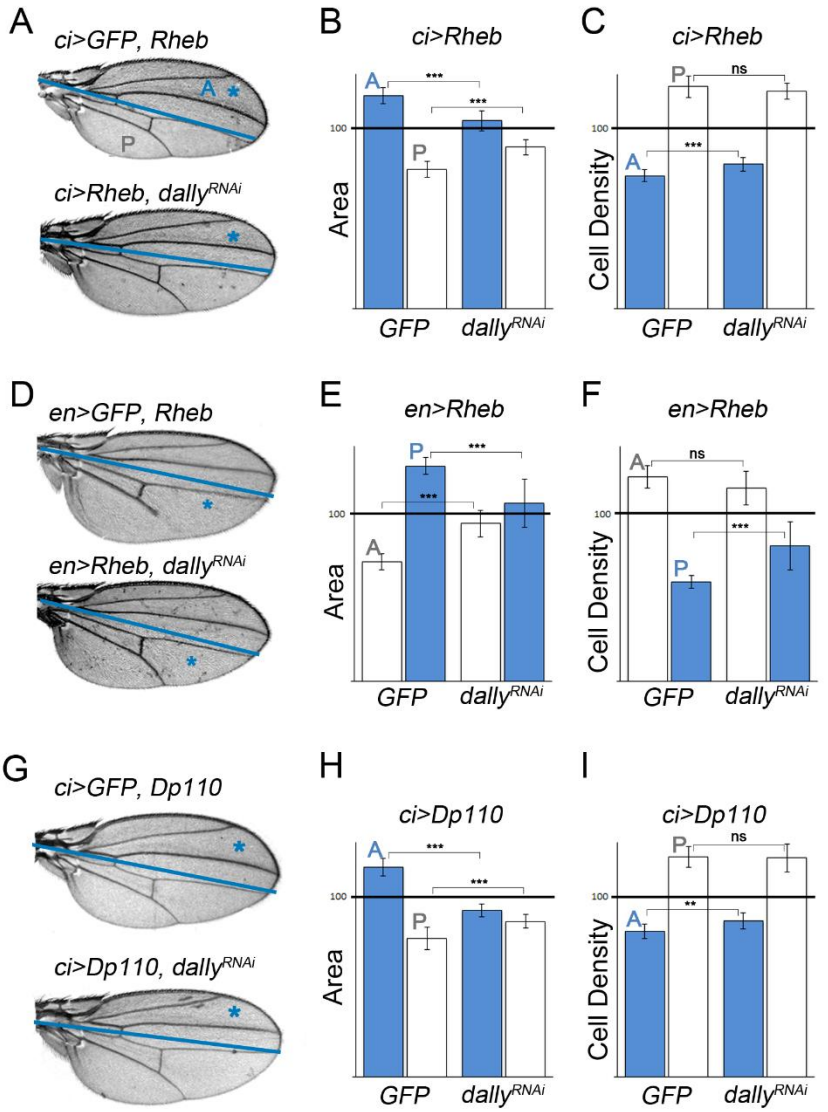

Figure 45. Dally contributes to the autonomous and non-autonomous effects of targeted activation of PI3K/PTEN and TSC/TOR pathways. (A, D, G) Cuticle preparations of adult wings expressing the indicated transgenes under the control of the *ci-gal4* (A, G) or *en-gal4* (D) drivers. The blue line marks the boundary between the anterior (A) and posterior (P) compartments and the domains of transgene expression are marked with a blue asterisk. (B, C, E, F, H, I) Histograms plotting tissue size (B, E, H) and cell density (C, F, I) values of the transgene-expressing (blue bars) or nonexpressing (white bars) compartments of adult wings driving expression of the indicated transgenes under the control of the *ci-gal4* (B, C, H, I) or *en-gal4* (E, F) drivers. Values are normalized as a percent of the control GFP-expressing wings .Error bars show the standard deviation. Number of wings analyzed per genotype ≥ 10. ***p < 0.001; ** p < 0.01; ns, not significant. See also Table 22.

Upon expression of a dsRNA against Dally in wing discs expressing Dp110/PI3K in the anterior compartment, the autonomous expansion of the Dpp activity gradient and the non-autonomous retraction caused by targeted expression of Dp110 were both largely rescued (Figure 46A). We observed a slight increase in Dpp signaling in the non-autonomous territory upon Dally depletion when compared to targeted activation of Dp110 alone (Figure 46B, white bars).

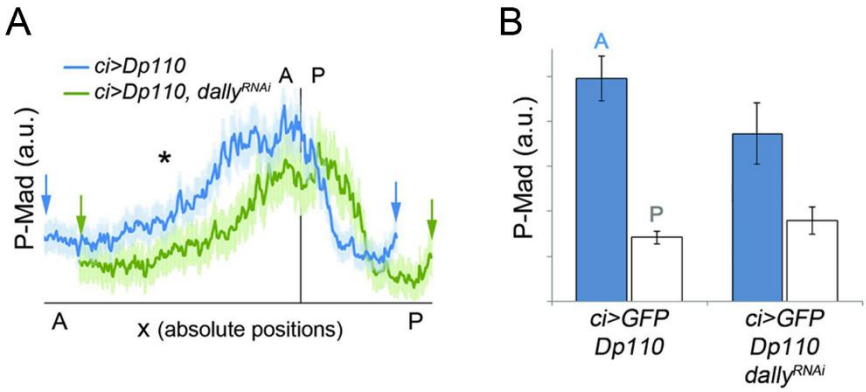

Figure 46. Dally contributes to the expansion of the Dpp activity gradient upon activation of growth. (A) Average pMAD profiles of wing discs expressing *GFP* and *Dp110* (blue line) or *GFP*, a dsRNA against *dally* and *Dp110* (green line) under the control of the *ci-gal4* driver. Profiles were taken along the AP axis and plotted in absolute positions. The standard error to the mean is shown in the corresponding color for each genotype. The AP boundary of both experiments was aligned to allow comparison of the profile in each compartment. Number of wing discs analyzed per genotype ≥ 5. The domains of transgene expression are marked with a black asterisk. Arrows mark the limits of the Dpp activity gradients. (B) Histogram plotting the total intensity of pMAD signal in a.u. of the anterior (blue bars) and posterior (white bars) compartments of *ci>GFP, Dp110* and *ci>Dp110, dallyRNAi* wing discs. Error bars indicate the standard error to the mean. Number of wing discs analyzed per genotype ≥ 5. ns, not significant. See also Table 23.

Sulfateless (Sfl), an enzyme needed for the modification of HS chains within glypicans (Lin and Perrimon, 1999), is essential in the biosynthetic cascade of Dally. Additionally, it has been shown that in *sfl* mutant clones Dpp-GFP movement is blocked (Belenkaya et al., 2004), probably due to lack of a functional form of Dally. When we depleted *sulfateless* in posterior cells with activated PI3K/PTEN signaling, we observed that both the autonomous increase and the non-autonomous reduction in tissue size were rescued (Figure 47A and 47B). The

drastic autonomous reduction in compartment size is most probably due to the strong impact on tissue size that depletion of this enzyme already causes in an otherwise wild type background (Figure 48A-D, blue bars). Most importantly, the targeted expression of dsRNA forms against *sfl* in otherwise wild type wings has little effect on growth of adjacent cell territories (Figure 48A-D, white bars). Overall, we conclude that Dally contributes to the autonomous and non-autonomous effects on tissue growth caused by activation of PI3K/PTEN and TSC/TOR signaling pathways. However, given the fact that depletion of Dally was not able to rescue the non-autonomous reduction in cell size caused by activation of these pathways (Figure 45C, 45F and 45I, white bars), we propose that cell size is non-autonomously regulated by the PI3K/PTEN and TSC/TOR pathways in a Dally-independent manner.

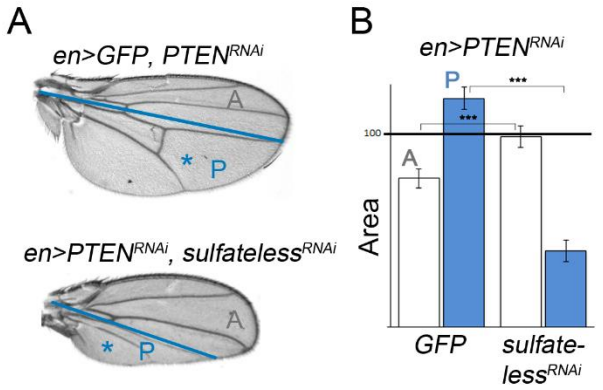

Figure 47. Depletion of *sfl* rescues the autonomous and non-autonomous effects on tissue growth. (A) Cuticle preparations of adult wings expressing *GFP* and *PTEN*^{RNAi} or *PTEN*^{RNAi} and *sulfateless*^{RNAi} under the control of the *en-gal4* driver. The blue line marks the boundary between the anterior (A) and posterior (P) compartments, and the domains of transgene expression are marked with a blue asterisk. (B) Histogram plotting tissue size of the transgene-expressing (blue bars) or nonexpressing (white bars) compartments of adult wings showed in A. Values are normalized as a percent of the control GFP-expressing wings. Error bars show the standard deviation. Number of wings analyzed per genotype ≥ 10. ***p < 0.001. See also Table 24.

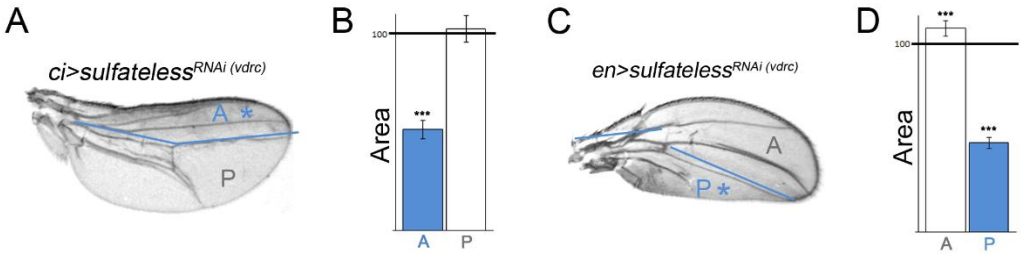

Figure 48. Depletion of *sfl* strongly reduces tissue size autonomously. (A, C) Cuticle preparations of adult wings expressing *sulfateless*^{RNAi} under the control of the *ci-gal4* (A) or the *en-gal4* (C) drivers. The blue line marks the boundary between the anterior (A) and posterior (P) compartments and the domains of transgene expression are marked with a blue asterisk. (B, D) Histograms plotting tissue size of the transgene-expressing (blue bars) or nonexpressing (white bars) compartments of adult wings of *ci>sulfateless*^{RNAi} (B) or *en>sulfateless*^{RNAi} (D). Values are normalized as a percent of the control GFP-expressing wings. Error bars show the standard deviation. Number of wings analyzed per genotype ≥ 10. ***p < 0.001; ns, not significant. See also Table 25.

Dally contributes to the autonomous and non-autonomous effects on tissue growth upon targeted inactivation of the Hippo signaling pathway

Inactivation of the Hippo pathway causes a reduction in tissue size in adjacent wild type cell populations

Mutations in the Hippo pathway, originally identified in *Drosophila* by their capacity to induce cell proliferation and organ growth, induce tumors in mouse models and occur in a broad range of human carcinomas, including lung, colorectal, ovarian, and liver cancers (reviewed in (Harvey et al., 2013)). Similar to what happened to TOR activation, deregulation of the Hippo/Yorkie pathway causes strong overgrowth and larval lethality (Justice et al., 1995). We thus induced a mild activation of the pathway by expressing a wild type form of the transcription factor Yorkie (Yki). Overexpression of Yki in the anterior or posterior compartments of the developing wing gave rise to a tissue-autonomous increase in size (Figure 49A, 49B, 49D and 49E, blue bars) and, most interestingly, a non-autonomous size reduction of the adjacent wild type territories (Figure 49A,

49B, 49D and 49E, white bars). Consisting with the role of Hippo signaling in driving cell proliferation, the cell densities were higher than GFP-expressing controls in the transgene expressing compartment (Figure 49C and 49F, blue bars). As shown before in the case of PI3K/PTEN and TSC/TOR activation, Yki overexpression also caused a non-autonomous decrease in cell size (Figure 49C and 49F, white bars).

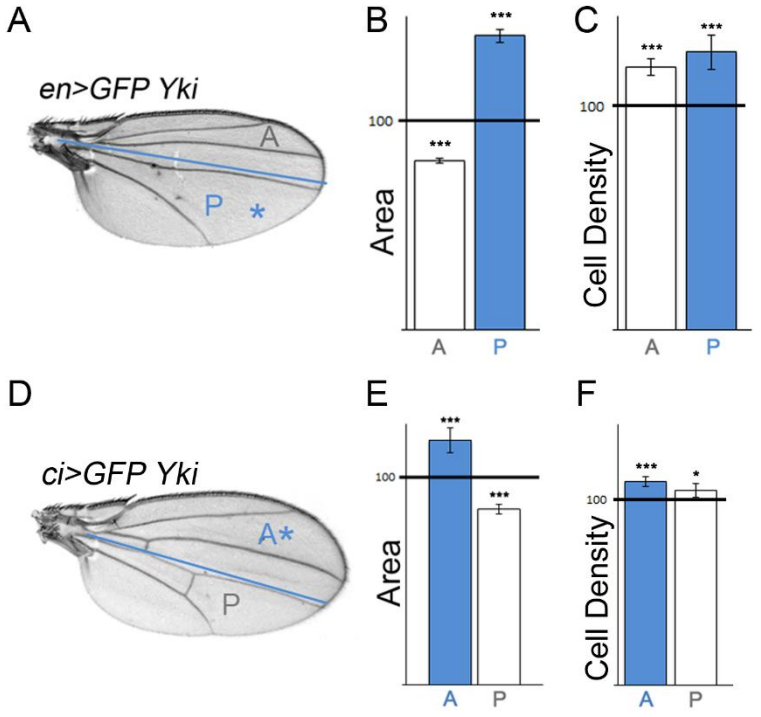

Figure 49. Yki overexpression causes a reduction in tissue and cell size of the adjacent domains. (A, D) Cuticle preparations of adult wings expressing *Yki* under the control of the *en-gal4* (A) or *ci-gal4* (D) drivers. The blue line marks the boundary between the anterior (A) and posterior (P) compartments and the domains of transgene expression are marked with a blue asterisk. (B, C, E, F) Histograms plotting tissue size (B, E) and cell density (C, F) of the transgene-expressing (blue bars) or nonexpressing (white bars) compartments of adult wings expressing *Yki* under the control of the *en-gal4* (B, C) or *ci-gal4* (E, F) drivers. Values are normalized as a percent of the control GFP-expressing wings .Error bars show the standard deviation. Number of wings analyzed per genotype ≥ 10. ***p < 0.001; * p < 0.05. See also Table 26.

Dally, and not Dally-like, contributes to the autonomous and non-autonomous effects on tissue growth upon targeted inactivation Hippo/Yorkie signaling

It was previously shown that the expression levels of the two existing *Drosophila* glypicans, Dally and Dally-like, are up-regulated upon deregulation of the Hippo/Yorkie pathway (Baena-Lopez et al., 2008). Indeed, overexpression of the wild type form of Yki in the anterior compartment caused an up-regulation of Dally at the transcriptional level (Figure 50A and 50B) and Dally-like protein levels (Figure 50C and 50D).

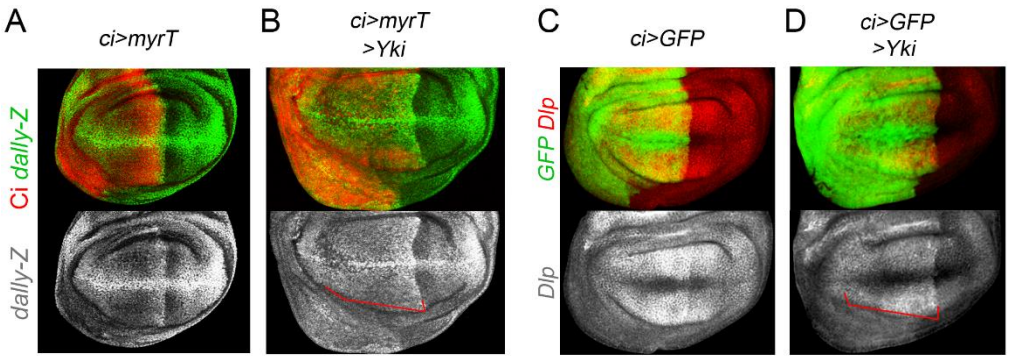

Figure 50. Yki overexpression upregulates levels of Dally and Dally-like. (A, B) Wing imaginal discs of *ci>myrT* (A) and *ci>myrT, Yki* (B) labelled to visualize *dally-lacZ* (antibody to β-Gal, green or white) and myrTomato (myrT, in red) expression to mark the transgene-expressing domain. Note stronger expression of *dally-lacZ* upon Yki overexpression (red brackets). (C, D) Wing imaginal discs of *ci>GFP* (C) and *ci>GFP, Yki* (D) labelled to visualize Dally-like protein (in red or white) and GFP expression to mark the transgene-expressing domain. Note higher levels of Dlp in Yki overexpressing cells (red brackets).

Loss of both Dally and Dally-like has been shown to rescue the overgrowth of clones of cells overexpressing Yorkie (Baena-Lopez et al., 2008). We thus revisited the contribution of these two glypicans to the autonomous effects on tissue growth caused by deregulation of the Hippo/Yorkie pathway and analyzed whether they also contribute to the non-autonomous effects on tissue size of the adjacent cell populations. Interestingly, Dally depletion in the Yki-overexpressing

domain was able to rescue both the autonomous and non-autonomous effects on tissue size (Figure 51A and 51B).

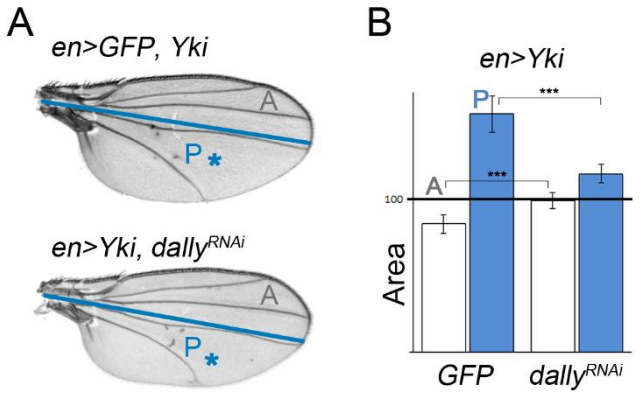

Figure 51. The autonomous and non-autonomous effects on tissue growth due to Yki overexpression depend on Dally. (A) Cuticle preparations of adult wings expressing *Yki* and *GFP* or *Yki* and *dally*^{RNAi} under the control of the *en-gal4* driver. The blue line marks the boundary between the anterior (A) and posterior (P) compartments and the domains of transgene expression are marked with a blue asterisk. (B) Histogram plotting tissue size of the transgene-expressing (blue bars) or nonexpressing (white bars) compartments of adult wings showed in A. Values are normalized as a percent of the control GFP-expressing wings. Error bars show the standard deviation. Number of wings analyzed per genotype ≥ 10. ***p < 0.001. See also Table 27.

By contrast, Dally-like depletion, using two different dsRNA forms able to reduce its protein levels (Figure 52C), was not able to rescue the non-autonomous decrease in tissue size caused by Yki activation (Figure 52A and 52B, white bars). It was previously described that Dally-like contributes to the overgrowth caused by Yki overexpression (Baena-Lopez et al., 2008). However, in our case depletion of Dally-like was not able to rescue the overgrowth of Yki overexpression (Figure 52A and 52B, blue bars).

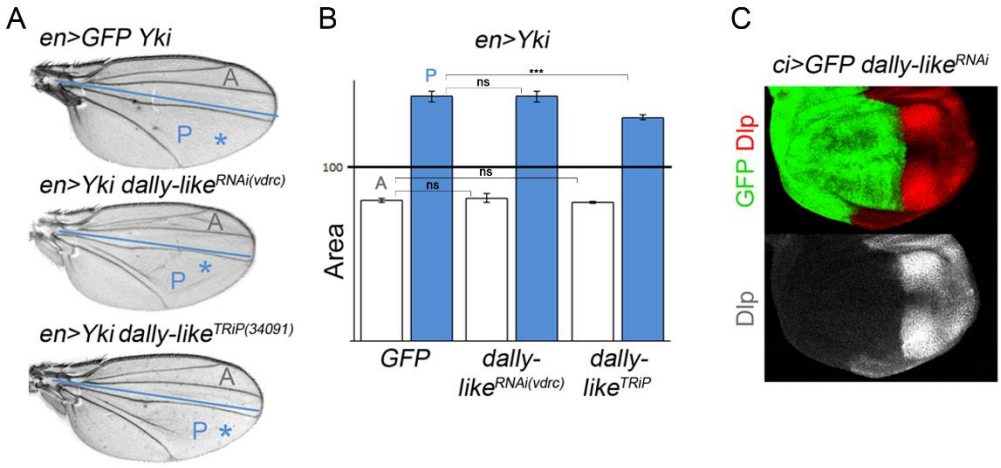

Figure 52. Dally-like does not contribute to the non-autonomous effects on tissue growth due to Yki overexpression. (A) Cuticle preparations of adult wings expressing *Yki* and *GFP* or *Yki* and two different dsRNA against Dally-like under the control of the *en-gal4* driver. The blue line marks the boundary between the anterior (A) and posterior (P) compartments and the domains of transgene expression are marked with a blue asterisk. (B) Histogram plotting tissue size of the transgene-expressing (blue bars) or nonexpressing (white bars) compartments of adult wings showed in A. Values are normalized as a percent of the control GFP-expressing wings. Error bars show the standard deviation. Number of wings analyzed per genotype ≥ 10. ***p < 0.001; ns, not significant. (C) Wing imaginal disc driving expression of a dsRNA against Dally-like in the anterior domain labelled to visualized Dlp protein levels (in red or white) and GFP (in green) expression to mark the transgene-expressing domain. Note that the *dally-like*^{RNAi} is able to strongly reduce Dally-like protein levels. See also Table 28.

Altogether, the results presented above indicate that Dally, and not Dally-like, contributes to the tissue-autonomous and non-autonomous effects on tissue growth caused by targeted deregulation of the PI3K/PTEN, TSC/TOR, and Hippo/Yorkie signaling pathways. These pathways exert their tissue-autonomous action through Dally, most probably by modulating the spreading of the Dpp morphogen and other secreted growth factors, as Dp110 overexpression was still able to induce growth in Dpp-depleted tissues (Figure 36B, blue bars). We hypothesize that the non-autonomous effects are a consequence of withdrawal of Dpp from neighboring cells. To further reinforce this idea, we carried out some experiments in which Dpp is trapped to specific territories in a Dally-independent manner.

Dpp trapping, by modulation of its receptor, also causes a non-autonomous reduction in tissue size

The Dpp type I receptor Thickveins (Tkv) has been shown to trap the Dpp ligand and limit its spreading. Clones of cells overexpressing the receptor show graded expression of Dpp target genes with higher levels closer to the Dpp source (Lecuit and Cohen, 1998). Therefore, we decided to analyze the capacity of Tkv to phenocopy the non-autonomous effects on tissue growth observed upon targeted deregulation of the PI3K/PTEN, TSC/TOR and Hippo/Yorkie pathways. For this purpose, we overexpressed a wild type or a dominant negative form of the receptor that is able to bind the Dpp ligand but unable to transduce the signal (Kumar and Moses, 2001). Driving expression of both transgenes in the anterior or in the posterior compartment of the wing primordia gave rise to an expected autonomous reduction in tissue size due to a dampening in the activity of the Dpp pathway (Figure 53, blue bars). Remarkably, it caused a non-autonomous size reduction of the adjacent wild type territories (Figure 53, white bars). Expression of the dominant negative form of Tkv did not influence cell size, since no major changes were observed in cell densities values in the autonomous nor in the non-autonomous compartment (Figure 53F and 53H). This latter observation is consistent with the fact that changes in Dpp signaling do not cause any effect on cell size (Martín-Castellanos and Edgar, 2002). This, together with the result that overexpression of Dally did not cause a non-autonomous reduction in cell size (Figure 40B and 40D), indicate that Dally and Dpp are regulating cell number but not cell size. Once again, these data reinforce the idea that the non-autonomous effects on cell size observed upon deregulation of the PI3K/PTEN, TSC/TOR, or Hippo/Yorkie pathways are Dally and Dpp independent.

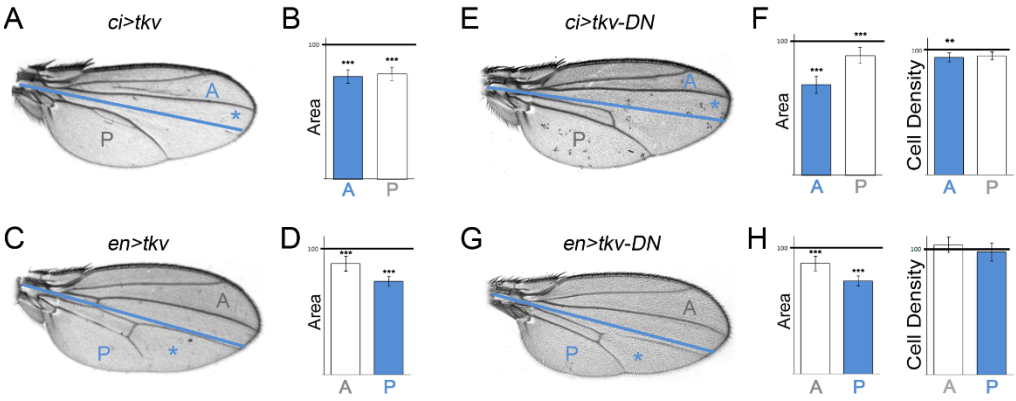

Figure 53. Increase Dpp trapping by Tkv causes a non-autonomous reduction in tissue size. (A, C, E, G) Cuticle preparations of adult wings expressing *tkv* (A, C) or *tkv*^{DN} (E, G) under the control of the *ci-gal4* (A, E) and the *en-gal4* (C, G) drivers. The blue line marks the boundary between the anterior (A) and posterior (P) compartments and the domains of transgene expression are marked with a blue asterisk. (B, D) Histograms plotting tissue size of the transgene-expressing (blue bars) or nonexpressing (white bars) compartments of adult wings showed in A and C respectively. (F, H) Histograms plotting tissue size (left) and cell density values (right) of the transgene-expressing (blue bars) or nonexpressing (white bars) compartments of adult wings showed in E and G respectively. Values are normalized as a percent of the control GFP-expressing wings. Error bars show the standard deviation. Number of wings analyzed per genotype ≥ 10. ***p < 0.001; **p < 0.01; ns, not significant. See also Table 29.

Thus, high levels of the Tkv receptor trap Dpp and trigger "competition" for the ligand, thus inducing a non-autonomous reduction in tissue size of neighboring wild type cell populations. Consistent with this, co-expression of the Tkv^{DN} together with a dsRNA against PTEN was able to further enhance the non-autonomous reduction in tissue size seen with depletion of PTEN alone (Figure 54, white bars), similarly to the overexpression of Dally (Figure 41). In this case, the size of the transgene expressing compartment was slightly rescued due to a reduction of Dpp activity caused by the dominant negative form of Tkv (Figure 54, blue bars). These results emphasize the role of Dpp in modulating the growth and pattern of different cell populations within a developing organ.

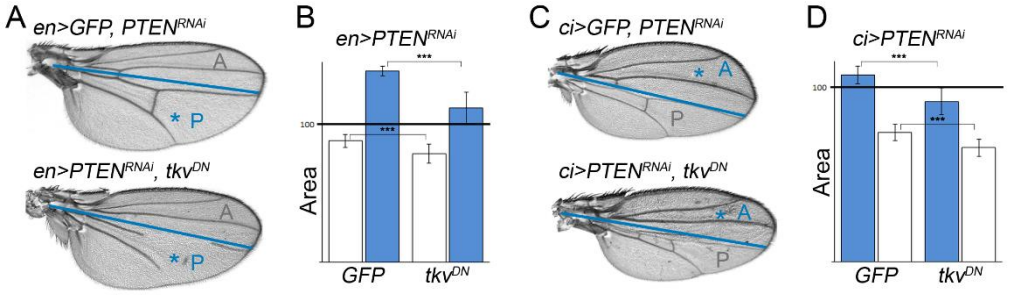

Figure 54. Increase Dpp trapping by Tkv upon targeted activation of PI3K/PTEN signaling pathway enhances the non-autonomous reduction in tissue size. (A, C) Cuticle preparations of adult wings expressing *GFP* and *PTEN*^{RNAi} or *PTEN*^{RNAi} and *tkv*^{DN} under the control of the *en-gal4* (A) and the *ci-gal4* (C) drivers. The blue line marks the boundary between the anterior (A) and posterior (P) compartments and the domains of transgene expression are marked with a blue asterisk. (B, D) Histograms plotting tissue size of the transgene-expressing (blue bars) or nonexpressing (white bars) compartments of adult wings showed in A and C respectively. Values are normalized as a percent of the control GFP-expressing wings. Error bars show the standard deviation. Number of wings analyzed per genotype ≥ 10. ***p < 0.001. See also Table 30.

Overall, we show that targeted activation of growth promoting pathways to specific territories of the wing imaginal disc triggers the trapping of the Dpp ligand towards those cells, due to an increase in Dally levels, and as such the adjacent wild type cell populations suffer a decrease in the growth and proliferation rates due to a reduction in Dpp activity. Moreover, trapping of the Dpp ligand by other means also showed a non-autonomous reduction in size of the adjacent territories. We speculate that this could be one strategy used by malignant mutation-carrying cells, in the early stages of tumorigenesis, to outcompete the surrounding wild type cells and, as such, accelerate their colonization.

Dally, a Molecular Bridge between Nutrition and Wing Scaling

Depletion of Dally rescues the overgrowth caused by activation of PI3K/PTEN and TSC/TOR signaling pathways

The PI3K/PTEN and TSC/TOR signaling pathways play a conserved role in nutrient sensing and tissue growth during normal development. In the *Drosophila* wing, they modulate the final size of the adult structure according to nutrient availability of the feeding animal [reviewed in (Grewal, 2009; Neufeld, 2003)], and Dpp plays an organ-intrinsic role in the coordination of growth and patterning [reviewed in (Restrepo et al., 2014; Wartlick et al., 2011b)]. The molecular mechanisms that integrate the organ-extrinsic with the organ-intrinsic regulators of growth remain mysterious. The identification of the proteoglycan Dally as the rate-limiting factor that contributes to the tissue-autonomous and non-autonomous effects on growth caused by targeted activation of the nutrient-sensing PI3K/PTEN and TSC/TOR pathways presented in this thesis suggests that Dally acts as a molecular bridge between the organ-intrinsic and organ-extrinsic mechanisms that regulate organ size. Consistent with this proposal, activation of the PI3K/PTEN or TSC/TOR pathways, which mimics conditions of high nutrient availability, led to an increase in Dally expression levels (Figure 39). Moreover, activation of both PI3K/PTEN or TSC/TOR signaling pathways in the wing pouch, using the *nub-gal4* driver, lead to larger adult wings (Figure 55, see also Figure 15), and depletion of Dally rescued that resulting overgrowth (Figure 55, see also Figure 45). These data indicate that Dally contributes to the tissue overgrowth caused by activation of these pathways.

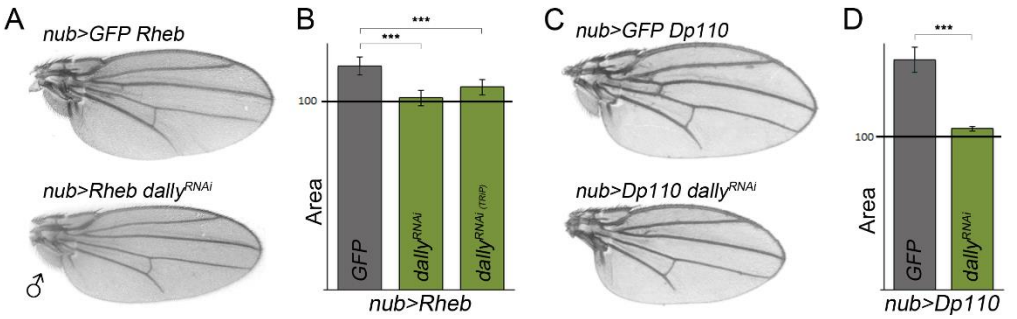

Figure 55. Dally depletion rescues the overgrowth caused by activation of PI3K/PTEN and TSC/TOR signaling. (A-D) Cuticle preparations (A, C) and histograms plotting tissue size normalized as a percent of the control wings (B, D) of *nub>Rheb* (A, B) or *nub>Dp110* (C, D) adult wings co-expressing either *GFP* or *dally*^{RNAi}. Two independent RNA interference (RNAi) lines were used in B. Error bars show the standard deviation. Number of wings analyzed per genotype ≥ 10. ***p < 0.001. See also Table 31.

Dally expression is reduced upon reduced PI3K/PTEN and TSC/TOR activity

We next addressed whether reduced wing size caused by inactivation of the PI3K/PTEN or TSC/TOR pathways, which mimics conditions of low nutrient availability, relies, at least in part, on reduced expression levels of Dally. Upon depletion of the PI3K/PTEN or TSC/TOR signaling pathways (by expressing dsRNA forms against the Insulin-like Receptor [InR] and Rheb, respectively) Dally expression levels, visualized by the *dally-lacZ* reporter, were reduced (Figure 56).

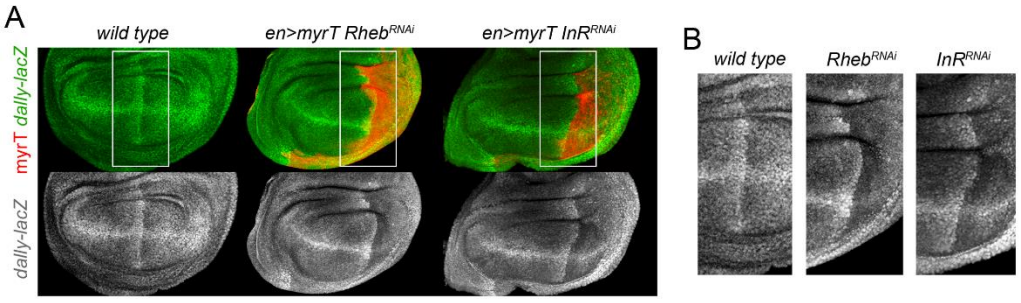

Figure 56. Dally levels are reduced upon inactivation of the PI3K/PTEN and TSC/TOR signaling. (A) Representative wing discs of the indicated genotypes labelled to visualize *dally-lacZ* (antibody to β-Gal, green or white) and myrT expression (in red) marks the transgene-expressing domain. (B) Higher magnification pictures of the squared regions shown in A. Note the reduced expression of *dally-lacZ* upon depletion of the TSC/TOR or PTEN/PI3K pathways.

To know whether the observed reduction in Dally expression levels was responsible for the tissue size defects caused by depletion of the PI3K/PTEN pathway, we overexpressed Dally in cells depleted for Dp110. We noticed that Dally overexpression was able to partially rescue the tissue size defects caused by depletion of the PI3K/PTEN signaling pathway (Figure 57A and 57B). As expected from the results obtained before, the cell size defects were not rescued upon Dally overexpression (Figure 57A, lower panels). These results indicate that the tissue size defects caused by depletion of this pathway rely, at least in part, on the observed reduction in Dally expression levels.

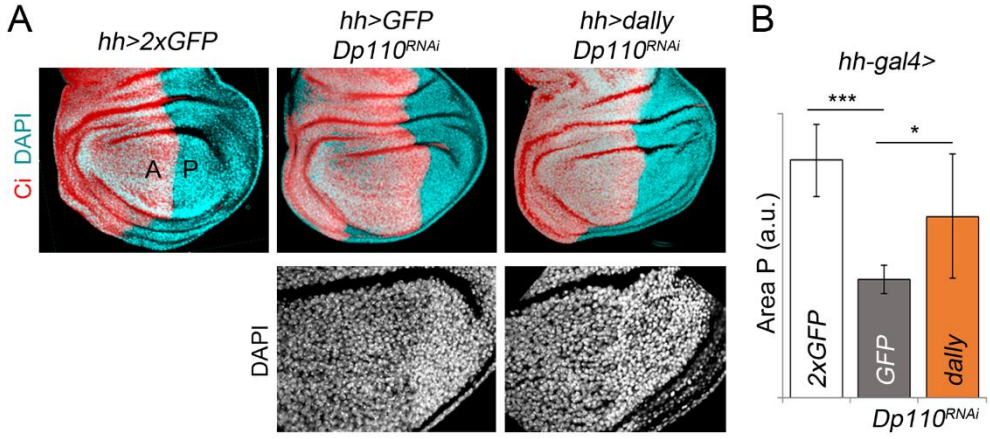

Figure 57. Overexpression of Dally partially rescues the defects of Dp110 depletion. (A) Representative wing discs of the indicated genotypes and labelled to visualize Ci protein (red) to label the anterior compartment and DAPI (in cyan). (B) Histogram plotting the P/A size ratio of wing discs of the indicated genotypes. Error bars show the standard deviation. Number of wing discs analyzed per genotype ≥ 10. ***p < 0.001; *p < 0.05. See also Table 32.

By contrast, Dally overexpression was only able to slightly rescue the tissue size defects caused by depletion of the TSC/TOR pathway (Figure 58A), again without any impact on cell size (Figure 58B) suggesting that other elements are required, together with Dally, to mediate TSC/TOR-dependent tissue growth.

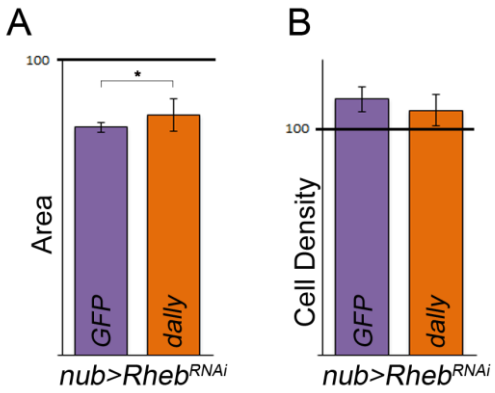

Figure 58. Overexpression of Dally slightly rescues the defects of Rheb depletion. (A, B) Histograms plotting tissue size (A) and cell density (B) values normalized as a percent of the control (*nub>GFP*) of *nub>Rheb*^{RNAi} adult wings co-expressing either *GFP* or *Dally*. Error bars show the standard deviation. Number of wings analyzed per genotype ≥ 10. *p < 0.05. See also Table 33.

In order to further reinforce the idea of Dally working as a molecular bridge between nutrient-sensing pathways and organ-intrinsic mechanisms, we subjected experimental and control larvae to media containing high (100 g/L yeast) or low (20 g/L yeast) levels of amino acids and analyzed the size of the resulting adult wings upon expression of Dally or a dsRNA form against Dally in the whole wing primordium. As expected, the total wing size of control *nub>GFP* animals was reduced in those larvae reared on food containing 20 g/L yeast (Figure 59, grey bars). Despite of that, the size of Dally-overexpressing wings (which slightly increases the range of Dpp signaling without affecting the shape of the activity gradient, see Figure 60) was comparable to that of animals receiving food containing 100 g/L yeast (Figure 59, orange bar). Similarly, despite the expected increase in animal size reared on food containing 100 g/L yeast, the size of Dally depleted wings was comparable to that of animals receiving 20 g/L yeast food (Figure 59, green bar).

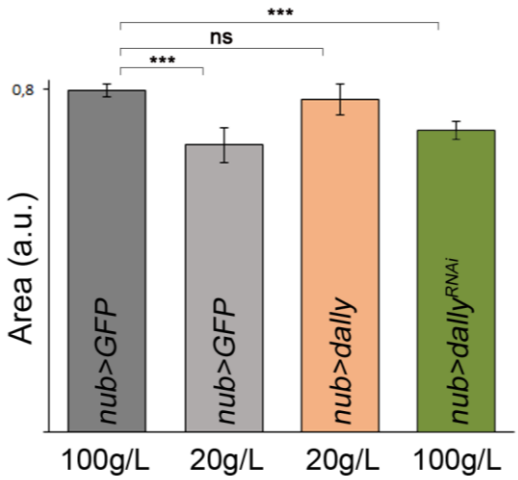

Figure 59. Modulation of Dally in different nutrient conditions. Histogram plotting absolute size in a.u. of adult wings of the indicated genotypes. Quantification was made in well-fed (100 g/L yeast food) and starved (20 g/L yeast food) animals. Error bars show the standard deviation. Number of wings analyzed per genotype ≥ 10. ***p < 0.001; ns, not significant. See also Table 34.

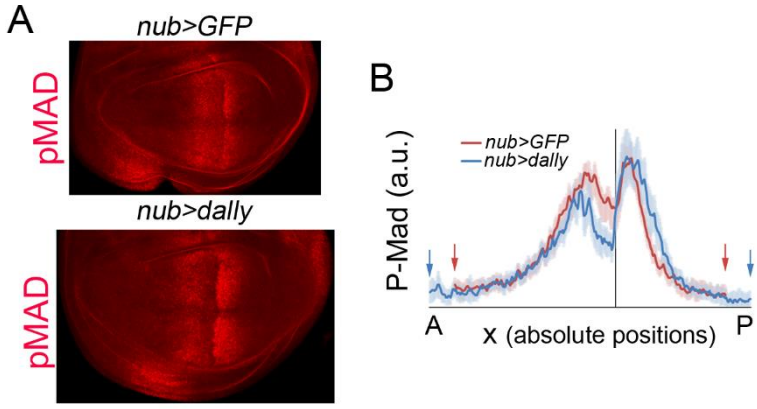

Figure 60. Dally overexpression in the wing pouch affects the range but not the shape of the activity gradient. (A) Wing imaginal discs of *nub>GFP* and *nub>dally* larvae labelled to visualize pMAD protein (in red). (B) Average pMAD profiles of wing discs expressing *GFP* (red line) or *Dally* (blue line) in the *nubbin* domain. Profiles were taken along the AP axis and plotted in absolute positions. The standard error to the mean is shown in the corresponding color for each genotype. The AP boundary of both experiments was aligned to allow comparison of the profile in each compartment. Number of wing discs analyzed per genotype ≥ 7. Arrows mark the limits of the Dpp activity gradients.

All together, these results reveal that Dally proteoglycan participates in integrating nutrient conditions into wing scaling, most probably through its ability to facilitate the spread of Dpp throughout the tissue.

Discussion

Discussion

During development, the coordination of growth between and within organs is fundamental to assure the emergence of animals with proper body/organ size and proportions. Nutrient conditions, through the activity of nutrient sensing pathways, such as the phosphatidylinositol 3-kinase (PI3K)–phosphatase with tensin homology (PTEN) and the tuberous sclerosis complex (TSC)–target of rapamycin (TOR) signaling pathways, cautiously modulate the final size of a developing organ. In addition, patterning signals operate in an autonomous way to control growth of an organ. How cells integrate distinct inputs (extrinsic and intrinsic signals) to generate organs of appropriate size and shape remains unknown. Interestingly, the PI3K/PTEN and TSC/TOR pathways are frequently activated in human cancer. This activation is often causative of tumorigenesis and raises the question of how cells acquiring mutations in tumor suppressor genes outcompete neighboring wild type cells. In order to tackle these two issues, we used the *Drosophila* wing to deregulate the PI3K/PTEN and TSC/TOR pathways in specific cell populations. The results presented in this thesis unravel a new role for the glypican Dally, which functions in regulating the spread of Dpp in *Drosophila* tissues, in contributing to the autonomous and non-autonomous effects of deregulation of these tumor suppressor pathways. The ability of Dally to trap the growth factor Dpp helps to integrate organ-extrinsic with organ-intrinsic signals that modulate the growth of the wing imaginal disc. Moreover, this strategy might be used by cancer cells to efficiently outcompete the neighboring wild type cells.

A new process of cell competition

Targeted deregulation of the PI3K/PTEN, TSC/TOR, or Hippo/Yorkie signaling pathways not only promotes tissue overgrowth in an autonomous manner by increasing the number and/or size of cells, but also induces a consistent non-autonomous reduction in tissue size of the adjacent wild type cell populations. This non-autonomous effect is a consequence of a reduction in both cell size and proliferation rates (cell number). The reduction in proliferation rates is most probably a consequence of longer cell division cycles as we did not see any obvious arrest in any particular cell cycle stage. The non-autonomous reduction in size resembles the process of cell competition described as the ability of cells with a growth advantage to eliminate the neighboring wild type cells by apoptosis. However, targeted activation of these pathways did not induce non-autonomous apoptosis and, moreover, reducing the apoptotic machinery by different means did not rescue the non-autonomous reduction in tissue size. Effector caspases and the Dp53 tumor suppressor protein have an important role in reducing the growth and proliferation rates of adjacent wild type territories upon targeted depletion of the translational machinery (Mesquita et al., 2010). Even though targeted deregulation of the PI3K/PTEN, TSC/TOR, or Hippo/Yorkie signaling pathways induced a clear autonomous increase in the number of apoptotic cells, neither the caspases nor Dp53 were responsible for the non-autonomous reduction in tissue size and proliferation rates in our case. Another possibility is that the non-autonomous reduction in size is a consequence of the withdrawal of nutrients from neighboring tissues by the overgrowing populations based on the observation that competition for nutrients contributes to the growth of *PTEN* mutant cells and to the out-competition of wild type surrounding cells (Nowak et al., 2013). However, this idea was over-ruled by the experimental observation that subjecting larvae to different amino acid diets did not have any impact on the size reduction of neighboring cell populations. This difference may rely on the fact that

Dpp is only required from growth in the wing imaginal disc while in the eye disc it is not.

Interestingly, we observed that the width of the Dpp activity gradient as well as the total amount of Dpp activity were both reduced in adjacent cell populations upon targeted de-regulation of these tumor suppressor pathways. This led us to propose that the non-autonomous reduction in tissue size is a consequence of reduced Dpp signaling, most probably reflecting increased number of Dpp molecules bound to the overgrowing tissue and a consequent reduction in the number of Dpp molecules available in the neighboring cell population (Figure 61). Consistent with this proposal, the non-autonomous effects on tissue size were no longer seen in the absence of the Dpp ligand, suggesting that targeted activation of growth promoting pathways triggers competition for the growth factor Dpp availability. It has been proposed that classical cell competition can be also due to competition for Dpp ligand availability, since loser cells upregulate Brk expression which triggers JNK activation and apoptosis (Moreno et al., 2002). Again, we did not see apoptosis in the territories with reduced Dpp activity. One possibility is that confronting cells with drastic differences in Brk expression levels is the responsible for triggering apoptosis. Another possibility is that elimination of loser clones could also be partially induced by the mechanical constraints imposed by the vicinity of fast growing clones and cell crowding. This could explain the insulating role of compartment boundaries on cell competition, which through the local upregulation of cortical tension, could mitigate the communication of mechanical stress from one compartment to the other (Landsberg et al., 2009).

Whether the term competition can be used to describe what we see upon targeted activation of growth might be controversial mainly because the concept of cell competition is tightly linked to apoptosis and also it does not cross the compartment boundaries of the wing imaginal disc. However, taking the concept of competition as a contest, between two or more groups, for resources, we can say that upon targeted activation of growth a competition for the amount of Dpp

ligand is being triggered. Nevertheless, this competition is not normally occurring during development, since making a territory less efficient in the trapping of the ligand (depleting Dally, for example) did not cause any overgrowth and/or an increase in Dpp activity in the neighboring cell populations. Finally, other pathways have been related to cell competition, and yet they differ from the classical view as they do not require induction of apoptosis. This includes activation of Ras (Hogan et al., 2009) and Scr in mammalian epithelial cultured cells (Kajita et al., 2010), and clones of cells mutant for Csk in *Drosophila* (Vidal et al., 2006) and, in those scenarios, their out-competition is due to context-dependent effects on epithelial cell extrusion. As mentioned before, competition for nutrients availability has also been shown to contribute to the out-competition of wild type cells by PTEN mutant cells (Nowak et al., 2013). All these examples may fit into a broader definition of cell competition than the one that is currently accepted.

A new role for Dally

We showed that the glypican Dally, which plays a major role in regulating the spread of Dpp in *Drosophila* tissues, is upregulated upon activation of the PI3K/PTEN, TSC/TOR, or Hippo/Yorkie signaling pathways and that the increase in Dally expression levels contributes to the autonomous effects on tissue size and to the non-autonomous reduction in cell number. Whereas the autonomous effects on tissue size caused by deregulation of these tumor suppressor pathways are most probably due to, as least in part, the capacity of Dally to facilitate Dpp spreading throughout the tissue, we propose that the non-autonomous effects on cell number are a consequence of withdrawal of Dpp from neighboring tissues (Figure 61). The non-autonomous reduction in tissue size is a consequence of reduced Dpp signaling, most probably reflecting increased number of Dpp

molecules bound to the overgrowing (Dally-upregulated) tissue and a consequent reduction in the number of Dpp molecules available in the neighboring cell population. This proposal is based on a number of observations. First, the width of the Dpp activity gradient, as well as the total amount of Dpp activity, was reduced in adjacent cell populations upon targeted depletion of tumor suppressor pathways. Second, the non-autonomous effects on tissue size did not occur in the absence of Dpp. Third, the non-autonomous effects on tissue size were fully rescued by Dally depletion, which has a rather specific role on the spread of Dpp when overexpressed. Fourth, the non-autonomous effects on tissue size, growth and proliferation rates, and/or Dpp availability and signaling can be phenocopied by overexpression of Dally. Fifth, increasing the levels of the Dpp receptor Tkv also causes a non-autonomous reduction in tissue size. Still, it would be very helpful to visualize Dpp distribution upon targeted activation of these pathways, which has some technical limitations. So far, the only way to do so is by overexpressing a Dpp-GFP construct in the Dpp expression domain. This non-physiological overexpression leads to strong overgrowth of the wing disc, which impairs the interpretation of the results. Boosting Dpp signaling to the maximum and showing that the non-autonomous effect is lost would also be very insightful. The main effector of Dpp signaling on growth is Brinker. We have increased Dpp signaling by different means (by using mutations in *brinker* or by overexpressing Dpp in its own expression domain using the lexA system) and, unfortunately, the resulting wing primordia were in all cases largely overgrown and no adult flies were isolated. Unluckily, Dp110 expression in the anterior domain in a *brk* mutant background was lethal in early larval development, and no larval primordia could be isolated.

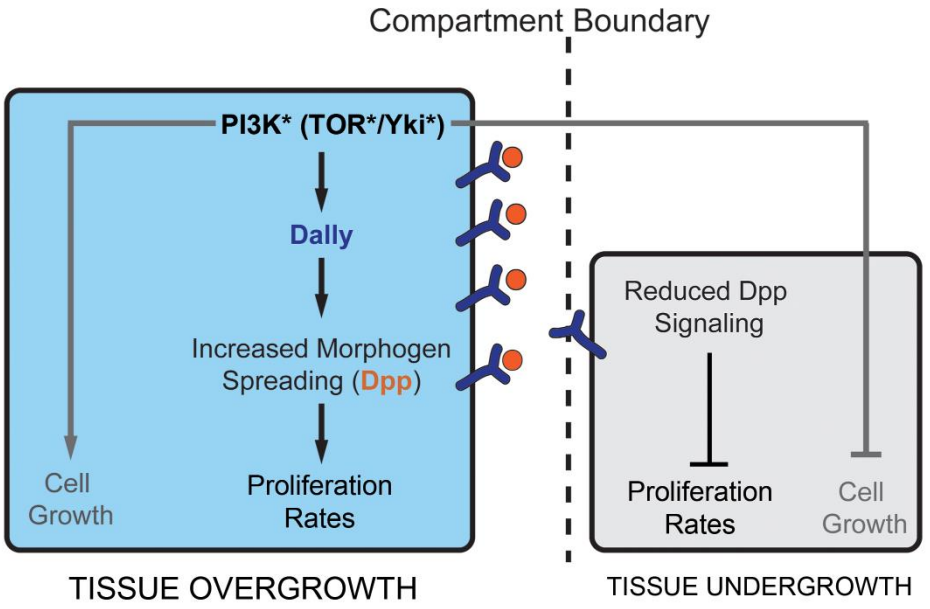

Figure 61. A role of Dally in mediating the non-autonomous effects on tissue growth. Activation of the PI3K/PTEN, TSC/TOR, or Hippo/Yorkie pathways in a defined cell population (in blue) increases cell and/or tissue size in an autonomous manner and induces a non-autonomous reduction in both cell size and number in neighboring cell populations (in grey). Whereas the autonomous and non-autonomous effects on tissue size are mediated by Dally, the effects on cell size are Dally independent. The non-autonomous reduction in tissue size is a consequence of reduced Dpp signaling, most probably reflecting increased number of Dpp molecules (in orange) bound to the overgrowing (Dally-upregulated, dark blue) tissue and a consequent reduction in the number of available Dpp molecules to the neighboring cell population.

We observed different strengths of the autonomous and non-autonomous effects upon deregulation of these tumor suppressor pathways (or overexpression of Dally) in either the A or P compartments. Despite the mild autonomous induction of tissue growth caused by the *ci-gal4* driver in A cells, it caused a relatively strong non-autonomous reduction of the neighboring compartment. On the contrary, the *en-gal4* driver caused a strong autonomous induction of tissue growth in P cells but a relatively weak non-autonomous reduction of the neighboring compartment. The differential autonomous response might simply reflect different strengths of these Gal4 drivers. Systemic effects due to expression of the Gal4 drivers in other places besides the compartments of the wing imaginal disc could affect the growth of the whole larvae. This possibility was rejected by the

fact that no changes in body size were observed upon targeted activation of these pathways in the wing disc. By contrast, the strongest non-autonomous effects caused by the *ci-gal4* driver (when compared to the *en-gal4* driver) might be because Dpp expression is restricted to the A compartment and increased levels of Dally in Dpp expressing cells are more efficient at titrating out the levels of this growth factor from the neighboring compartment. Additionally, studies of a second *Drosophila* BMP-family member, Glass bottom boat (Gbb), suggest that Dpp might not act alone in specifying BMP signaling-dependent positional information along the anteroposterior axis. Either alone or in heterodimers with Dpp, Gbb uses the same signal transduction system as Dpp. Gbb seems to contribute to the BMP morphogen gradient, most strongly in the posterior compartment (Bangi and Wharton, 2006a; Bangi and Wharton, 2006b). It might be that Dally is also able to cause the withdrawal of Gbb from the extracellular matrix.

We noticed that the non-autonomous effects on cell size observed upon deregulation of the PI3K/PTEN, TSC/TOR, or Hippo/Yorkie pathways are Dally independent, as overexpression of Dally did not cause a non-autonomous reduction in cell size. Moreover, depletion of Dally did not rescue the non-autonomous reduction in cell size caused by activation of these pathways. These results are consistent with the fact that changes in Dpp signaling do not cause any effect on cell size (Martín-Castellanos and Edgar, 2002), which is also confirmed by the overexpression of a dominant negative form of the Thickveins receptor, thus indicating that Dally and Dpp regulate cell number but not cell size. A Dally-independent mechanism, triggered by activation of these signaling pathways, may be at work in order to induce a non-autonomous reduction in cell size. It is known that experimentally induced alterations in cell proliferation are often compensated by changes in cell size (Weigmann et al., 1997). However, since Dally depletion rescues cell number and proliferation rates, but not cell size, these compensation mechanism seems not to be functioning in this situation. Given the fact that in the wing imaginal disc we could not observe the reduction in cell size

it might be that the reduction seen in the adult wing is due to an adjustment of cell size during pupal stages. It is known that during pupal development, wing cells go through two rounds of cell division and the pattern of cell proliferation is spatially heterogeneous associated with wing vein and intervein regions (García-Bellido et al., 1994; Milan et al., 1996).

Still, one open question is how Dally is commonly regulated by the PI3K/PTEN, TSC/TOR and Hippo/Yorkie signaling pathways. Dally regulation is indeed occurring at the transcriptional level, since the *dally-lacZ* reporter was upregulated upon activation of these growth promoting pathways. One possibility is that regulation of Dally by the PI3K/PTEN and TSC/TOR signaling pathways goes through regulation of Yki. This hypothesis is based on the fact that both IIS and TOR signaling regulate Yki expression or activity *in vivo* (Parker and Struhl, 2015; Straßburger et al., 2012). It was shown that IIS activates Yki *in vivo*, and that Yki plays an important role in the ability of IIS to drive cell proliferation in wing cells (Straßburger et al., 2012). TOR signaling has been shown to govern Yki action after it reaches the nucleus by allowing it to gain access to its target genes (Parker and Struhl, 2015). A less likely alternative could be that the three signaling pathways independently activate Dally through its respective transcription factors. In this sense, identification and characterization of putative binding sites for each transcription factor in the Dally locus/regulatory region could be very insightful.

Dpp signaling in growth control

Interestingly, deregulation of these pathways, and the resulting tissue overgrowth, leads to the expansion of the Dpp gradient without affecting the total levels of Dpp signaling. These results imply that Dpp activity levels do not play an instructive role in promoting tissue growth but rather that it is the range of the Dpp gradient what regulates final tissue size. Consistent with this proposal,

depletion of Dally levels in one compartment (which might lead to increased levels of available Dpp to the neighboring cell population) does not cause any visible non-autonomous effect in tissue size. This could be due to the capacity of Dpp to restrict its own spreading through the repression of Pentagone, a diffusible protein that interacts with Dally and contributes to the expansion of the Dpp gradient (Ben-Zvi et al., 2011; Hamaratoglu et al., 2011; Vuilleumier et al., 2010).

The graded distribution of Dpp leads, via the interaction with its receptor complex, to the graded activation of Mad/Medea, which in turn represses the transcription of *brinker* (*brk*). This creates a gradient of Brk expression that is reciprocal to the Dpp gradient. Brk is a transcriptional repressor that acts negatively to establish, in a dose-dependent manner, the expression domain of Dpp target genes like *spalt* (Campbell and Tomlinson, 1999; Jaźwińska et al., 1999; Minami et al., 1999). Thus, Dpp regulates the expression of target genes by repressing *brinker*. Remarkably, the reduced size of the wing primordium observed in hypomorphic alleles of *dpp* is restored when combined with *brk* mutants (Schwank et al., 2008). This experimental evidence indicates that Dpp controls wing growth entirely via repression of *brk*. The Dally-mediated increase in the width of the Dpp gradient observed upon deregulation of the PI3K/PTEN or TSC/TOR pathways might contribute to restrict the expression domain of *brk* to the lateral sides of the wing primordium. Similarly, the non-autonomous decrease in the width of the Dpp gradient might cause an expansion of the *brk* domain, which is known to repress growth.

However, an issue that has been a matter of intense debate is how graded Dpp activity drives uniform proliferation throughout the wing imaginal discs. It has been suggested that Dpp sustains proliferation of the central cells, by removal of the growth repressor Brinker. A recent report shows that in the absence of Dpp spreading, by trapping Dpp at its source, lateral cells still divide at normal rates, while medial cells divide at a lower rate (Harmansa et al., 2015). Our results of targeted Dally overexpression experiments are consistent with this idea in the sense that the adjacent wild type territory, which has reduced Dpp spreading

presents a lower proliferation rate. We assume that this occurs especially in the medial region of the posterior compartment.

Although we show that Dally has a rather specific impact on the Dpp morphogen, Dally-mediated spreading of other secreted growth factors might also contribute to the autonomous effects on tissue growth caused by deregulation of the PI3K/PTEN, TSC/TOR, or Hippo/Yorkie pathways. This is revealed by the fact that Dally depletion rescues both the autonomous and the non-autonomous effects, whereas deregulation of these pathways are still able to induce some growth upon Dpp knock down.

Downstream of Dally and Dpp in growth

It is clear that Dally and Dpp signaling have an impact on tissue growth. Dally overexpression gives rise to an increase in tissue size as well as an increase in Dpp signaling by different means. The role of Dpp in driving tissue growth has been shown to be exclusively through repression of Brinker and the creation of an inverse gradient of its expression levels. In fact, in a similar fashion as overexpression of Dpp throughout the wing imaginal disc, Brk mutant discs present a dramatic increase in tissue size.

The identification of downstream effectors of the Dpp pathway on growth remains largely mysterious. Only a few transcriptional target genes of Brk are known, such as *vestigial* (*vg*), the microRNA *bantam* known to promote cell survival and proliferation (Nolo et al., 2006; Thompson and Cohen, 2006), and the proto-oncogene dMyc (Doumpas et al., 2013). Dally has been shown to affect cell cycle progression via Cyclin A in the optic lobe and retina of the *Drosophila* eye primordium, but whether it does so via Dpp signaling remains unknown (Nakato et al., 2002).

To generate larger structures, an increase/accumulation of mass has to occur, and this implies uptake of more nutrients required for protein synthesis and organelle

biogenesis. Given the fact that activation of the Dpp signaling pathway generates a remarkable increase in tissue mass, it must by any mean lead to a higher nutrient uptake. Which are the downstream targets/effectors of Dpp signaling that allow this to occur remain unidentified.

Biological relevance of this mechanism

Somatic mutations in tumor suppressor genes such as PTEN or TSC are frequently observed in early events of tumor development, and these mutations are thought to contribute to the selection of tumorigenic cells. Competition for available growth factors, by modulating the levels of glypicans, such as Dally, might contribute to the out-competition of wild type cells and to the selection of malignant mutation-carrying cells in human cancer. Tumor cells, by acquiring an advantage in tethering growth factors from the media, might cause a reduction in the amount of these factors available to the surrounding cells, thus causing a non-autonomous reduction in growth and proliferate rates. Interestingly, in *Drosophila* epithelial cells it was demonstrated that the secreted proteoglycan Perlecan can cooperate with EGFR to promote tumorigenesis (Herranz et al., 2014). Coexpression of Perlecan in the EGFR-expressing epithelial cells potentiates endogenous Wg and Dpp signals from the epithelial cells to support expansion of tumor cells. Wg activity is required in the epithelial compartment, whereas Dpp activity is required non-autonomously in the mesenchymal compartment (Herranz et al., 2014). In mammalian epithelial cells, it has been shown that insulin, through Akt activation, enhances the delivery of TGF-β receptors at the cell surface thereby enhancing TGF-β responsiveness which promotes the migration of these cells (Budi et al., 2015). The authors proposed that this mechanism may help to explain the progression/malignancy of cancers in which Akt is activated.

The PI3K/PTEN and TSC/TOR signaling pathways play a role not only in disease but also during normal development. These two pathways modulate the final size of the developing organism according to nutrient availability. In a condition of high nutrient availability, which leads to the activation of the nutrient-sensing PI3K/PTEN and TSC/TOR pathways, increased levels of Dally facilitate the spread of the Dpp morphogen throughout the growing tissue and contribute to the generation of larger but well-proportioned and scaled adult structures. Depletion of Dally expression levels rescues the tissue growth caused by high levels of nutrients or activation of the nutrient-sensing pathways and gives rise to smaller and, again, well-proportioned and scaled adult structures. Of remarkable interest is the capacity of Dally to induce tissue overgrowth when overexpressed or to mediate the overgrowth upon deregulation of the PI3K/PTEN, TSC/TOR, or Hippo/Yorkie pathways. In this context, our results identify Dally as a molecular bridge between nutrient sensing and wing scaling in *Drosophila* (Figure 62).

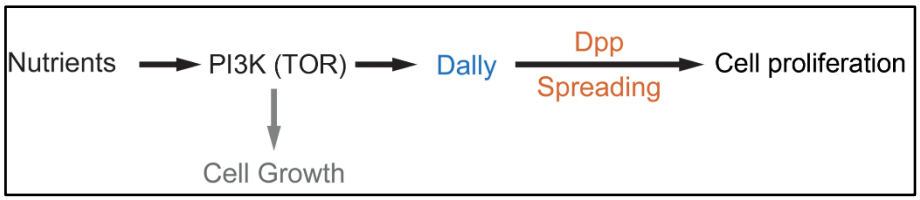

Figure 62. A role of Dally in tissue growth. Within the feeding animal, the PI3K/PTEN and TSC/TOR pathways sense nutrient conditions and modulate both cell and tissue size. Whereas the effects on tissue size are mediated by the glypican Dally, which modulates the spreading of the Dpp morphogen throughout the tissue, the effects on cell size are Dally independent.

Compartments and coordination of growth

Compartments have been proposed to be individual units of growth control (Martín and Morata, 2006). In other words, the size of each compartment is controlled independently. Our results on the lack of non-autonomous effects on tissue growth upon depletion of Dally or Sulfateless, the enzyme needed for the

modification of HS chains within glypicans, indicate that this is the case. Targeted depletion of glypican expression or activity in developing compartments gave rise to an autonomous reduction in tissue size without affecting the neighboring compartment. However, independent lines of evidence support the view that adjacent compartments buffer local variations in tissue growth caused by different means, including a non-autonomous reduction in tissue size upon depletion of the protein biosynthetic machinery (Mesquita et al., 2010) or reduced epidermal growth factor receptor (EGFR) activity (García-Bellido et al., 1994). Our results on the capacity of overgrowing compartments to withdraw Dpp from neighboring tissues and to cause a non-autonomous reduction in growth and proliferation rates reinforce the view that compartments are susceptible to modulate their growth rates upon different types of stress, including depletion of tumor suppressor genes.

Interestingly, the halteres and wings of *Drosophila* are homologous thoracic appendages, and the activity of the Ultrabithorax (Ubx) Hox gene in the haltere imaginal discs contributes to defining its reduced size. The reason for the small posterior compartment of the haltere is that Ubx, together with Engrailed, downregulates Dpp signaling in the posterior compartment. Interestingly, it does so by reducing the expression levels of Dally and Tkv (Crickmore and Mann, 2006; Crickmore and Mann, 2007; de Navas et al., 2006; Makhijani et al., 2007), thus reinforcing the role of Dally in modulating tissue growth in epithelial organs. Furthermore, overexpression of Dally in the P compartment gives rise to an overall increase in size of haltere discs, and a non-autonomous reduction in pMAD labeling in the A cells immediately adjacent to the AP boundary (Crickmore and Mann, 2007). It would be interesting to known whether activation of PI3K/PTEN and TSC/TOR signaling in P cells of the halteres is able to upregulate Dally expression levels even in the presence of Ubx.

Upon reduction of growth in one compartment, the adjacent cell populations reduce its growth rates (Mesquita et al., 2010), favoring the maintenance of the proportions between the distinct territories. In this thesis we showed that upon

activation of growth in one territory, the adjacent cell populations reduce its growth rates, favoring the maintenance of roughly its normal total size. So, the wing rather favors maintenance of proportions or of total final size. Which are the biological constrains behind this choice is an interesting question. Preservation of proportional wings is important for maximum functionality. However, up to certain point, since very small wings would not allow the animal to fly. Conservation of total final size at the expense of the proportionality could be due to weight issues, since very large wings might be incompatible with flying.

The results presented in this thesis unravel properties of the system not described so far: cells can compete for available growth factors such as Dpp. Moreover, the unraveled mechanism by which activation of the PI3K/PTEN, TSC/TOR and Hippo/Yorkie pathways induce a non-autonomous tissue undergrowth might contribute to the understanding of these pathways in tumorigenesis. In addition, the fact that Dally influences Dpp gradient formation and its expression is controlled by the nutrient sensing pathways, demonstrates that it might act as a molecular bridge between organ-extrinsic and organ-intrinsic factors that control wing growth during development of the fly.

Conclusions

Conclusions

1. Targeted activation of PI3K/PTEN, TSC/TOR and Hippo/Yorkie signaling pathways induces a non-autonomous reduction in tissue size of adjacent wild type cell populations.

2. The non-autonomous reduction in tissue size is a consequence of a reduction in both growth and proliferation rates throughout development.

3. The non-autonomous response is independent of apoptosis–and does not rely on competition for nutrients.

4. The activation of PI3K/PTEN and TSC/TOR pathways affects the spreading, but not activity, of the Dpp morphogen, and consequently Dpp activity levels are reduced in adjacent wild type populations.

5. The activity of the PI3K/PTEN, TSC/TOR and Hippo/Yorkie pathways regulate Dally expression levels.

6. Dally overexpression causes an autonomous increase in tissue size accompanied by an increase in cell number and higher Dpp activity levels.

7. The non-autonomous effects on tissue size, growth and proliferation rates, and/or Dpp availability and signaling are phenocopied by targeted overexpression of Dally.

8. Trapping of the Dpp morphogen by increasing the levels of its receptor causes a non-autonomous reduction in tissue size.

9. Dally contributes to the autonomous and non-autonomous effects on tissue size upon targeted activation of PI3K/PTEN, TSC/TOR and Hippo/Yorkie pathways.

10. Dally couples the organ-extrinsic (nutrient-sensing pathways) to the organ-intrinsic (Dpp signaling) growth properties in the wing imaginal disc.

Material and Methods

Material and Methods

Drosophila Strains

Flies were raised at 25° C (unless otherwise specified) in a 12/12 h day/night period on standard *Drosophila* medium containing 4% glucose, 55 g/L yeast, 0,65% agar, 28 g/L wheat flour, 4 ml/L propionic acid and 1,1 g/L nipagin).

Gal4 driver lines: *en-gal4*, *hh-gal4*, *ci-gal4, nub-gal4* were from the Bloomington Stock Center and are described in Flybase; *spalt^{PE}-gal4* (Barrio and de Celis, 2004).

UAS – lines: *UAS-PTEN^{RNAi}* (ID 101475), *UAS-dally^{RNAi}* (ID 14136), *UAS-dally-like^{RNAi}* (ID 100268), *UAS-sulfateless^{RNAi}* (ID 5070), *UAS-InR^{RNAi}* (ID 992), *UAS-Dp110^{RNAi}* (ID 38985) were obtained from the Vienna *Drosophila* RNAi Center; *UAS-Rheb^{RNAi}* (HMS00923), *UAS-dally^{RNAi}* (HMS00905), *UAS-dally-like^{RNAi}* (HMS00875 and HMS00903), *UAS-sulfateless^{RNAi}* (HMS00543), *UAS-dpp^{RNAi}* (JF01371) were obtained from the Bloomington Stock Center TRiP collection; *UAS-p35* (Hay et al., 1994); *UAS-yki* (kind gift from S. Cohen); *UAS-tkv* and *UAS-tkv^{DN}* (a dominant negative version of *tkv* that lacked the cytoplasmic kinase domain necessary for signal transduction (Kumar and Moses, 2001)); *UAS-dp53^{ct}* (a dominant negative version of Dp53, (Brodsky et al., 2000)); *UAS-dally* ((Nakato et al., 1995), kind gift from E. Sánchez-Herrero); *UAS-cyclin-E* and *UAS-string* (kind gifts from B. Edgar), *UAS–Dp110/PI3K* and *UAS-Rheb* were obtained from the Bloomington Stock Center and are described in Flybase.

Other lines: *dally-YFP* (115511), *tkv-YFP* (115298) were obtained from the DGRC; *tkv-lacZ* (*P(lacZ)tkvk16713*) was obtained from Bloomington Stock Center and is described in Flybase; *dally-lacZ* (*P(lacZ)dally06464*, (Nakato et al., 1995), kind gift

from E. Sánchez-Herrero); *Df(3L)H99* (a deficiency that covers the pro-apoptotic genes hid, grim, and reaper, (Steller, 2008)); *dpp-lacZ* (Basler and Struhl, 1994).

Mosaic analysis

FRT clones**.** The following *Drosophila* genotypes were used to generate loss-of-function clones in wing discs by the FLP/FRT system (Xu and Rubin, 1993):
(1) *hs-FLP, ubi-nls-RFP, FRT19A/FRT19A; ci-gal4, UAS-GFP/+,*
(2) *hs-FLP, ubi-nls-RFP, FRT19A/FRT19A; ci-gal4,UAS-GFP/UAS-Dp110*
(3) *hs-FLP, ubi-nls-RFP, FRT19A/FRT19A; ci-gal4, UAS-GFP/UAS-Dally*
Heat-shock (1h at 38°C) was induced at early third instar (72h AEL), grown at 25°C and wing discs were dissected 72h after clone induction. The clones were marked by the absence of RFP expression.

Antibodies

The antibodies used were rabbit anti-Spalt (a kind gift from R. Barrio, (Barrio and de Celis, 2004)), rabbit anti-pMAD (a kind gift from G. Morata), guinea-pig anti-Dally (kind gift from A. Gallet (Ayers et al., 2012)), mouse anti-Distalless (kind gift from S. Cohen), rabbit anti–phosphorylated histone 3 (PH3) (Cell Signaling), rat anti-BrdU (Abcam), rabbit anti-βgal (Cappel), rat anti-Ci (2A1, DSHB), mouse anti-Patched (*Drosophila* Ptc - Apa 1, DSHB), mouse anti-Wingless (4D4, DSHB) and mouse anti-Dally-like (13G8, DSHB). The fluorescent secondary antibodies that have been used are from Molecular Probes (used 1/500).

Immunostaining

Larvae were dissected in PBS, fixed for 20 minutes in PBS + 4% formaldehyde, rinsed 3 times during 15 minutes with PBT (PBS + 0.1% Triton X-100), and blocked for 1 hour with BBT (PBT + BSA 0'3% + 250 mM NaCl). Incubation with primary antibodies in 50µl of BBT was performed overnight at 4°C. After incubation, samples were rinsed 4 times during 15 minutes with BBT and stained

with secondary antibodies conjugated with different Alexa-fluorophores in 100µl of BBT for 2 hours at room temperature. DAPI was added to the last 15 minutes of secondary antibody staining to detect DNA. Samples were finally rinsed with PBT and mounted in mounting medium (40ml Glycerol + 5ml PBS10X + 400µl N-propyl-gallate 50% diluted in ethanol). Images were captured using a Leica TCS SP2 confocal microscope and process and treated with Fiji Software (NIH, USA) and Adobe Photoshop Software.

TUNEL Assay

TUNEL analysis was performed as described in (Milán et al., 1996) and it was used to label the DNA break of death cells (kit provided by Roche Diagnostics).

BrdU incorporation

BrdU incorporation was performed as described in (Milán et al., 1996). It was used to measure DNA synthesis (S phase) in proliferating cells. 5-bromo2'-deoxy-uridine (BrdU) was incorporated into DNA in place of thymidine. Then, cells which have incorporated BrdU into DNA were detected using an antibody against BrdU.

In situ hybridization

In situ hybridization was performed as described in (Milán et al., 1996). The antisense probes of *string* and *cycE* were previously generated in the laboratory (Mesquita et al., 2010).

Quantification of Tissue and Cell Size in Adult Wings

Virgins of the different *gal4*-lines were crossed with males carrying different UAS-transgenes and allowed to lay eggs for 24h at 25°C. The resulting larvae developed at 25°C until adulthood. The sizes of the wing and of the A and P compartments were measured using Fiji Software (NIH, USA). Cell density was measured as the number of hairs (each wing cell differentiates a hair) per defined area. Two conserved regions between veins L4 and L5 (P compartment) and veins L2 and L3

(A compartment) were used to measure cell densities. The final area and cell density values were normalized as a percent of the control values of GFP expressing samples under the corresponding *gal4*-drivers. At least ten adult wings per genotype were scored. Only adult males were scored. The average values and the corresponding standard deviation were calculated, and a *t*-test analysis was carried out. The average values, the corresponding standard deviations, and the corresponding p-values are included in the annexes tables.

Quantification of Tissue Growth in Developing Wing Discs

Hatched first instar larvae were sorted from egg laying plates (egg laying period of 4h at 25°C), transferred to fresh tubes, allowed to growth at 25°C, and dissected at three time points of development (72h, 96h and 140h). The size of the A and P compartments in the wing primordia was measured using Fiji Software (NIH, USA). At least ten wing discs per genotype and per time point were scored. The corresponding standard deviation was calculated, and a *t*-test analysis was carried out. The average values, the corresponding standard deviations, and the corresponding p-values are included in the annexes tables.

Proliferation and Growth Rate Measurements by Clonal Analysis

Early third instar (72h AEL) larvae of the following genotypes: (1) *hs-FLP, ubi-nls-RFP, FRT19A/FRT19A; ci-gal4, UAS-GFP/+*, (2) *hs-FLP, ubi-nls-RFP, FRT19A/FRT19A; ci-gal4, UAS-GFP/UAS-Dp110*, and (3) *hs-FLP, ubi-nls-RFP, FRT19A/FRT19A; ci-gal4, UAS-GFP/UAS-Dally*, were heat-shocked at 38°C for 1h and then transferred to 25°C. Wing discs were dissected 72h after clone induction. The size of clones, visualized by the absence of RFP expression, was quantified from confocal images with Fiji Software (NIH, USA). Wing discs were also labeled with DAPI to quantify cell number. At least 30 clones were quantified. Average values and the corresponding standard deviations were calculated, and a t-test

analysis was carried out. Clones in the three different genotypes were induced and dissected in parallel, and the same control wing discs (genotype nr 1) were used in Figures 23 and 40. The average values, the corresponding standard deviations, and the corresponding p-values are included in the annexes tables.

Flow Cytometry Analysis

Wing imaginal discs of each genotype were dissected in cold PBS, dissociated with trypsin-EDTA at 32°C for 45 min, and fixed with 4% formaldehyde for 20 min. Cells were centrifuged at 2,000 rpm for 2 min, resuspended in 1 ml of 70% ethanol, and incubated for 1 h at room temperature (RT). After centrifugation, the pellet was resuspended in PBS with DAPI 1 mg/ml and RNase 100 mg/ml and incubated for 1h at RT. DAPI fluorescence was determined by flow cytometry using a FacsAria I SORP sorter (Beckton Dickinson, San Jose, California). Excitation with the blue line of the laser (488 nm) permits the acquisition of scatter parameters. Blue laser (488 nm) was used for GFP excitation, and a UV laser (350 nm) for DAPI excitation. Doublets were discriminated using an integral/peak dot plot of DAPI fluorescence. Cell cycle histograms were obtained on each sample according to the GFP fluorescence, and cell cycle analysis was done on DAPI fluorescence collected at 440 nm. DNA analysis on single fluorescence histograms was done using Summit software (Dako Colorado).

pMAD Expression Profile

In order to obtain the pMAD expression profile at the same developmental stage in all genotypes analyzed, larvae were fed with food complemented with bromophenol blue (0,2 g in 100 ml of fly food), as described in (Andres and Thummel, 1994)), and wandering larvae with empty (white) gut, corresponding to 1–6h before the entry into pupal stage, were used to dissect the wing discs. As previously described in (Hamaratoglu et al., 2011), all wing discs from a dataset (GFP control and experimental discs) were fixed and stained together to avoid variability between discs and mounted on the same slide to reduce potential

variation in thickness between the slide and the coverslip across different samples. All discs from a dataset were imaged under identical settings using a Leica SP2 confocal microscope (0.36 μm of step size). Confocal conditions were adjusted to avoid saturated pixels with maximal intensity. After image acquisition, four consecutive slices (above and below the brightest slice from each stack) were manually selected by visual inspection, and a mean projection of these nine slices was subsequently performed. Using a reduced number of slices and performing the mean projection allowed us to reduce the noise as well as to avoid the signal from the peripodial membrane. Indeed, we made sure that these nine slices contained signal from the columnar cells of the pouch only. All discs were rotated to have anterior to the left and dorsal upwards orientation. The remaining analyses were applied solely to the wing pouch. We extracted the profiles along the anterior–posterior (AP) axis parallel to the dorsal-ventral (DV) boundary in four different offsets (two in the dorsal compartment and two in the ventral one). The positioning of the AP boundary was scored by the GFP expression driven by the *gal4* line. To quantify total pMAD signaling of a particular region of interest (A or P compartments or the whole wing pouch), signal intensities per pixel were first collected from raw images taken with the same laser confocal conditions using the histogram function of Fiji Software (NIH, USA). Confocal conditions were adjusted to avoid saturated pixels with maximal intensity. Total pMAD signaling per region of interest was quantified as the sum of all pixel intensities. All wing discs from a dataset (GFP control and experimental discs) were fixed and stained together. All of the image processing and data extraction were performed using Fiji Software (NIH, USA). At least five discs per genotype were analyzed. The average values, the corresponding standard deviations, and the corresponding p-values are included in the annexes tables.

Fly Food with Varying Concentrations of Yeast

We adapted the food recipe described in (Bass et al., 2007). The following recipes were used to vary the concentration of yeast: (A) 100 g/L yeast food: 1 liter of standard fly medium contains 100 g of fresh yeast, 100 g of sucrose, 27 g bacteriological agar, 3 mL of propionic acid, and 30 mL of nipagin; and (B) 20 g/L yeast food (starvation): it was generated by reducing the amount of fresh yeast without altering the other ingredients. Hatched first instar larvae were sorted from egg laying plates (egg laying period of 8h at 25°C), transferred to tubes with the different yeast concentration foods and allowed to grow at 25°C to adulthood. Control animals were analyzed in parallel in each experimental condition.

Statistical Analyses

The average values, the corresponding standard deviations or standard error to the mean, and the corresponding p-values were calculated using the Microsoft Excel. In all quantifications, the Student's *t*-test (two-tailed) was used to test for significance. Significance is indicated in the figures using the following symbols: *p < 0.05, **p < 0.01, ***p < 0.001. Error bars represent either the standard deviation (in the case of tissue size and cell density measurements) or the standard error to the mean (in the case of quantification of mitotic figures, apoptotic cells, and pMAD signal intensity).

Quantification of Pupal Volume

Hatched first instar female larvae were sorted from egg laying plates (egg laying period of 4h at 25°C), transferred to fresh tubes, allowed to growth at 25°C until pupa formation to determine pupa volume. For pupal size measurements pictures were taken with an Olympus MVX10 Macroscope, measures were done using Fiji Software (NIH, USA), and volume was given by the formula $4/3\pi(L/2)(l/2)2$ (L, length; l, diameter). The corresponding standard deviation was calculated, and a *t*-test analysis was carried out.

Bibliography

Bibliography

Abrams, J. M. (2002). Competition and compensation: Coupled to death in development and cancer. *Cell* **110**, 403–406.

Adachi-Yamada, T. and O'Connor, M. B. (2002). Morphogenetic Apoptosis: A Mechanism for Correcting Discontinuities in Morphogen Gradients. *Dev. Biol.* **251**, 74–90.

Adachi-Yamada, T., Fujimura-Kamada, K., Nishida, Y. and Matsumoto, K. (1999). Distortion of proximodistal information causes JNK-dependent apoptosis in *Drosophila* wing. *Nature* **400**, 166–169.

Adams, M. D., Celniker, S. E., Holt, R. a, Evans, C. a, Gocayne, J. D., Amanatides, P. G., Scherer, S. E., Li, P. W., Hoskins, R. a, Galle, R. F., et al. (2000). The genome sequence of *Drosophila* melanogaster. *Science* **287**, 2185–2195.

Agrawal, N., Joshi, S., Kango, M., Saha, D., Mishra, A. and Sinha, P. (1995). Epithelial Hyperplasia of Imaginal Discs Induced by Mutations in *Drosophila* Tumor Suppressor Genes: Growth and Pattern Formation in Genetic Mosaics. *Dev. Biol.* **169**, 387–398.

Akiyama, T., Kamimura, K., Firkus, C., Takeo, S., Shimmi, O. and Nakato, H. (2008). Dally regulates Dpp morphogen gradient formation by stabilizing Dpp on the cell surface. *Dev. Biol.* **313**, 408–419.

Alexandre, C., Jacinto, A. and Ingham, P. W. (1996). Transcriptional activation of hedgehog target genes in *Drosophila* is mediated directly by the Cubitus interruptus protein, a member of the GLI family of zinc finger DNA-binding proteins. *Genes Dev.* **10**, 2003–2013.

Amoyel, M. and Bach, E. a (2014). Cell competition: how to eliminate your neighbours. *Development* **141**, 988–1000.

Andres, A. J. and Thummel, C. S. (1994). Methods for quantitative analysis of transcription in larvae and prepupae. **44**, 565–573.

Avruch, J., Long, X., Ortiz-Vega, S., Rapley, J., Papageorgiou, A. and Dai, N. (2009). Amino acid regulation of TOR complex 1. *Am. J. …* **1**, 592–602.

Ayers, K. L., Mteirek, R., Cervantes, a., Lavenant-Staccini, L., Therond, P. P. and Gallet, a. (2012). Dally and Notum regulate the switch between low and high level Hedgehog pathway signalling. *Development* **139**, 3168–3179.

Baena-Lopez, L. a and García-Bellido, a (2006). Control of growth and positional information by the graded vestigial expression pattern in the wing of *Drosophila melanogaster*. *Proc. Natl. Acad. Sci. U. S. A.* **103**, 13734–13739.

Baena-Lopez, L. A., Rodríguez, I. and Baonza, A. (2008). The tumor suppressor genes dachsous and fat modulate different signalling pathways by regulating dally and dally-like. *Proc. Natl. Acad. Sci. U. S. A.* **105**, 9645–9650.

Baena-Lopez, L. A., Franch-Marro, X. and Vincent, J.-P. (2009). Wingless promotes proliferative growth in a gradient-independent manner. *Sci. Signal.* **2**, ra60.

Ballesteros-Arias, L., Saavedra, V. and Morata, G. (2013). Cell competition may function either as tumour-suppressing or as tumour-stimulating factor in *Drosophila*. *Oncogene* 1–8.

Bangi, E. and Wharton, K. (2006a). Dual function of the *Drosophila* Alk1/Alk2 ortholog Saxophone shapes the Bmp activity gradient in the wing imaginal disc. *Development* **133**, 3295–303.

Bangi, E. and Wharton, K. (2006b). Dpp and Gbb exhibit different effective ranges in the establishment of the BMP activity gradient critical for *Drosophila* wing patterning. *Dev. Biol.* **295**, 178–193.

Barrio, R. and de Celis, J. F. (2004). Regulation of spalt expression in the *Drosophila* wing blade in response to the Decapentaplegic signaling pathway. *Proc. Natl. Acad. Sci. U. S. A.* **101**, 6021–6026.

Basler, K. and Struhl, G. (1994). Compartment boundaries and the control of *Drosophila* limb pattern by hedgehog protein. *Nature* **368**, 208–214.

Bass, T. M., Grandison, R. C., Wong, R., Martinez, P., Partridge, L. and Piper, M. D. W. (2007). Optimization of dietary restriction protocols in *Drosophila*. *J. Gerontol. A. Biol. Sci. Med. Sci.* **62**, 1071–1081.

Baumgartner, R., Poernbacher, I., Buser, N., Hafen, E. and Stocker, H. (2010). The WW Domain Protein Kibra Acts Upstream of Hippo in *Drosophila*. *Dev. Cell* **18**, 309–316.

Belenkaya, T. Y., Han, C., Yan, D., Opoka, R. J., Khodoun, M., Liu, H. and Lin, X. (2004). *Drosophila* Dpp morphogen movement is independent of dynamin-mediated endocytosis but regulated by the glypican members of heparan sulfate proteoglycans. *Cell* **119**, 231–244.

Bennett, F. C. and Harvey, K. F. (2006). Fat Cadherin Modulates Organ Size in *Drosophila* via the Salvador/Warts/Hippo Signaling Pathway. *Curr. Biol.* **16**, 2101–2110.

Ben-Zvi, D. and Barkai, N. (2010). Scaling of morphogen gradients by an expansion-repression integral feedback control. *Proc. Natl. Acad. Sci. U. S. A.* **107**, 6924–6929.

Ben-Zvi, D., Pyrowolakis, G., Barkai, N. and Shilo, B. Z. (2011). Expansion-repression mechanism for scaling the Dpp activation gradient in *drosophila* wing imaginal discs. *Curr. Biol.* **21**, 1391–1396.

Bernfield, M., Götte, M., Park, P. W., Reizes, O., Fitzgerald, M. L., Lincecum, J. and Zako, M. (1999). Functions of Cell Surface Heparan sulfate Proteoglycans. *Annu. Rev. Biochem.* 729–777.

Böhni, R., Riesgo-Escovar, J., Oldham, S., Brogiolo, W., Stocker, H., Andruss, B. F., Beckingham, K. and Hafen, E. (1999). Autonomous Control of Cell and Organ Size by CHICO, a< i> Drosophila</i> Homolog of Vertebrate IRS1--4. *Cell* **97**, 865–875.

Brand, a H. and Perrimon, N. (1993). Targeted gene expression as a means of altering cell fates and generating dominant phenotypes. *Development* **118**, 401–415.

Brodsky, M. H., Nordstrom, W., Tsang, G., Kwan, E., Rubin, G. M. and Abrams, J. M. (2000). Drosophila p53 binds a damage response element at the reaper locus. *Cell* **101**, 103–113.

Bryant, P. and Simpson, P. (1984). Intrinsic and extrinsic control of growth in developing organs. *Q. Rev. Biol.* **59**, 387–415.

Budi, E. H., Muthusamy, B. and Derynck, R. (2015). The insulin response integrates increased TGF- b signaling through Akt-induced enhancement of cell surface delivery of TGF- b receptors. **8**, 1–16.

Burke, R. and Basler, K. (1996). Dpp receptors are autonomously required for cell proliferation in the entire developing Drosophila wing. *Development* **122**, 2261–2269.

Butler, M. J., Jacobsen, T. L., Cain, D. M., Jarman, M. G., Hubank, M., Whittle, J. R. S., Phillips, R. and Simcox, A. (2003). Discovery of genes with highly restricted expression patterns in the Drosophila wing disc using DNA oligonucleotide microarrays. *Development* **130**, 659–670.

Campbell, G. and Tomlinson, a (1999). Transducing the Dpp morphogen gradient in the wing of Drosophila: regulation of Dpp targets by brinker. *Cell* **96**, 553–562.

Capdevila, J. and Guerrero, I. (1994). Targeted expression of the signaling molecule decapentaplegic induces pattern duplications and growth alterations in Drosophila wings. *EMBO J.* **13**, 4459–4468.

Chang, C.-H., Qiu, J., O'Sullivan, D., Buck, M. D., Noguchi, T., Curtis, J. D., Chen, Q., Gindin, M., Gubin, M. M., van der Windt, G. J. W., et al. (2015). Metabolic Competition in the Tumor Microenvironment Is a Driver of Cancer Progression. *Cell* **162**, 1229–1241.

Chen, C.-L., Gajewski, K. M., Hamaratoglu, F., Bossuyt, W., Sansores-Garcia, L., Tao, C. and Halder, G. (2010). The apical-basal cell polarity determinant Crumbs regulates Hippo signaling in *Drosophila*. *Proc. Natl. Acad. Sci. U. S. A.* **107**, 15810–15815.

Cho, E., Feng, Y., Rauskolb, C., Maitra, S., Fehon, R. and Irvine, K. D. (2006). Delineation of a Fat tumor suppressor pathway. *Nat. Genet.* **38**, 1142–1150.

Clavería, C., Giovinazzo, G., Sierra, R. and Torres, M. (2013). Myc-driven endogenous cell competition in the early mammalian embryo. *Nature* **500**, 39–44.

Colombani, J., Andersen, D. S. and Leopold, P. (2012). Secreted Peptide Dilp8 Coordinates *Drosophila* Tissue Growth with Developmental Timing. *Science (80-.).* **336**, 582–585.

Colombani, J., Andersen, D. S., Boulan, L., Boone, E., Romero, N., Virolle, V., Texada, M. and Léopold, P. (2015). *Drosophila* Lgr3 Couples Organ Growth with Maturation and Ensures Developmental Stability. *Curr. Biol.* 2723–2729.

Crick, F. H. and Lawrence, P. a (1975). Compartments and polyclones in insect development. *Science (80-.).* **189**, 340–347.

Crickmore, M. a and Mann, R. S. (2006). Hox control of organ size by regulation of morphogen production and mobility. *Science* **313**, 63–68.

Crickmore, M. a and Mann, R. S. (2007). Hox control of morphogen mobility and organ development through regulation of glypican expression. *Development* **134**, 327–334.

Cully, M., You, H., Levine, A. J. and Mak, T. W. (2006). Beyond PTEN mutations: the PI3K pathway as an integrator of multiple inputs during tumorigenesis. *Nat. Rev. Cancer* **6**, 184–192.

Day, S. J. and Lawrence, P. a (2000). Measuring dimensions: the regulation of size and shape. *Development* **127**, 2977–2987.

De Celis, J. F. (2003). Pattern formation in the *Drosophila* wing: The development of the veins. *BioEssays* **25**, 443–451.

De La Cova, C., Abril, M., Bellosta, P., Gallant, P. and Johnston, L. a. (2004). *Drosophila* myc regulates organ size by inducing cell competition. *Cell* **117**, 107–116.

de Navas, L. F., Garaulet, D. L. and Sánchez-Herrero, E. (2006). The ultrabithorax Hox gene of *Drosophila* controls haltere size by regulating the Dpp pathway. *Development* **133**, 4495–4506.

De Nooij, J. C., Letendre, M. A. and Hariharan, I. K. (1996). A cyclin-dependent kinase inhibitor, dacapo, is necessary for timely exit from the cell cycle during *Drosophila* embryogenesis. *Cell* **87**, 1237–1247.

Dekanty, A., Barrio, L., Muzzopappa, M., Auer, H. and Milán, M. (2012). Aneuploidy-induced delaminating cells drive tumorigenesis in *Drosophila* epithelia. *Proc. Natl. Acad. Sci. U. S. A.* **109**, 20549–54.

Diaz-Benjumea, F. J. and Cohen, S. M. (1993). Interaction between dorsal and ventral cells in the imaginal disc directs wing development in *Drosophila*. *Cell* **75**, 741–752.

Diaz-Benjumea, F. J. and Cohen, S. M. (1995). Serrate signals through Notch to establish a Wingless-dependent organizer at the dorsal/ventral compartment boundary of the *Drosophila* wing. *Development* **121**, 4215–4225.

Diez Del Corral, R., Aroca, P., Gómez-Skarmeta, J. L., Cavodeassi, F. and Modolell, J. (1999). The iroquois homeodomain proteins are required to specify body wall identity in *Drosophila*. *Genes Dev.* **13**, 1754–1761.

Doherty, D., Feger, G., Younger-Shepherd, S., Jan, L. Y. and Jan, Y. N. (1996). Delta is a ventral to dorsal signal complementary to Serrate, another notch ligand, in *Drosophila* wing formation. *Genes Dev.* **10**, 421–434.

Dong, J. and Pan, D. (2004). Tsc2 is not a critical target of Akt during normal *Drosophila* development. *Genes Dev.* **18**, 2479–2484.

Doumpas, N., Ruiz-Romero, M., Blanco, E., Edgar, B., Corominas, M. and Teleman, A. a (2013). Brk regulates wing disc growth in part via repression of Myc expression. *EMBO Rep.* **14**, 261–8.

Du, W. E. I., Vidal, M., Xie, J.-E. and Dyson, N. (1996). RBF, a nove RB-related gene that regulates E2F activvity and interacts with cyclin E in *Drosophila*. *Genes Dev.* **10**, 1206–1218.

Dynlacht, B. D., Brook, a, Dembski, M., Yenush, L. and Dyson, N. (1994). DNA-binding and trans-activation properties of *Drosophila* E2F and DP proteins. *Proc. Natl. Acad. Sci. U. S. A.* **91**, 6359–6363.

Edgar, B. a and O'Farrell, P. H. (1989). Genetic control of cell division patterns in the *Drosophila* embryo. *Cell* **57**, 177–187.

Engelman, J. a, Luo, J. and Cantley, L. C. (2006). The evolution of phosphatidylinositol 3-kinases as regulators of growth and metabolism. *Nat. Rev. Genet.* **7**, 606–619.

Enomoto, M. and Igaki, T. (2012). Src controls tumorigenesis via JNK-dependent regulation of the Hippo pathway in *Drosophila*. *EMBO Rep.* **14**, 65–72.

Enomoto, M., Vaughen, J. and Igaki, T. (2015). Non-autonomous overgrowth by oncogenic niche cells: cellular cooperation and competition in tumorigenesis. *Cancer Sci.* n/a–n/a.

Entchev, E. V, Schwabedissen, a and González-Gaitán, M. (2000). Gradient formation of the TGF-beta homolog Dpp. *Cell* **103**, 981–991.

Froldi, F., Ziosi, M., Garoia, F., Pession, A., Grzeschik, N. a, Bellosta, P., Strand, D., Richardson, H. E., Pession, A. and Grifoni, D. (2010). The lethal giant larvae tumour suppressor mutation requires dMyc oncoprotein to promote clonal malignancy. *BMC Biol.* **8**, 33.

Fujise, M., Izumi, S., Selleck, S. B. and Nakato, H. (2001). Regulation of dally, an integral membrane proteoglycan, and its function during adult sensory organ formation of *Drosophila*. *Dev. Biol.* **235**, 433–448.

Fujise, M., Takeo, S., Kamimura, K., Matsuo, T., Aigaki, T., Izumi, S. and Nakato, H. (2003). Dally regulates Dpp morphogen gradient formation in the *Drosophila* wing. *Development* **130**, 1515–1522.

Gabay, M., Li, Y. and Felsher, D. W. (2014). MYC activation is a hallmark of cancer initiation and maintenance. *Cold Spring Harb. Perspect. Med.* **4**, 1–14.

Gao, X. and Pan, D. (2001). TSC1 and TSC2 tumor suppressors antagonize insulin signaling in cell growth. *Genes Dev.* 1383–1392.

Garcia-Bellido, a and Merriam, J. R. (1971). Parameters of the wing imaginal disc development of *Drosophila* melanogaster. *Dev. Biol.* **24**, 61–87.

Garcia-Bellido, A., Ripoll, P. and Morata, G. (1973). Developmental compartimentalisation of the wing disk of *Drosophila*. *Nat New Biol* **245**, 251–3.

García-Bellido, a, Cortés, F. and Milán, M. (1994). Cell interactions in the control of size in *Drosophila* wings. *Proc. Natl. Acad. Sci. U. S. A.* **91**, 10222–10226.

Garelli, a., Gontijo, a. M., Miguela, V., Caparros, E. and Dominguez, M. (2012). Imaginal Discs Secrete Insulin-Like Peptide 8 to Mediate Plasticity of Growth and Maturation. *Science (80-.).* **336**, 579–582.

Garofalo, R. S. (2002). Genetic analysis of insulin signaling in *Drosophila*. *Trends Endocrinol. Metab.* **13**, 156–162.

Genevet, A., Wehr, M. C., Brain, R., Thompson, B. J. and Tapon, N. (2010). Kibra Is a Regulator of the Salvador/Warts/Hippo Signaling Network. *Dev. Cell* **18**, 300–308.

Giraldez, A. J. and Cohen, S. M. (2003). Wingless and Notch signaling provide cell survival cues and control cell proliferation during wing development. *Development* **130**, 6533–6543.

Glise, B., Miller, C. a., Crozatier, M., Halbisen, M. a., Wise, S., Olson, D. J., Vincent, A. and Blair, S. S. (2005). Shifted, the *Drosophila* ortholog of Wnt inhibitory factor-1, controls the distribution and movement of hedgehog. *Dev. Cell* **8**, 255–266.

Goberdhan, D. C. I., Paricio, N., Goodman, E. C., Mlodzik, M. and Wilson, C. (1999). *Drosophila* tumor suppressor PTEN controls cell size and number by antagonizing the Chico / PI3-kinase signaling pathway. *Genes Dev.* 3244–3258.

Gonzalez-Gaitan, M. a., Micol, J. L. and Garcia-Bellido, a. (1990). Developmental genetic analysis of Contrabithorax mutations in *Drosophila* melanogaster. *Genetics* **126**, 139–155.

González-Gaitán, M. and Jäckle, H. (1999). The range of spalt-activating Dpp signalling is reduced in endocytosis-defective *Drosophila* wing discs. *Mech. Dev.* **87**, 143–151.

Gorfinkiel, N., Sierra, J., Callejo, A., Ibañez, C. and Guerrero, I. (2005). The *Drosophila* ortholog of the human Wnt inhibitor factor shifted controls the diffusion of lipid-modified hedgehog. *Dev. Cell* **8**, 241–253.

Grewal, S. S. (2009). Insulin/TOR signaling in growth and homeostasis: A view from the fly world. *Int. J. Biochem. Cell Biol.* **41**, 1006–1010.

Grewal, S. S., Li, L., Orian, A., Eisenman, R. N. and Edgar, B. a (2005). Myc-dependent regulation of ribosomal RNA synthesis during *Drosophila* development. *Nat. Cell Biol.* **7**, 295–302.

Groppe, J., Rumpel, K., Economides, A. N., Stahl, N., Sebald, W. and Affolter, M. (1998). Biochemical and biophysical characterization of refolded *Drosophila* DPP, a homolog of bone morphogenetic proteins 2 and 4. *J. Biol. Chem.* **273**, 29052–29065.

Grzeschik, N. a., Parsons, L. M., Allott, M. L., Harvey, K. F. and Richardson, H. E. (2010a). Lgl, aPKC, and Crumbs Regulate the Salvador/Warts/Hippo Pathway through Two Distinct Mechanisms. *Curr. Biol.* **20**, 573–581.

Grzeschik, N. a., Parsons, L. M. and Richardson, H. E. (2010b). Lgl, the SWH pathway and tumorigenesis: It's a matter of context & competition! *Cell Cycle* **9**, 3202–3212.

Hamaratoglu, F., de Lachapelle, A. M., Pyrowolakis, G., Bergmann, S. and Affolter, M. (2011). Dpp signaling activity requires pentagone to scale with tissue size in the growing *drosophila* wing imaginal disc. *PLoS Biol.* **9**, e1001182.

Hamaratoglu, F., Affolter, M. and Pyrowolakis, G. (2014). Dpp/BMP signaling in flies: From molecules to biology. *Semin. Cell Dev. Biol.* **32**, 128–136.

Han, C., Belenkaya, T. Y., Wang, B. and Lin, X. (2004). *Drosophila* glypicans control the cell-to-cell movement of Hedgehog by a dynamin-independent process. *Development* **131**, 601–611.

Han, C., Yan, D., Belenkaya, T. Y. and Lin, X. (2005). *Drosophila* glypicans Dally and Dally-like shape the extracellular Wingless morphogen gradient in the wing disc. *Development* **132**, 667–679.

Hardie, D. G. (2007). AMP-activated/SNF1 protein kinases: conserved guardians of cellular energy. *Nat. Rev. Mol. Cell Biol.* **8**, 774–785.

Harmansa, S., Hamaratoglu, F., Affolter, M. and Caussinus, E. (2015). Dpp spreading is required for medial but not for lateral wing disc growth. *Nature* 1–18.

Harvey, K. F., Zhang, X. and Thomas, D. M. (2013). The Hippo pathway and human cancer. *Nat Rev Cancer* **13**, 246–257.

Hay, B. a, Wolff, T. and Rubin, G. M. (1994). Expression of baculovirus P35 prevents cell death in *Drosophila*. *Development* **120**, 2121–2129.

Hayashi, Y., Sexton, T. R., Dejima, K., Perry, D. W., Takemura, M., Kobayashi, S., Nakato, H. and Harrison, D. a. (2012). Glypicans regulate JAK/STAT signaling and distribution of the Unpaired morphogen. *Development* **139**, 4162–4171.

Herranz, H., Weng, R. and Cohen, S. M. (2014). Crosstalk between epithelial and mesenchymal tissues in tumorigenesis and imaginal disc development. *Curr. Biol.* **24**, 1476–1484.

Hietakangas, V. and Cohen, S. M. (2009). Regulation of tissue growth through nutrient sensing. *Annu. Rev. Genet.* **43**, 389–410.

Hogan, C., Dupré-Crochet, S., Norman, M., Kajita, M., Zimmermann, C., Pelling, A. E., Piddini, E., Baena-López, L. A., Vincent, J.-P., Itoh, Y., et al. (2009). Characterization of the interface between normal and transformed epithelial cells. *Nat. Cell Biol.* **11**, 460–467.

Holz, M. K., Ballif, B. A., Gygi, S. P. and Blenis, J. (2005). mTOR and S6K1 mediate assembly of the translation preinitiation complex through dynamic protein interchange and ordered phosphorylation events. *Cell* **123**, 569–580.

Hsiung, F., Ramirez-Weber, F.-A., Iwaki, D. D. and Kornberg, T. B. (2005). Dependence of *Drosophila* wing imaginal disc cytonemes on Decapentaplegic. *Nature* **437**, 8–11.

Huang, H., Potter, C. J., Tao, W., Li, D., Brogiolo, W. and Hafen, E. (1999). PTEN affects cell size , cell proliferation and apoptosis during *Drosophila* eye development. **5372**, 5365–5372.

Huang, J., Wu, S., Barrera, J., Matthews, K. and Pan, D. (2005). The Hippo signaling pathway coordinately regulates cell proliferation and apoptosis by inactivating Yorkie, the *Drosophila* homolog of YAP. *Cell* **122**, 421–434.

Huang, Q., Li, F., Liu, X., Li, W., Shi, W., Liu, F.-F., O'Sullivan, B., He, Z., Peng, Y., Tan, A.-C., et al. (2011). Caspase 3–mediated stimulation of tumor cell repopulation during cancer radiotherapy. *Nat. Med.* **17**, 860–866.

Huh, J. R., Guo, M. and Hay, B. A. (2004). Compensatory Proliferation Induced by Cell Death in the *Drosophila* Wing Disc Requires Activity of the Apical Cell Death Caspase Dronc in a Nonapoptotic Role. *Curr. Biol.* **14**, 1262–1266.

Inoki, K., Li, Y., Xu, T. and Guan, K.-L. (2003a). Rheb GTPase is a direct target of TSC2 GAP activity and regulates mTOR signaling. *Genes Dev.* **17**, 1829–1834.

Inoki, K., Zhu, T. and Guan, K.-L. (2003b). TSC2 mediates cellular energy response to control cell growth and survival. *Cell* **115**, 577–590.

Inoki, K., Corradetti, M. N. and Guan, K.-L. (2005). Dysregulation of the TSC-mTOR pathway in human disease. *Nat. Genet.* **37**, 19–24.

Irvine, K. D. and Vogt, T. F. (1997). Dorsal-ventral signaling in limb development. *Curr. Opin. Cell Biol.* **9**, 867–876.

Ito, N. and Rubin, G. M. (1999). gigas, a *Drosophila* Homolog of Tuberous Sclerosis Gene Product-2, Regulates the Cell Cycle. *Cell* **105**, 415.

Jackson, S. M., Nakato, H., Sugiura, M., Jannuzi, a, Oakes, R., Kaluza, V., Golden, C. and Selleck, S. B. (1997). dally, a *Drosophila* glypican, controls cellular responses to the TGF-beta-related morphogen, Dpp. *Development* **124**, 4113–4120.

Jastrzebski, K., Hannan, K. M., Tchoubrieva, E. B., Hannan, R. D. and Pearson, R. B. (2007). Coordinate regulation of ribosome biogenesis and function by the ribosomal protein S6 kinase, a key mediator of mTOR function. *Growth Factors* **25**, 209–226.

Jaźwińska, a, Kirov, N., Wieschaus, E., Roth, S. and Rushlow, C. (1999). The *Drosophila* gene brinker reveals a novel mechanism of Dpp target gene regulation. *Cell* **96**, 563–573.

Johnston, L. a and Sanders, A. L. (2003). Wingless promotes cell survival but constrains growth during *Drosophila* wing development. *Nat. Cell Biol.* **5**, 827–833.

Johnston, L. a and Schubiger, G. (1996). Ectopic expression of wingless in imaginal discs interferes with decapentaplegic expression and alters cell determination. *Development* **122**, 3519–3529.

Johnston, L. a., Prober, D. a., Edgar, B. a., Eisenman, R. N. and Gallant, P. (1999). *Drosophila* myc regulates cellular growth during development. *Cell* **98**, 779–790.

Jünger, M. a, Rintelen, F., Stocker, H., Wasserman, J. D., Végh, M., Radimerski, T., Greenberg, M. E. and Hafen, E. (2003). The *Drosophila* forkhead transcription factor FOXO mediates the reduction in cell number associated with reduced insulin signaling. *J. Biol.*

Justice, R. W., Zilian, O., Woods, D. F., Noll, M. and Bryant, P. J. (1995). The *Drosophila* tumor suppressor gene warts encodes a homolog of human myotonic dystrophy kinase and is required for the control of cell shape and proliferation. *Genes Dev.* **9**, 534–546.

Kajita, M., Hogan, C., Harris, A. R., Dupre-Crochet, S., Itasaki, N., Kawakami, K., Charras, G., Tada, M. and Fujita, Y. (2010). Interaction with surrounding normal epithelial cells influences signalling pathways and behaviour of Src-transformed cells. *J. Cell Sci.* **123**, 171–180.

Kalaany, N. Y. and Sabatini, D. M. (2009). Tumours with PI3K activation are resistant to dietary restriction. *Nature* **458**, 725–731.

Kim, J., Johnson, K., Chen, H. J., Carroll, S. and Laughon, a (1997). *Drosophila* Mad binds to DNA and directly mediates activation of vestigial by Decapentaplegic. *Nature* **388**, 304–308.

Kim, E., Goraksha-Hicks, P., Li, L., Neufeld, T. P. and Guan, K.-L. (2008). Regulation of TORC1 by Rag GTPases in nutrient response. *Nat. Cell Biol.* **10**, 935–945.

Kirkpatrick, H., Johnson, K. and Laughon, A. (2001). Repression of Dpp Targets by Binding of Brinker to Mad Sites. *J. Biol. Chem.* **276**, 18216–18222.

Kobayashi, T., Minowa, O., Sugitani, Y., Takai, S., Mitani, H., Kobayashi, E., Noda, T. and Hino, O. (2001). A germ-line Tsc1 mutation causes tumor development and embryonic lethality that are similar, but not identical to, those caused by Tsc2 mutation in mice. *Proc. Natl. Acad. Sci. U. S. A.* **98**, 8762–8767.

Kornberg, T., Sidén, I., O'Farrell, P. and Simon, M. (1985). The engrailed locus of *Drosophila*: in situ localization of transcripts reveals compartment-specific expression. *Cell* **40**, 45–53.

Kramer, J. M., Davidge, J. T., Lockyer, J. M. and Staveley, B. E. (2003). Expression of *Drosophila* FOXO regulates growth and can phenocopy starvation. *BMC Dev. Biol.* **3**, 5.

Kumar, J. P. and Moses, K. (2001). The EGF receptor and notch signaling pathways control the initiation of the morphogenetic furrow during *Drosophila* eye development. *Development* **128**, 2689–2697.

Landsberg, K. P., Farhadifar, R., Ranft, J., Umetsu, D., Widmann, T. J., Bittig, T., Said, A., Jülicher, F. and Dahmann, C. (2009). Increased Cell Bond Tension Governs Cell Sorting at the *Drosophila* Anteroposterior Compartment Boundary. *Curr. Biol.* **19**, 1950–1955.

Lane, M. E., Sauer, K., Wallace, K., Jan, Y. N., Lehner, C. F. and Vaessin, H. (1996). Dacapo, a cyclin-dependent kinase inhibitor, stops cell proliferation during *Drosophila* development. *Cell* **87**, 1225–1235.

Lecuit, T. and Cohen, S. M. (1998). Dpp receptor levels contribute to shaping the Dpp morphogen gradient in the *Drosophila* wing imaginal disc. *Development* **125**, 4901–4907.

Lecuit, T., Brook, W. J., Ng, M., Calleja, M., Sun, H. and Cohen, S. M. (1996). Two distinct mechanisms for long-range patterning by Decapentaplegic in the *Drosophila* wing. *Nature* **381**, 387–393.

Leevers, S. J., Weinkove, D., MacDougall, L. K., Hafen, E. and Waterfield, M. D. (1996). The *Drosophila* phosphoinositide 3-kinase Dp110 promotes cell growth. *EMBO J.* **15**, 6584–6594.

Levayer, R. and Moreno, E. (2013). Mechanisms of cell competition: Themes and variations. *J. Cell Biol.* **200**, 689–698.

Levine, A. J. (1997). P53, the Cellular Gatekeeper for Growth and Division. *Cell* **88**, 323–331.

Lin, X. and Perrimon, N. (1999). Dally cooperates with *Drosophila* Frizzled 2 to transduce Wingless signalling. *Nature* **400**, 281–284.

Ling, C., Zheng, Y., Yin, F., Yu, J., Huang, J., Hong, Y., Wu, S. and Pan, D. (2010). The apical transmembrane protein Crumbs functions as a tumor suppressor that regulates Hippo signaling by binding to Expanded. *Proc. Natl. Acad. Sci. U. S. A.* **107**, 10532–10537.

Makhijani, K., Kalyani, C., Srividya, T. and Shashidhara, L. S. (2007). Modulation of Decapentaplegic gradient during haltere specification in *Drosophila*. *Dev. Biol.* **302**, 243–255.

Martín, F. a and Morata, G. (2006). Compartments and the control of growth in the *Drosophila* wing imaginal disc. *Development* **133**, 4421–4426.

Martín, F. a, Pérez-Garijo, A., Moreno, E. and Morata, G. (2004). The brinker gradient controls wing growth in *Drosophila*. *Development* **131**, 4921–4930.

Martín, F. a, Herrera, S. C. and Morata, G. (2009). Cell competition, growth and size control in the *Drosophila* wing imaginal disc. *Development* **136**, 3747–3756.

Martín-Castellanos, C. and Edgar, B. a (2002). A characterization of the effects of Dpp signaling on cell growth and proliferation in the *Drosophila* wing. *Development* **129**, 1003–1013.

Martins, V. C., Busch, K., Juraeva, D., Blum, C., Ludwig, C., Rasche, V., Lasitschka, F., Mastitsky, S. E., Brors, B., Hielscher, T., et al. (2014). Cell competition is a tumour suppressor mechanism in the thymus. *Nature* **509**, 465–70.

Mata, J., Curado, S., Ephrussi, a and Rørth, P. (2000). Tribbles coordinates mitosis and morphogenesis in *Drosophila* by regulating string/CDC25 proteolysis. *Cell* **101**, 511–522.

McBride, A., Ghilagaber, S., Nikolaev, A. and Hardie, D. G. (2009). The Glycogen-Binding Domain on the AMPK β Subunit Allows the Kinase to Act as a Glycogen Sensor. *Cell Metab.* **9**, 23–34.

McCartney, B. M., Kulikauskas, R. M., LaJeunesse, D. R. and Fehon, R. G. (2000). The neurofibromatosis-2 homologue, Merlin, and the tumor suppressor expanded function together in *Drosophila* to regulate cell proliferation and differentiation. *Development* **127**, 1315–1324.

Menéndez, J., Pérez-Garijo, A., Calleja, M. and Morata, G. (2010). A tumor-suppressing mechanism in *Drosophila* involving cell competition and the Hippo pathway. *Proc. Natl. Acad. Sci. U. S. A.* **107**, 14651–14656.

Merino, M. M., Rhiner, C., Lopez-gay, J. M., Buechel, D., Hauert, B. and Moreno, E. (2015). Article Elimination of Unfit Cells Maintains Tissue Health and Prolongs Lifespan. *Cell* **160**, 461–476.

Mesquita, D., Dekanty, A. and Milán, M. (2010). A dp53-dependent mechanism involved in coordinating tissue growth in *Drosophila*. *PLoS Biol.* **8**, e1000566.

Milan, M., Campuzano, S. and GarciaBellido, A. (1996). Cell cycling and patterned cell proliferation in the *Drosophila* wing during metamorphosis. **93**, 11687–11692.

Milan, M., Perez, L. and Cohen, S. M. (2002). Short-range cell interactions and cell survival in the *Drosophila* wing. *Dev. Cell* **2**, 797–805.

Milán, M. (2002). Survival of the fittest. Cell competition in the *Drosophila* wing. *EMBO Rep.* **3**, 724–725.

Milán, M., Campuzano, S. and García-Bellido, a (1996). Cell cycling and patterned cell proliferation in the wing primordium of *Drosophila*. *Proc. Natl. Acad. Sci. U. S. A.* **93**, 640–645.

Milán, M., Campuzano, S. and García-Bellido, a (1997). Developmental parameters of cell death in the wing disc of *Drosophila*. *Proc. Natl. Acad. Sci. U. S. A.* **94**, 5691–5696.

Milán, M., Weihe, U., Pérez, L. and Cohen, S. M. (2001). The LRR proteins Capricious and Tartan mediate cell interactions during DV boundary formation in the *Drosophila* wing. *Cell* **106**, 785–794.

Minami, M., Kinoshita, N., Kamoshida, Y., Tanimoto, H. and Tabata, T. (1999). brinker is a target of Dpp in *Drosophila* that negatively regulates Dpp-dependent genes. *Nature* **398**, 242–246.

Mirantes, C., Eritja, N., Dosil, M. A., Santacana, M., Pallares, J., Gatius, S., Bergadà, L., Maiques, O., Matias-Guiu, X. and Dolcet, X. (2013). An inducible knockout mouse to model the cell-autonomous role of PTEN in initiating endometrial, prostate and thyroid neoplasias. *Dis. Model. Mech.* **6**, 710–20.

Morata, G. and Ripoll, P. (1975). Minutes: mutants of *drosophila* autonomously affecting cell division rate. *Dev. Biol.* **42**, 211–221.

Moreno, E. (2008). Is cell competition relevant to cancer? *Nat. Rev. Cancer* **8**, 141–147.

Moreno, E. and Basler, K. (2004). dMyc transforms cells into super-competitors. *Cell* **117**, 117–129.

Moreno, E., Basler, K. and Morata, G. (2002). Cells compete for decapentaplegic survival factor to prevent apoptosis in *Drosophila* wing development. *Nature* **416**, 755–759.

Moser, M. and Campbell, G. (2005). Generating and interpreting the Brinker gradient in the *Drosophila* wing. *Dev. Biol.* **286**, 647–658.

Müller, B., Hartmann, B., Pyrowolakis, G., Affolter, M. and Basler, K. (2003). Conversion of an extracellular Dpp/BMP morphogen gradient into an inverse transcriptional gradient. *Cell* **113**, 221–233.

Müller, P., Rogers, K. W., Yu, S. R., Brand, M. and Schier, A. F. (2013). Morphogen transport. *Development* **140**, 1621–38.

Nakae, J., Kido, Y. and Accili, D. (2001). Distinct and overlapping functions of insulin and IGF-I receptors. *Endocr. Rev.* **22**, 818–835.

Nakato, H., Futch, T. a and Selleck, S. B. (1995). The division abnormally delayed (dally) gene: a putative integral membrane proteoglycan required for cell division patterning during postembryonic development of the nervous system in *Drosophila*. *Development* **121**, 3687–3702.

Nakato, H., Fox, B. and Selleck, S. B. (2002). dally, a *Drosophila* member of the glypican family of integral membrane proteoglycans, affects cell cycle progression and morphogenesis via a Cyclin A-mediated process. *J. Cell Sci.* **115**, 123–30.

Nellen, D., Burke, R., Struhl, G. and Basler, K. (1996). Direct and Long-Range Action of a DPP Morphogen Gradient. *Cell* **85**, 357–368.

Neto-Silva, R. M., de Beco, S. and Johnston, L. a. (2010). Evidence for a growth-stabilizing regulatory feedback mechanism between Myc and Yorkie, the *drosophila* homolog of Yap. *Dev. Cell* **19**, 507–520.

Neufeld, T. P. (2003). Body building: Regulation of shape and size by PI3K/TOR signaling during development. *Mech. Dev.* **120**, 1283–1296.

Neufeld, T. P., de la Cruz, a F., Johnston, L. a and Edgar, B. a (1998). Coordination of growth and cell division in the *Drosophila* wing. *Cell* **93**, 1183–93.

Neumann, C. and Cohen, S. (1997). Morphogens and pattern formation. *Bioessays* **19**, 721–729.

Ng, M., Diaz-Benjumea, F. J., Vincent, J. P., Wu, J. and Cohen, S. M. (1996). Specification of the wing by localized expression of wingless protein. *Nature* **381**, 316–318.

Nolo, R., Morrison, C. M., Tao, C., Zhang, X. and Halder, G. (2006). The bantam MicroRNA Is a Target of the Hippo Tumor-Suppressor Pathway. *Curr. Biol.* **16**, 1895–1904.

Norman, M., Wisniewska, K., Lawrenson, K., Garcia-Miranda, P., Tada, M., Kajita, M., Mano, H., Ishikawa, S., Ikegawa, M., Shimada, T., et al. (2012). Loss of Scribble causes cell competition in mammalian cells. *J. Cell Sci.*

Nowak, K., Seisenbacher, G., Hafen, E. and Stocker, H. (2013). Nutrient restriction enhances the proliferative potential of cells lacking the tumor suppressor PTEN in mitotic tissues. *Elife* **2013**, e00380–e00380.

Oliver, E. R., Saunders, T. L., Tarlé, S. a and Glaser, T. (2004). Ribosomal protein L24 defect in belly spot and tail (Bst), a mouse Minute. *Development* **131**, 3907–3920.

Pallares-Cartes, C., Cakan-Akdogan, G. and Teleman, A. a. (2012). Tissue-Specific Coupling between Insulin/IGF and TORC1 Signaling via PRAS40 in *Drosophila*. *Dev. Cell* **22**, 172–182.

Parker, J. (2011). Morphogens, nutrients, and the basis of organ scaling. *Evol. Dev.* **13**, 304–314.

Parker, J. and Struhl, G. (2015). Scaling the *Drosophila* Wing: TOR-Dependent Target Gene Access by the Hippo Pathway Transducer Yorkie. *PLOS Biol.* **13**, e1002274.

Pérez-Garijo, A., Martín, F. a and Morata, G. (2004). Caspase inhibition during apoptosis causes abnormal signalling and developmental aberrations in *Drosophila*. *Development* **131**, 5591–5598.

Pérez-Garijo, A., Fuchs, Y. and Steller, H. (2013). Apoptotic cells can induce non-autonomous apoptosis through the TNF pathway. *Elife* **2013**, e01004.

Potter, C. J., Huang, H. and Xu, T. (2001). *Drosophila* Tsc1 functions with Tsc2 to antagonize insulin signaling in regulating cell growth, cell proliferation, and organ size. *Cell* **105**, 357–368.

Potter, C. J., Pedraza, L. G. and Xu, T. (2002). Akt regulates growth by directly phosphorylating Tsc2. *Nat. Cell Biol.* **4**, 658–665.

Puig, O., Marr, M. T. M., Ruhf, M. L. and Tjian, R. (2003). Control of cell number by *Drosophila* FOXO : downstream and feedback regulation of the insulin receptor pathway. *Genes Dev.* **17**, 2006–2020.

Pyrowolakis, G., Hartmann, B., Müller, B., Basler, K. and Affolter, M. (2004). A simple molecular complex mediates widespread BMP-induced repression during *Drosophila* development. *Dev. Cell* **7**, 229–240.

Reiter, L. T. and Bier, E. (2002). Using *Drosophila* melanogaster to uncover human disease gene function and potential drug target proteins. *Expert Opin. Ther. Targets* **6**, 387–399.

Restrepo, S., Zartman, J. J. and Basler, K. (2014). Coordination of patterning and growth by the morphogen DPP. *Curr. Biol.* **24**, R245–R255.

Riley, M. a and Wertz, J. E. (2002). Bacteriocins: evolution, ecology, and application. *Annu. Rev. Microbiol.* **56**, 117–137.

Robinson, B. S., Huang, J., Hong, Y. and Moberg, K. H. (2010). Crumbs Regulates Salvador/Warts/Hippo Signaling in *Drosophila* via the FERM-Domain Protein Expanded. *Curr. Biol.* **20**, 582–590.

Rodrigues, a. B., Zoranovic, T., Ayala-Camargo, a., Grewal, S., Reyes-Robles, T., Krasny, M., Wu, D. C., Johnston, L. a. and Bach, E. a. (2012). Activated STAT regulates growth and induces competitive interactions independently of Myc, Yorkie, Wingless and ribosome biogenesis. *Development* **139**, 4051–4061.

Rogulja, D. and Irvine, K. D. (2005). Regulation of cell proliferation by a morphogen gradient. *Cell* **123**, 449–461.

Rogulja, D., Rauskolb, C. and Irvine, K. D. (2008). Morphogen Control of Wing Growth through the Fat Signaling Pathway. *Dev. Cell* **15**, 309–321.

Roy, S., Hsiung, F. and Kornberg, T. B. (2011). Specificity of *Drosophila* Cytonemes for Distinct Signaling Pathways. *Science (80-.).* **332**, 354–359.

Ruberte, E., Marty, T., Nellen, D., Affolter, M. and Basler, K. (1995). An absolute requirement for both the type II and type I receptors, punt and thick veins, for dpp signaling in vivo. *Cell* **80**, 889–897.

Ryoo, H. D., Gorenc, T. and Steller, H. (2004). Apoptotic cells can induce compensatory cell proliferation through the JNK and the wingless signaling pathways. *Dev. Cell* **7**, 491–501.

Sancak, Y., Thoreen, C. C., Peterson, T. R., Lindquist, R. a., Kang, S. a., Spooner, E., Carr, S. a. and Sabatini, D. M. (2007). PRAS40 Is an Insulin-Regulated Inhibitor of the mTORC1 Protein Kinase. *Mol. Cell* **25**, 903–915.

Sancak, Y., Peterson, T. R., Shaul, Y. D., Lindquist, R. A., Thoreen, C. C., Bar-Peled, L. and Sabatini, D. M. (2008). The Rag GTPases bind raptor and mediate amino acid signaling to mTORC1. *Science (80-.).* **320**, 1496–1501.

Sancho, M., Di-Gregorio, A., George, N., Pozzi, S., Sánchez, J., Pernaute, B. and Rodríguez, T. (2013). Competitive interactions eliminate unfit embryonic stem cells at the onset of differentiation. *Dev. Cell* **26**, 19–30.

Saucedo, L. J., Gao, X., Chiarelli, D. a, Li, L., Pan, D. and Edgar, B. a (2003a). Rheb promotes cell growth as a component of the insulin/TOR signalling network. *Nat. Cell Biol.* **5**, 566–571.

Saucedo, L. J., Gao, X., Chiarelli, D. A., Li, L., Pan, D. and Edgar, B. A. (2003b). Rheb promotes cell growth as a component of the insulin/TOR signalling network. *Nat Cell Biol* **5**, 566–571.

Schleich, S. and Teleman, A. a. (2009). Akt phosphorylates both Tsc1 and Tsc2 in *drosophila*, but neither phosphorylation is required for normal animal growth. *PLoS One* **4**,.

Schwank, G. and Basler, K. (2010). Regulation of organ growth by morphogen gradients. *Cold Spring Harb. Perspect. Biol.* **2**, a001669.

Schwank, G., Restrepo, S. and Basler, K. (2008). Growth regulation by Dpp: an essential role for Brinker and a non-essential role for graded signaling levels. *Development* **135**, 4003–4013.

Schwank, G., Tauriello, G., Yagi, R., Kranz, E., Koumoutsakos, P. and Basler, K. (2011). Antagonistic Growth Regulation by Dpp and Fat Drives Uniform Cell Proliferation. *Dev. Cell* **20**, 123–130.

Serrano, N. and O'Farrell, P. H. (1997). Limb morphogenesis: connections between patterning and growth. *Curr. Biol.* **7**, R186–R195.

Shraiman, B. I. (2005). Mechanical feedback as a possible regulator of tissue growth. *Proc. Natl. Acad. Sci. U. S. A.* **102**, 3318–3323.

Simpson, P. (1979). Parameters of cell competition in the compartments of the wing disc of *Drosophila*. *Dev. Biol.* **69**, 182–193.

Simpson, P. and Morata, G. (1981). Differential mitotic rates and patterns of growth in compartments in the *Drosophila* wing. *Dev. Biol.* **85**, 299–308.

Smith, E. M., Finn, S. G., Tee, A. R., Brownei, G. J. and Proud, C. G. (2005). The tuberous sclerosis protein TSC2 is not required for the regulation of the mammalian target of rapamycin by amino acids and certain cellular stresses. *J. Biol. Chem.* **280**, 18717–18727.

Steller, H. (2008). Regulation of apoptosis in *Drosophila*. *Cell Death Differ.* **15**, 1132–1138.

Stocker, H., Radimerski, T., Schindelholz, B., Wittwer, F., Belawat, P., Daram, P., Breuer, S., Thomas, G. and Hafen, E. (2003). Rheb is an essential regulator of S6K in controlling cell growth in *Drosophila*. *Nat. Cell Biol.* **5**, 559–565.

Straßburger, K., Tiebe, M., Pinna, F., Breuhahn, K. and Teleman, A. a. (2012). Insulin/IGF signaling drives cell proliferation in part via Yorkie/YAP. *Dev. Biol.* **367**, 187–196.

Strigini, M. and Cohen, S. M. (1997). A Hedgehog activity gradient contributes to AP axial patterning of the *Drosophila* wing. *Development* **124**, 4697–4705.

Struhl, G. and Basler, K. (1993). Organizing activity of wingless protein in *Drosophila*. *Cell* **72**, 527–540.

Takino, K., Ohsawa, S. and Igaki, T. (2014). Loss of Rab5 drives non-autonomous cell proliferation through TNF and Ras signaling in *Drosophila*. *Dev. Biol.* **395**, 19–28.

Tamori, Y., Bialucha, C. U., Tian, A. G., Kajita, M., Huang, Y. C., Norman, M., Harrison, N., Poulton, J., Ivanovitch, K., Disch, L., et al. (2010). Involvement of Lgl and Mahjong/VprBP in Cell Competition. *PLoS Biol.* **8**, 1–10.

Taniguchi, C. M., Emanuelli, B. and Kahn, C. R. (2006). Critical nodes in signalling pathways: insights into insulin action. *Nat. Rev. Mol. Cell Biol.* **7**, 85–96.

Tapon, N., Ito, N., Dickson, B. J., Treisman, J. E. and Hariharan, I. K. (2001). The *Drosophila* tuberous sclerosis complex gene homologs restrict cell growth and cell proliferation. *Cell* **105**, 345–355.

Tapon, N., Harvey, K. F., Bell, D. W., Wahrer, D. C. R., Schiripo, T. a., Haber, D. a. and Hariharan, I. K. (2002). salvador promotes both cell cycle exit and apoptosis in *Drosophila* and is mutated in human cancer cell lines. *Cell* **110**, 467–478.

Tee, A. R., Manning, B. D., Roux, P. P., Cantley, L. C. and Blenis, J. (2003). Tuberous sclerosis complex gene products, Tuberin and Hamartin, control mTOR signaling by acting as a GTPase-activating protein complex toward Rheb. *Curr. Biol.* **13**, 1259–1268.

Teleman, a a and Cohen, S. M. (2000). Dpp gradient formation in the *Drosophila* wing imaginal disc. *Cell* **103**, 971–980.

Teleman, A. a., Hietakangas, V., Sayadian, A. C. and Cohen, S. M. (2008). Nutritional Control of Protein Biosynthetic Capacity by Insulin via Myc in *Drosophila*. *Cell Metab.* **7**, 21–32.

Thompson, B. J. and Cohen, S. M. (2006). The Hippo Pathway Regulates the bantam microRNA to Control Cell Proliferation and Apoptosis in *Drosophila*. *Cell* **126**, 767–774.

Tiebe, M., Lutz, M., De La Garza, A., Buechling, T., Boutros, M. and Teleman, A. A. (2015). REPTOR and REPTOR-BP Regulate Organismal Metabolism and Transcription Downstream of TORC1. *Dev. Cell* **33**, 272–284.

Tsuda, M., Kamimura, K., Nakato, H., Archer, M., Staatz, W., Fox, B., Humphrey, M., Olson, S., Futch, T., Kaluza, V., et al. (1999). The cell-surface proteoglycan Dally regulates Wingless signalling in *Drosophila*. *Nature* **400**, 276–280.

Tsuneizumi, K., Nakayama, T., Kamoshida, Y., Kornberg, T. B., Christian, J. L. and Tabata, T. (1997). Daughters against dpp modulates dpp organizing activity in *Drosophila* wing development. *Nature* **389**, 627–631.

Tyler, D. M., Li, W., Zhuo, N., Pellock, B. and Baker, N. E. (2007). Genes Affecting Cell Competition in *Drosophila*. *Genetics* **175**, 643–657.

Udan, R. S., Kango-Singh, M., Nolo, R., Tao, C. and Halder, G. (2003). Hippo promotes proliferation arrest and apoptosis in the Salvador/Warts pathway. *Nat. Cell Biol.* **5**, 914–920.

Vallejo, D. M., Juarez-Carreño, S., Bolivar, J., Morante, J. and Dominguez, M. (2015). A brain circuit that synchronizes growth and maturation revealed through Dilp8 binding to Lgr3. *Science (80-.).* 1–16.

Vander Haar, E., Lee, S.-I., Bandhakavi, S., Griffin, T. J. and Kim, D.-H. (2007). Insulin signalling to mTOR mediated by the Akt/PKB substrate PRAS40. *Nat. Cell Biol.* **9**, 316–323.

Vidal, M., Larson, D. E. and Cagan, R. L. (2006). Csk-Deficient Boundary Cells Are Eliminated from Normal *Drosophila* Epithelia by Exclusion, Migration, and Apoptosis. *Dev. Cell* **10**, 33–44.

Vuilleumier, R., Springhorn, A., Patterson, L., Koidl, S., Hammerschmidt, M., Affolter, M. and Pyrowolakis, G. (2010). Control of Dpp morphogen signalling by a secreted feedback regulator. *Nat. Cell Biol.* **12**, 611–617.

Wang, S. H., Simcox, A. and Campbell, G. (2000). Dual role for *Drosophila* epidermal growth factor receptor signaling in early wing disc development. *Genes Dev.* **14**, 2271–2276.

Wang, X., Li, W., Williams, M., Terada, N., Alessi, D. R. and Proud, C. G. (2001). Regulation of elongation factor 2 kinase by p90(RSK1) and p70 S6 kinase. *Eur. Mol. Biol. Organ. J.* **20**, 4370–4379.

Wartlick, O., Mumcu, P., Kicheva, a, Bittig, T., Seum, C., Jülicher, F. and González-Gaitán, M. (2011a). Dynamics of Dpp signaling and proliferation control. *Science* **331**, 1154–1159.

Wartlick, O., Mumcu, P., Jülicher, F. and Gonzalez-Gaitan, M. (2011b). Understanding morphogenetic growth control - lessons from flies. *Nat. Rev. Mol. Cell Biol.* **12**, 594–604.

Weigmann, K., Cohen, S. M. and Lehner, C. F. (1997). Cell cycle progression, growth and patterning in imaginal discs despite inhibition of cell division after inactivation of *Drosophila* Cdc2 kinase. *Development* **124**, 3555–3563.

Winter, S. E. and Campbell, G. (2004). Repression of Dpp targets in the *Drosophila* wing by Brinker. *Development* **131**, 6071–6081.

Wu, Q. and Brown, M. R. (2006). Signaling and function of insulin-like peptides in insects. *Annu. Rev. Entomol.* **51**, 1–24.

Wu, J. and Cohen, S. M. (2002). Repression of Teashirt marks the initiation of wing development. *Development* **129**, 2411–2418.

Wu, S., Huang, J., Dong, J. and Pan, D. (2003). hippo encodes a Ste-20 family protein kinase that restricts cell proliferation and promotes apoptosis in conjunction with salvador and warts. *Cell* **114**, 445–456.

Xu, T. and Rubin, G. M. (1993). Analysis of genetic mosaics in developing and adult *Drosophila* tissues. *Development* **117**, 1223–1237.

Yan, D. and Lin, X. (2009). Shaping morphogen gradients by proteoglycans. *Cold Spring Harb. Perspect. Biol.* **1**, a002493.

Yu, J., Zheng, Y., Dong, J., Klusza, S., Deng, W. M. and Pan, D. (2010). Kibra Functions as a Tumor Suppressor Protein that Regulates Hippo Signaling in Conjunction with Merlin and Expanded. *Dev. Cell* **18**, 288–299.

Yuan, T. L. and Cantley, L. C. (2008). PI3K pathway alterations in cancer: variations on a theme. *Oncogene* **27**, 5497–5510.

Zecca, M. and Struhl, G. (2002a). Control of growth and patterning of the *Drosophila* wing imaginal disc by EGFR-mediated signaling. *Development* **129**, 1369–1376.

Zecca, M. and Struhl, G. (2002b). Subdivision of the *Drosophila* wing imaginal disc by EGFR-mediated signaling. *Development* **129**, 1357–1368.

Zecca, M., Basler, K. and Struhl, G. (1995). Sequential organizing activities of engrailed, hedgehog and decapentaplegic in the *Drosophila* wing. *Development* **121**, 2265–2278.

Zecca, M., Basler, K. and Struhl, G. (1996). Direct and long-range action of a wingless morphogen gradient. *Cell* **87**, 833–844.

Zhang, H., Stallock, J. P., Ng, J. C., Reinhard, C. and Neufeld, T. P. (2000). Regulation of cellular growth by the *Drosophila* target of rapamycin dTOR. *Genes Dev.* **14**, 2712–2724.

Zhang, Y., Gao, X., Saucedo, L. J., Ru, B., Edgar, B. A. and Pan, D. (2003). Rheb is a direct target of the tuberous sclerosis tumour suppressor proteins. *Nat Cell Biol* **5**, 578–581.

Zhang, Y., You, J., Ren, W. and Lin, X. (2013). *Drosophila* glypicans Dally and Dally-like are essential regulators for JAK/STAT signaling and Unpaired distribution in eye development. *Dev. Biol.* **375**, 23–32.

Zhao, M., Szafranski, P., Hall, C. A. and Goode, S. (2008). Basolateral junctions utilize warts signaling to control epithelial-mesenchymal transition and proliferation crucial for migration and invasion of *drosophila* ovarian epithelial cells. *Genetics* **178**, 1947–1971.

Zhao, B., Tumaneng, K. and Guan, K.-L. (2011). The Hippo pathway in organ size control, tissue regeneration and stem cell self-renewal. *Nat. Cell Biol.* **13**, 877–883.

Zhou, S., Lo, W. C., Suhalim, J. L., Digman, M. a., Gratton, E., Nie, Q. and Lander, A. D. (2012). Free extracellular diffusion creates the Dpp morphogen gradient of the *Drosophila* wing disc. *Curr. Biol.* **22**, 668–675.

Ziosi, M., Baena-López, L. A., Grifoni, D., Froldi, F., Pession, A., Garoia, F., Trotta, V., Bellosta, P., Cavicchi, S. and Pession, A. (2010). dMyc Functions Downstream of Yorkie to Promote the Supercompetitive Behavior of Hippo Pathway Mutant Cells. *PLoS Genet.* **6**, e1001140.

Supporting Tables

Supporting Tables

AREA (% CONTROL) ± STD DEV						
Genotype	Total	p-value	Anterior	p-value	Posterior	p-value
nub>GFP	100 ± 1,0	-	100 ± 1,9	-	100 ± 2,1	-
nub>Dp110	136 ± 6,4	10^{-12}	142 ± 6,5	10^{-13}	129 ± 2,0	10^{-11}
nub>PTEN^{RNAi}	126 ± 3,7	10^{-15}	125 ± 3,3	10^{-15}	127 ± 4,2	10^{-14}
nub>Rheb	109 ± 6,7	10^{-4}	110 ± 1,8	10^{-5}	107 ± 2,6	0,02

CELL DENSITY (% CONTROL) ± STD DEV				
Genotype	Anterior	p-value	Posterior	p-value
nub>GFP	100 ± 5,9	-	100 ± 2,4	-
nub>Dp110	94 ± 5,7	0,03	93 ± 6,8	0,004
nub>PTEN^{RNAi}	90 ± 2,5	10^{-4}	88 ± 4,0	10^{-7}
nub>Rheb	90 ± 11,3	0,02	95 ± 7,2	0,04

Table 1. Quantitative measurements regarding Figure 15. Tissue size values of whole wings (total) and its anterior and posterior compartments of flies expressing *Dp110*, *PTEN^{RNAi}* or *Rheb* transgenes in the *nub* domain measured as a ratio (in percentage) with respect to control wings expressing *GFP* in the same domain. Cell density values of both anterior and posterior compartments measured as a ratio (in percentage) with respect to control wings expressing *GFP* in the same domains. These values correspond to the average of 10 adult wings with their corresponding standard deviations. A t-test was carried out to calculate the p-value as a measurement of the statistical significance of the difference between transgene expressing and GFP expressing wings. Total, anterior and posterior areas were significantly increased. Cell density values were significantly reduced in both compartments.

AREA (% CONTROL) ± STD DEV						
Genotype	Total	p-value	Anterior	p-value	Posterior	p-value
ci>GFP	100 ± 2,5	-	100 ± 3,5	-	100 ± 2,9	-
ci>Dp110	93 ± 2,8	10^{-5}	113 ± 3,9	10^{-7}	77 ± 3,0	10^{-12}
ci>PTEN^{RNAi}	96 ± 4,5	0,03	118 ± 4,7	10^{-10}	77 ± 4,9	10^{-12}
ci>Rheb	96 ± 4,4	0,02	114 ± 6,2	10^{-6}	80 ± 3,8	10^{-10}
CELL DENSITY (% CONTROL) ± STD DEV						
Genotype	Anterior	p-value	Posterior	p-value		
ci>GFP	100 ± 3,2	-	100 ± 5,5	-		
ci>Dp110	97 ± 5,3	0,1	123 ± 6,4	10^{-8}		
ci>PTEN^{RNAi}	91 ± 3,3	10^{-6}	126 ± 4,4	10^{-9}		
ci>Rheb	82 ± 4,1	10^{-9}	114 ± 4,1	10^{-6}		

Table 2. Quantitative measurements regarding Figure 16. Tissue size values of whole wings (total) and its anterior and posterior compartments of flies expressing *Dp110*, *PTEN^{RNAi}* or *Rheb* transgenes in the *ci* domain measured as a ratio (in percentage) with respect to control wings expressing *GFP* in the same domain. Cell density values of both anterior and posterior compartments measured as a ratio (in percentage) with respect to control wings expressing *GFP* in the same domain. These values correspond to the average of 10 adult wings with their corresponding standard deviations. A t-test was carried out to calculate the p-value as a measurement of the statistical significance of the difference between transgene expressing and GFP expressing wings. Total and anterior were significantly increased while posterior areas were significantly reduced. Cell density values were significantly increased in the transgene non-expressing compartment.

AREA (% CONTROL) ± STD DEV						
Genotype	Total	p-value	Anterior	p-value	Posterior	p-value
en>GFP	100 ± 3,8	-	100 ± 4,1	-	100 ± 2,8	-
en>Dp110	115 ± 4,0	10^{-9}	90 ± 2,7	10^{-8}	138 ± 5,6	10^{-14}
en>PTEN^{RNAi}	110 ± 3,5	10^{-6}	89 ± 4,6	10^{-6}	129 ± 4,2	10^{-14}
en>Rheb	115 ± 3,9	10^{-8}	84 ± 5,8	10^{-7}	139 ± 4,3	10^{-15}
CELL DENSITY (% CONTROL) ± STD DEV						
Genotype	Anterior	p-value	Posterior	p-value		
en>GFP	100 ± 6,4	-	100 ± 4,1	-		
en>Dp110	118 ± 5,1	10^{-7}	84 ± 3,0	10^{-9}		
en>PTEN^{RNAi}	113 ± 4,0	10^{-5}	87 ± 1,6	10^{-8}		
en>Rheb	111 ± 2,8	10^{-4}	71 ± 2,7	10^{-13}		

Table 3. Quantitative measurements regarding Figure 17. Tissue size values of whole wings (total) and its anterior and posterior compartments of flies expressing *Dp110*, *PTEN^{RNAi}* or *Rheb* transgenes in the *en* domain measured as a ratio (in percentage) with respect to control wings expressing *GFP* in the same domain. Cell density values of both anterior and posterior compartments measured as a ratio (in percentage) with respect to control wings expressing *GFP* in the same domain. These values correspond to the average of 10 adult wings with their corresponding standard deviations. A t-test was carried out to calculate the p-value as a measurement of the statistical significance of the difference between transgene expressing and GFP expressing wings. Total and posterior were significantly increased while anterior areas were significantly reduced. Cell density values were significantly increased in the transgene non-expressing compartment.

AREA (% CONTROL) ± STD DEV						
Genotype	Total	p-value	Anterior	p-value	Posterior	p-value
hh>GFP	100 ± 3,1	-	100 ± 4,7	-	100 ± 4,1	-
hh>PTEN^{RNAi}	111 ± 3,0	10^{-4}	74 ± 6,7	10^{-12}	147 ± 2,8	10^{-14}
hh>Rheb	109 ± 7,1	10^{-4}	67 ± 6,9	10^{-12}	150 ± 8,9	10^{-14}

CELL DENSITY (% CONTROL) ± STD DEV				
Genotype	Anterior	p-value	Posterior	p-value
hh>GFP	100 ± 3,1	-	100 ± 3,6	-
hh>PTEN^{RNAi}	116 ± 4,5	10^{-8}	77 ± 3,0	10^{-12}
hh>Rheb	119 ± 5,2	10^{-8}	66 ± 3,4	10^{-14}

Table 4. Quantitative measurements regarding Figure 18. Tissue size values of whole wings (total) and its anterior and posterior compartments of flies expressing *Dp110*, *PTEN^{RNAi}* or *Rheb* transgenes in the *hh* domain measured as a ratio (in percentage) with respect to control wings expressing *GFP* in the same domain. Cell density values of both anterior and posterior compartments measured as a ratio (in percentage) with respect to control wings expressing *GFP* in the same domain. These values correspond to the average of 10 adult wings with their corresponding standard deviations. A t-test was carried out to calculate the p-value as a measurement of the statistical significance of the difference between transgene expressing and GFP expressing wings. Total and posterior were significantly increased while anterior areas were significantly reduced. Cell density values were significantly increased in the transgene non-expressing compartment.

AREA (% CONTROL) ± STD DEV						
Genotype	Total	p-value	Medial	p-value	Lateral	p-value
spalt^{PE}>GFP	100 ± 3,0	-	100 ± 3,2	-	100 ± 3,1	-
spalt^{PE}>PTEN^{RNAi}	110 ± 5,3	10^{-6}	115 ± 5,0	10^{-9}	85 ± 1,8	10^{-6}

CELL DENSITY (% CONTROL) ± STD DEV				
Genotype	Medial	p-value	Lateral	p-value
spalt^{PE}>GFP	100 ± 3,5	-	100 ± 2,3	-
spalt^{PE}>PTEN^{RNAi}	95 ± 3,6	0,003	109 ± 9,4	0,007

Table 5. Quantitative measurements regarding Figure 19. Tissue size values of whole wings (total), medial and lateral regions of the wings of flies expressing *PTEN^{RNAi}* in the *spalt* domain measured as a ratio (in percentage) with respect to control wings expressing *GFP* in the same domain. Cell density values of both medial and lateral regions measured as a ratio (in percentage) with respect to control wings expressing *GFP* in the same domain. These values correspond to the average of 10 adult wings with their corresponding standard deviations. A t-test was carried out to calculate the p-value as a measurement of the statistical significance of the difference between transgene expressing and GFP expressing wings. Total and medial areas were significantly increased while lateral areas were significantly reduced. Cell density values were significantly increased in the transgene non-expressing domain.

AREA (% CONTROL) ± STD DEV						
Genotype	Total	p-value	Anterior	p-value	Posterior	p-value
ci>GFP	100 ± 2,5	-	100 ± 3,5	-	100 ± 2,9	-
ci>GFP, stg:cycE	98 ± 4,6	0,2	95 ± 4,7	0,005	102 ± 4,8	0,2

CELL DENSITY (% CONTROL) ± STD DEV				
Genotype	Anterior	p-value	Posterior	p-value
ci>GFP	100 ± 3,2	-	100 ± 5,5	-
ci>GFP, stg:cycE	139 ± 7,1	10^{-11}	100 ± 6,9	0,9

Table 6. Quantitative measurements regarding Figure 20. Tissue size values of whole wings (total), anterior and posterior compartments of the wing of flies expressing *stg:cycE* in the *ci* domain measured as a ratio (in percentage) with respect to control wings expressing *GFP* in the same domain. Cell density values of both anterior and posterior compartments measured as a ratio (in percentage) with respect to control wings expressing *GFP* in the same domain. These values correspond to the average of 10 adult wings with their corresponding standard deviations. A t-test was carried out to calculate the p-value as a measurement of the statistical significance of the difference between transgene expressing and GFP expressing wings. Anterior area was significantly reduced while total and posterior areas were unchanged. Cell density values were significantly increased in the transgene expressing domain.

AREA (a.u.) ± STD DEV					
Genotype	Hours AEL	Anterior	p-value	Posterior	p-value
ci>GFP	72h	8182410 ± 2962836	-	3503880 ± 1415256	-
ci>Dp110		8917929 ± 1891782	0,53	2425304 ± 564358	0,05
ci>Rheb		9159519 ± 2152243	0,35	3311393 ± 780111	0,68
ci>GFP	96h	34534581 ± 8828190	-	17853186 ± 4972073	-
ci>Dp110		54019999 ± 7312248	10^{-11}	14733415 ± 1903948	0,005
ci>Rheb		37851396 ± 7855633	0,17	14055889 ± 2426341	0,001
ci>GFP	140h	88998852 ± 20829964	-	53998521 ± 12343187	-
ci>Dp110		149811761 ± 30924178	10^{-10}	43848257 ± 8465028	0,002
ci>Rheb		123603449 ± 17092310	10^{-5}	39487669 ± 8321698	0,002

Table 7. Quantitative measurements regarding Figure 22. Tissue size values (in arbitrary units) of anterior and posterior compartments of the wing imaginal discs of flies expressing *GFP, Dp110* and *Rheb* in the *ci* domain in three different time points during development. These values correspond to the average of ≥ 15 wing imaginal discs per genotype and per time point with their corresponding standard deviations. A t-test was carried out to calculate the p-value as a measurement of the statistical significance of the difference between transgene expressing and GFP expressing discs. The nonautonomous reduction in tissue size is already statistically significant at 96h AEL.

CLONE AREA (a.u.) ± STD DEV				
Genotype	Anterior	p-value	Posterior	p-value
ci>GFP	388 ± 141	-	348 ± 140	-
ci>GFP, Dp110	587 ± 249	10^{-4}	114 ± 67	10^{-13}
NUMBER OF CELLS/CLONE ± STD DEV				
Genotype	Anterior	p-value	Posterior	p-value
ci>GFP	20 ± 7	-	23 ± 7	-
ci>GFP, Dp110	23 ± 8	0,21	9 ± 4	10^{-14}

Table 8. Quantitative measurements regarding Figure 23. Size values (in arbitrary units) and number of cells of wild type clones in anterior and posterior compartments of wing imaginal discs of flies expressing *GFP* and *Dp110* in the *ci* domain. Clones were generated at the beginning of the third instar period and quantified 72h later in late third instar wing discs. These values correspond to the average of ≥ 30 clones with their corresponding standard deviations. A t-test was carried out to calculate the p-value as a measurement of the statistical significance of the difference between transgene expressing and GFP expressing discs. Clonal size and number of cells/clone values were significantly increased and decrease respectively in the transgene nonexpressing domain.

MITOTIC FIGURES/AREA (A.U.) ± STD DEV				
Genotype	Anterior	p-value	Posterior	p-value
ci>GFP	3,397 ± 0,001	-	4,358 ± 0,001	-
ci>GFP, Rheb	3,276 ± 0,001	0,7	4,626 ± 0,001	0,6
ci>GFP, Dp110	2,954 ± 0,001	0,2	3,711 ± 0,001	0,2
Genotype	Anterior	p-value	Posterior	p-value
en>GFP	6,542 ± 0,001	-	6,495 ± 0,002	-
en>GFP, Rheb	5,260 ± 0,001	0,02	5,204 ± 0,001	0,08
en>GFP, Dp110	8,135 ± 0,001	0,06	7,555 ± 0,001	0,07

Table 9. Quantitative measurements regarding Figure 24. Mitotic figures/area (in arbitrary units) in anterior and posterior compartments of wing imaginal discs of flies expressing *GFP*, *Rheb* or *Dp110* in the *ci* or *en* domains. A t-test was carried out to calculate the p-value as a measurement of the statistical significance of the difference between transgene expressing and GFP expressing discs. No significant changes were observed.

PUPAL VOLUME (% CONTROL) ± STD DEV		
Genotype	Pupal Volume	p-value
ci>GFP	100 ± 13,4	-
ci>GFP, Rheb	86 ± 8,7	0,01
ci>GFP, Dp110	109 ± 15,2	0,2
ci>GFP, PTEN^{RNAi}	93 ± 15,4	0,3
Genotype	Pupal Volume	p-value
en>GFP	100 ± 4,3	-
en>GFP, Rheb	105 ± 5,5	0,3
en>GFP, Dp110	112 ± 13,9	0,2
en>GFP, PTEN^{RNAi}	101 ± 13,2	0,8

Table 10. Quantitative measurements regarding Figure 27. Pupa volume values of animals expressing *Rheb, Dp110 or PTEN^{RNAi}* either with *ci-gal4* or *en-gal4* driver measured as a ratio (in percentage) with respect to controls expressing *GFP* in the same domain. These values correspond to the average of at least 10 pupae with their corresponding standard deviations. A t-test was carried out to calculate the p-value as a measurement of the statistical significance of the difference between transgene expressing and GFP expressing animals. No significant changes were observed.

APOPTOTIC CELLS (A.U.) ± STD DEV				
Genotype	Anterior	p-value	Posterior	p-value
ci>GFP	4,4 ± 4,2	-	5,5 ± 4,7	-
ci>GFP, Rheb	72,0 ± 26,5	10^{-10}	2,0 ± 1,7	0,02
ci>GFP, Dp110	91,4 ± 25,4	10^{-12}	5,5 ± 3,4	0,98

Table 11. Quantitative measurements regarding Figure 28. Absolute number of apoptotic cells in anterior and posterior compartments of wing imaginal discs of flies expressing *GFP*, *Rheb* or *Dp110* in the *ci* domain. A t-test was carried out to calculate the p-value as a measurement of the statistical significance of the difference between transgene expressing and GFP expressing discs. No significant changes were observed in the nonautonomous domain.

AREA (% CONTROL) ± STD DEV						
Genotype	Total	p-value	Anterior	p-value	Posterior	p-value
en>2xGFP	100 ± 2,1	-	100 ± 3,3	-	100 ± 2,1	-
en>GFP, Rheb; +/+	113 ± 3,1	10^{-9}	90 ± 6,0	10^{-4}	129 ± 3,4	10^{-15}
en>GFP, Rheb; H99/+	104 ± 3,8	10^{-5}	83 ± 2,9	0,003	118 ± 5,0	10^{-5}
en>GFP, Rheb, dp53^{ct}	106 ± 1,8	10^{-6}	85 ± 3,9	0,04	120 ± 1,8	10^{-7}
ci>2xGFP	100 ± 1,9	-	100 ± 1,8	-	100 ± 2,5	-
ci>GFP, Dp110; +/+	88 ± 3,6	10^{-8}	120 ± 3,9	10^{-11}	74 ± 4,1	10^{-12}
ci>GFP, Dp110; H99/+	99 ± 3,3	10^{-6}	126 ± 5,5	0,02	79 ± 3,2	0,007

CELL DENSITY (% CONTROL) ± STD DEV				
Genotype	Anterior	p-value	Posterior	p-value
en>2xGFP	100 ± 3,4	-	100 ± 3,3	-
en>GFP, Rheb; +/+	108 ± 4,6	10^{-4}	70 ± 3,3	10^{-14}
en>GFP, Rheb; H99/+	113 ± 5,9	0,08	73 ± 2,4	0,02
en>GFP, Rheb, dp53^{ct}	110 ± 2,3	0,3	72 ± 3,4	0,2

APOPTOTIC CELLS (A.U) ± STD DEV				
Genotype	Anterior	p-value	Posterior	p-value
en>2xGFP	4 ± 4,2	-	5 ± 4,7	-
en>GFP, Rheb; +/+	14 ± 7,8	10^{-4}	191 ± 23,2	10^{-19}
en>GFP, Rheb; H99/+	23 ± 12,5	0,09	137 ± 31,0	0,001
en>GFP, Rheb, dp53^{ct}	6 ± 6,9	0,03	122 ± 40,5	10^{-4}

Table 12. Quantitative measurements regarding Figure 29. Tissue size values of whole wings (total), anterior and posterior compartments of the wing of flies of the indicated genotypes measured as a ratio (in percentage) with respect to control wings expressing GFP in the same domain. Cell density values of both anterior and posterior compartments measured as a ratio (in percentage) with respect to control wings expressing the indicated transgenes in the *en* domain. These values correspond to the average of 10 adult wings with their corresponding standard deviations. A t-test was carried out to calculate the p-value as a measurement of the statistical significance of the difference between transgene expressing and GFP expressing wings. Absolute number of apoptotic cells in anterior and posterior compartments of wing imaginal discs of flies of the indicated genotypes. A t-test was carried out to calculate the p-value as a measurement of the statistical significance of the difference between transgene expressing and GFP expressing discs.

AREA (% CONTROL) ± STD DEV						
Genotype	Total	p-value	Anterior	p-value	Posterior	p-value
en>2xGFP	100 ± 1,5	-	100 ± 2,6	-	100 ± 1,3	-
en>GFP, Rheb	118 ± 3,1	10^{-12}	91 ± 2,0	10^{-7}	142 ± 4,7	10^{-16}
en>p35, Rheb	97 ± 14,4	10^{-4}	69 ± 15,8	10^{-4}	121 ± 13,9	10^{-4}

CELL DENSITY (% CONTROL) ± STD DEV				
Genotype	Anterior	p-value	Posterior	p-value
en>2xGFP	100 ± 2,2	-	100 ± 4,6	-
en>GFP, Rheb	113 ± 3,1	10^{-9}	68 ± 3,3	10^{-13}
en>p35, Rheb	121 ± 8,2	0,01	84 ± 7,3	10^{-6}

MITOTIC FIGURES/AREA (A.U.) ± STD DEV				
Genotype	Anterior	p-value	Posterior	p-value
en>2xGFP	6,542 ± 0,001	-	6,495 ± 0,002	-
en>GFP, Rheb	5,260 ± 0,001	0,02	5,204 ± 0,001	0,08
en>p35, Rheb	9,6 ± 0,002	0,002	8,4 ± 0,002	0,05
en>GFP, Dp110	8,135 ± 0,001	0,06	7,555 ± 0,001	0,07
en>p35, Dp110	10,6 ± 0,002	10^{-4}	9,8 ± 0,003	0,04

Table 13. Quantitative measurements regarding Figure 30. Tissue size values of whole wings (total), anterior and posterior compartments of the wing of flies of the indicated genotypes measured as a ratio (in percentage) with respect to control wings expressing GFP in the *en* domain. Cell density values of both anterior and posterior compartments measured as a ratio (in percentage) with respect to control wings expressing the indicated transgenes in the *en* domain. These values correspond to the average of 10 adult wings with their corresponding standard deviations. Number of mitotic figures/area in anterior and posterior compartments of wing imaginal discs of flies of the indicated genotypes. A t-test was carried out to calculate the p-value as a measurement of the statistical significance of the difference between transgene expressing and GFP expressing discs.

AREA (% CONTROL) ± STD DEV							
Genotype	Yeast	Total	p-value	Anterior	p-value	Posterior	p-value
ci>2xGFP	100 g/L	100 ± 2,4	-	100 ± 2,9	-	100 ± 2,2	-
ci>GFP, Rheb		95 ± 6,0	0,02	116 ± 6,7	10^{-6}	78 ± 6,0	10^{-8}
en>2xGFP		100 ± 5,9	-	100 ± 5,5	-	100 ± 6,7	-
en>GFP, PTEN^{RNAi}		118 ± 4,3	10^{-7}	82 ± 4,1	10^{-7}	149 ± 5,8	10^{-12}
ci>2xGFP	20 g/L	100 ± 2,1	-	100 ± 3,3	-	100 ± 1,6	-
ci>GFP, Rheb		101 ± 7,7	0,7	115 ± 6,3	10^{-5}	90 ± 9,2	0,004
en>2xGFP		100 ± 6,3	-	100 ± 5,0	-	100 ± 17,3	-
en>GFP, PTEN^{RNAi}		124 ± 6,7	0,01	81 ± 6,1	0,02	159 ± 8,0	10^{-5}

Table 14. Quantitative measurements regarding Figure 31. Tissue size values of whole wings (total), anterior and posterior compartments of the wing of flies of the indicated genotypes measured as a ratio (in percentage) with respect to control wings expressing GFP in the *ci* or *en* domains in animals raised in food with two different concentrations of yeast. These values correspond to the average of 10 adult wings with their corresponding standard deviations.

P-MAD INTENSITY (A.U.) ± STD DEV				
Genotype	Anterior	p-value	Posterior	p-value
ci>2xGFP	4607545 ± 543956	-	2833571 ± 367250	-
ci>GFP, Dp110	5304664 ± 744489	0,1	1160516 ± 183531	10^{-6}
ci>2xGFP	2182006 ± 467961	-	1064266 ± 208610	-
ci>GFP, Rheb	2116653 ± 306063	0,8	604659 ± 48722	10^{-5}
en>2xGFP	3457660 ± 718594	-	2623238 ± 597625	-
en>GFP, PTEN^{RNAi}	2563141 ± 327462	0,05	3198569 ± 704604	0,2

Table 15. Quantitative measurements regarding Figure 33. P-MAD intensity values, in arbitrary units, of anterior and posterior compartments of the wing imaginal discs of the indicated genotypes. These values correspond to the average of at least 5 wing discs with their corresponding standard deviations. Note reduced p-MAD intensity in the nonautonomous compartments.

P-MAD INTENSITY (A.U.) ± STD DEV		
Genotype	Wing pouch	p-value
nub>GFP	6292233 ± 907108	-
nub> Dp110	6502790 ± 339713	0,6

Table 16. Quantitative measurements regarding Figure 34. P-MAD intensity values, in arbitrary units, of the wing pouch region of imaginal discs of the indicated genotypes. These values correspond to the average of at least 5 wing discs with their corresponding standard deviations. No statistical significance between control and experiment was observed.

AREA (a.u.) ± STD DEV				
Genotype	Anterior	p-value	Posterior	p-value
ci>2xGFP	88998852 ± 20829964	-	53998521 ± 12343187	-
ci>GFP, Dp110	149811761 ± 30924178	10-10	43848257 ± 8465028	0,002
ci>GFP, Dpp^{RNAi}	51455732 ± 9535773	-	22527304 ± 4171354	-
ci>Dp110, Dpp^{RNAi}	96182227 ± 24732022	10-7	29010165 ± 6287990	0,002

Table 17. Quantitative measurements regarding Figure 36. Tissue size values (in arbitrary units) of anterior and posterior compartments of the wing imaginal discs of late third wing imaginal discs expressing *GFP* or *Dp110* in the *ci* domain in the presence or absence of Dpp. These values correspond to the average of ≥ 15 wing imaginal discs per genotype with their corresponding standard deviations. A t-test was carried out to calculate the p-value as a measurement of the statistical significance of the difference between Dp110-expressing discs and its corresponding controls. Note that, in the absence of Dpp, the nonautonomous compartment no longer reduces its size.

AREA (% CONTROL) ± STD DEV						
Genotype	Total	p-value	Anterior	p-value	Posterior	p-value
ci>2xGFP	100 ± 2,5	-	100 ± 3,5	-	100 ± 2,9	-
ci>GFP, dally	103 ± 5,4	0,1	121 ± 6,9	10^{-9}	86 ± 5,1	10^{-8}
en>2xGFP	100 ± 2,1	-	100 ± 2,6	-	100 ± 2,6	-
en>GFP, dally	128 ± 5,3	10^{-12}	95 ± 4,1	0,003	155 ± 7,7	10^{-15}

CELL DENSITY (% CONTROL) ± STD DEV				
Genotype	Anterior	p-value	Posterior	p-value
ci>2xGFP	100 ± 3,2	-	100 ± 5,5	-
ci>GFP, dally	107 ± 3,2	10^{-5}	93 ± 4,2	0,006
en>2xGFP	100 ± 3,0	-	100 ± 2,0	-
en>GFP, dally	95 ± 5,0	0,08	108 ± 2,7	10^{-5}

CLONE AREA (a.u.) ± STD DEV				
Genotype	Anterior	p-value	Posterior	p-value
ci-Gal4>GFP	388 ± 141	-	348 ± 140	-
ci-Gal4>GFP, Dally	537 ± 169	10^{-4}	182 ± 89	10^{-7}

NUMBER OF CELLS/CLONE ± STD DEV				
Genotype	Anterior	p-value	Posterior	p-value
ci-Gal4>GFP	20 ± 7	-	23 ± 7	-
ci-Gal4>GFP, Dally	28 ± 12	0,005	10 ± 4	10^{-13}

Table 18. Quantitative measurements regarding Figure 40. Tissue size values of whole wings (total), anterior and posterior compartments of the wing of flies of the indicated genotypes measured as a ratio (in percentage) with respect to control wings expressing GFP in the *ci* or *en* domains in animals raised in food with two different concentrations of yeast. These values correspond to the average of 10 adult wings with their corresponding standard deviations. Size values (in arbitrary units) and number of cells of wild type clones in anterior and posterior compartments of wing imaginal discs of flies expressing *GFP* or *Dally* in the *ci* domain. Clones were generated at the beginning of the third instar period and quantified 72h later in late third instar wing discs. These values correspond to the average of ≥ 30 clones with their corresponding standard deviations. A t-test was carried out to calculate the p-value as a measurement of the statistical significance of the difference between transgene expressing and GFP expressing discs.

P-MAD INTENSITY (A.U.) ± STD DEV				
Genotype	Anterior	p-value	Posterior	p-value
ci>2xGFP	3803191 ± 834391	-	1881774 ± 282834	-
ci>GFP, Dally	4974308 ± 817762	0,004	1287812 ± 354951	10^{-4}

Table 19. Quantitative measurements regarding Figure 41. P-MAD intensity values, in arbitrary units, of anterior and posterior compartments of the wing imaginal discs of the indicated genotypes. These values correspond to the average of at least 5 wing discs with their corresponding standard deviations. Note statistically significant increased p-MAD intensity in the Dally-expressing domain and reduced in the nonautonomous compartments.

AREA (% CONTROL) ± STD DEV						
Genotype	Total	p-value	Anterior	p-value	Posterior	p-value
ci>2xGFP	100 ± 2,5	-	100 ± 3,5	-	100 ± 2,9	-
ci>GFP, Dp110	91 ± 4,1	10^{-6}	112 ± 5,3	10^{-7}	74 ± 3,2	10^{-16}
ci>Dp110, dally	102 ± 5,0	10^{-5}	139 ± 8,6	10^{-8}	70 ± 3,2	0,02
ci>GFP, PTEN^{RNAi}	90 ± 4,8	10^{-6}	107 ± 5,1	0,001	74 ± 4,7	10^{-16}
ci>PTEN^{RNAi}, dally	94 ± 7,5	0,1	127 ± 6,4	10^{-6}	63 ± 8,6	0,002

CELL DENSITY (% CONTROL) ± STD DEV				
Genotype	Anterior	p-value	Posterior	p-value
ci>2xGFP	100 ± 3,2	-	100 ± 5,5	-
ci>GFP, Dp110	88 ± 5,3	10^{-4}	120 ± 6,4	10^{-7}
ci>Dp110, dally	91 ± 5,8	0,2	119 ± 10,3	0,7
ci>GFP, PTEN^{RNAi}	91 ± 3,3	10^{-6}	126 ± 4,4	10^{-9}
ci>PTEN^{RNAi}, dally	95 ± 4,5	0,06	121 ± 9,9	0,2

Table 20. Quantitative measurements regarding Figure 43. Tissue size values of whole wings (total), anterior and posterior compartments of the wing of flies of the indicated genotypes measured as a ratio (in percentage) with respect to control wings expressing GFP in the *ci* domain. Cell density values of both anterior and posterior compartments measured as a ratio (in percentage) with respect to control wings expressing the indicated transgenes in the *ci* domain. These values correspond to the average of 10 adult wings with their corresponding standard deviations. A t-test was carried out to calculate the p-value as a measurement of the statistical significance.

AREA (% CONTROL) ± STD DEV						
Genotype	Total	p-value	Anterior	p-value	Posterior	p-value
ci>2xGFP	100 ± 1,9	-	100 ± 2,9	-	100 ± 2,0	-
ci>GFP, dally^{RNAi}	92 ± 1,9	10^{-9}	82 ± 1,7	10^{-14}	98 ± 2,8	0,08
en>2xGFP	100 ± 1,8	-	100 ± 2,7	-	100 ± 3,4	-
en>GFP, dally^{RNAi}	86 ± 1,5	10^{-14}	97 ± 2,4	0,03	76 ± 2,0	10^{-14}

CELL DENSITY (% CONTROL) ± STD DEV				
Genotype	Anterior	p-value	Posterior	p-value
ci>2xGFP	100 ± 2,8	-	100 ± 4,2	-
ci>GFP, dally^{RNAi}	89 ± 6,1	10^{-5}	104 ± 5,9	0,1
en>2xGFP	100 ± 2,9	-	100 ± 2,4	-
en>GFP, dally^{RNAi}	105 ± 4,5	0,01	94 ± 5,3	0,007

Table 21. Quantitative measurements regarding Figure 44. Tissue size values of whole wings (total), anterior and posterior compartments of the wing of flies of the indicated genotypes measured as a ratio (in percentage) with respect to control wings expressing GFP in the same domain. Cell density values of both anterior and posterior compartments measured as a ratio (in percentage) with respect to control wings expressing the indicated transgenes in the same domain. These values correspond to the average of 10 adult wings with their corresponding standard deviations. A t-test was carried out to calculate the p-value as a measurement of the statistical significance.

AREA (% CONTROL) ± STD DEV						
Genotype	Total	p-value	Anterior	p-value	Posterior	p-value
ci>2xGFP	100 ± 1,9	-	100 ± 2,9	-	100 ± 2,0	-
ci>GFP, Rheb	93 ± 4,0	10^{-5}	118 ± 4,6	10^{-9}	77 ± 4,5	10^{-12}
ci>Rheb, dally^{RNAi}	95 ± 2,5	0,1	104 ± 5,5	10^{-6}	90 ± 4,2	10^{-6}
en>2xGFP	100 ± 1,8	-	100 ± 2,7	-	100 ± 3,4	-
en>GFP, Rheb	101 ± 4,3	0,7	71 ± 4,7	10^{-12}	128 ± 5,0	10^{-11}
en>Rheb, dally^{RNAi}	100 ± 5,2	0,9	94 ± 7,7	10^{-7}	106 ± 14,4	10^{-4}
ci>2xGFP	100 ± 2,5	-	100 ± 3,0	-	100 ± 3,7	-
ci>GFP, Dp110	92 ± 5,0	10^{-4}	116 ± 4,8	10^{-8}	77 ± 6,2	10^{-9}
ci>Dp110, dally^{RNAi}	89 ± 2,6	0,05	92 ± 3,4	10^{-10}	86 ± 3,6	10^{-4}

CELL DENSITY (% CONTROL) ± STD DEV				
Genotype	Anterior	p-value	Posterior	p-value
ci>2xGFP	100 ± 2,8	-	100 ± 4,2	-
ci>GFP, Rheb	84 ± 3,0	10^{-9}	118 ± 5,1	10^{-7}
ci>Rheb, dally^{RNAi}	80 ± 3,7	10^{-11}	121 ± 4,5	10^{-9}
en>2xGFP	100 ± 2,9	-	100 ± 2,4	-
en>GFP, Rheb	122 ± 6,7	10^{-8}	59 ± 3,8	10^{-16}
en>Rheb, dally^{RNAi}	115 ± 10,1	0,09	81 ± 14,5	10^{-4}
ci>2xGFP	100 ± 4,0	-	100 ± 3,6	-
ci>GFP, Dp110	81 ± 4,0	10^{-9}	122 ± 5,6	10^{-9}
ci>Dp110, dally^{RNAi}	87 ± 4,6	0,01	122 ± 7,9	0,9

Table 22. Quantitative measurements regarding Figure 45. Tissue size values of whole wings (total), anterior and posterior compartments of the wing of flies of the indicated genotypes measured as a ratio (in percentage) with respect to control wings expressing GFP in the same domain. Cell density values of both anterior and posterior compartments measured as a ratio (in percentage) with respect to control wings expressing the indicated transgenes in the same domain. These values correspond to the average of 10 adult wings with their corresponding standard deviations. A t-test was carried out to calculate the p-value as a measurement of the statistical significance.

P-MAD INTENSITY (A.U.) ± STD DEV				
Genotype	Anterior	p-value	Posterior	p-value
ci>GFP, Dp110	2479183 ± 497488	-	709408 ± 143401	-
ci>Dp110, dally^{RNAi}	1864771 ± 754103	0,2	892940 ± 334898	0,3

Table 23. Quantitative measurements regarding Figure 46. P-MAD intensity values, in arbitrary units, of anterior and posterior compartments of the wing imaginal discs of the indicated genotypes. These values correspond to the average of at least 5 wing discs with their corresponding standard deviations. A t-test was carried out to calculate the p-value as a measurement of the statistical significance.

AREA (% CONTROL) ± STD DEV						
Genotype	Total	p-value	Anterior	p-value	Posterior	p-value
en>2xGFP	100 ± 3,8	-	100 ± 2,8	-	100 ± 4,1	-
en>GFP, PTEN^{RNAi}	116 ± 3,2	10^{-9}	139 ± 3,5	10^{-17}	88 ± 2,8	10^{-7}
en>PTEN^{RNAi}, sulfateless^{RNAi}	67 ± 5,3	10^{-17}	39 ± 5,8	10^{-22}	98 ± 5,6	10^{-5}

Table 24. Quantitative measurements regarding Figure 47. Tissue size values of whole wings (total), anterior and posterior compartments of the wing of flies of the indicated genotypes measured as a ratio (in percentage) with respect to control wings expressing GFP in the *en* domain. These values correspond to the average of 10 adult wings with their corresponding standard deviations. A t-test was carried out to calculate the p-value as a measurement of the statistical significance.

AREA (% CONTROL) ± STD DEV						
Genotype	Total	p-value	Anterior	p-value	Posterior	p-value
ci>2xGFP	100 ± 3,1	-	100 ± 2,8	-	100 ± 2,7	-
ci>GFP, sulfateless^{RNAi}	79 ± 6,1	10^{-9}	51 ± 4,8	10^{-17}	103 ± 6,9	0,3
en>2xGFP	100 ± 2,1	-	100 ± 2,6	-	100 ± 2,6	-
en>GFP, sulfateless^{RNAi}	77 ± 2,8	10^{-16}	108 ± 4,1	10^{-5}	47 ± 3,0	10^{-22}

Table 25. Quantitative measurements regarding Figure 48. Tissue size values of whole wings (total), anterior and posterior compartments of the wing of flies of the indicated genotypes measured as a ratio (in percentage) with respect to control wings expressing GFP in the *en* domain. These values correspond to the average of 10 adult wings with their corresponding standard deviations. A t-test was carried out to calculate the p-value as a measurement of the statistical significance.

AREA (% CONTROL) ± STD DEV						
Genotype	Total	p-value	Anterior	p-value	Posterior	p-value
ci>2xGFP	100 ± 2,5	-	100 ± 3,5	-	100 ± 2,9	-
ci>GFP, Yki	99 ± 3,5	0,6	117 ± 5,8	10^{-8}	84 ± 2,4	10^{-11}
en>2xGFP	100 ± 2,1	-	100 ± 2,6	-	100 ± 2,6	-
en>GFP, Yki	124 ± 8,1	10^{-8}	84 ± 6,1	10^{-7}	156 ± 11,9	10^{-11}

CELL DENSITY (% CONTROL) ± STD DEV				
Genotype	Anterior	p-value	Posterior	p-value
ci>2xGFP	100 ± 3,2	-	100 ± 5,5	-
ci>GFP, Yki	109 ± 2,9	10^{-6}	104 ± 3,7	0,04
en>2xGFP	100 ± 6,4	-	100 ± 4,1	-
en>GFP, Yki	117 ± 3,9	10^{-7}	124 ± 7,8	10^{-8}

Table 26. Quantitative measurements regarding Figure 49. Tissue size values of whole wings (total), anterior and posterior compartments of the wing of flies of the indicated genotypes measured as a ratio (in percentage) with respect to control wings expressing GFP in the same domain. Cell density values of both anterior and posterior compartments measured as a ratio (in percentage) with respect to control wings expressing the indicated transgenes in the same domain. These values correspond to the average of 10 adult wings with their corresponding standard deviations. A t-test was carried out to calculate the p-value as a measurement of the statistical significance.

AREA (% CONTROL) ± STD DEV						
Genotype	Total	p-value	Anterior	p-value	Posterior	p-value
en>2xGFP	100 ± 2,1	-	100 ± 2,6	-	100 ± 2,6	-
en>GFP, Yki	124 ± 8,1	10^{-8}	84 ± 6,1	10^{-7}	156 ± 11,9	10^{-11}
en>Yki, dally^{RNAi}	110 ± 5,3	10^{-5}	99 ± 5,3	10^{-6}	117 ± 6,2	10^{-9}

Table 27. Quantitative measurements regarding Figure 51. Tissue size values of whole wings (total), anterior and posterior compartments of the wing of flies of the indicated genotypes measured as a ratio (in percentage) with respect to control wings expressing GFP in the same domain. These values correspond to the average of 10 adult wings with their corresponding standard deviations. A t-test was carried out to calculate the p-value as a measurement of the statistical significance.

AREA (% CONTROL) ± STD DEV						
Genotype	Total	p-value	Anterior	p-value	Posterior	p-value
en>2xGFP	100 ± 2,1	-	100 ± 2,6	-	100 ± 2,6	-
en>GFP, Yki	124 ± 8,1	10^{-8}	84 ± 6,1	10^{-7}	156 ± 11,9	10^{-11}
en>Yki, dally-like^{RNAi}	113 ± 8,9	0,008	82 ± 9,1	0,7	141 ± 10,9	0,005
en>2xGFP	100 ± 2,1	-	100 ± 2,4	-	100 ± 2,0	-
en>GFP, Yki	112 ± 6,0	10^{-7}	81 ± 3,1	10^{-14}	141 ± 10,2	10^{-12}
en>Yki, dally-like^{TRiP}	105 ± 3,1	10^{-4}	80 ± 2,2	0,4	129 ± 4,8	10^{-4}

Table 28. Quantitative measurements regarding Figure 52. Tissue size values of whole wings (total), anterior and posterior compartments of the wing of flies of the indicated genotypes measured as a ratio (in percentage) with respect to control wings expressing GFP in the same domain. These values correspond to the average of 10 adult wings with their corresponding standard deviations. A t-test was carried out to calculate the p-value as a measurement of the statistical significance.

AREA (% CONTROL) ± STD DEV						
Genotype	Total	p-value	Anterior	p-value	Posterior	p-value
ci>2xGFP	100 ± 2,5	-	100 ± 3,5	-	100 ± 2,9	-
ci>GFP, tkv	78 ± 1,8	10^{-16}	76 ± 4,9	10^{-11}	78 ± 4,9	10^{-11}
ci>GFP, tkv^{DN}	79 ± 6,1	10^{-9}	67 ± 6,3	10^{-12}	89 ± 5,8	10^{-5}
en>2xGFP	100 ± 3,8	-	100 ± 4,1	-	100 ± 2,8	-
en>GFP, tkv	87 ± 5,6	10^{-6}	91 ± 6,3	10^{-4}	81 ± 4,5	10^{-10}
en>GFP, tkv^{DN}	82 ± 4,5	10^{-9}	88 ± 5,7	10^{-5}	74 ± 4,2	10^{-13}
CELL DENSITY (% CONTROL) ± STD DEV						
Genotype	Anterior	p-value	Posterior	p-value		
ci>2xGFP	100 ± 3,2	-	100 ± 5,5	-		
ci>GFP, tkv^{DN}	95 ± 3,6	0,002	96 ± 3,0	0,06		
en>2xGFP	100 ± 6,4	-	100 ± 4,1	-		
en>GFP, tkv^{DN}	103 ± 6,0	0,3	97 ± 7,1	0,3		

Table 29. Quantitative measurements regarding Figure 53. Tissue size values of whole wings (total), anterior and posterior compartments of the wing of flies of the indicated genotypes measured as a ratio (in percentage) with respect to control wings expressing GFP in the same domain. Cell density values of both anterior and posterior compartments measured as a ratio (in percentage) with respect to control wings expressing the indicated transgenes in the same domain. These values correspond to the average of 10 adult wings with their corresponding standard deviations. A t-test was carried out to calculate the p-value as a measurement of the statistical significance.

AREA (% CONTROL) ± STD DEV						
Genotype	Total	p-value	Anterior	p-value	Posterior	p-value
en>2xGFP	100 ± 3,8	-	100 ± 4,1	-	100 ± 2,8	-
en>GFP, PTEN^{RNAi}	116 ± 3,2	10^{-9}	88 ± 4,8	10^{-6}	139 ± 3,5	10^{-17}
en>PTEN^{RNAi}, tkv^{DN}	98 ± 8,5	10^{-4}	79 ± 7,0	10^{-4}	112 ± 11,3	10^{-4}
ci>2xGFP	100 ± 2,5	-	100 ± 3,5	-	100 ± 2,9	-
ci>GFP, PTEN^{RNAi}	90 ± 4,7	10^{-6}	107 ± 5,1	0,001	74 ± 4,7	10^{-12}
ci>PTEN^{RNAi}, tkv^{DN}	78 ± 5,0	10^{-4}	92 ± 7,6	10^{-5}	65 ± 4,9	10^{-4}

Table 30. Quantitative measurements regarding Figure 54. Tissue size values of whole wings (total), anterior and posterior compartments of the wing of flies of the indicated genotypes measured as a ratio (in percentage) with respect to control wings expressing GFP in the same domain. These values correspond to the average of 10 adult wings with their corresponding standard deviations. A t-test was carried out to calculate the p-value as a measurement of the statistical significance.

AREA (% CONTROL) ± STD DEV		
Genotype	Total	p-value
nub>GFP	100 ± 3,3	-
nub>Rheb	118 ± 4,8	10^{-9}
nub>Rheb, dally^{RNAi}	102 ± 4,0	10^{-8}
nub>Rheb, dally^{TRiP}	107 ± 4,0	10^{-6}
nub>Dp110	150 ± 8,3	10^{-13}
nub>Dp110, dally^{TRiP}	105 ± 1,4	10^{-12}

Table 31. Quantitative measurements regarding Figure 55. Total tissue size values of wing of flies of the indicated genotypes measured as a ratio (in percentage) with respect to control wings expressing GFP in the same domain. These values correspond to the average of 10 adult wings with their corresponding standard deviations. A t-test was carried out to calculate the p-value as a measurement of the statistical significance.

AREA (A.U.) ± STD DEV				
Genotype	Anterior	p-value	Posterior	p-value
hh>2xGFP	83275 ± 10603	-	46027 ± 6994	-
hh>GFP, Dp110^{RNAi}	81912 ± 5270	0,8	22901 ± 2740	10^{-5}
hh>Dp110^{RNAi}, dally	84869 ± 27895	0,8	35151 ± 12007	0,03

Table 32. Quantitative measurements regarding Figure 57. Tissue size values (in arbitrary units) of the posterior and anterior compartments of late third instar wing discs of larvae of the indicated genotypes. These values correspond to the average of 10 adult wings with their corresponding standard deviations. A t-test was carried out to calculate the p-value as a measurement of the statistical significance.

AREA (% CONTROL) ± STD DEV		
Genotype	Total	p-value
nub>GFP	100 ± 3,1	-
nub>Rheb^{RNAi}	77 ± 1,6	10^{-15}
nub>Rheb^{RNAi}, dally	82 ± 5,4	0,02
CELL DENSITY (% CONTROL) ± STD DEV		
Genotype	Total	p-value
nub>GFP	100 ± 7,9	-
nub>Rheb^{RNAi}	113 ± 5,5	10^{-4}
nub>Rheb^{RNAi}, dally	108 ± 6,8	0,09

Table 33. Quantitative measurements regarding Figure 58. Total tissue size values of wings of flies of the indicated genotypes measured as a ratio (in percentage) with respect to control wings expressing GFP in the same domain. Cell density values of wings of the indicated genotypes measured as a ratio (in percentage) with respect to control wings expressing GFP in the same domain. These values correspond to the average of 10 adult wings with their corresponding standard deviations. A t-test was carried out to calculate the p-value as a measurement of the statistical significance.

AREA (% CONTROL) ± STD DEV			
Genotype	Yeast	Total	p-value
nub>GFP	100g/L	100 ± 1,8	-
nub>GFP	20g/L	84 ± 5,1	10^{-8}
nub>dally	20g/L	97 ± 4,6	0,1
nub>dally^{TRiP}	100g/L	88 ± 2,7	10^{-9}

Table 34. Quantitative measurements regarding Figure 59. Total tissue size values of wings of flies of the indicated genotypes raised in food varying the yeast content measured as a ratio (in percentage) with respect to control wings expressing GFP in the same domain in 100g/L of yeast content. These values correspond to the average of 10 adult wings with their corresponding standard deviations. A t-test was carried out to calculate the p-value as a measurement of the statistical significance. Note that dally-overexpressing wings of animals raised in 20g/L of yeast food are similar in size to control wings of animals raised in 100g/L of yeast food. Also, wings depleted for dally of animals raised in 100g/L of yeast food are similar to wild type wings of animals raised in 20g/L of yeast food.

Index of Figures

Abbreviations

4EBP: Eukaryotic translation initiation factor 4E-binding protein

A: Anterior

AEL: After Egg Laying

AMPK: AMP-activated protein kinase

AP: Anterior-Posterior

BrdU: Bromodeoxyuridine

Brk: Brinker

CDK: Cyclin-dependent kinases

Ci: Cubitus Interuptus

CycE: Cyclin E

D: Dorsal

Dad: Daughters against dpp

Dally: Division abnormally delayed

Diap1: Death-associated inhibitor of apoptosis 1

DILPs: *Drosophila* Insulin-like Peptides

Dlg: Discs-large

Dlp: Dally-like protein

DNA: Deoxyribonucleic Acid

Dpp: Decapentaplegic

Dll: Distalless

Ds: dachsous

dsRNA: double strand ribonucleic acid

DV: Dorsal-Ventral

ECM: Extracellular Matrix

eIF4E: Eukaryotic translation initiation factor 4E

En: Engrailed

Ex: Expanded

FACs: Fluorescence-activated cell sorting

FOXO: Forkhead box, sub-group O

FRAP: Fluorescence recovery after photobleaching

FSC: Forward Scatter

GAG: glycosaminoglycan

GFP: Green Fluorescent Protein

GPI: Glycosylphosphatidyl inositol

Hh: Hedgehog

HPSGs: Heparan sulfate proteoglycans

Hpo: Hippo

HS: Heparan sulfate

Hth: Homothorax

IGF: Insulin-like Growth Factors

IIS: insulin/insulin growth factor signaling

InR: Insulin Receptor

IRS: Insulin receptor substrate

L1: First larval stage

L2: Second larval stage

L3: Third larval stage

Lgl: lethal (2) giant larvae
MAD: Mothers against decapentaplegic
Mats: mob as tumor suppressor
Mer: Merlin
mRNA: Messenger Ribonucleic Acid
Omb: Optomotor-blind
ONCs: Oncogenic Niche Cells
P: Posterior
Pent: Pentagone
PI3K: Phosphotidylinositol 3 Kinase
PIP2: Phosphatidylinositol 4,5-bisphosphate
PIP3: Phosphatidylinositol (3,4,5)-trisphosphate
PH3: Phosphorylated Histone 3
PRAS40: Proline-rich AKT1 substrate 1 protein
Ptc: Patched
PTEN: Phosphatase and Tensin Homolog
RBF: Retinoblastoma-family protein
RNAi: RNA interference
Rheb: Ras homolog enriched in brain ortholog
Sal: Spalt
Sav: Salvador
Scrib: Scribble
Sd: Scalloped
Sens: Senseless
Sfl: Sulfateless
S6K: Ribosomal protein S6 kinase
Stg: String
TGFβ: Transforming growth factor beta
Tkv: Thickveins
TOR: Target of Rapamycin
TSC1: tuberous sclerosis complex 1
TSC2: tuberous sclerosis complex 2
Tsh: Teashirt
UAS: Upstream Activation Sequence
V: Ventral
Vg: Vestigial
Wg: Wingless
Wts: Warts

Resumen en castellano

Para obtener organismos estructuralmente funcionales, el tamaño de sus órganos tiene que estar altamente regulado durante el desarrollo. Por un lado, dicho tamaño final depende del estado nutricional del organismo y de la actividad de vías de señalización que responden a la disponibilidad de nutrientes. Por otro lado, existen señales intrínsecas en estos órganos que operan de forma autónoma para controlar su crecimiento y su forma. Cómo integran las células y los tejidos estas señales extrínsecas e intrínsecas para generar órganos del tamaño y forma apropiados sigue siendo, en gran parte, una incógnita.

Las vías de señalización PI3K (Phosphatidylinositol 3-Kinase)/PTEN (Phosphatase with Tensin Homology) y TSC (Tuberous Sclerosis Complex)/TOR (Target of Rapamycin) que responden a la disponibilidad de nutrientes están involucradas en el control del crecimiento. Además, se encuentran hiper-activadas con frecuencia en diferentes cánceres humanos, y su activación es muchas veces la causa inicial del desarrollo de los tumores. Una pregunta interesante, y todavía poco explorada, es entender cómo células mutantes para genes supresores de tumores compiten con las células adyacentes salvajes durante las primeras etapas de la tumorigénesis y hasta llegar a eliminarlas completamente.

Para analizar el impacto de la activación restringida a determinadas regiones de estas vías de señalización sobre poblaciones celulares adyacentes de tipo salvaje, hemos utilizado como sistema modelo los primordios imaginales de *Drosophila*, tejidos epiteliales altamente proliferativos y en continuo crecimiento durante el desarrollo larvario.

Los resultados presentados en esta tesis demuestran que la activación restringida a determinadas regiones de estas vías genera, como esperábamos, un sobre-crecimiento del tejido afectado y, sorprendentemente, una clara reducción del

crecimiento y la proliferación de las poblaciones celulares adyacentes no afectadas. Demostramos que esta respuesta no autónoma: (1) se produce independientemente de la región dentro del primordio dónde se activan estas vías; (2) es funcional durante todo el desarrollo; (3) es independiente a la inducción de muerte celular y, por tanto, distinta de la competición celular; y (4) no se ve influenciada por el estado nutricional del organismo.

También identificamos el mecanismo molecular involucrado en dichos fenotipos. Demostramos que los efectos observados en el crecimiento de los tejidos, tanto autónomos como no autónomos, están mediados por Dally, un proteoglicano implicado en la regulación de la difusión, la estabilidad y la actividad del factor de crecimiento Dpp (Decapentaplegic)/ TGF- β (Transforming Growth Factor β). Activación de las vías de señalización PI3K/PTEN y TSC/TOR aumenta los niveles de expresión de Dally; la sobreexpresión de Dally fenocopia los efectos producidos por la activación de estas vías a nivel autónomo y no autónomo tanto en el crecimiento como en la proliferación celular, y finalmente, la disminución de los niveles de Dally es capaz de rescatar los efectos en la proliferación celular y en el tamaño inducidos por estas vías.

En nuestro modelo, proponemos que la reducción no autónoma del tamaño del tejido se genera debido a una reducción en los niveles de señalización de la vía de Dpp. El incremento en los niveles de Dally inducido por la activación de estas vías conlleva un mayor secuestro de moléculas de Dpp y, como consecuencia, una reducción del número de moléculas de Dpp disponibles para las poblaciones celulares adyacentes. Asimismo, sugerimos que ambas poblaciones celulares compiten por la cantidad de moléculas de Dpp, y que la reducción de estas promueve la eliminación de las células salvajes por parte de la población celular que está sobrecreciendo. Consistente con esta hipótesis, un aumento de los niveles del receptor de Dpp, Thickveins, capaz de retirar/internalizar el ligando Dpp del espacio extracelular, también causa una reducción no autónoma del tamaño del tejido adyacente.

Mientras que las vías de señalización que detectan los nutrientes modulan el tamaño final de las estructuras adultas de un organismo en función a la disponibilidad de nutrientes, Dpp juega un papel intrínseco a nivel del órgano en la coordinación de crecimiento con la generación de patrón. Por lo tanto, nuestros resultados revelan una función de Dally como un puente molecular entre los mecanismos intrínsecos y extrínsecos que regulan el tamaño final de los órganos. Como tal, contribuye a integrar la disponibilidad de nutrientes con el "scaling" de los órganos.

Annexes

Annexes

In addition to the project addressed in this PhD thesis and that has been successfully published in PLOS Biology in 2015 **(Main Publication)**, I have also contributed to a different research project that resulted in another publication from the lab.

In collaboration with Laura Boulan, I was involved in a project related with the interaction between TRIM-NHL proteins and dMyc specifically and exclusively in growth control in epithelial cells that lead to publication of one original research article **(Publication 2)**. For this paper, I contributed to conduct all the experiments.

TRIM-NHL proteins are a family of translational regulators that control cell growth, proliferation, and differentiation during development. *Drosophila* Brat and Mei-P26 TRIM-NHL proteins serve as tumor suppressors in stem cell lineages and have been proposed to exert this action, in part, via the repression of the protooncogene dMyc. We analyzed the role of Brat, Mei-P26, and dMyc in regulating growth in *Drosophila* imaginal discs. As in stem cell lineages, we found that Brat and Mei-P26 repress dMyc in epithelial cells by acting at the post-transcriptional and protein level, respectively. Loss-of-function of *brat* and overexpression of dMyc induce overgrowth in stem cell lineages and eventually can participate in tumor formation. In contrast, we found that an increase in Mei-P26 levels inhibits growth of epithelial cells in these two conditions. Upon depletion of Brat, Mei-P26 up-regulation prevents an increase in dMyc protein levels and leads to tissue undergrowth. This mechanism appears to be tissue-specific since we did not observe Mei-P26 upregulation in brain tumors resulting from *brat* loss-of-function. We observed that driving Mei-P26 expression in these tumors —mimicking the situation in epithelial cells— is sufficient to prevent dMyc accumulation, thus rescuing the overgrowth. Finally, we showed that Mei-

P26 upregulation mediates dMyc-induced apoptosis and limits dMyc growth potential in epithelial cells. These findings shed light on the tumor suppressor roles of TRIM-NHL proteins and underscore a new mechanism that maintains tissue homeostasis upon dMyc deregulation.

Main Publication

"Dally Proteoglycan Mediates the Autonomous and Nonautonomous Effects on Tissue Growth Caused by Activation of the PI3K and TOR Pathways"

PLOS | BIOLOGY

RESEARCH ARTICLE

Dally Proteoglycan Mediates the Autonomous and Nonautonomous Effects on Tissue Growth Caused by Activation of the PI3K and TOR Pathways

Ana Ferreira[1], **Marco Milán**[1,2]*

1 Institute for Research in Biomedicine (IRB Barcelona), Barcelona, Spain, **2** Institucio Catalana de Recerca i Estudis Avançats (ICREA), Barcelona, Spain

* marco.milan@irbbarcelona.org

OPEN ACCESS

Citation: Ferreira A, Milán M (2015) Dally Proteoglycan Mediates the Autonomous and Nonautonomous Effects on Tissue Growth Caused by Activation of the PI3K and TOR Pathways. PLoS Biol 13(8): e1002239. doi:10.1371/journal.pbio.1002239

Academic Editor: Konrad Basler, University of Zurich, SWITZERLAND

Received: December 19, 2014

Accepted: July 31, 2015

Published: August 27, 2015

Data Availability Statement: All relevant data are within the paper and its Supporting Information files.

Funding: This work was funded by the Ministerio de Economia y Competitividad (BFU2010-21123 and BFU2013-44485 grants), AGAUR (2005 SGR 00118 grant), and Fundação para a Ciência e a Tecnologia (SFRH/BD/68745/2010 grant). The funders had no role in study design, data collection and analysis, decision to publish, or preparation of the manuscript.

Competing Interests: The authors have declared that no competing interests exist.

Abstract

How cells acquiring mutations in tumor suppressor genes outcompete neighboring wild-type cells is poorly understood. The phosphatidylinositol 3-kinase (PI3K)–phosphatase with tensin homology (PTEN) and tuberous sclerosis complex (TSC)-target of rapamycin (TOR) pathways are frequently activated in human cancer, and this activation is often causative of tumorigenesis. We utilized the Gal4-UAS system in *Drosophila* imaginal primordia, highly proliferative and growing tissues, to analyze the impact of restricted activation of these pathways on neighboring wild-type cell populations. Activation of these pathways leads to an autonomous induction of tissue overgrowth and to a remarkable nonautonomous reduction in growth and proliferation rates of adjacent cell populations. This nonautonomous response occurs independently of where these pathways are activated, is functional all throughout development, takes place across compartments, and is distinct from cell competition. The observed autonomous and nonautonomous effects on tissue growth rely on the up-regulation of the proteoglycan Dally, a major element involved in modulating the spreading, stability, and activity of the growth promoting Decapentaplegic (Dpp)/transforming growth factor β(TGF-β) signaling molecule. Our findings indicate that a reduction in the amount of available growth factors contributes to the outcompetition of wild-type cells by overgrowing cell populations. During normal development, the PI3K/PTEN and TSC/TOR pathways play a major role in sensing nutrient availability and modulating the final size of any developing organ. We present evidence that Dally also contributes to integrating nutrient sensing and organ scaling, the fitting of pattern to size.

Author Summary

The final size of a developing organ is finely modulated by nutrient conditions through the activity of nutrient sensing pathways, and deregulation of these pathways is often causative of tumorigenesis. Besides the well-known roles of these pathways in inducing tissue and

Abbreviations: βGal, β-galactosidase; A, anterior; AEL, after egg laying; AP, anterior–posterior; a.u., arbitrary units; *brk*, *brinker*; *cycE*, *cyclin E*; Dpp, Decapentaplegic; DSHB, Developmental Studies Hybridoma Bank; dsRNA, double-stranded RNA; DV, dorsal-ventral; EGFR, epidermal growth factor receptor; FACS, fluorescence-activated cell sorter; GFP, green fluorescent protein; GPI, glycosylphosphatidylinositol; GTP, guanosine-5'-triphosphate; HS, heparan sulfate; HSPG, heparan sulfate proteoglycan; InR, insulin-like receptor; MAD, Mothers against Dpp; P, posterior; PH3, phosphorylated histone H3; PI3K, phosphatidylinositol 3-kinase; PTEN, phosphatase and tensin homolog; RFP, red fluorescent protein; RNAi, RNA interference; RT, room temperature; Sfl, Sulfateless; *stg*, *string*; TGF-β, transforming growth factor β; Tkv, Thickveins; TOR, target of rapamycin; TSC, tuberous sclerosis complex; TUNEL, terminal deoxynucleotidyl transferase dUTP nick end labeling; UAS, upstream activation sequence; *Ubx*, *Ultrabithorax*; VDRC, Vienna Drosophila RNAi Center

cell growth, here we identify a nonautonomous effect of activation of these pathways on growth and proliferation rates and on the final size of neighboring cell populations. We reveal that the observed autonomous and nonautonomous effects on tissue growth and proliferation rates rely on the up-regulation of the proteoglycan Dally, a major factor involved in modulating the spreading, stability, and activity of the growth promoting Decapentaplegic (Dpp)/transforming growth factor β(TGF-β) signaling molecule. Our data indicate that a reduction in the amount of available growth factors contributes to the outcompetition of wild-type cells by overgrowing cell populations. Whereas nutrient-sensing pathways modulate the final size of the adult structure according to nutrient availability to the feeding animal, Dpp plays an organ-intrinsic role in the coordination of growth and patterning. We identify the proteoglycan Dally as the rate-limiting factor that contributes to the tissue-autonomous and nonautonomous effects on growth caused by targeted activation of the nutrient-sensing pathways. Thus, our results unravel a role of Dally as a molecular bridge between the organ-intrinsic and organ-extrinsic mechanisms that regulate organ size.

Introduction

Several conserved signaling pathways involved in the control of organ size in many species are frequently deregulated in a broad range of human cancers, and this deregulation is often causative of tumorigenesis. The phosphatidylinositol 3-kinase (PI3K)–phosphatase with tensin homology (PTEN) is one of the most commonly altered pathways in human tumors. Deletion of PTEN is associated with aggressive metastatic potential and poor prognosis (reviewed in [1]), and targeted depletion of PTEN in epithelial cells leads to rapid development of endometrial, prostate, and thyroid neoplasias in mouse models [2]. Mutations in tuberous sclerosis complex 1 (TSC1) and tuberous sclerosis complex 2 (TSC2) that lead to hyperactivation of the target of rapamycin (TOR) pathway are causative of tuberous sclerosis, a hamartoma syndrome associated with a predisposition to malignancy [3], and heterozygous *Tsc1* or *Tsc2* mutant mice develop renal and extrarenal tumors such as hepatic hemangiomas [4].

In *Drosophila*, the PI3K/PTEN and TSC/TOR pathways modulate the final size of the developing organism according to nutrient availability, and their activation promotes cell and tissue growth (reviewed in [5,6]). Thus, the identification of the molecular players and cellular interactions underlying the induction of growth upon loss of these tumor suppressor genes in model organisms will bring new insight into their contribution to the initial steps of tumorigenesis, as somatic mutations in these pathways appear to be frequently accumulated in early events of tumor development. In this context, the imaginal primordia of *Drosophila*, monolayered epithelial tissues that grow and proliferate 1,000-fold in size in about five days inside the feeding larvae, have proved to be a valuable model system to address the impact of tumor suppressor genes in the early events of tumorigenesis (reviewed in [7,8]). Their simple architecture enables both the labelling and tracking of cell populations that can be genetically manipulated with the help of sophisticated tools as well as the analysis of the cell-autonomous and nonautonomous impact of loss of these tumor suppressor genes.

Of particular interest is the understanding of how cells depleted of tumor suppressor genes outcompete neighboring wild-type cells, especially during early stages of tumorigenesis following initial mutagenesis and transformation. Cell competition, a process favoring fit over weak or harmful cells, was originally identified in *Drosophila* [9] and has been proposed to play a protumoral role in this process [10]. However, cell competition has been recently shown to

play a tumor suppressor role in the mammalian thymus as it prevents the selection of faulty cells, which become tumorigenic [11]. Thus, the initial proposal of cell competition as a driving force in tumor progression remains elusive. Work in *Drosophila* imaginal primordia has also shown that competition for nutrients contributes to the growth of *PTEN* mutant cells and the outcompetition of wild-type surrounding cells [12]. These results explain the resistance of tumors lacking PTEN or with increased PI3K activity to dietary restriction [13].

Here, we used the developing wing primordium of *Drosophila* to analyze the autonomous and nonautonomous impact of *PI3K/PTEN* and *TSC/TOR* pathway activation. We utilized the GAL4/ upstream activation sequence (UAS) system to target these pathways in restricted cell populations that correspond to the developing compartments—cell populations that do not mix and give rise to defined structures of the adult wing [14]. We present evidence that activation of these two pathways, well known to induce tissue growth in an autonomous manner, causes a nonautonomous reduction in the growth and proliferation rates as well as in the resulting tissue size of adjacent cell populations. The observed autonomous and nonautonomous effects on tissue growth rely on the up-regulation of the proteoglycan Dally, a major element involved in modulating the spread, stability, and activity of the growth-promoting Decapentaplegic (Dpp)/transforming growth factor β (TGF-β) signaling molecule. These results shed new light on the selection process that takes place during the early stages of tumorigenesis following initial mutagenesis and transformation, in which competition for secreted growth-promoting factors might play a fundamental role. During normal development, the PI3K/PTEN and TSC/TOR signaling pathways modulate the final size of the adult wing as a function of nutrient availability (reviewed in [15,16]), whereas Dpp plays an organ-intrinsic role in the coordination of growth and patterning within the developing wing primordium (reviewed in [17,18]). Our results also identify Dally as a molecular bridge between nutrient sensing and wing scaling, the latter defined as the fitting of pattern to size.

Results

Targeted Activation of the PI3K/PTEN or TSC/TOR Pathways Induces a Nonautonomous Reduction in Tissue Size of the Adjacent Cell Populations

The activation of the PI3K/PTEN and TSC/TOR pathways induces tissue growth in the developing imaginal primordia and gives rise to overgrown adult structures [19–23]. Interestingly, these pathways exert this action by affecting cell size and cell proliferation in different manners. Activation of the PI3K/PTEN pathway in the whole wing (with the *nubbin-gal4* driver, Fig 1A), either by expression of *PI3K-92E* (also termed *Drosophila p110* or *Dp110*) or a double-stranded RNA (dsRNA) form of *PTEN* (a negative regulator of PI3K/Dp110), gave rise to larger wings than those of control flies expressing green fluorescent protein (GFP) (Fig 1A and 1B). The increase in tissue size was a consequence of both an increase in cell size (reflected by a reduction in cell densities in the adult wing, Fig 1D) and in cell number (note the increase in tissue size in Fig 1B and 1C is much larger than the reduction in cell densities in Fig 1D). Activation of the TOR pathway, by depletion of *TSC1 or TSC2*, leads to strongly overgrown tissues and larval lethality [24]. In order to reduce larval lethality and to analyze the resulting adult wings, we induced mild activation of the TOR pathway by overexpressing the guanosine-5'-triphosphate (GTP)-binding protein Rheb, which binds and activates TOR [25–27]. Rheb overexpression gives rise to overgrown adult wings (Fig 1B). The observed increase in tissue size is mainly a consequence of an increase in cell size (Fig 1D, note the reduction in cell densities is to a similar extent as the increase in tissue size shown in Fig 1B and 1C). The adult wing is subdivided into an anterior (A) and a posterior (P) compartment, and the boundary between these

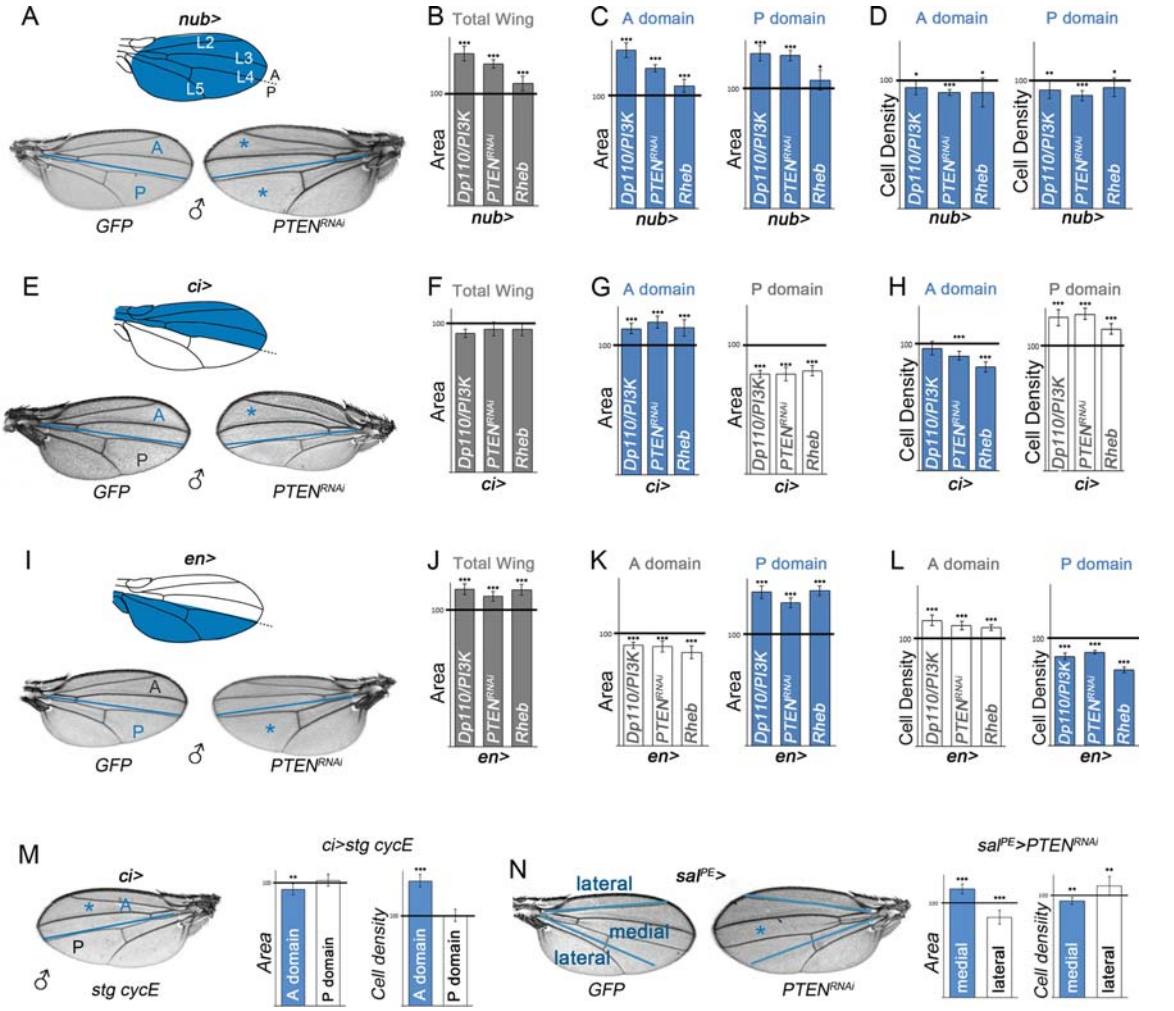

Fig 1. Nonautonomous effects on tissue size upon targeted activation of PI3K/PTEN and TSC/TOR pathways. (A, E, I) Schemes of adult wings with the *nub* (A), *ci* (E), and *en* (I) expression domains marked in blue and cuticle preparations of male adult wings expressing *GFP* or *PTEN*^{RNAi} under the control of the *nub-gal4* (A), *ci-gal4* (E), and *en-gal4* (I) drivers. The blue line marks the boundary between anterior (A) and posterior (P) compartments. The wing is decorated with four longitudinal veins (L2–L5), and the anterior side of L4 corresponds to the AP compartment boundary. (B–D, F–H, J–L) Histograms plotting tissue size (B, C, F, G, J, K) and cell density (D, H, L) of the whole wing (B, F, J), or the A and P compartments of adult wings expressing the indicated transgenes in the *nub* (B–D), *ci* (F–H) or *en* (J–L) domains normalized as a percent of the control wings. Note a consistent reduction in tissue size of the adjacent cell populations in G and K (white bars). (M) Cuticle preparation of a *ci>stg*, *cycE* adult wing. The blue line marks the boundary between the A and P compartments. On the right are histograms plotting tissue size and cell density values of the A (blue bars) and P (white bars) domains of *ci>stg*, *cycE* adult wings normalized as a percent of the control (*ci>GFP*) wings. *ci-gal4* drives gene expression to the A compartment of the wing. (N) Cuticle preparations of *spalt*^{PE}*>GFP* and *spalt*^{PE}*>PTEN*^{RNAi} adult wings. The blue lines mark the lateral and medial regions of the wing. On the right are histograms plotting tissue size and cell density values of the medial (blue bars) and lateral (white bars) regions of *spalt*^{PE}*>PTEN*^{RNAi} adult wings normalized as a percent of the control (*spalt*^{PE}*>GFP*) wings. *spalt-gal4* drives gene expression to the medial part of the wing. The domains of transgene expression in A, E, I, M, and N are marked with a blue asterisk. Error bars show the standard deviation. Number of wings analyzed per genotype $\geq$ 10. ***$p < 0.001$; **$p < 0.01$; *$p < 0.05$. Area and cell density values of the cell populations driving transgene expression are labeled in blue, and the values of the nonexpressing domain are represented in white.

doi:10.1371/journal.pbio.1002239.g001

two cell populations is easily identified in the adult wing (Fig 1A), as it corresponds to the anterior side of the fourth longitudinal vein (L4, Fig 1A). The observed increase in tissue size upon activation of the PI3K/PTEN or TSC/TOR pathways in the whole wing was similar in both compartments (Fig 1C).

To address the potential nonautonomous roles of the *PTEN* and *TSC* tumor suppressor genes on neighboring wild-type cell populations, we drove transgene expression in either the A (with the *ci-gal4* driver) or P (with the *en-gal4* or *hh-gal4* drivers) compartments of the developing *Drosophila* wing (Fig 1E and 1I and S1 Fig) and quantified the size of the adjacent compartments in the resulting adult structures. The autonomous capacity of these transgenes to induce tissue and/or cell growth and cell proliferation was also observed with these Gal4 drivers (Fig 1E, 1G, 1H and 1K and 1L and S1 Fig, blue bars). Interestingly, the size of neighboring wild-type tissues decreased in all cases (Fig 1E, 1G, 1I and 1K and S1 Fig, white bars), and this decrease was accompanied by a reduction in cell size (reflected by an increase in cell densities in the adult wing (Fig 1H and 1L and S1 Fig, white bars). Whether the reductions in cell and tissue size are two independent processes nonautonomously regulated by the PI3K/PTEN and TSC/TOR pathways or whether there is a causal relationship between them is further analyzed in the following sections. The nonautonomous effects on tissue growth were also obtained with other Gal4 drivers not specific to compartments (Fig 1N). Increased cell proliferation, by means of overexpression of the cell cycle regulators String/Dcdc25 and CycE (which drive G2/M and G1/S transitions, respectively [28–30]), gave rise to a higher number of cells as a consequence of increased mitotic activity (Fig 1M and S1 Fig, see also [31]) but was not sufficient to promote tissue growth (Fig 1M, blue bar). The transgene-expressing compartment was, if anything, slightly smaller (Fig 1M, blue bar), most probably because of the observed increase in the number of apoptotic cells in the tissue (S1 Fig, see also [31]). Thus, the capacity of PI3K/PTEN to promote tissue growth does not depend only on increased cell proliferation rates. Driving cell proliferation was not sufficient to exert any nonautonomous effects on tissue or cell growth either (Fig 1M, white bars). All together, these results indicate that tissue overgrowth, induced by different means and independently of whether it is a consequence of increased cell size and/or cell number, causes a nonautonomous reduction in tissue size of adjacent cell populations.

Targeted Activation of the PI3K/PTEN or TSC/TOR Pathways Induces a Nonautonomous Reduction of Growth Rates in Adjacent Cell Populations

The results presented so far indicate that induction of tissue overgrowth in defined territories of the wing primordia causes a nonautonomous decrease in tissue size of nearby cell populations. To understand whether this nonautonomous response is an active mechanism that takes place during development, we monitored the size of the A and P compartments throughout development after targeted expression of growth-promoting transgenes in anterior cells. Larvae expressing PI3K/Dp110, Rheb, or GFP in the A compartment (with the *ci-gal4* driver) were grown at 25°C, and the absolute size of the transgene-expressing (A) and nonexpressing (P) compartments was quantified at a range of time points of larval development. We focused our attention on third instar wing discs (from 72 to 140 h after egg laying [AEL]), as primordia of the future adult wings are specified in late second instar (around 60 h AEL, [32]). The autonomous impact of PI3K/Dp110 or Rheb on tissue growth was already visible in mid–late third instar wing discs (96–140 h AEL), and, most interestingly, this was accompanied by a clear reduction in tissue size of the neighboring P compartment (Fig 2A and 2B). Thus, activation of growth promoting pathways in one territory causes a nonautonomous reduction in growth rates of the adjacent cell population.

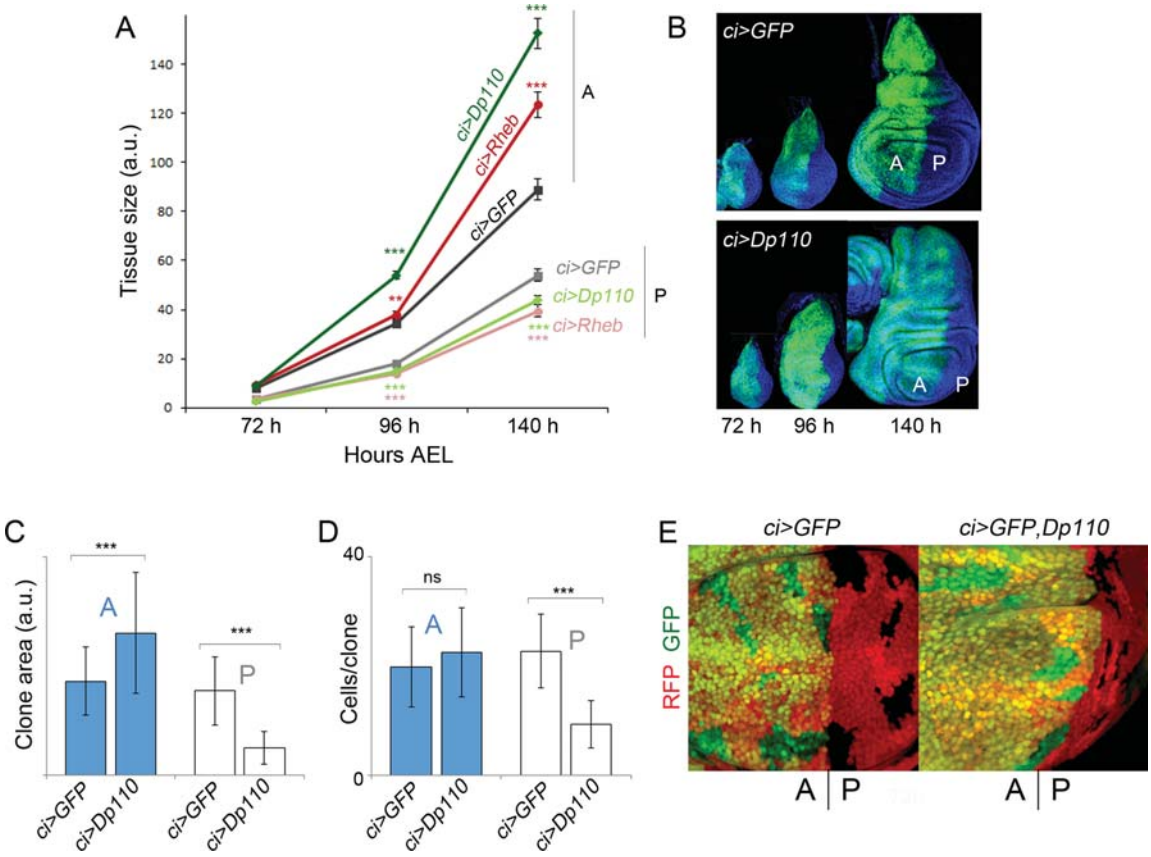

Fig 2. Targeted activation of the PI3K/PTEN and TSC/TOR pathways induces a nonautonomous reduction in growth rates in adjacent cell populations. (A) Quantification of tissue size (in arbitrary units [a.u.]) of both anterior (A) and posterior (P) domains of wing imaginal discs of the indicated genotypes in three distinct time points during development (in hours [h] AEL). Error bars show the standard deviation. Number of wing discs analyzed per genotype $\geq$ 15. ***$p < 0.001$; **$p < 0.01$. (B) Examples of *ci>GFP* (upper panel) and *ci>GFP*, *Dp110* (lower panel) wing imaginal discs in the developmental time points shown in panel A. The transgene-expressing domain is marked with GFP (in green), and the disc is labelled with DAPI (in blue). The A and P compartments are indicated. (C, D) Histograms plotting the size of clones (in a.u., C) and the number of cells per clone (D) located in the A or P compartment of *ci-gal4*,*UAS-GFP* and *ci-gal4*, *UAS-GFP*/*UAS-Dp110* wing discs. Clones were generated at the beginning of the third instar period and quantified 72 h later in late third instar wing discs. Error bars indicate the standard deviation. Number of clones analyzed per genotype $\geq$ 30. ***$p < 0.001$. Size of clones (A compartment, a.u.): ci>GFP = 388 ± 141; ci>GFP, Dp110 = 587 ± 249. Size of clones (P compartment, a.u.): ci>GFP = 348 ± 140; ci>GFP, Dp110 = 114 ± 67. Number of cells per clone (A compartment): ci>GFP = 20 ± 7; ci>GFP, Dp110 = 23 ± 8. Number of cells per clone (P compartment): ci>GFP = 23 ± 7; ci>GFP, Dp110 = 9 ± 4. (E) Examples of clones of cells in *ci>GFP* (left panel) and *ci>GFP*, *Dp110* (right panel) wing discs and induced in the developmental time points shown in C and D. The transgene-expressing domain is marked with GFP (in green), and the clones are labeled by the absence of nuclear red fluorescent protein (RFP, red) expression. The A and P compartments are indicated.

doi:10.1371/journal.pbio.1002239.g002

In order to investigate whether cell proliferation rates are also regulated in a nonautonomous manner, we induced neutral clones of cells at the beginning of the third instar period (72 h AEL) and examined the size of these clones 72 h later in late third instar wing discs. Clone size (in arbitrary units [a.u.]) and number of cells per clone were measured in *ci-gal4; UAS-GFP/UAS-Dp110* wing discs, and these two measurements were compared to those of control clones induced in *ci-gal4; UAS-GFP/+* wing discs and grown in parallel. In

Dp110-expressing wing discs, the size of the clones in the A compartment was, as expected, significantly larger than the size of clones quantified in the A compartment of GFP-expressing discs (Fig 2C–2E). Interestingly, the clone size and the number of cells per clone were significantly smaller in the P compartment of *Dp110*-expressing wing discs than in GFP-expressing discs (Fig 2C–2E). We also used a fluorescence-activated cell sorter (FACS) to collect data about the DNA content of dissociated cells from 120 h AEL wing discs expressing Dp110 or GFP under the control of the *ci-gal4* driver. As shown in S1 Fig, the cell cycle profile of A and P cells was very similar in the two genotypes analyzed. Taken together, these results indicate that activation of growth promoting pathways causes a nonautonomous reduction in proliferation rates, without any obvious arrest in any particular cell cycle stage, and imply that the nonautonomous reduction in tissue size observed in adult wings is a consequence of not only reduced cell size but also cell number.

Nonautonomous Effects on Tissue Growth Are Independent of Apoptosis and Dietary Restriction

The nonautonomous reduction in growth rates caused by activation of the PI3K/PTEN or TSC/TOR pathways in defined cell populations of the developing wing primordia is reminiscent of cell competition, a short-range elimination of slow-dividing cells through apoptosis when confronted with a faster-growing cell population [33]. We thus performed a terminal deoxynucleotidyl transferase dUTP nick end labeling (TUNEL) assay to label DNA strand breaks induced by apoptotic cell death and quantified the number of apoptotic cells in the transgene-expressing and nonexpressing cell populations. A clear increase in TUNEL-positive cells was observed in those territories expressing Rheb or Dp110/PI3K when compared to GFP-expressing tissues (Fig 3A and 3B, green bars). A similar cell autonomous induction of apoptosis was previously observed in *PTEN* mutant cells [12], most probably reflecting a deleterious effect of nonphysiological activation of these pathways in proliferating cells. However, the number of apoptotic cells in adjacent cell populations was small and very similar to that found in control tissues expressing GFP (Fig 3A and 3B, grey bars, see also [34]). We next analyzed a potential contribution of apoptotic cell death to the nonautonomous reduction in growth rates caused by Rheb or Dp110/PI3K expression. When apoptosis was reduced in the whole animal by halving the dose of the proapoptotic genes *hid*, *grim*, and *reaper* (in *Df(H99)/+* larvae, [35]), the number of apoptotic cells in the tissue was reduced (S1 Fig), but the nonautonomous reduction in tissue size was unaffected (Fig 3C, 3C', 3D and 3D'). The transcription factor and tumor suppressor p53, a short-lived, nonabundant protein in healthy cells, plays a fundamental role in regulating the response of mammalian cells to stress, in part through the transcriptional activation of genes involved in apoptosis and cell cycle regulation [36]. Impaired protein translation in *Drosophila* tissues has been previously shown to induce Dp53 activation and Dp53-dependent inhibition of growth and proliferation rates in adjacent tissues [37]. However, the nonautonomous effects on tissue growth caused by Rheb or Dp110/PI3K overexpression were unaffected by expression of a dominant negative version of Dp53 ($Dp53^{ct}$, Fig 3C and 3C'). Taken together, all these results indicate that Dp53 is not required in the overgrown territory to nonautonomously reduce the growth rates in neighboring cell populations and that the nonautonomous decrease in growth rates is not a consequence of programmed cell death.

Apoptotic cells can produce signals to instruct neighboring cells either to undergo additional proliferation or apoptosis [34,38–40]. We thus analyzed whether the apoptotic cells observed in the transgene-expressing compartment exerted any nonautonomous effect on the neighboring compartment. Expression of p35, a baculovirus protein well known to block

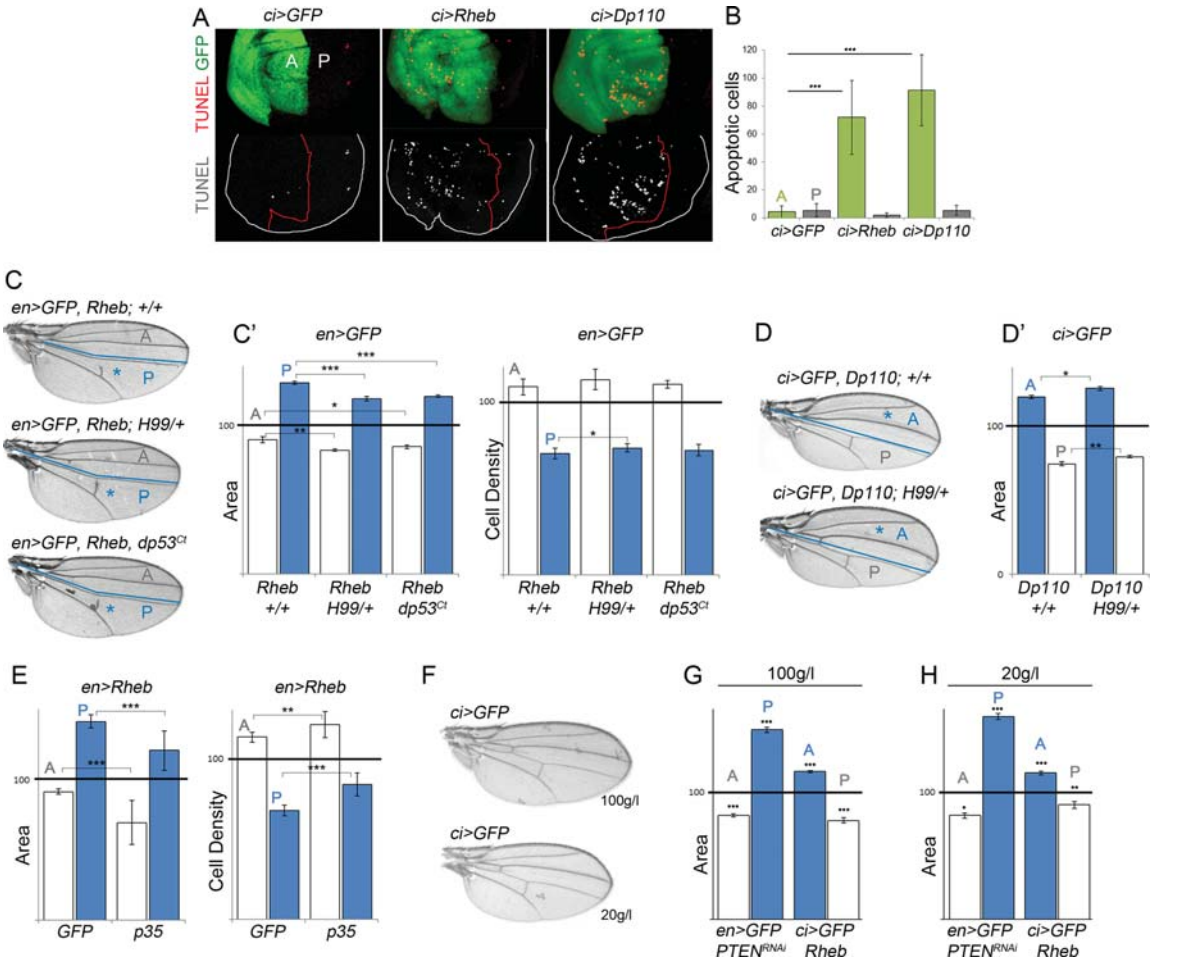

Fig 3. The nonautonomous reduction in tissue size upon targeted activation of the PI3K/PTEN and TSC/TOR pathways does not rely on Dp53 activity and apoptosis and is not affected by nutrient restriction. (A) *ci>GFP*, *ci>Rheb*, and *ci>Dp110* wing imaginal discs labelled with TUNEL to visualize apoptotic cells (in red or white). The *ci* domain is labelled with GFP (in green), and the boundary between A and P cells is marked by a red line. (B) Histogram plotting the quantification of the absolute number of TUNEL-positive cells in the A (light green bars) and P (grey bars) compartments of the indicated genotypes. Error bars indicate the standard deviation. Number of wing discs analyzed per genotype $\geq$ 10. ***$p < 0.001$. (C, D) Cuticle preparations of *en>GFP*, *Rheb* (C), and *ci>GFP*, *Dp110* (D) adult wings either in a wild-type background, in a heterozygous background for *H99* (a deficiency that uncovers *reaper*, *hid*, and *grim* proapoptotic genes), or coexpressing a dominant negative form of Dp53 ($Dp53^{Ct}$). The blue line marks the boundary between the A and P compartments. The domains of transgene expression are marked with a blue asterisk. (C', D', E) Histograms plotting tissue size (C', D', E) and cell density values (C', E) of the transgene-expressing compartment (blue bars) and the adjacent cell populations (white bars) of adult wings with the indicated genotypes normalized as a percent of the control wings. Error bars show the standard deviation. Number of wings analyzed per genotype $\geq$ 10. ***$p < 0.001$; **$p < 0.01$; *$p < 0.05$. (F) Cuticle preparations of *ci>GFP* adult wings of well-fed (100 g/L yeast food, top) and starved (20 g/L yeast food, bottom) animals. Note the reduction in wing size caused by starvation. (G, H) Histograms plotting tissue size of the transgene-expressing compartment (blue bars) and the adjacent cell populations (white bars) of adult wings with the indicated genotypes normalized as a percent of the control wings. Error bars show the standard deviation. Number of wings analyzed per genotype $\geq$ 10. ***$p < 0.001$; **$p < 0.01$; *$p < 0.05$. Quantification was made in well-fed (100 g/L yeast food, left histogram) and starved (20 g/L yeast food, right histogram) animals of identical genotypes.

doi:10.1371/journal.pbio.1002239.g003

apoptosis at the level of the effector apoptotic Caspases [41], was not able to rescue the nonautonomous decrease in tissue growth caused by Rheb overexpression (Fig 3E). We found out that p35 expression caused an increase in cell density in both the transgene-expressing compartment and in the neighboring one, most probably reflecting apoptosis-induced cell proliferation caused by undead cells. Indeed, mitotic activity was increased in the developing primordia expressing p35 (S1 Fig). These results indicate that dying cells in the transgene-expressing compartment do not contribute to the nonautonomous reduction in tissue and cell size.

PTEN mutant cells generated in *Drosophila* tissues have been recently shown to acquire a growth advantage under starvation conditions at the expense of the wild-type neighboring cells, and this growth advantage has been proposed to rely on the withdrawal of nutrients from neighboring cells [12]. To assess the impact of nutrient availability on the autonomous and nonautonomous effects caused by expression of Rheb or *PTEN-RNAi* in defined territories of the wing primordium, larvae expressing these transgenes in either the A or P compartment were reared on food with varying yeast content, the main source of micronutrients and amino acids in fly media. Our standard medium contains 50 g/l yeast. We thus subjected experimental larvae expressing either a dsRNA form of PTEN or Rheb and control larvae expressing GFP to media containing 100 g/l and 20 g/l yeast and analyzed the size of the transgene-expressing and nonexpressing cell populations in the resulting adult wings. Despite the expected reduction in the size of wings of animals reared on food containing 20 g/l yeast (Fig 3F), the extent (in percentage) of the nonautonomous decrease in tissue size caused by transgene expression was similar to that observed in animals reared on food containing 100 g/l yeast (Fig 3G and 3H). Thus, the nonautonomous reduction in growth rates is not a consequence of the withdrawal of nutrients from neighboring cells.

Autonomous and Nonautonomous Effects on the Dpp Activity Gradient

We noticed that activation of the PI3K/PTEN or TSC/TOR pathways in defined populations of the wing primordium gave rise to larger but well-proportioned adult structures (Fig 4A, see also Fig 1). The adjacent wild-type territories were reduced in size, but the patterning elements (e.g., longitudinal veins) were also proportionally well located. The signaling molecule Dpp, a member of the TGF-β superfamily, is expressed at the boundary between the A and P compartments in the developing wing (Fig 4B) and plays a major role in positioning the wing veins along the anterior–posterior axis [42]. Interestingly, the Dpp gradient scales with size in order to correctly maintain the wing proportions [43–46], and Dpp is well known to promote tissue growth (reviewed in [17,18]). Thus, the autonomous and nonautonomous effects of Rheb or Dp110/PI3K overexpression on tissue growth might rely on modulating the range of Dpp activity. Since *dpp* expression was largely unaffected in transgene-expressing tissues (Fig 4B), we monitored the range of the Dpp activity gradient, visualized by the expression of the Dpp target gene Spalt (Fig 4C, [47]) and with an antibody against the phosphorylated form of the Dpp transducer Mothers Against Dpp (pMAD, Fig 4D). As expected and as a result of the capacity of the Dpp gradient to scale with tissue size, the range of the Dpp activity gradient was expanded in the overgrowing transgene-expressing compartment (Fig 4C and 4D). In order to quantify the cell-autonomous impact of tissue growth on the Dpp activity gradient, we extracted the pMAD profiles along four lines perpendicular to the *dpp* expression domain (yellow lines in Fig 4D) and plotted the average pMAD values along the AP axis in experimental (blue in Fig 4E, 4F, 4H and 4I) and control (red in Fig 4E, 4F, 4H and 4I) wing primordia raised in the same conditions and immunolabeled in the same tube (as previously done in [45]). Since the boundary between A and P cells is out of phase in control and Dp110-expressing wing

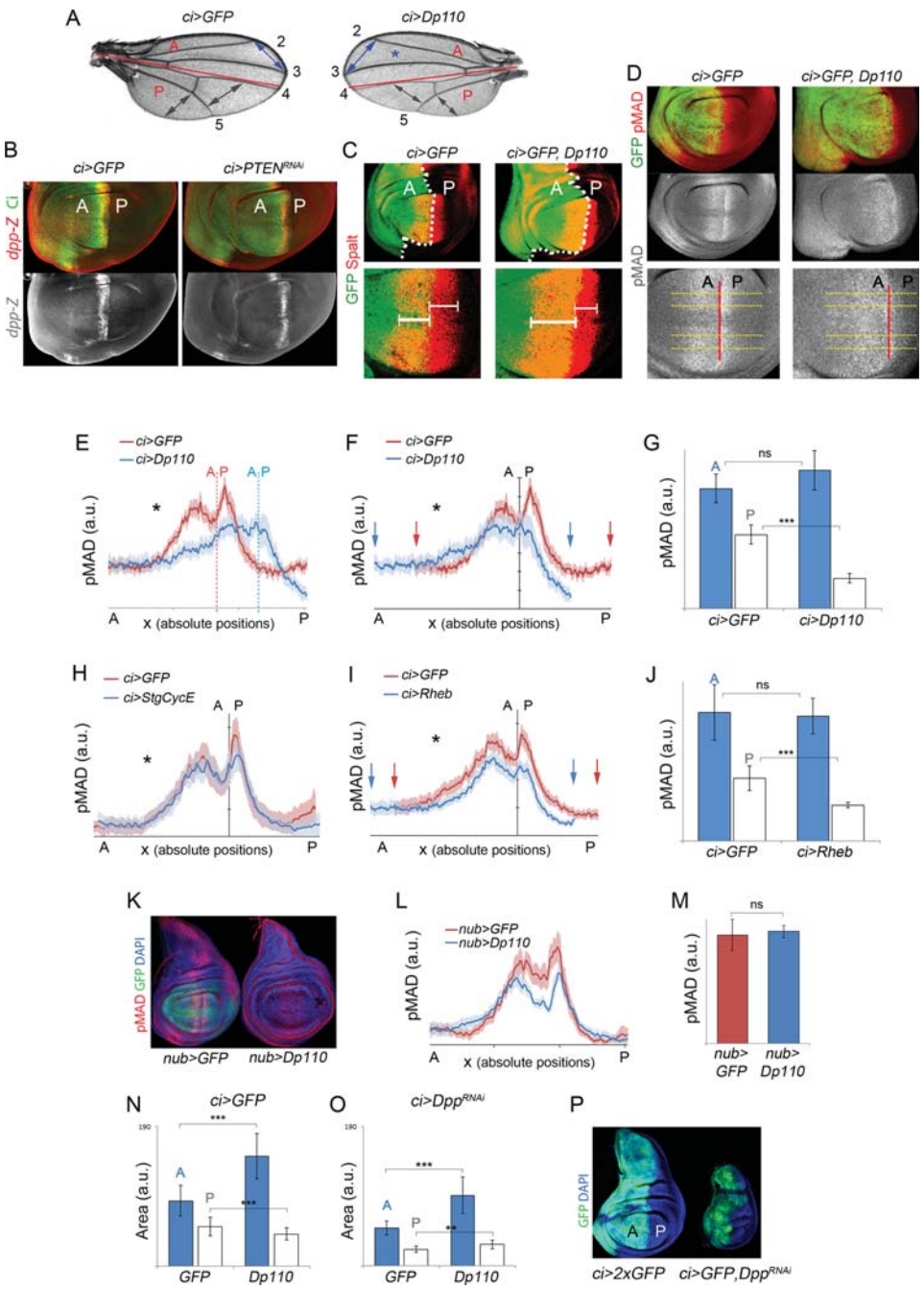

Fig 4. Autonomous and nonautonomous effects on Dpp activity levels upon targeted activation of the PI3K/PTEN and TSC/TOR pathways. (A) Cuticle preparation of adult wings expressing *GFP* or *Dp110* under the control of the *ci-gal4* driver, which drives transgene expression in the anterior

compartment. Note the expansion of the anterior intervein regions (blue arrows) upon induction of growth and the corresponding reduction of the posterior intervein regions (grey arrows). The anterior (A) and posterior (P) compartments are labeled, and the AP boundary is marked by a red line. (B) Wing imaginal disc of *ci>GFP* and *ci>PTEN*^{RNAi} larvae labelled to visualized Ci protein (in green) and β-galactosidase (βGal) (in red or white) to visualize *dpp* (dpp-lacZ) expression. The width of the *dpp-lacZ* stripe (normalized with respect to the width of the wing pouch) was *ci>GFP* = 0.082 ± 0.005; *ci>PTEN*^{RNAi} = 0.088 ± 0.003; $p = 0.55$; $n > 6$. (C) Wing imaginal discs of *ci>GFP* and *ci>GFP*, *Dp110* larva labelled to visualize Spalt (in red) and GFP (in green) protein expression. The white dashed line marks the boundary between A and P cells. The lower panels show magnification of the Spalt domain. Note that the anterior Spalt domain is wider upon Dp110 expression (thick bracket) whereas the posterior Spalt domain (thin brackets) gets reduced. (D) Wing imaginal discs of *ci>GFP* and *ci>GFP*, *Dp110* larva labelled to visualize pMAD protein (in red or white) and GFP (in green). Lower panels show magnifications of the pMAD domains, and the red line marks the boundary between the A and P compartments. Horizontal yellow lines were used to generate the pMAD profiles shown in E–I. (E, F, H, I) Average pMAD profiles of wing discs expressing *GFP* (red line) or *GFP* and the corresponding transgenes (blue line) under the control of the *ci-gal4* driver. Profiles were taken along the AP axis and plotted in absolute positions. The standard error to the mean is shown in the corresponding color for each genotype. In E, the AP boundary of each experiment is marked by a dashed line of the corresponding color. In F, the AP boundary of both experiments was aligned to allow comparison of the profile in each compartment. Number of wing discs analyzed per genotype ≥ 5. The domains of transgene expression are marked with a black asterisk. Arrows mark the limits of the Dpp activity gradients. (G, J) Histograms plotting the total intensity of the pMAD signal in a.u. of the anterior (blue bars) and posterior (white bars) compartments of *ci>GFP* (G, J) and *ci>Dp110* (G) or *ci>Rheb* (J) wing discs. Error bars indicate the standard deviation. Number of wing discs analyzed per genotype ≥ 5. ***$p < 0.001$. (K) Wing imaginal discs of *nub>GFP* and *nub>Dp110* larvae labelled to visualize pMAD protein (in red), GFP (in green), and DAPI (in blue, to visualize nuclei). (L) Average pMAD profile of wing discs expressing *GFP* (red line) or *Dp110* (blue line) in the *nubbin* domain. Profiles were taken along the AP axis and plotted in absolute positions. The standard error to the mean is shown in the corresponding color for each genotype. Number of wing discs analyzed per genotype ≥ 7. (M) Histogram plotting the total intensity of the pMAD signal in a.u. of the *nubbin* domain of *nub>GFP* (red bar) and *nub>Dp110* (blue bar) discs. Error bars indicate the standard deviation. Number of wing discs analyzed per genotype ≥ 5. (N) Histogram plotting the area (in a.u.) of anterior (blue) and posterior (white) domains of wing discs expressing *GFP* or *GFP* and *Dp110* in the *ci* domain. Error bars show the standard deviation. Number of wing discs analyzed per genotype ≥ 15. ***$p < 0.001$ (O) Histogram plotting the area (in a.u.) of anterior (blue) and posterior (white) domains of wing discs expressing either *GFP* or *Dp110* in the *ci* domain together with a dsRNA form against *dpp*. Error bars show the standard deviation. Number of wing discs analyzed per genotype ≥ 15. ***$p < 0.001$, **$p < 0.01$. (P) Wing imaginal discs of *ci>GFP* and *ci>dpp*^{RNAi} larvae labelled to visualize GFP (in green) and DAPI (in blue, to visualize nuclei).

doi:10.1371/journal.pbio.1002239.g004

discs (Fig 4E), the pMAD profiles were aligned with respect to the AP boundary to better visualize the autonomous and nonautonomous effects on the Dpp activity gradient (Fig 4F and 4I). Despite the visible expansion along the AP axis of the pMAD gradient in the overgrowing compartment (black asterisk in Fig 4E, 4F and 4I, see also S2 Fig), the total amount of pMAD, quantified as total pixel intensity within each compartment (see Materials and Methods), was comparable in overgrowing and control compartments (Fig 4G and 4J, see also S2 Fig). A similar relationship between the range of the pMAD gradient and the total amount of pMAD was observed when transgene expression was driven in the whole wing primordium (Fig 4K–4M). These results indicate that tissue growth has a major impact in Dpp spreading but not signaling. Two observations suggest that the tissue-autonomous expansion of the pMAD gradient is a consequence of increased tissue size, and that this expansion is not solely a consequence of increased number of cells. First, Rheb overexpression increased tissue and cell size, but not cell number, and led to the expansion of the pMAD gradient (Fig 4I, black asterisk). Second, increased cell number without affecting tissue size (by means of expression of the cell cycle regulators CycE and String/Dcdc25) did not have any impact on the pMAD gradient (Fig 4H, black asterisk).

Interestingly, both the width of the Dpp activity gradient, monitored by the expression of Spalt (Fig 4C) and pMAD (Fig 4D, 4E, 4F and 4I and S2 Fig), and the total amount of pMAD signaling (Fig 4G and 4J and S2 Fig) were reduced in adjacent wild-type territories. This nonautonomous effect was not observed upon expression of cell cycle regulators CycE and String/Dcdc25 (Fig 4H). We next addressed whether the nonautonomous reduction in tissue size relied on the capacity of the tissue to compete for the Dpp ligand. For this purpose, we compared the size of PI3K/Dp110-expressing and nonexpressing compartments upon depletion of Dpp, by means of expression of a dsRNA form against *dpp* in the A compartment (Fig 4N and 4O). Expression of a dsRNA form against *dpp* in A cells gave rise to a strong reduction in tissue size (Fig 4P). Whereas PI3K/Dp110 was still able to induce overgrowth of the transgene-expressing territory (Fig 4N and 4O, blue bars), the nonautonomous reduction in tissue size was largely rescued (compare Fig 4N and 4O, white bars). Taken together, these results indicate

that tissue growth has a major impact in Dpp spreading but not signaling and that the nonautonomous reduction in tissue size is most probably a consequence of reduced Dpp signaling.

Dally Contributes to the Autonomous and Nonautonomous Effects on Tissue Growth

Heparan sulfate proteoglycans (HSPGs) of the glypican family play key roles in the regulation of morphogen signaling and distribution (reviewed in [48]). Glypicans are glycosylphosphatidylinositol (GPI)-anchored HSPGs that have a protein core to which heparan sulfate (HS) chains are covalently attached. HS chains provide binding sites for many growth factors, and the glypican Dally contributes to the spreading of the Dpp ligand over the wing primordium [49–52]. Interestingly, the expression levels of Dally (visualized with two distinct reporters, an enhancer-trap and a proteintrap, see Fig 5A and 5B and S2 Fig) were clearly increased upon activation of the PI3K/PTEN or TSC/TOR pathways. We next monitored the capacity of targeted overexpression of Dally to phenocopy the autonomous and nonautonomous effects on tissue growth, proliferation rates, and Dpp gradient formation observed upon activation of these two pathways. Overexpression of Dally in the A or P compartments of the developing wing gave rise to a tissue-autonomous increase in size (Fig 5C–5F, blue bars) and, most importantly, a nonautonomous reduction in size of the adjacent wild-type territories (Fig 5C–5F, white bars). The increase in tissue size was accompanied by an increase in cell number (note the higher cell density in the transgene expressing compartment, Fig 5D, blue bars). In contrast to the PI3K/PTEN and TSC/TOR pathways, the nonautonomous reduction in tissue size caused by Dally overexpression was not accompanied by a decrease in cell size (note that cell densities, if anything, decreased, Fig 5D and 5F, white bars). Thus, other elements regulated by the growth-promoting pathways, apart from Dally, might have a nonautonomous impact on cell size. In order to address whether growth and proliferation rates are also regulated in a nonautonomous manner by the overexpression of Dally, we induced neutral clones of cells at the beginning of the third instar period (72 h AEL) and examined the size of these clones 72 h later in late third instar wing discs. Clone size and number of cells per clone were measured in the A and P compartments of *ci-gal4; UAS-GFP/UAS-Dally* wing discs, and these two measurements were compared to those of control clones induced in *ci-gal4; UAS-GFP/+* wing discs and grown in parallel. In Dally-overexpressing wing discs, the size of the clones and the number of cells per clone in the A compartment were significantly bigger than the size of clones quantified in the A compartment of GFP-expressing discs (Fig 5G and 5H). Interestingly, clone size and number of cells per clone were significantly smaller in the P compartment of Dally-expressing wing discs than in GFP-expressing discs (Fig 5G and 5H). These results indicate that overexpression of Dally causes a nonautonomous reduction in proliferation rates and imply that the nonautonomous reduction in tissue size observed in adult wings is a consequence of reduced cell number. Targeted overexpression of Dally also gave rise to a tissue-autonomous increase in the width of the pMAD signaling gradient and to a remarkable reduction in pMAD signaling in nearby territories (Fig 5I–5K). In this case, the total amount of pMAD was higher in Dally-overexpressing compartments than in the control one (Fig 5K). We noticed that the patterning elements, including wing veins and the wing margin, were well located and formed, thus indicating that Dally overexpression exerts a specific role on Dpp gradient formation and a minor role on the other secreted signaling molecules involved in wing growth and patterning.

We next monitored the contribution of Dally to the autonomous and nonautonomous effects on tissue growth caused by targeted deregulation of the PI3K/PTEN and TSC/TOR pathways. For this purpose, we expressed a dsRNA form of *Dally* together with Dp110/PI3K or Rheb. Expression of a dsRNA form of *Dally* in otherwise wild-type wings caused a mild

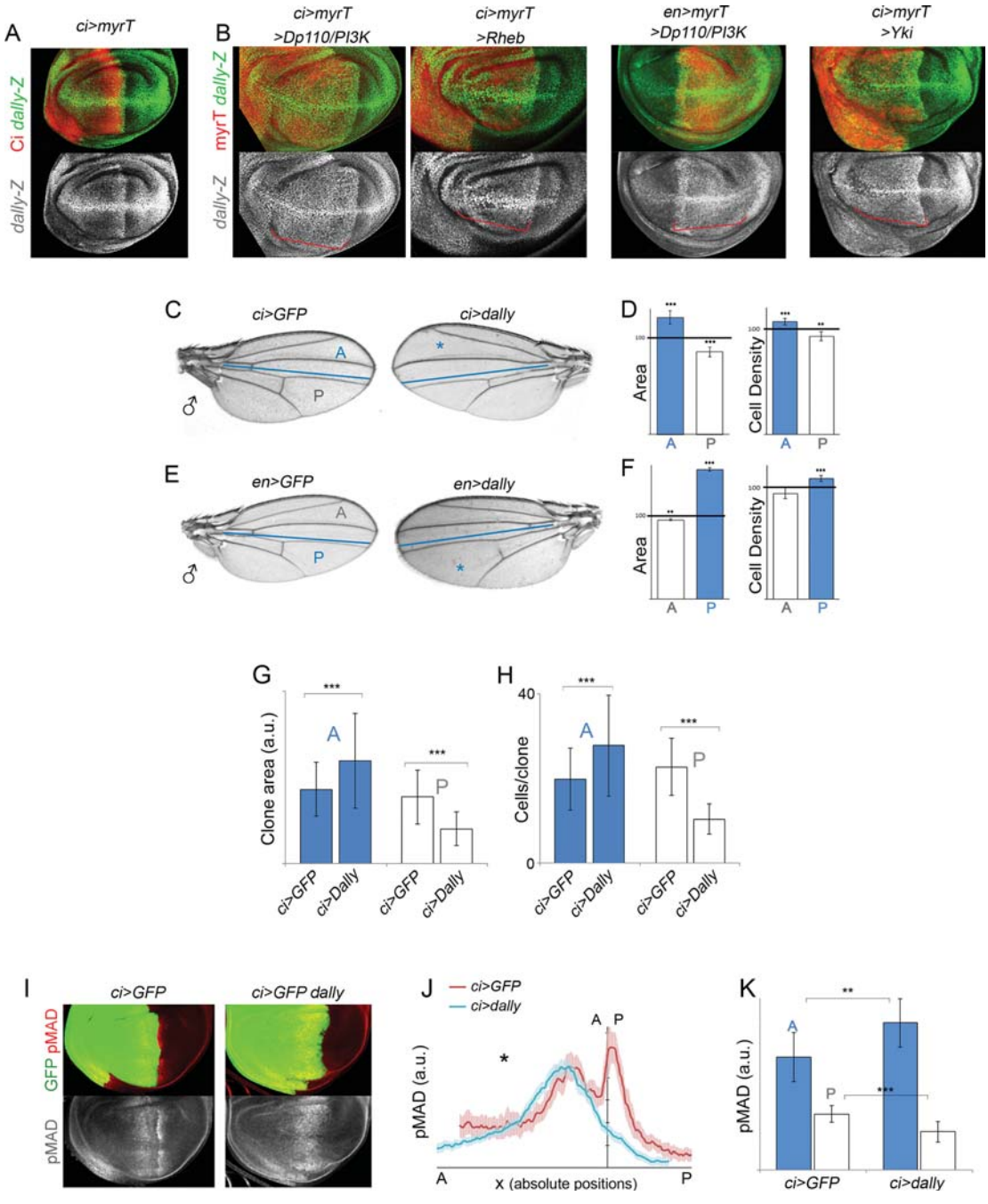
A
ci>myrT
Ci dally-Z
dally-Z
B
ci>myrT >Dp110/PI3K
ci>myrT >Rheb
en>myrT >Dp110/PI3K
ci>myrT >Yki
myrT dally-Z
dally-Z
C
ci>GFP
ci>dally
A
P
D
Area
Cell Density
E
en>GFP
en>dally
F
G
Clone area (a.u.)
H
Cells/clone
40
0
ci>GFP
ci>Dally
I
ci>GFP
ci>GFP dally
GFP pMAD
pMAD
J
ci>GFP
ci>dally
pMAD (a.u.)
x (absolute positions)
K
pMAD (a.u.)

Fig 5. Overexpression of Dally phenocopies the autonomous and nonautonomous effects of targeted activation of the PI3K/PTEN and TSC/TOR pathways. (A, B) Representative wing discs of the indicated genotypes labeled to visualize *dally-lacZ* (antibody to β-Gal, green or white) and myrTomato (myrT, in red) expression to mark the transgene-expressing domain. Note stronger expression of *dally-lacZ* upon activation of the PI3K/PTEN, TSC/TOR, or hippo/Yorkie pathways (red brackets). (C, E) Cuticle preparations of male adult wings overexpressing Dally under the control of the *ci-gal4* (C) or *en-gal4* (E) drivers. The blue line marks the boundary between the anterior (A) and posterior (P) compartments, and the domains of Dally overexpression are marked with a blue asterisk. (D, F). Histograms plotting tissue size (left) and cell density values (right) of the Dally-expressing domains (blue bars) and the adjacent compartments (white bars) of adult wings overexpressing Dally under the control of the *ci-gal4* (D) or *en-gal4* (F) drivers. Values are normalized as a percent of the control (GFP-expressing) wings. Error bars show the standard deviation. Number of wings analyzed per genotype $\geq$ 10. ***$p < 0.001$; **$p < 0.01$. (G, H) Histograms plotting the size of clones (in a.u., G) and the number of cells per clone (H) located in the A or P compartment of *ci-gal4*, *UAS-GFP* and *ci-gal4*, *UAS-GFP/UAS-Dally* wing discs. Clones were generated at the beginning of the third instar period and quantified 72 h later in late third instar wing discs. Error bars indicate the standard deviation. Number of clones analyzed per genotype $\geq$ 30. ***$p < 0.001$. Size of clones (A compartment, a.u.): ci>GFP = 388 ± 141; ci>GFP, Dally = 537 ± 169. Size of clones (P compartment, a.u.): ci>GFP = 348 ± 140; ci>GFP, Dally = 182 ± 89. Number of cells per clone (A compartment): ci>GFP = 20 ± 7; ci>GFP, Dally = 28 ± 12. Number of cells per clone (P compartment): ci>GFP = 23 ± 7; ci>GFP, Dally = 10 ± 4. (I) Wing imaginal discs of *ci>GFP* and *ci>GFP*, *Dally* larvae labelled to visualize pMAD protein (in red or white) and GFP (in green). (J) Average pMAD profiles of wing discs expressing *GFP* (red line) or *GFP* and *Dally* (blue line) under the control of the *ci-gal4* driver. Profiles were taken along the AP axis and plotted in absolute positions. The standard error to the mean is shown in the corresponding color for each genotype. The AP boundary of both experiments was aligned to allow comparison of the profile in each compartment. Number of wing discs analyzed per genotype $\geq$ 5. (K) Histogram plotting the total intensity of the pMAD signal in a.u. of the anterior (blue bars) and posterior (white bars) compartments of *ci>GFP* and *ci>Dally*, *GFP* wing discs. Error bars indicate the standard deviation. Number of wing discs analyzed per genotype $\geq$ 5. ***$p < 0.001$; **$p < 0.01$.

doi:10.1371/journal.pbio.1002239.g005

tissue-autonomous size reduction (S2 Fig, blue bars), but no visible effect was observed in adjacent cell territories (S2 Fig, white bars). The width of the Dpp activity gradient was mildly reduced in the transgene-expressing compartment (S2 Fig). Interestingly, depletion of Dally was able to largely rescue not only the autonomous but also the nonautonomous effects on tissue growth caused by Rheb or PI3K/Dp110 expression (Fig 6A–6C). The autonomous expansion of the Dpp activity gradient and the nonautonomous retraction caused by targeted expression of Dp110 was also largely rescued by the dsRNA form of *Dally* (S2 Fig). Depletion of Sulfateless (Sfl), an enzyme needed for the modification of HS chains within glypicans [53], also rescued the autonomous and nonautonomous effects on tissue growth caused by *PTEN* depletion (Fig 6E). Targeted expression of dsRNA forms of *sfl* in otherwise wild-type wings caused a strong tissue-autonomous size reduction (S2 Fig, blue bars), but little effect was observed in adjacent cell territories (S2 Fig, white bars). Interestingly, depletion of Dally was not able to rescue the nonautonomous reduction in cell size caused by activation of the PI3K/PTEN and TSC/TOR pathways (Fig 6A–6C), reinforcing the proposal that cell size is nonautonomously regulated by the PI3K/PTEN and TSC/TOR pathways in a Dally-independent manner.

Mutations in the *hippo* pathway, originally identified in *Drosophila* by their capacity to induce cell proliferation and organ growth, induce tumors in mouse models and occur in a broad range of human carcinomas, including lung, colorectal, ovarian, and liver cancers (reviewed in [54]). Interestingly, the expression levels of the two existing *Drosophila* glypicans, Dally and Dally-like, are up-regulated upon deregulation of the *hippo/Yorkie* pathway (Fig 5B and [55]). Moreover, simultaneous mutations of both *Dally* and *Dally-like* have been shown to rescue the overgrowth caused by clones of cells overexpressing Yorkie [55]. We thus revisited the contribution of these two glypicans to the autonomous effects on tissue growth caused by deregulation of the hippo/Yorkie pathway and analyzed the potential nonautonomous effects on tissue size of the adjacent cell populations. Similar to what happened to TOR activation, deregulation of the hippo/Yorkie pathway causes strong overgrowth and larval lethality [56]. We thus induced a mild activation of the pathway by expressing a wild-type form of the transcription factor Yorkie. Overexpression of Yorkie in the A or P compartments of the developing wing gave rise to a tissue-autonomous increase in size and, most interestingly, a nonautonomous size reduction of the adjacent wild-type territories (Fig 6D and S2 Fig). Interestingly, both the autonomous and nonautonomous effects on tissue size were rescued by depletion of

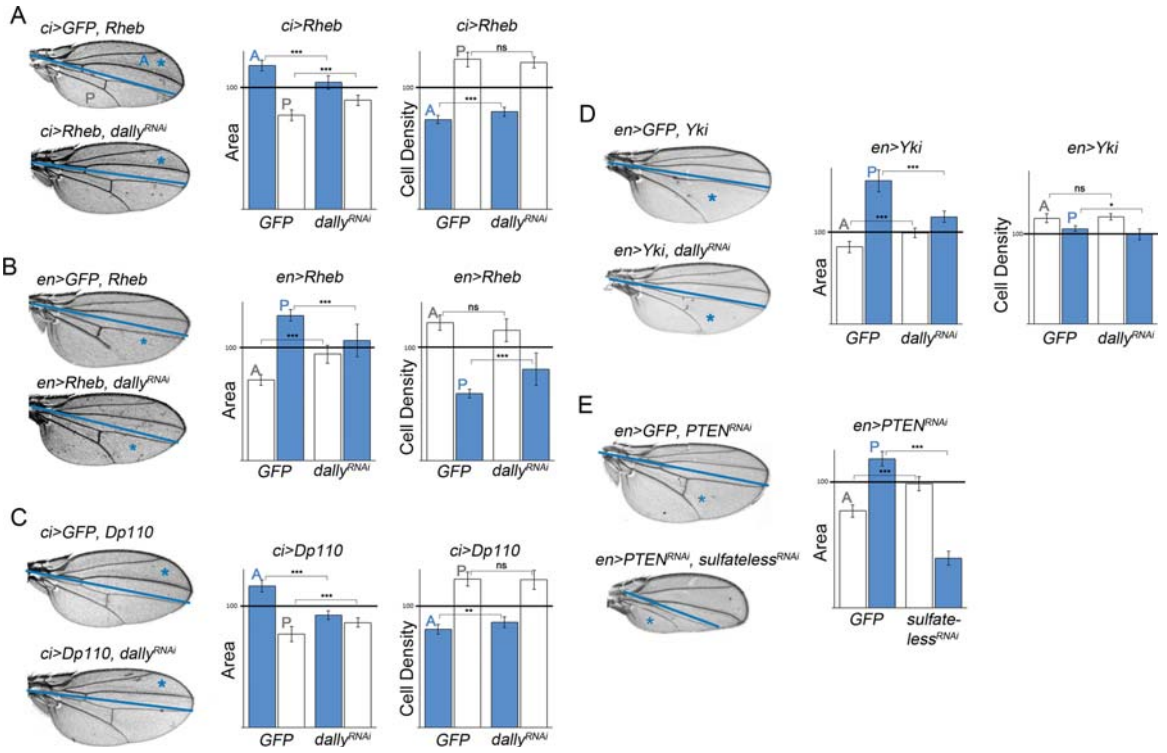

Fig 6. Dally contributes to the autonomous and nonautonomous effects of targeted deregulation of the PI3K/PTEN, TSC/TOR, and hippo/yorkie pathways. (A–E) Cuticle preparations of adult wings expressing the indicated transgenes under the control of the *ci-gal4* (A, C) or *en-gal4* (B, D, E) drivers. The blue line marks the boundary between the anterior (A) and posterior (P) compartments, and the domains of transgene expression are marked with a blue asterisk. On the right side of each panel, histograms plotting tissue size (A–E) and cell density (A–D) of the transgene-expressing (blue bars) or nonexpressing (white bars) compartments of adult wings expressing the indicated transgenes. Error bars show the standard deviation. Number of wings analyzed per genotype $\geq$ 10. ***$p < 0.001$; ** $p < 0.01$; *$p < 0.05$.

doi:10.1371/journal.pbio.1002239.g006

Dally (Fig 6D). In contrast, depletion of Dally-like, using two different dsRNA forms able to reduce its protein levels, did not have this effect (S2 Fig).

Taken together, the above results indicate that Dally, and not Dally-like, contributes to the tissue-autonomous and nonautonomous effects on tissue growth caused by targeted deregulation of the PI3K/PTEN, TSC/TOR, and hippo/Yorkie pathways. These pathways exert their tissue-autonomous action through Dally, most probably by modulating the spreading of the Dpp morphogen and other secreted growth factors, as Dp110 overexpression was still able to induce some growth in Dpp-depleted tissues (Fig 4O). We hypothesize that the nonautonomous effects are a consequence of withdrawal of Dpp from neighboring cells. In order to reinforce the latter notion, we analyzed the capacity of the Dpp type I receptor Thickveins (Tkv), which has been shown to trap Dpp and limit its spreading [43,57], to phenocopy the nonautonomous effects on tissue growth observed upon targeted deregulation of these pathways. Although the expression levels of Tkv (visualized with both an enhancer and a protein trap) were unaffected by targeted deregulation of the PI3K/PTEN pathway (S3 Fig), targeted expression of a wild-type form of Tkv or a dominant negative form of the receptor able to bind Dpp but unable to

transduce the signal (Tkv-DN, [58]) gave rise to a nonautonomous size reduction of the adjacent wild-type territories (S3 Fig, white bars). These results emphasize the role of Dpp in modulating the growth and pattern of different cell populations within a developing organ.

Dally, a Molecular Bridge between Nutrition and Wing Scaling

Besides the roles of the PI3K/PTEN and TSC/TOR signaling pathways in inducing tumor growth [2,4], these two pathways play a conserved role in nutrient sensing and tissue growth during normal development. In the *Drosophila* wing, they modulate the final size of the adult structure according to nutrient availability of the feeding animal (reviewed in [15,16]), and Dpp plays an organ-intrinsic role in the coordination of growth and patterning (reviewed in [17,18]). The identification of the proteoglycan Dally as the rate-limiting factor that contributes to the tissue-autonomous and nonautonomous effects on growth caused by targeted activation of the nutrient-sensing PI3K/PTEN and TSC/TOR pathways suggests that Dally acts as a molecular bridge between the organ-intrinsic and organ-extrinsic mechanisms that regulate organ size. Consistent with this proposal, activation of the PI3K/PTEN or TSC/TOR pathways, which mimics conditions of high nutrient availability, led to an increase in Dally expression levels (Fig 5B) and larger wings (Fig 7A–7D), and depletion of Dally rescued the resulting tissue overgrowth (Fig 7A–7D, see also Fig 6A–6C). These data indicate that Dally contributes to the tissue overgrowth caused by activation of these pathways. We next addressed whether reduced wing size caused by inactivation of the PI3K/PTEN or TSC/TOR pathways, which mimics conditions of low nutrient availability, relies, at least in part, on reduced expression levels of Dally. Interestingly, Dally expression levels were reduced upon targeted depletion of the PI3K/PTEN or TSC/TOR signaling pathways (by expressing dsRNA forms of the insulin-like receptor [InR] and Rheb, respectively; Fig 7E and S4 Fig), and, most interestingly, Dally overexpression was able to partially rescue the tissue size defects caused by depletion of the PI3K/PTEN pathway (Fig 7F and 7G). As expected, the cell size defects were not rescued upon Dally overexpression. These results indicate that the tissue size defects caused by depletion of this pathway rely, at least in part, on the observed reduction in Dally expression levels. Dally overexpression was able only to slightly rescue the tissue size defects of Rheb-depleted wings (S4 Fig), suggesting that other elements are required, together with Dally, to mediate TSC/TOR-dependent tissue growth.

In order to further analyze the role of Dally as a molecular bridge between nutrient-sensing pathways and organ-intrinsic mechanisms, we subjected experimental and control larvae to media containing high (100 g/l yeast) or low (20 g/l yeast) levels of amino acids and analyzed the size of the resulting adult wings upon expression of Dally or a dsRNA form of Dally in the whole wing primordium. Despite the expected reduction in the size of animals reared on food containing 20 g/l yeast, the size of Dally-overexpressing wings (which slightly increases the range of Dpp signaling without affecting the shape of the activity gradient, S4 Fig) was comparable to that of animals receiving food containing 100 g/l yeast (Fig 7H). Similarly, despite the expected increase in animal size reared on food containing 100 g/l yeast, the size of Dally-depleted wings was comparable to that of animals receiving 20 g/l yeast food (Fig 7H). All together, these results reveal that Dally proteoglycan participates in integrating nutrient conditions into wing scaling, most probably through its ability to facilitate the spread of Dpp throughout the tissue.

Discussion

Here we present evidence that targeted deregulation of the PI3K/PTEN, TSC/TOR, or hippo/Yorkie pathways, known to promote tissue overgrowth by increasing the number and/or size

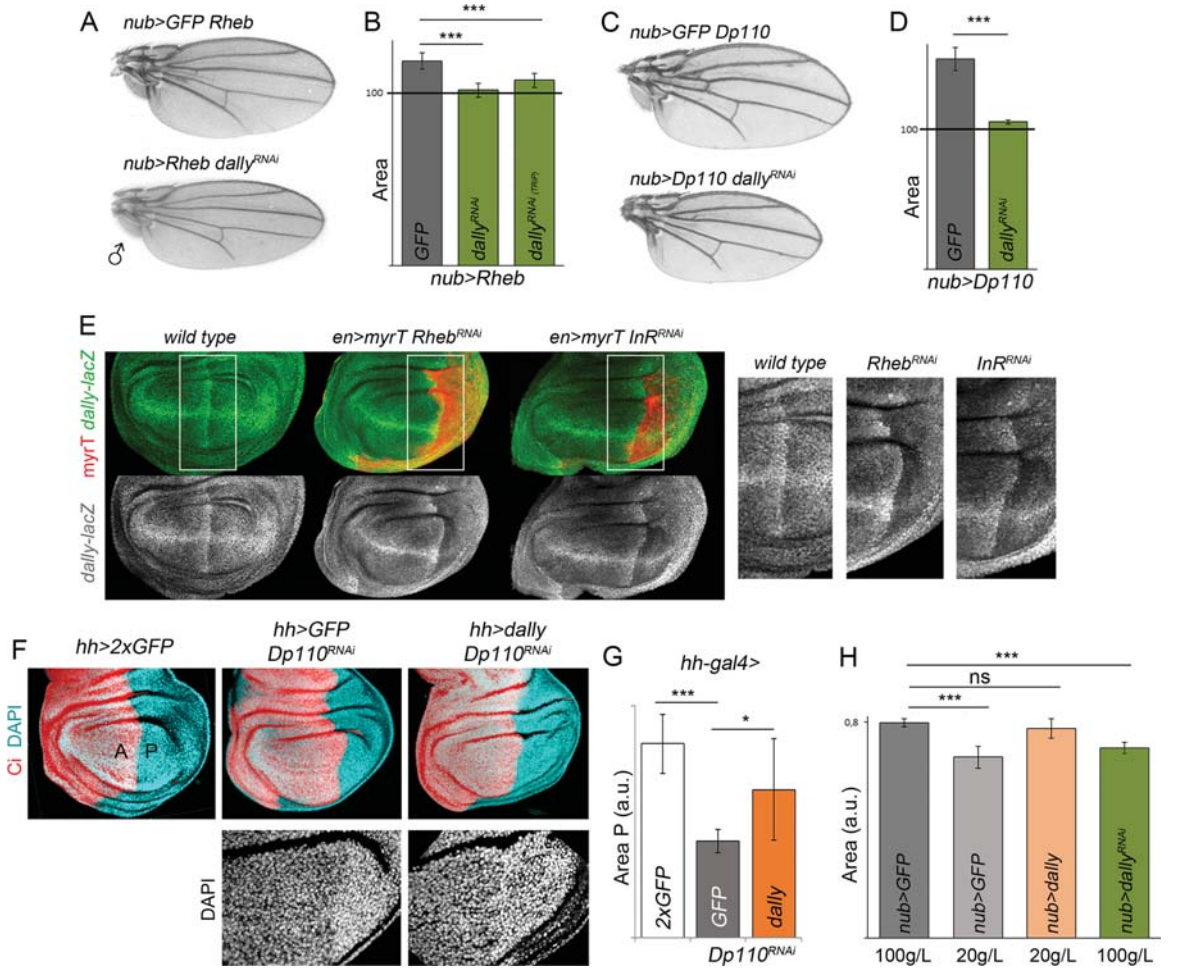

Fig 7. Dally acts as a bridge between nutrient sensing and wing scaling. (A–D) Cuticle preparations (A, C) and histograms plotting tissue size normalized as a percent of the control wings (B, D) of *nub>Rheb* (A, B) or *nub>Dp110* (C, D) adult wings coexpressing either *GFP* or *dally*^{RNAi}. Two independent RNA interference (RNAi) lines were used in B. Error bars show the standard deviation. Number of wings analyzed per genotype $\geq$ 10. ***$p < 0.001$. (E) Representative wing discs of the indicated genotypes labeled to visualize *dally-lacZ* (antibody to β-Gal, green or white) and myrT expression (in red) to mark the transgene-expressing domain. Higher magnification pictures of the squared regions are shown on the right side. Note the reduced expression of *dally-lacZ* upon depletion of the TSC/TOR or PTEN/PI3K pathways. (F) Representative wing discs of the indicated genotypes and labeled to visualize Ci (red) and DAPI (in blue). Ci labels the anterior compartment. A, anterior compartment; P, posterior compartment. (G) Histogram plotting the P/A size ratio of wing discs of the indicated genotypes. Error bars show the standard deviation. Number of wing discs analyzed per genotype $\geq$ 10. ***$p < 0.001$. P/A ratios: hh>2XGFP = 0.55 ± 0.02; hh>GFP, Dp110-RNAi = 0.29 ± 0.06; hh>dally, Dp110-RNAi = 0.42 ± 0.07. (H) Histogram plotting absolute size in a.u. of adult wings of the indicated genotypes. Quantification was made in well-fed (100 g/L yeast food) and starved (20 g/L yeast food) animals. Error bars show the standard deviation. Number of wings analyzed per genotype $\geq$ 10. ***$p < 0.001$. ns, not significant.

doi:10.1371/journal.pbio.1002239.g007

of cells, induces a nonautonomous reduction in tissue size of adjacent cell populations. This nonautonomous effect is a consequence of a reduction in both cell size and proliferation rates (cell number), and it is not a consequence of programmed cell death or the withdrawal of nutrients from neighboring tissues, as reducing the levels of proapoptotic genes or subjecting larvae

to different amino-acid diets does not have any impact on the size reduction of neighboring cell populations. We show that the glypican Dally, which plays a major role in regulating the spread of Dpp in *Drosophila* tissues [49–52,59], is up-regulated upon deregulation of these tumor suppressor pathways and that the increase in Dally expression levels contributes to the autonomous effects on tissue size and to the nonautonomous reduction in cell number. Whereas the autonomous effects on tissue size caused by deregulation of these tumor suppressor pathways are most probably due, as least in part (see below), to the capacity of Dally to facilitate Dpp spreading throughout the tissue, we propose that the nonautonomous effects on cell number are a consequence of withdrawal of Dpp from neighboring tissues (Fig 8A). This proposal is based on a number of observations. First, the width of the Dpp activity gradient as well as the total amount of Dpp activity was reduced in adjacent cell populations upon targeted depletion of tumor suppressor pathways. Second, the nonautonomous effects on tissue size were fully rescued by Dally depletion, which has a rather specific role on the spread of Dpp when overexpressed. Third, the nonautonomous effects on tissue size, growth and proliferation rates, and/or Dpp availability and signaling can be phenocopied by overexpression of Dally or the Dpp receptor Tkv. We observed different strengths of the autonomous and nonautonomous effects upon deregulation of these tumor suppressor pathways or overexpression of Dally in either the A or P compartments (Fig 1 and Fig 6). Despite the mild autonomous induction of tissue growth caused by the *ci-gal4* driver in A cells, it caused a relatively strong nonautonomous reduction of the neighboring compartment. On the contrary, the *en-gal4* driver caused a strong autonomous induction of tissue growth in P cells but a relatively weak nonautonomous reduction of the neighboring compartment. The differential autonomous response might simply reflect different strengths of these Gal4 drivers. By contrast, the strongest nonautonomous effects caused by the *ci-gal4* driver (when compared to the *en-gal4* driver) might be because Dpp expression is restricted to the A compartment and increased levels of Dally in Dpp expressing cells are more efficient at titrating out the levels of this growth factor from the neighboring compartment. We noticed that the nonautonomous effects on cell size observed upon deregulation of the PI3K/PTEN, TSC/TOR, or hippo/Yorkie pathways are Dally independent, as overexpression of Dally did not cause a nonautonomous reduction in cell size. Moreover, depletion of Dally did not rescue the nonautonomous reduction in cell size caused by activation of these pathways. These results are consistent with the fact that changes in Dpp signaling do not cause any effect on cell size (S3 Fig, see also [60]) and indicate that Dally and Dpp are regulating cell number but not cell size. Somatic mutations in tumor suppressor genes such as PTEN or TSC are frequently accumulated in early events of tumor development, and these mutations are thought to contribute to the selection of tumorigenic cells. Competition for available growth factors, by modulating the levels of glypicans, such as Dally, might contribute to the outcompetition of wild-type cells and to the selection of malignant mutation-carrying cells in human cancer.

The PI3K/PTEN and TSC/TOR signaling pathways play a role not only in disease but also during normal development. These two pathways modulate the final size of the developing organism according to nutrient availability. Our results also identify, in this context, Dally as a molecular bridge between nutrient sensing and wing scaling in *Drosophila* (Fig 8B). In a condition of high nutrient availability, which leads to the activation of the nutrient-sensing PI3K/PTEN and TSC/TOR pathways, increased levels of Dally facilitate the spread of Dpp throughout the growing tissue and contribute to the generation of larger but well-proportioned and scaled adult structures. Depletion of Dally expression levels rescues the tissue growth caused by high levels of nutrients or activation of the nutrient-sensing pathways and gives rise to smaller and, again, well-proportioned and scaled adult structures. Of remarkable interest is the capacity of Dally to induce tissue overgrowth when overexpressed or to mediate tissue growth upon

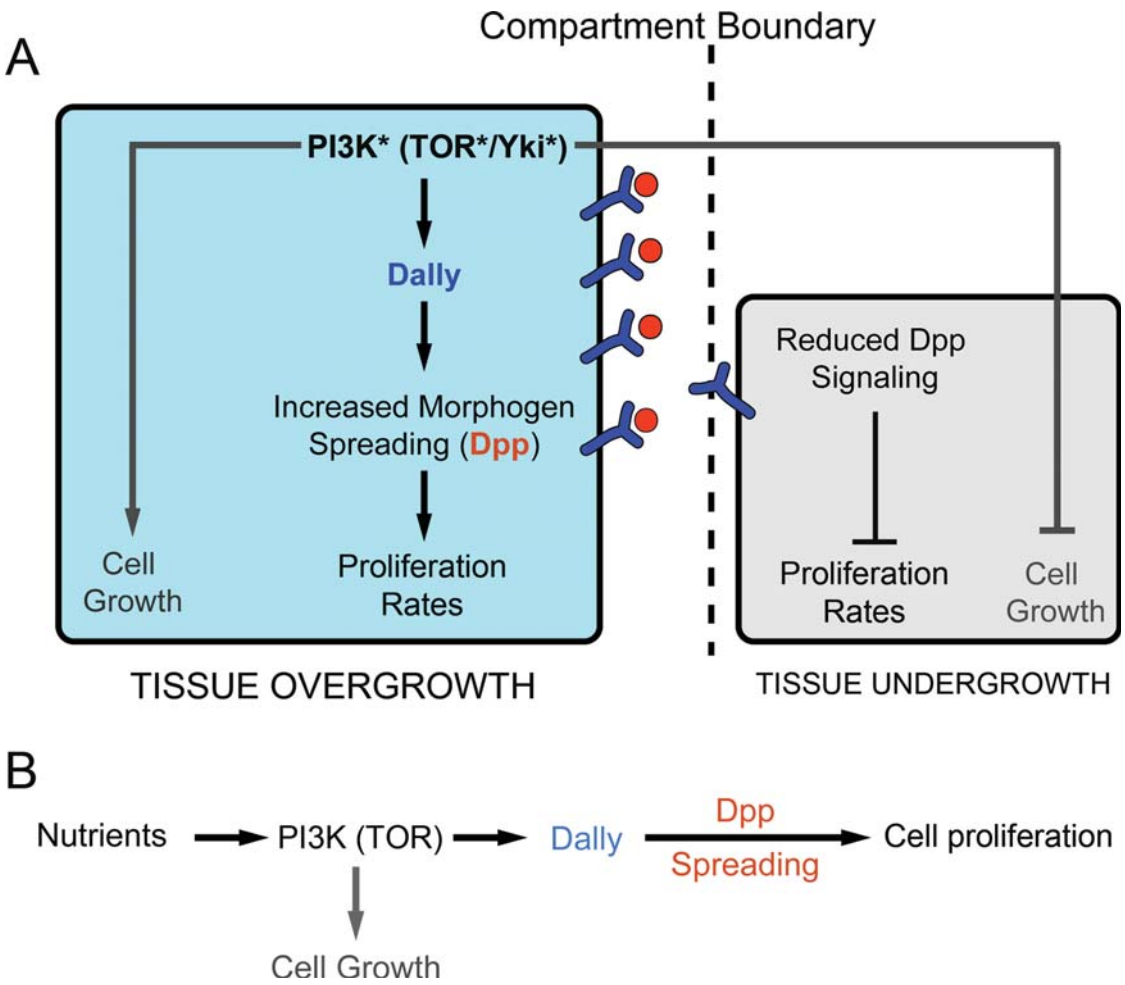

Fig 8. A role of Dally in tissue growth. (A) Activation of the PI3K/PTEN, TSC/TOR, or Yorkie pathways in a defined cell population (in blue) increases cell and/or tissue size in an autonomous manner and induces a nonautonomous reduction in both cell size and number in neighboring cell populations (in grey). Whereas the autonomous and nonautonomous effects on tissue size are mediated by Dally, the effects on cell size are Dally independent. The nonautonomous reduction in tissue size is a consequence of reduced Dpp signaling, most probably reflecting increased number of Dpp molecules bound to the overgrowing (Dally overexpressing) tissue and a consequent reduction in the number of available Dpp molecules to the neighboring cell population. (B) Within the feeding animal, the PI3K/PTEN and TSC/TOR pathways sense nutrient conditions and modulate both cell and tissue size. Whereas the effects on tissue size are mediated by the glypican Dally, which modulates the spreading of the Dpp morphogen throughout the tissue, the effects on cell size are Dally independent.

doi:10.1371/journal.pbio.1002239.g008

deregulation of the PI3K/PTEN, TSC/TOR, or hippo/Yorkie pathways. Interestingly, deregulation of these pathways, and the resulting tissue overgrowth, leads to the expansion of the Dpp gradient without affecting the total levels of Dpp signaling. These results imply that Dpp activity levels do not play an instructive role in promoting tissue growth but rather that it is the range of the Dpp gradient that regulates final tissue size. Consistent with this proposal, depletion of Dally levels in one compartment (which might lead to increased levels of available Dpp

in the neighboring cell population) does not cause any visible nonautonomous effect in tissue size (S2 Fig). These results are reminiscent of the capacity of Dpp to restrict its own spreading through the repression of Pentagone, a diffusible protein that interacts with Dally and contributes to the expansion of the Dpp gradient [45,46,61]. The graded distribution of Dpp leads, via the interaction with its receptor complex, to the graded activation of Mad/Medea, which in turn represses the transcription of *brinker* (*brk*, reviewed in [42]). This creates a gradient of Brk expression that is reciprocal to the Dpp gradient. Brk is a transcriptional repressor that acts negatively to establish, in a dose-dependent manner, the expression domain of Dpp target genes like *spalt* [62–64]. Thus, Dpp regulates the expression of target genes by repressing *brinker*. Remarkably, the reduced size of the wing primordium observed in hypomorphic alleles of *dpp* is restored when combined with *brk* mutants [65]. This experimental evidence indicates that Dpp controls wing growth entirely via repression of *brk*. The Dally-mediated increase in the width of the Dpp gradient observed upon deregulation of the PI3K/PTEN, TSC/TOR, or hippo/Yorkie pathways might contribute to restrict the expression domain of *brk* to the lateral sides of the wing primordium. Similarly, the nonautonomous decrease in the width of the Dpp gradient might cause an expansion of the *brk* domain, which is known to repress growth. Interestingly, Dally-mediated spreading of other secreted growth factors might also contribute to the autonomous effects on tissue growth caused by deregulation of the PI3K/PTEN, TSC/TOR, or hippo/Yorkie pathways. This is revealed by the fact that Dally depletion rescues both the autonomous and the nonautonomous effects (Fig 6), whereas deregulation of these pathways are still able to induce some growth upon knocking down Dpp (Fig 4O).

Compartments have been proposed to be units of growth control [66]. In other words, the size of each compartment is controlled independently. Our results on the lack of nonautonomous effects on tissue growth upon depletion of Dally or Sfl, the enzyme needed for the modification of HS chains within glypicans, indicate that this is the case. Targeted depletion of glypican expression or activity in the developing compartments gave rise to an autonomous reduction in tissue size without affecting the neighboring compartment (S2 Fig). However, independent lines of evidence support the view that adjacent compartments buffer local variations in tissue growth caused by different means, including a nonautonomous reduction in tissue size upon depletion of the protein biosynthetic machinery [37] or reduced epidermal growth factor receptor (EGFR) activity [67]. Our results on the capacity of overgrowing compartments to withdraw Dpp from neighboring tissues upon targeted deregulation of the PI3K/PTEN, TSC/TOR, or hippo/Yorkie pathways and to cause a nonautonomous reduction in growth and proliferation rates reinforce the view that compartments are susceptible to modulate their growth rates upon different types of stress, including depletion of tumor suppressor genes. Interestingly, the halteres and wings of *Drosophila* are homologous thoracic appendages, and the activity of the *Ultrabithorax* (*Ubx*) *Hox* gene in the haltere discs contributes to defining its reduced size. Remarkably, it does so by reducing the expression levels of *Dally* [68–71], thus reinforcing the role of Dally in modulating tissue growth in epithelial organs.

Materials and Methods

Drosophila Strains

The *Drosophila* strains used were *UAS–PTEN*^{RNAi} (ID 101475, VDRC); *UAS-Rheb*^{RNAi} (HMS00923, TRiP); *UAS-dally*^{RNAi} (ID 14136, VDRC and HMS00905, TRiP); *UAS-dlp*^{RNAi} (ID 100268, VDRC; HMS00875, TRiP and HMS00903, TRiP); *UAS-sulfateless*^{RNAi} (ID 5070, VDRC and HMS00543, TRiP); *UAS-dpp*^{RNAi} (JF01371, TRiP); *UAS-InR*^{RNAi} (ID 992, VDRC); *UAS-Dp110*^{RNAi} (ID 38985, VDRC); *dally-YFP* (115511, DGRC); *tkv-YFP* (115298, DGRC); *tkv-lacZ* (*P(lacZ)tkv*^{k16713}, Bloomington), *UAS-dally* and *dally-lacZ* (*P(lacZ)dally*^{06464}, [50], kind gifts

from E. Sánchez-Herrero); *UAS-dp53*^{ct} (a dominant negative version of Dp53, [72]); *Df(3L)H99* (a deficiency that covers the pro-apoptotic genes *hid*, *grim*, and *reaper*, [35]); *sal*^{PE}*-Gal4* [47]; *dpp-lacZ* [73]. *en-gal4*, *ci-gal4*, *nub-gal4*, *UAS-dlp*, *UAS-cyclin-E* and *UAS-string* (kind gifts from B. Edgar), *UAS-tkv* and *UAS-tkv*^{DN} (a dominant negative version of tkv that lacked the cytoplasmic kinase domain necessary for signal transduction [58]), *UAS–yki* (a kind gift from S. Cohen), *UAS–Dp110/PI3K* and *UAS-Rheb* are described in Flybase.

Immunohistochemistry

The antibodies used were rabbit anti-Spalt (a kind gift from R. Barrio, [47]), rabbit anti-pMAD (a kind gift from G. Morata), rabbit anti–phosphorylated histone 3 (PH3) (Cell Signaling), rabbit anti-βgal (Cappel), rat anti-Ci (2A1, DSHB), and mouse anti-Dally-like (13G8, DSHB). Secondary antibodies were obtained from Molecular Probes. TUNEL analysis was performed as described in [74].

Quantification of Tissue and Cell Size in Adult Wings

The sizes of the wing and of the A and P compartments were measured using Image J Software (NIH, United States). Cell density was measured as the number of hairs (each wing cell differentiates a hair) per defined area. Two conserved regions between veins L4 and L5 (P compartment) and veins L2 and L3 (A compartment) were used to measure cell densities. The final area and cell density values were normalized as a percent of the control values of GFP expressing samples under the corresponding Gal4-drivers. At least ten adult wings per genotype were scored. Only adult males were scored. The average values and the corresponding standard deviation were calculated, and a *t*-test analysis was carried out. The average values, the corresponding standard deviations, and the corresponding *p*-values are included in S1 Data.

Quantification of Tissue Growth in Developing Wing Discs

Hatched first instar larvae were sorted from egg laying plates (egg laying period of 4 h at 25°C), transferred to fresh tubes, allowed to growth at 25°C, and dissected at three time points of development (72 h, 96 h and 140 h). The size of the A and P compartments in the wing primordia was measured using Fiji Software (NIH, US). At least ten wing discs per genotype and per time point were scored. The corresponding standard deviation was calculated, and a *t*-test analysis was carried out. The average values, the corresponding standard deviations, and the corresponding *p*-values are included in S1 Data.

Proliferation and Growth Rate Measurements by Clonal Analysis

Early third instar (72 h AEL) larvae of the following genotypes: (1) *hs-FLP*, *ubi-nls-RFP*, *FRT19A/FRT19A*; *ci-gal4*, *UAS-GFP/+*, (2) *hs-FLP*, *ubi-nls-RFP*, *FRT19A/FRT19A*; *ci-gal4*, *UAS-GFP/UAS-Dp110*, and (3) *hs-FLP*, *ubi-nls-RFP*, *FRT19A/FRT19A*; *ci-gal4*, *UAS-GFP/UAS-Dally*, were heat-shocked at 38°C for 1 h and then transferred to 25°C. Wing discs were dissected 72 h after clone induction. The size of clones, visualized by the absence of RFP expression, was quantified from confocal images with ImageJ software (NIH, US). Wing discs were also labelled with DAPI to quantify cell number. At least 30 clones were quantified. Average values and the corresponding standard deviations were calculated, and a *t*-test analysis was carried out. Clones in the three different genotypes were induced and dissected in parallel, and the same control wing discs (genotype nr 1) were used in Figs 2 and 5. The average values, the corresponding standard deviations, and the corresponding *p*-values are included in S1 Data.

Flow Cytometry Analysis

Wing imaginal discs of each genotype were dissected in cold PBS, dissociated with trypsin-EDTA at 32°C for 45 min, and fixed with 4% formaldehyde for 20 min. Cells were centrifuged at 2,000 rpm for 2 min, resuspended in 1 ml of 70% ethanol, and incubated for 1 h at room temperature (RT). After centrifugation, the pellet was resuspended in PBS with DAPI 1 mg/ml and RNase 100 mg/ml and incubated for 1 h at RT. DAPI fluorescence was determined by flow cytometry using a FacsAria I SORP sorter (Beckton Dickinson, San Jose, California). Excitation with the blue line of the laser (488 nm) permits the acquisition of scatter parameters. Blue laser (488 nm) was used for GFP excitation, and a UV laser (350 nm) for DAPI excitation. Doublets were discriminated using an integral/peak dot plot of DAPI fluorescence. Cell cycle histograms were obtained on each sample according to the GFP fluorescence, and cell cycle analysis was done on DAPI fluorescence collected at 440 nm. DNA analysis on single fluorescence histograms was done using Summit software (Dako Colorado).

pMAD Expression Profile

In order to obtain the pMAD expression profile at the same developmental stage in all genotypes analyzed, larvae were fed with food complemented with bromophenol blue (0,2 g in 100 ml of fly food), as described in [75], and wandering larvae with empty (white) gut, corresponding to 1–6 h before the entry into pupal stage, were used to dissect the wing discs. As previously described in [45], all wing discs from a dataset (GFP control and experimental discs) were fixed and stained together to avoid variability between discs and mounted on the same slide to reduce potential variation in thickness between the slide and the coverslip across different samples. All discs from a dataset were imaged under identical settings using a Leica SP2 confocal microscope (0.36 μm of step size). Confocal conditions were adjusted to avoid saturated pixels with maximal intensity. After image acquisition, four consecutive slices (above and below the brightest slice from each stack) were manually selected by visual inspection, and a mean projection of these nine slices was subsequently performed. Using a reduced number of slices and performing the mean projection allowed us to reduce the noise as well as to avoid the signal from the peripodial membrane. Indeed, we made sure that these nine slices contained signal from the columnar cells of the pouch only. All discs were rotated to have anterior to the left and dorsal upwards orientation. The remaining analyses were applied solely to the wing pouch. We extracted the profiles along the anterior–posterior (AP) axis parallel to the dorsal-ventral (DV) boundary in four different offsets (two in the dorsal compartment and two in the ventral one). The positioning of the AP boundary was scored by the GFP expression driven by the *gal4* line. Data are included in S1 Data. To quantify total pMAD signaling of a particular region of interest (A or P compartments or the whole wing pouch), signal intensities per pixel were first collected from raw images taken with the same laser confocal conditions using the histogram function of Fiji Software (NIH, US). Confocal conditions were adjusted to avoid saturated pixels with maximal intensity. Total pMAD signaling per region of interest was quantified as the sum of all pixel intensities. All wing discs from a dataset (GFP control and experimental discs) were fixed and stained together. All of the image processing and data extraction were performed using Fiji Software (NIH, USA). At least five discs per genotype were analyzed. The average values, the corresponding standard deviations, and the corresponding *p*-values are included in S1 Data.

Fly Food with Varying Concentrations of Yeast

We adapted the food recipe described in [76]. The following recipes were used to vary the concentration of yeast: (A) 100 g/L yeast food: 1 liter of standard fly medium contains 100 g of

fresh yeast, 100 g of sucrose, 27 g bacto agar, 3 mL of propionic acid, and 30 mL of nipagin; and (B) 20 g/L yeast food (starvation): it was generated by reducing the amount of fresh yeast without altering the other ingredients.

Hatched first instar larvae were sorted from egg laying plates (egg laying period of 8 h at 25°C), transferred to tubes with the different yeast concentration foods and allowed to grow at 25°C to adulthood. Control animals were analyzed in parallel in each experimental condition.

Statistical Analyses

In all quantifications, the Student's *t*-test (two-tailed) was used to test for significance. Significance is indicated in the figures using the following symbols: $^{*}p < 0.05$, $^{**}p < 0.01$, $^{***}p < 0.001$. Error bars represent either the standard deviation (in the case of tissue size and cell density measurements) or the standard error to the mean (in the case of quantification of mitotic figures, apoptotic cells, and pMAD signal intensity).

Supporting Information

S1 Data. Quantitative measurements with their corresponding standard deviations of tissue size and/or cell density values in adult wings (Figs 1–3, Figs 5–7, and S1–S4 Figs) or wing imaginal discs (Fig 4 and Fig 7), clonal area and number of cells per clone (Fig 2 and Fig 5), number of apoptotic cells (Fig 3 and S1 Fig), pMAD intensity (Fig 4, Fig 5, and S2 Fig), and mitotic figures (S1 Fig) of individuals expressing the indicated transgenes under the control of the corresponding Gal4 drivers. A *t*-test was carried out to calculate the *p*-value as a measurement of the statistical significance. Data are ordered with respect to the corresponding main or supplementary figures. Further tabs present the underlying numerical data used to generate the pMAD profiles shown in Figs 4E, 4F, 4H, 4I, 4L, and 5J and S2A, S2J, S2K and S4C Figs.
(XLSX)

S1 Fig. Nonautonomous effects on tissue size upon targeted activation of PI3K/PTEN and TSC/TOR pathways. (A) Cuticle preparations of male adult wings expressing *GFP* or $PTEN^{R\text{-}NAi}$ under the control of the *hh-gal4* driver. The blue line marks the boundary between the anterior (A) and posterior (P) compartments. (B–D) Histograms plotting tissue size of the whole wing (B) and tissue size and cell density of A (white bars) and P (blue bars) compartments (C, D) of adult wings expressing the indicated transgenes in the *hh* domain normalized as a percent of the control wings. Note a consistent reduction in tissue size of the adjacent cell populations (white bars). Error bars indicate the standard deviation. Number of wings analyzed per genotype ≥ 10. $^{***}p < 0.001$. (E, F) *ci>GFP*, *CycE*, *string* wing imaginal discs labelled with TUNEL to visualize apoptotic cells (in red, E) or with an antibody against phosphorylated histone 3 (PH3, in magenta or white) to visualize mitotic cells (F). The *ci* domain is labelled with GFP (in green). (G, H) DNA-content profile of FACS-sorted GFP-expressing and nonexpressing cells dissociated from *ci>GFP* and *ci>GFP*, *Dp110* wing imaginal discs. Percentage of cells in G1, G2, and S is indicated. (I) Histogram plotting the quantification of mitotic figures per area in the A (grey bars) and P (blue bars) compartments of the indicated genotypes. Error bars indicate the standard deviation. Number of wing discs analyzed per genotype ≥ 10. $^{***}p < 0.001$; $^{**}p < 0.01$; $^{*}p < 0.05$. (J) Histogram plotting the quantification of the absolute number of TUNEL-positive cells in the P (light green bars) and A (grey bars) compartments of the indicated genotypes. Error bars indicate the standard deviation. Number of wing discs analyzed per genotype ≥ 10. $^{***}p < 0.001$.
(TIF)

S2 Fig. Glypicans and tissue growth. (A) Average pMAD profile of wing discs expressing *GFP* (red line) or *GFP* and the corresponding transgenes (blue line) under the control of the *en-gal4* driver. Profiles were taken along the AP axis and plotted in absolute positions. The standard error to the mean is shown in the corresponding color for each genotype. The AP boundary of both experiments was aligned to allow comparison of the profile in each compartment. Number of wing discs analyzed per genotype ≥ 5. The domains of transgene expression are marked with a black asterisk. Arrows mark the limits of the Dpp activity gradients. (A') Histograms plotting the total intensity of pMAD signal in a.u. of the posterior (blue bars) and anterior (white bars) compartments of *en>2xGFP* and *en>GFP*, $PTEN^{RNAi}$ wing discs. Error bars indicate the standard error to the mean. Number of wing discs analyzed per genotype ≥ 5. $^{*}p < 0.05$ (B) Wing imaginal discs of the indicated genotypes labelled to visualize Dally expression. Expression of Dally was analyzed in flies carrying *a Dally-YFP* reporter. Red brackets indicate the domain of transgene (*myrT* or $PTEN^{RNAi}$) expression. High magnification of the squared region is shown in the right panel. (C–H) On the left, cuticle preparations of adult wings of the indicated genotypes. On the right, histograms plotting tissue size (C–H) and cell density (C, D) values of the transgene-expressing compartment (blue bars) and adjacent compartment (white bars), normalized as a percent of the control wings. Error bars show the standard deviation. Number of wings analyzed per genotype ≥ 10. $^{***}p < 0.001$; $^{**}p < 0.01$; $^{*}p < 0.05$. The blue line marks the boundary between the A and P compartments, and the domains of transgene expression are marked with a blue asterisk. (I) Wing imaginal disc of the indicated genotype labelled to visualize Dally-like (in red or white) and GFP (in green) protein expression. (J) Average pMAD profiles of wing discs expressing *GFP* and Dp110 (blue line) or *GFP*, a dsRNA form against *Dally* and *Dp110* (green line) under the control of the *ci-gal4* driver. Profiles were taken along the AP axis and plotted in absolute positions. The standard error to the mean is shown in the corresponding color for each genotype. The AP boundary of both experiments was aligned to allow comparison of the profile in each compartment. Number of wing discs analyzed per genotype ≥ 5. The domains of transgene expression are marked with a black asterisk. Arrows mark the limits of the Dpp activity gradients. (J') Histograms plotting the total intensity of pMAD signal in a.u. of the anterior (blue bars) and posterior (white bars) compartments of *ci>GFP*, *Dp110* and *ci>Dp110*, *Dally-RNAi* wing discs. Error bars indicate the standard error to the mean. Number of wing discs analyzed per genotype ≥ 5. (K) Wing imaginal discs (left panels) of *ci>GFP* and *ci>dally* ^{RNAi} larvae labelled to visualize pMAD protein (in white) and average pMAD profiles (right panels) of wing discs expressing *GFP* (red line) or *dally* ^{RNAi} (green line) in the *ci* domain. Profiles were taken along the AP axis and plotted in absolute positions. The standard error to the mean is shown in the corresponding color for each genotype. The AP boundary of both experiments was aligned to allow comparison of the profile in each compartment. Number of wing discs analyzed per genotype ≥ 7. The domains of transgene expression are marked with a black asterisk. Arrows mark the limits of the Dpp activity gradients.
(TIF)

S3 Fig. Thickveins and tissue growth. (A, B) Wing imaginal discs of the indicated genotypes labelled to visualize *thickveins* expression. Expression of *thickveins* was analyzed in flies carrying *tkv-lacZ* (A) or *tkv-YFP* (B) reporters. Red brackets indicate the domain of transgene (*myrT* or $PTEN^{RNAi}$) expression. (C, D) On the left, cuticle preparations of adult wings of the indicated genotypes. On the right, histograms plotting tissue size (C,D) and cell density (D) values of the transgene-expressing compartment (blue bars) and of the adjacent compartment (white bars), normalized as a percent of the control wings. Error bars show the standard deviation. Number of wings analyzed per genotype ≥ 10. $^{***}p < 0.001$; $^{**}p < 0.01$; $^{*}p < 0.05$. The

blue line marks the boundary between the anterior (A) and posterior (P) compartments, and the domains of transgene expression are marked with a blue asterisk.
(TIF)

S4 Fig. Regulation of Dally by the PI3K and TOR pathways. (A) Wing imaginal discs of the indicated genotypes labelled to visualize Dally expression (in red or white) and DAPI (in blue to visualize nuclei). The transgene-expressing domain is labelled with GFP (in green). Expression of Dally was analyzed in flies carrying *a Dally-lacZ* reporter. (B) Histogram plotting tissue size and cell density values normalized as a percent of the control (*nub>GFP*) of $nub>Rheb^{R\text{-}NAi}$ adult wings coexpressing either *GFP* or *Dally*. Error bars show the standard deviation. Number of wings analyzed per genotype ≥ 10. $^{*}p < 0.05$. (C) Wing imaginal discs (left panels) of *nub>GFP* and *nub>dally* larvae labelled to visualize pMAD protein (in red) and average pMAD profiles (right panels) of wing discs expressing *GFP* (red line) or *Dally* (blue line) in the *nubbin* domain. Profiles were taken along the AP axis and plotted in absolute positions. The standard error to the mean is shown in the corresponding color for each genotype. The AP boundary of both experiments was aligned to allow comparison of the profile in each compartment. Number of wing discs analyzed per genotype ≥ 7. Arrows mark the limits of the Dpp activity gradients.
(TIF)

Acknowledgments

We thank R. Barrio, S. Cohen, B. Edgar, G. Morata, E. Sánchez-Herrero, the Bloomington Stock Center, the Developmental Studies Hybridoma Bank (DSHB), and the Vienna Drosophila RNAi Center (VDRC) for flies and reagents, T. Yates for text editing, and L. Boulan, L. Barrio, C. Recasens, and A. Terriente-Félix for comments on the manuscript.

Author Contributions

Conceived and designed the experiments: AF MM. Performed the experiments: AF. Analyzed the data: AF MM. Wrote the paper: MM.

References

1. Cully M, You H, Levine AJ, Mak TW. Beyond PTEN mutations: the PI3K pathway as an integrator of multiple inputs during tumorigenesis. Nat Rev Cancer. 2006; 6(3):184–92. PMID: 16453012
2. Mirantes C, Eritja N, Dosil MA, Santacana M, Pallares J, Gatius S, et al. An inducible knockout mouse to model the cell-autonomous role of PTEN in initiating endometrial, prostate and thyroid neoplasias. Dis Model Mech. 2013; 6(3):710–20. doi: 10.1242/dmm.011445 PMID: 23471917
3. Inoki K, Corradetti MN, Guan KL. Dysregulation of the TSC-mTOR pathway in human disease. Nat Genet. 2005; 37(1):19–24. PMID: 15624019
4. Kobayashi T, Minowa O, Sugitani Y, Takai S, Mitani H, Kobayashi E, et al. A germ-line Tsc1 mutation causes tumor development and embryonic lethality that are similar, but not identical to, those caused by Tsc2 mutation in mice. Proc Natl Acad Sci U S A. 2001; 98(15):8762–7. PMID: 11438694
5. Hariharan IK, Bilder D. Regulation of imaginal disc growth by tumor-suppressor genes in Drosophila. Annu Rev Genet. 2006; 40:335–61. PMID: 16872256
6. Hietakangas V, Cohen SM. Regulation of tissue growth through nutrient sensing. Annu Rev Genet. 2009; 43:389–410. doi: 10.1146/annurev-genet-102108-134815 PMID: 19694515
7. Pastor-Pareja JC, Xu T. Dissecting social cell biology and tumors using Drosophila genetics. Annu Rev Genet. 2013; 47:51–74. doi: 10.1146/annurev-genet-110711-155414 PMID: 23988119
8. Brumby AM, Richardson HE. Using Drosophila melanogaster to map human cancer pathways. Nat Rev Cancer. 2005; 5(8):626–39. PMID: 16034367
9. Morata G, Ripoll P. Minutes: mutants of drosophila autonomously affecting cell division rate. Dev Biol. 1975; 42(2):211–21. PMID: 1116643

10. Moreno E. Is cell competition relevant to cancer? Nat Rev Cancer. 2008; 8(2):141–7. doi: 10.1038/nrc2252 PMID: 18185517

11. Martins VC, Busch K, Juraeva D, Blum C, Ludwig C, Rasche V, et al. Cell competition is a tumour suppressor mechanism in the thymus. Nature. 2014; 509(7501):465–70. doi: 10.1038/nature13317 PMID: 24828041

12. Nowak K, Seisenbacher G, Hafen E, Stocker H. Nutrient restriction enhances the proliferative potential of cells lacking the tumor suppressor PTEN in mitotic tissues. Elife. 2013; 2:e00380. doi: 10.7554/eLife.00380 PMID: 23853709

13. Kalaany NY, Sabatini DM. Tumours with PI3K activation are resistant to dietary restriction. Nature. 2009; 458(7239):725–31. doi: 10.1038/nature07782 PMID: 19279572

14. Garcia-Bellido A, Ripoll P, Morata G. Developmental compartmentalisation of the wing disk of Drosophila. Nature: New biology. 1973; 245(147):251–3.

15. Neufeld TP. Body building: regulation of shape and size by PI3K/TOR signaling during development. Mech Dev. 2003; 120(11):1283–96. PMID: 14623438

16. Grewal SS. Insulin/TOR signaling in growth and homeostasis: a view from the fly world. Int J Biochem Cell Biol. 2009; 41(5):1006–10. doi: 10.1016/j.biocel.2008.10.010 PMID: 18992839

17. Restrepo S, Zartman JJ, Basler K. Coordination of patterning and growth by the morphogen DPP. Curr Biol. 2014; 24(6):R245–55. doi: 10.1016/j.cub.2014.01.055 PMID: 24650915

18. Wartlick O, Mumcu P, Julicher F, Gonzalez-Gaitan M. Understanding morphogenetic growth control—lessons from flies. Nat Rev Mol Cell Biol. 2011; 12(9):594–604. doi: 10.1038/nrm3169 PMID: 21850035

19. Goberdhan DC, Paricio N, Goodman EC, Mlodzik M, Wilson C. Drosophila tumor suppressor PTEN controls cell size and number by antagonizing the Chico/PI3-kinase signaling pathway. Genes Dev. 1999; 13(24):3244–58. PMID: 10617573

20. Ito N, Rubin GM. gigas, a Drosophila homolog of tuberous sclerosis gene product-2, regulates the cell cycle. Cell. 1999; 96(4):529–39. PMID: 10052455

21. Huang H, Potter CJ, Tao W, Li DM, Brogiolo W, Hafen E, et al. PTEN affects cell size, cell proliferation and apoptosis during Drosophila eye development. Development. 1999; 126(23):5365–72. PMID: 10556061

22. Gao X, Pan D. TSC1 and TSC2 tumor suppressors antagonize insulin signaling in cell growth. Genes Dev. 2001; 15(11):1383–92. PMID: 11390358

23. Tapon N, Ito N, Dickson BJ, Treisman JE, Hariharan IK. The Drosophila tuberous sclerosis complex gene homologs restrict cell growth and cell proliferation. Cell. 2001; 105(3):345–55. PMID: 11348591

24. Radimerski T, Montagne J, Hemmings-Mieszczak M, Thomas G. Lethality of Drosophila lacking TSC tumor suppressor function rescued by reducing dS6K signaling. Genes Dev. 2002; 16(20):2627–32. PMID: 12381661

25. Stocker H, Radimerski T, Schindelholz B, Wittwer F, Belawat P, Daram P, et al. Rheb is an essential regulator of S6K in controlling cell growth in Drosophila. Nat Cell Biol. 2003; 5(6):559–65. PMID: 12766775

26. Zhang Y, Gao X, Saucedo LJ, Ru B, Edgar BA, Pan D. Rheb is a direct target of the tuberous sclerosis tumour suppressor proteins. Nat Cell Biol. 2003; 5(6):578–81. PMID: 12771962

27. Saucedo LJ, Gao X, Chiarelli DA, Li L, Pan D, Edgar BA. Rheb promotes cell growth as a component of the insulin/TOR signalling network. Nat Cell Biol. 2003; 5(6):566–71. PMID: 12766776

28. Edgar BA, O'Farrell PH. The three postblastoderm cell cycles of Drosophila embryogenesis are regulated in G2 by string. Cell. 1990; 62(3):469–80. PMID: 2199063

29. Knoblich JA, Sauer K, Jones L, Richardson H, Saint R, Lehner CF. Cyclin E controls S phase progression and its down-regulation during Drosophila embryogenesis is required for the arrest of cell proliferation. Cell. 1994; 77(1):107–20. PMID: 8156587

30. Milan M, Campuzano S, Garcia-Bellido A. Cell cycling and patterned cell proliferation in the Drosophila wing during metamorphosis. Proc Natl Acad Sci U S A. 1996; 93(21):11687–92. PMID: 8876197

31. Neufeld TP, de la Cruz AF, Johnston LA, Edgar BA. Coordination of growth and cell division in the Drosophila wing. Cell. 1998; 93(7):1183–93. PMID: 9657151

32. Ng M, Diaz-Benjumea FJ, Vincent JP, Wu J, Cohen SM. Specification of the wing by localized expression of wingless protein. Nature. 1996; 381(6580):316–8. PMID: 8692268

33. Moreno E, Basler K, Morata G. Cells compete for decapentaplegic survival factor to prevent apoptosis in Drosophila wing development. Nature. 2002; 416(6882):755–9. PMID: 11961558

34. Milan M, Campuzano S, Garcia-Bellido A. Developmental parameters of cell death in the wing disc of Drosophila. Proc Natl Acad Sci U S A. 1997; 94(11):5691–6. PMID: 9159134

35. Steller H. Regulation of apoptosis in Drosophila. Cell Death Differ. 2008; 15(7):1132–8. doi: 10.1038/cdd.2008.50 PMID: 18437164

36. Levine AJ. p53, the cellular gatekeeper for growth and division. Cell. 1997; 88(3):323–31. PMID: 9039259

37. Mesquita D, Dekanty A, Milan M. A dp53-dependent mechanism involved in coordinating tissue growth in Drosophila. PLoS Biol. 2010; 8(12):e1000566. doi: 10.1371/journal.pbio.1000566 PMID: 21179433

38. Perez-Garijo A, Fuchs Y, Steller H. Apoptotic cells can induce non-autonomous apoptosis through the TNF pathway. Elife. 2013; 2:e01004. doi: 10.7554/eLife.01004 PMID: 24066226

39. Ryoo HD, Gorenc T, Steller H. Apoptotic cells can induce compensatory cell proliferation through the JNK and the Wingless signaling pathways. Dev Cell. 2004; 7(4):491–501. PMID: 15469838

40. Perez-Garijo A, Shlevkov E, Morata G. The role of Dpp and Wg in compensatory proliferation and in the formation of hyperplastic overgrowths caused by apoptotic cells in the Drosophila wing disc. Development. 2009; 136(7):1169–77. doi: 10.1242/dev.034017 PMID: 19244279

41. Hay BA, Wolff T, Rubin GM. Expression of baculovirus P35 prevents cell death in Drosophila. Development. 1994; 120(8):2121–9. PMID: 7925015

42. Affolter M, Basler K. The Decapentaplegic morphogen gradient: from pattern formation to growth regulation. Nat Rev Genet. 2007; 8(9):663–74. PMID: 17703237

43. Teleman AA, Cohen SM. Dpp gradient formation in the Drosophila wing imaginal disc. Cell. 2000; 103 (6):971–80. PMID: 11136981

44. Wartlick O, Mumcu P, Kicheva A, Bittig T, Seum C, Julicher F, et al. Dynamics of Dpp signaling and proliferation control. Science. 2011; 331(6021):1154–9. doi: 10.1126/science.1200037 PMID: 21385708

45. Hamaratoglu F, de Lachapelle AM, Pyrowolakis G, Bergmann S, Affolter M. Dpp signaling activity requires Pentagone to scale with tissue size in the growing Drosophila wing imaginal disc. PLoS Biol. 2011; 9(10):e1001182. doi: 10.1371/journal.pbio.1001182 PMID: 22039350

46. Ben-Zvi D, Pyrowolakis G, Barkai N, Shilo BZ. Expansion-repression mechanism for scaling the Dpp activation gradient in Drosophila wing imaginal discs. Curr Biol. 2011; 21(16):1391–6. doi: 10.1016/j.cub.2011.07.015 PMID: 21835621

47. Barrio R, de Celis JF. Regulation of spalt expression in the Drosophila wing blade in response to the Decapentaplegic signaling pathway. Proc Natl Acad Sci U S A. 2004; 101(16):6021–6. PMID: 15079076

48. Yan D, Lin X. Shaping morphogen gradients by proteoglycans. Cold Spring Harb Perspect Biol. 2009; 1 (3):a002493. doi: 10.1101/cshperspect.a002493 PMID: 20066107

49. Jackson SM, Nakato H, Sugiura M, Jannuzi A, Oakes R, Kaluza V, et al. dally, a Drosophila glypican, controls cellular responses to the TGF-beta-related morphogen, Dpp. Development. 1997; 124 (20):4113–20. PMID: 9374407

50. Nakato H, Futch TA, Selleck SB. The division abnormally delayed (dally) gene: a putative integral membrane proteoglycan required for cell division patterning during postembryonic development of the nervous system in Drosophila. Development. 1995; 121(11):3687–702. PMID: 8582281

51. Fujise M, Takeo S, Kamimura K, Matsuo T, Aigaki T, Izumi S, et al. Dally regulates Dpp morphogen gradient formation in the Drosophila wing. Development. 2003; 130(8):1515–22. PMID: 12620978

52. Khare N, Baumgartner S. Dally-like protein, a new Drosophila glypican with expression overlapping with wingless. Mech Dev. 2000; 99(1–2):199–202. PMID: 11091094

53. Lin X, Perrimon N. Dally cooperates with *Drosophila* Frizzled 2 to transduce Wingless signalling. Nature. 1999; 400(6741):281–4. PMID: 10421372

54. Harvey KF, Zhang X, Thomas DM. The Hippo pathway and human cancer. Nat Rev Cancer. 2013; 13 (4):246–57. doi: 10.1038/nrc3458 PMID: 23467301

55. Baena-Lopez LA, Rodriguez I, Baonza A. The tumor suppressor genes dachsous and fat modulate different signalling pathways by regulating dally and dally-like. Proc Natl Acad Sci U S A. 2008; 105 (28):9645–50. doi: 10.1073/pnas.0803747105 PMID: 18621676

56. Justice RW, Zilian O, Woods DF, Noll M, Bryant PJ. The Drosophila tumor suppressor gene warts encodes a homolog of human myotonic dystrophy kinase and is required for the control of cell shape and proliferation. Genes Dev. 1995; 9(5):534–46. PMID: 7698644

57. Lecuit T, Cohen SM. Dpp receptor levels contribute to shaping the Dpp morphogen gradient in the Drosophila wing imaginal disc. Development. 1998; 125(24):4901–7. PMID: 9811574

58. Kumar JP, Moses K. The EGF receptor and notch signaling pathways control the initiation of the morphogenetic furrow during Drosophila eye development. Development. 2001; 128(14):2689–97. PMID: 11526075

59. Belenkaya TY, Han C, Yan D, Opoka RJ, Khodoun M, Liu H, et al. Drosophila Dpp morphogen movement is independent of dynamin-mediated endocytosis but regulated by the glypican members of heparan sulfate proteoglycans. Cell. 2004; 119(2):231–44. PMID: 15479640

60. Martin-Castellanos C, Edgar BA. A characterization of the effects of Dpp signaling on cell growth and proliferation in the Drosophila wing. Development. 2002; 129(4):1003–13. PMID: 11861483

61. Vuilleumier R, Springhorn A, Patterson L, Koidl S, Hammerschmidt M, Affolter M, et al. Control of Dpp morphogen signalling by a secreted feedback regulator. Nat Cell Biol. 2010; 12(6):611–7. doi: 10.1038/ncb2064 PMID: 20453847

62. Minami M, Kinoshita N, Kamoshida Y, Tanimoto H, Tabata T. brinker is a target of Dpp in Drosophila that negatively regulates Dpp-dependent genes. Nature. 1999; 398(6724):242–6. PMID: 10094047

63. Campbell G, Tomlinson A. Transducing the Dpp morphogen gradient in the wing of Drosophila: regulation of Dpp targets by brinker. Cell. 1999; 96(4):553–62. PMID: 10052457

64. Jazwinska A, Kirov N, Wieschaus E, Roth S, Rushlow C. The Drosophila gene brinker reveals a novel mechanism of Dpp target gene regulation. Cell. 1999; 96(4):563–73. PMID: 10052458

65. Schwank G, Restrepo S, Basler K. Growth regulation by Dpp: an essential role for Brinker and a non-essential role for graded signaling levels. Development. 2008; 135(24):4003–13. doi: 10.1242/dev.025635 PMID: 19029041

66. Martin FA, Morata G. Compartments and the control of growth in the Drosophila wing imaginal disc. Development. 2006; 133(22):4421–6. PMID: 17035294

67. Garcia-Bellido A, Cortes F, Milan M. Cell interactions in the control of size in Drosophila wings. Proc Natl Acad Sci U S A. 1994; 91(21):10222–6. PMID: 7937866

68. de Navas LF, Garaulet DL, Sanchez-Herrero E. The ultrabithorax Hox gene of Drosophila controls haltere size by regulating the Dpp pathway. Development. 2006; 133(22):4495–506. PMID: 17050628

69. Crickmore MA, Mann RS. Hox control of organ size by regulation of morphogen production and mobility. Science. 2006; 313(5783):63–8. PMID: 16741075

70. Makhijani K, Kalyani C, Srividya T, Shashidhara LS. Modulation of Decapentaplegic gradient during haltere specification in Drosophila. Dev Biol. 2007; 302(1):243–55. PMID: 17045257

71. Crickmore MA, Mann RS. Hox control of morphogen mobility and organ development through regulation of glypican expression. Development. 2007; 134(2):327–34. PMID: 17166918

72. Brodsky MH, Nordstrom W, Tsang G, Kwan E, Rubin GM, Abrams JM. Drosophila p53 binds a damage response element at the reaper locus. Cell. 2000; 101(1):103–13. PMID: 10778860

73. Basler K, Struhl G. Compartment boundaries and the control of *Drosophila* limb pattern by *hedgehog* protein. Nature. 1994; 368(6468):208–14. PMID: 8145818

74. Milan M, Campuzano S, Garcia-Bellido A. Cell cycling and patterned cell proliferation in the wing primordium of Drosophila. Proc Natl Acad Sci U S A. 1996; 93(2):640–5. PMID: 8570608

75. Andres AJ, Thummel CS. Methods for quantitative analysis of transcription in larvae and prepupae. Methods in cell biology. 1994; 44:565–73. PMID: 7535884

76. Bass TM, Grandison RC, Wong R, Martinez P, Partridge L, Piper MD. Optimization of dietary restriction protocols in Drosophila. The journals of gerontology Series A, Biological sciences and medical sciences. 2007; 62(10):1071–81. PMID: 17921418

Publication 2

"Mei-P26 Mediates Tissue-Specific Responses to the Brat Tumor Suppressor and the dMyc Proto-Oncogene in *Drosophila*"

Mei-P26 Mediates Tissue-Specific Responses to the Brat Tumor Suppressor and the dMyc Proto-Oncogene in *Drosophila*

Ana Ferreira,*,[1] Laura Boulan,*,[1] Lidia Perez,* and Marco Milán*,†,[2]
*Institute for Research in Biomedicine (IRB Barcelona), 08028 Barcelona, Spain, and †Institució Catalana de Recerca i Estudis Avançats (ICREA), 08010 Barcelona, Spain

ABSTRACT TRIM-NHL proteins are a family of translational regulators that control cell growth, proliferation, and differentiation during development. *Drosophila* Brat and Mei-P26 TRIM-NHL proteins serve as tumor suppressors in stem cell lineages and have been proposed to exert this action, in part, via the repression of the protooncogene dMyc. Here we analyze the role of Brat, Mei-P26, and dMyc in regulating growth in *Drosophila* imaginal discs. As in stem cell lineages, Brat and Mei-P26 repress dMyc in epithelial cells by acting at the post-transcriptional and protein level, respectively. Analysis of cell and organ size unravel that Mei-P26 mediates tissue-specific responses to Brat and dMyc activities. Loss-of-function of *brat* and overexpression of dMyc induce overgrowth in stem cell lineages and eventually can participate in tumor formation. In contrast, an increase in Mei-P26 levels inhibits growth of epithelial cells in these two conditions. Upon depletion of Brat, Mei-P26 up-regulation prevents an increase in dMyc protein levels and leads to tissue undergrowth. This mechanism appears to be tissue-specific since Mei-P26 is not upregulated in brain tumors resulting from *brat* loss-of-function. Driving Mei-P26 expression in these tumors —mimicking the situation in epithelial cells— is sufficient to prevent dMyc accumulation, thus rescuing the overgrowth. Finally, we show that Mei-P26 upregulation mediates dMyc-induced apoptosis and limits dMyc growth potential in epithelial cells. These findings shed light on the tumor suppressor roles of TRIM-NHL proteins and underscore a new mechanism that maintains tissue homeostasis upon dMyc deregulation.

TRIM-NHL proteins, which are present in many animal species ranging from *Caenorhabditis elegans* to mammals, are characterized by the presence of a tripartite motif, namely RING, B-box, and coil-coiled domains, in their N terminal. The RING domain confers these proteins E3-ubiquitin ligase activity (Meroni and Diez-Roux 2005). In the C-terminal part, these proteins carry several repeats of a NHL domain (first identified in NCL-1, HT2A, and LIN-41 proteins; Slack and Ruvkun 1998), which mediate specific protein–protein interactions and translational inhibition (Sonoda and Wharton 2001; Loedige *et al.* 2013). The highly conserved structure of these proteins points to common biological functions, such as the regulation of asymmetric cell division or microRNA levels (Neumüller *et al.* 2008; Kohlmaier and Edgar 2008; Hammell *et al.* 2009; Loedige and Filipowicz 2009; Schwamborn *et al.* 2009). TRIM-NHL proteins have also been shown to act as translational inhibitors (Sonoda and Wharton 2001; Harris *et al.* 2011; Loedige *et al.* 2013). Of the four members present in *Drosophila*, Brat and Mei-P26 act as tumor suppressors in stem cell lineages, as mutations in these two proteins give rise to tumor formation in the brain and in the germline, respectively (Arama *et al.* 2000; Page *et al.* 2000).

During the cell division of larval neuroblasts, the asymmetric segregation of Brat promotes differentiation and inhibits cell growth and proliferation (Bello *et al.* 2006; Betschinger *et al.* 2006; Lee *et al.* 2006). Consequently, *brat* loss of function results in the malignant proliferation of a subset of neural progenitors at the expense of differentiated neurons (Bowman *et al.* 2008). Similarly, Mei-P26 activity in transit-amplifying cells in the female germline inhibits cell growth and proliferation and promotes differentiation (Neumüller *et al.* 2008). A recent study also unraveled a tumor suppressor function for TRIM3 in mammals (Liu *et al.* 2014), suggesting that this role might constitute a key feature of TRIM-NHL proteins. Studies

doi: 10.1534/genetics.114.167502
Manuscript received January 1, 2014; accepted for publication June 24, 2014; published Early Online July 1, 2014.
Supporting information is available online at http://www.genetics.org/lookup/suppl/doi:10.1534/genetics.114.167502/-/DC1.
[1]These authors contributed equally to this work.
[2]Corresponding author: Baldiri Reixac, 10-12, 08028 Barcelona, Spain. E-mail: marco.milan@irbbarcelona.org

in stem cell lineages have proposed that both Brat and Mei-P26 inhibit cell growth by repressing the protooncogene dMyc (Betschinger *et al.* 2006; Neumüller *et al.*, 2008). Interestingly, their closest mammalian ortholog, TRIM32, also prevents the self-renewal of mouse neural progenitors and induces neuronal differentiation by targeting c-Myc for degradation (Schwamborn *et al.* 2009).

The conserved transcription factor Myc is a key regulator of many biological activities (Gallant 2013). It also functions as an oncogene that contributes to the formation of many human cancers and thus constitutes a therapeutic target (Vita and Henriksson 2006; Dang 2012). As such, it has been extensively studied both in developmental and cancer biology. In *Drosophila*, dMyc promotes cell growth and ribosome biogenesis (Johnston *et al.* 1999; Grewal *et al.* 2005). In addition, as in mammalian tumors, dMyc overexpression also induces apoptosis through an unknown mechanism (Montero *et al.* 2008). This dual role of dMyc in triggering both cell growth and cell death has been proposed to be responsible for the maintenance of final tissue size (De La Cova *et al.* 2004).

The complex relationship between growth and differentiation in stem cell lineages makes it difficult to study the interaction between TRIM-NHL proteins and dMyc specifically and exclusively in growth control. We therefore addressed this question in a highly proliferating epithelial tissue, the wing primordium. The development of this tissue has the advantage that growth and differentiation are separated in time: growth takes place mainly during the juvenile period (larval stages), while differentiation is restricted to metamorphosis (Cohen 1993). Our results reveal that, unlike stem cell lineages, epithelial cells possess a tissue-specific mechanism based on the interaction between TRIM-NHL tumor suppressors and the dMyc protooncogene. Modifications of Mei-P26 levels appear to constitute a safety mechanism that helps to maintain tissue homeostasis upon *brat* loss of function and dMyc overexpression.

Materials and Methods

Drosophila strains

The *Drosophila* strains used in this study are as follows: *UAS-Mei-P26$^{\Delta NHL}$* (kind gift from S. M. Cohen) (Li *et al.* 2012); *UAS-dMyc^{42}* (Johnston *et al.* 1999); *bantam* sensor and control sensor (Brennecke *et al.* 2003); *UAS-brat^{RNAi}* and *UAS-mei-P26^{RNAi}* (ID nos. 105054 and 101060, Vienna *Drosophila* RNAi Center, Austria); and *brat^{192}*, *UAS-Brat*, and *UAS-Mei-P26* from the Bloomington Stock Center. Other stocks are described in FlyBase.

Immunohistochemistry and in situ hybridization

For the overexpression of Mei-P26, larvae were raised at 18° and exposed to 29° 18 h before dissection to potentiate the UAS-Gal4 system. To generate MARCM clones, a heat shock of 45 min at 37° was given during early second instar to the following genotypes: (1) *hs-FLP*; *FRT40A/tub-Gal80 FRT40A*; *tub-Gal4 UAS-GFP/+*; (2) *hs-FLP*; *brat^{192} FRT40A/tub-Gal80 FRT40A*; *tub-Gal4 UAS-GFP/+*; and (3) *hs-FLP*; *brat^{192} FRT40A/tub-Gal80 FRT40A*; *and UAS-Mei-P26/tub-Gal4 UAS-GFP*. Wing imaginal discs were dissected 72 h and 96 h after clone induction, and clones were marked by the presence of GFP.

For the generation of *brat* mutant clones in the wing disc, *hs-FLP*; *brat^{192}FRT40A /arm-lacZ FRT40A* larvae were grown at 25°, heat shocked for 60 min at 37° during early second instar, and dissected 72 h later. Mutant cells were marked by the absence of GFP expression and their twins by the expression of two copies of GFP.

Samples were dissected in ice-cold PBS and fixed for 20 min at room temperature in 4% formaldehyde. Rabbit anti-Brat (kindly provided by G. Morata), guinea pig anti-dMyc (Herranz *et al.* 2008), rabbit anti-Mei-P26 (Liu *et al.* 2009), rat anti-Elav (Hybridoma Bank), and rabbit anti-βGal (Cappel) were used. Secondary antibodies were obtained from Molecular Probes. TUNEL staining and *in situ* hybridizations were performed as previously described (Herranz *et al.* 2010).

Generation of the GFP-3′-UTR sensors

For the GFP-dMyc-3′-UTR sensor, the 3′-UTR of *dMyc* was amplified from genomic DNA by PCR with the following primers: dMyc-UTR-Fwd: 5′-CCTCGAGTGTTGTCTCATACTATCGGCTT-3′; dMyc-UTR-Rev: 5′-ATTTGCGGCCGCGTTTTTCCCTTCAGTT TCTTT-3′; digested with *Xho*I/*Not*I and cloned into the control sensor plasmid (P-Casper-tub-GFP) via the *Xho*I/*Not*I site.

For the GFP-Mei-P26-3′-UTR sensor, the 3′-UTR of *mei-P26* was amplified from genomic DNA by PCR with the following primers: mei-P26-UTR-Fwd: 5′-TCAGAATGCGGCCGCAGTCCT GAACACCCTCTATGTT-3′; mei-P26-UTR-Rev: 5′-CCGCTCG AGGTAACATGTAAAGTAGTCGTGTTTGTG-3′; digested with *Xho*I/*Not*I and cloned into the control sensor plasmid (P-Casper-tub-GFP) via the *Xho*I/*Not*I site.

Quantification of cell and tissue growth parameters in adult wings and wing discs

The size of the *nubbin (nub)*, *engrailed (en)*, and *cubitus interruptus (ci)* domains was measured using ImageJ software (National Institutes of Health). Cell density was measured as the number of hairs (each wing cell differentiates a hair) per defined area. The following areas were used to measure cell densities: a conserved region between veins L2 and L3 (*ci* domain) in the *ci-Gal4* experiments and a conserved region between veins L4 and L5 (*en* domain) in the *en-Gal4* and *nub-Gal4* experiments. At least 10 female adult wings per genotype were scored. A *T*-test analysis was performed.

Results

dMyc is repressed by Brat and Mei-P26 in epithelial cells

Brat acts as a translational inhibitor by binding to the 3′-UTR of target mRNAs (Sonoda and Wharton 2001) and

was shown to repress dMyc translation in neural progenitors (Betschinger *et al.* 2006). To analyze the post-transcriptional regulation of dMyc expression, we constructed a *dMyc-3′UTR* sensor transgene consisting of the *dMyc 3′UTR* cloned into a *tubulin*-promoter-EGFP reporter plasmid (*dMyc-3′UTR* sensor, Figure 1A). On one hand, targeted overexpression of Brat to specific territories within the developing wing primordium induced a clear reduction in GFP levels of the *dMyc-3′UTR* sensor (Figure 1B), while a *control* GFP sensor (Brennecke *et al.* 2003) remained unaffected (Supporting Information, Figure S1A). On the other hand, clones of cells mutant for a genetically null allele of *brat* ($brat^{192}$) displayed a cell-autonomous increase in GFP expression levels of the *dMyc-3′UTR* sensor (Figure 1C, red arrows). A similar de-repression of the sensor was obtained by targeted expression of a *dsRNA* form of *brat* ($brat^{RNAi}$, Figure 1D). These results imply a conserved role of Brat in the negative regulation of dMyc translation, in both neural progenitors and epithelial cells.

The vertebrate TRIM-NHL protein TRIM32 displays ubiquitin ligase activity and binds and targets c-Myc for degradation (Schwamborn *et al.* 2009). Similarly, the overexpression of Mei-P26, the *Drosophila* ortholog of TRIM32 (Page *et al.* 2000), strongly reduces dMyc protein levels in a proteasome-dependent manner ((Herranz *et al.* 2010) (see also Figure S2A). In contrast, overexpressing a form of Mei-P26 lacking the NHL domain, which mediates specific protein–protein interactions, did not affect dMyc levels (Figure S2B). Equivalent amounts of full-length Mei-P26 and the truncated version were found to be expressed with the GAL4/UAS system in the *Drosophila* ovary (Li *et al.* 2012). Thus, both the ubiquitin ligase activity (Herranz *et al.* 2010) and the NHL domain (this work) of Mei-P26 are required to target dMyc for degradation. These observations confirm that the overexpression of Brat or Mei-P26 also reduces dMyc levels in epithelial cells, acting at the mRNA and protein levels, respectively.

Brat depletion does not affect dMyc protein levels and does not cause tissue overgrowth

Consistent with the repression of the *dMyc-3′UTR* sensor upon Brat overexpression, dMyc protein levels were also diminished when compared to neighboring wild-type cells (Figure 1, E and F). By using two different Gal4 lines to overexpress Brat in specific territories of the wing, we found that increased Brat levels lead to smaller wings (Figure S1, B and C) as a result of a reduced cell size (Figure S1D). These findings, together with previous observations (Frank *et al.* 2002), show that Brat overexpression inhibits cell growth and represses dMyc expression.

Surprisingly, dMyc protein levels were unaffected in $brat^{192}$ mutant and in $brat^{RNAi}$-expressing cells (Figure 1, G and H), whereas the *dMyc-3′UTR* sensor was derepressed under the same experimental conditions (Figure 1, C and D). Moreover, targeted depletion of *brat* in specific territories of the wing primordium resulted in decreased cell and tissue size of the resulting adult structure (Figure 1, I–K). Thus, in contrast to what happens in neural progenitors, *brat* loss of function in epithelial cells has no effect on dMyc protein levels and causes tissue undergrowth. We next addressed the molecular bases mediating the tissue-specific activities of Brat.

Mei-P26 mediates tissue undergrowth and prevents dMyc up-regulation upon depletion of brat in epithelial cells

The observation that the *dMyc-3′UTR* sensor, but not dMyc protein, is up-regulated in epithelial cells in the absence of Brat suggests that dMyc is finely regulated at the protein level in this condition. Interestingly, we observed an increase in Mei-P26 protein levels in $brat^{192}$ mutant as well as in $brat^{RNAi}$-expressing cells when compared to the wild-type neighboring tissue (Figure 2, A and B). Moreover, the depletion of Brat led to increased *mei-P26* mRNA levels (Figure 2, C and C′).

Brat binds AGO1 (Neumüller *et al.* 2008), and several TRIM-NHL proteins regulate microRNAs (Neumüller *et al.* 2008; Hammell *et al.* 2009; Schwamborn *et al.* 2009). Since Mei-P26 is controlled by several miRNAs in the wing epithelium (Herranz *et al.* 2010), we addressed whether Brat modulates Mei-P26 levels by regulating microRNAs. We found no changes in mature miRNA levels (Figure S3A) or in the activity of the well-described growth-promoting miRNA *bantam* (Brennecke *et al.* 2003; Figure S3, B–D) upon *brat* depletion. These observations thus suggest that miRNAs do not mediate Brat functions in this tissue. Furthermore, depletion of *brat* did not affect a *GFP-mei-P26-3′UTR* sensor (Figure 2, D and F), suggesting that the repression of *mei-P26* by Brat most probably occurs at the transcriptional level.

The simultaneous expression of $mei\text{-}P26^{RNAi}$ in *brat*-depleted cells resulted in the up-regulation of dMyc protein (Figure 2E). Consistent with the role of dMyc in promoting cell growth (Figure S2), the double knockdown of *brat* and *mei-P26* led to increased cell size in wing discs (reflected by a reduction in nuclear density, Figure 2, G and H) and adult wings (reflected by a reduction in cell density, Figure 2K). It also rescued the tissue undergrowth observed upon depletion of *brat* alone (Figure 2, I and J). Mei-P26 is normally present at very low levels in the wing epithelium (Herranz *et al.* 2010), and its depletion alone did not have any impact on dMyc levels or cell or tissue size (Figure S2, C–F).

Taken together, these findings reveal that the increase in Mei-P26 levels observed in *brat* mutant cells inhibits growth and prevents dMyc upregulation in the wing epithelium. Surprisingly, the up-regulation of dMyc protein caused by the double knockdown of *brat* and *mei-P26* increased cell but not tissue size under these conditions, suggesting that other homeostatic mechanisms might dampen the capacity of dMyc up-regulation to induce tissue overgrowth (see *Discussion*).

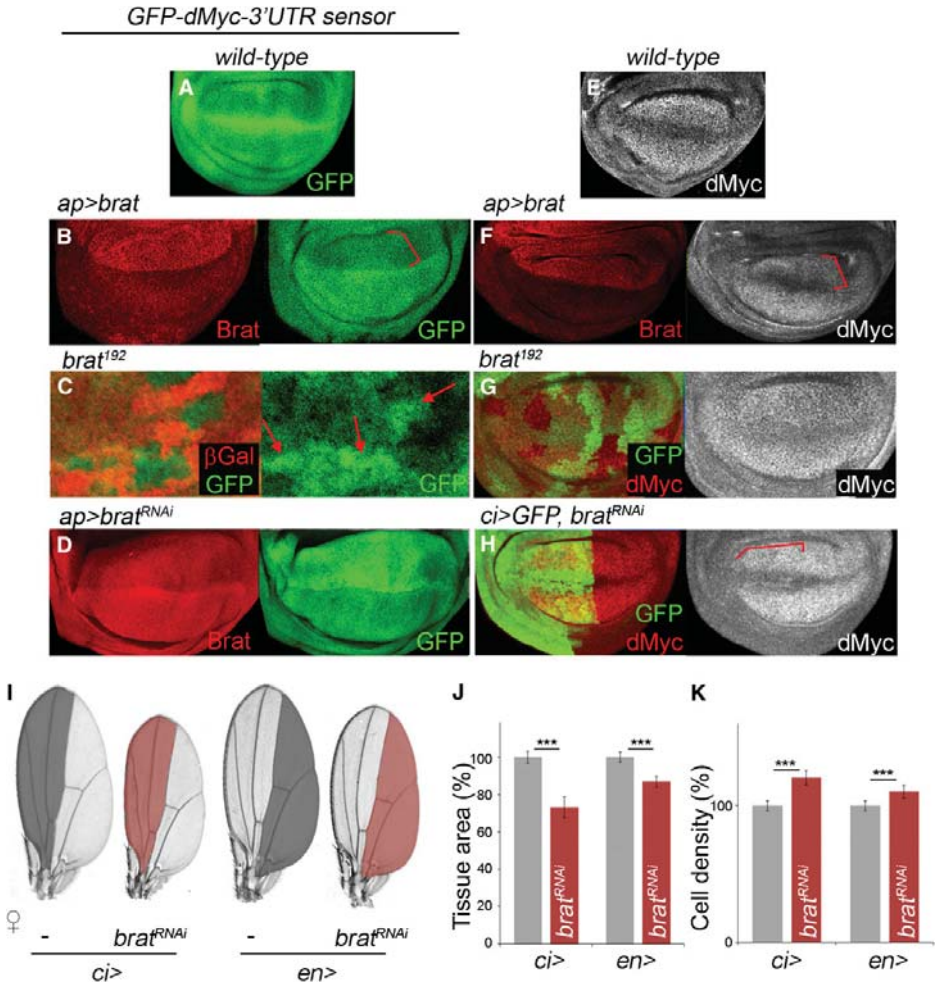

Figure 1 *brat* loss of function induces tissue undergrowth in epithelial cells. (A–D) Wing imaginal discs carrying the *dMyc-3′UTR* sensor (in green or white) in a wild-type background (A), in larvae overexpressing *brat* in the *apterous* domain (B, red brackets), in $brat^{192}$ homozygous mutant clones marked by absence of βGal (C, in red) and in larvae expressing $brat^{RNAi}$ in the *apterous* domain (D, red brackets). Wing discs in B and D were stained for Brat protein in red. (E) Wild-type wing imaginal disc labeled to visualize dMyc protein (in white). (F) Larval wing primordium overexpressing *brat* in the *apterous* domain (red brackets), labeled to visualize Brat (in red) and dMyc (in white) proteins. (G and H) Larval wing primordia labeled to visualize dMyc protein (red or white) and GFP (green) in $brat^{192}$ homozygous mutant clones marked by the absence of GFP (G) and in $brat^{RNAi}$-expressing cells (H, transgene expressed in the *ci* domain). (I) Cuticle preparations of female adult wings, expressing either the driver alone or $brat^{RNAi}$ in the *ci* or *en* domains (highlighted in gray and red in controls and experiments, respectively). (J and K) Histograms plotting tissue size (J) and cell density values (K) of the *ci* and *en* domains expressing $brat^{RNAi}$, normalized as a percentage of control wing values. In both *ci* > $brat^{RNAi}$ and *en* > $brat^{RNAi}$ adult wings, a significant reduction in tissue and cell size was observed in the anterior and posterior compartments, respectively, when compared to control wings raised in the same conditions. Errors bars represent standard deviation. $***P < 0.001$. Number of wings analyzed per genotype, ≥10.

No crosstalk between Brat and Mei-P26 in the neural lineage

To analyze the crosstalk between Brat and Mei-P26 in the neural lineage, we first generated MARCM clones mutant for *brat* and considered only those induced in specific regions of the larval brain where the loss of Brat leads to tumor formation (Bowman *et al.* 2008). As previously described (Bello *et al.* 2006; Betschinger *et al.* 2006; Lee *et al.* 2006), these clones displayed strong overgrowth and increased dMyc protein levels when compared to wild-type clones 96 hr after induction (Figure 3, A, A′, and B). The overgrowth was already seen 72 hr after clone induction (Figure 3B). Unlike in epithelial cells, *brat* mutant clones in the brain did not show increased levels of Mei-P26

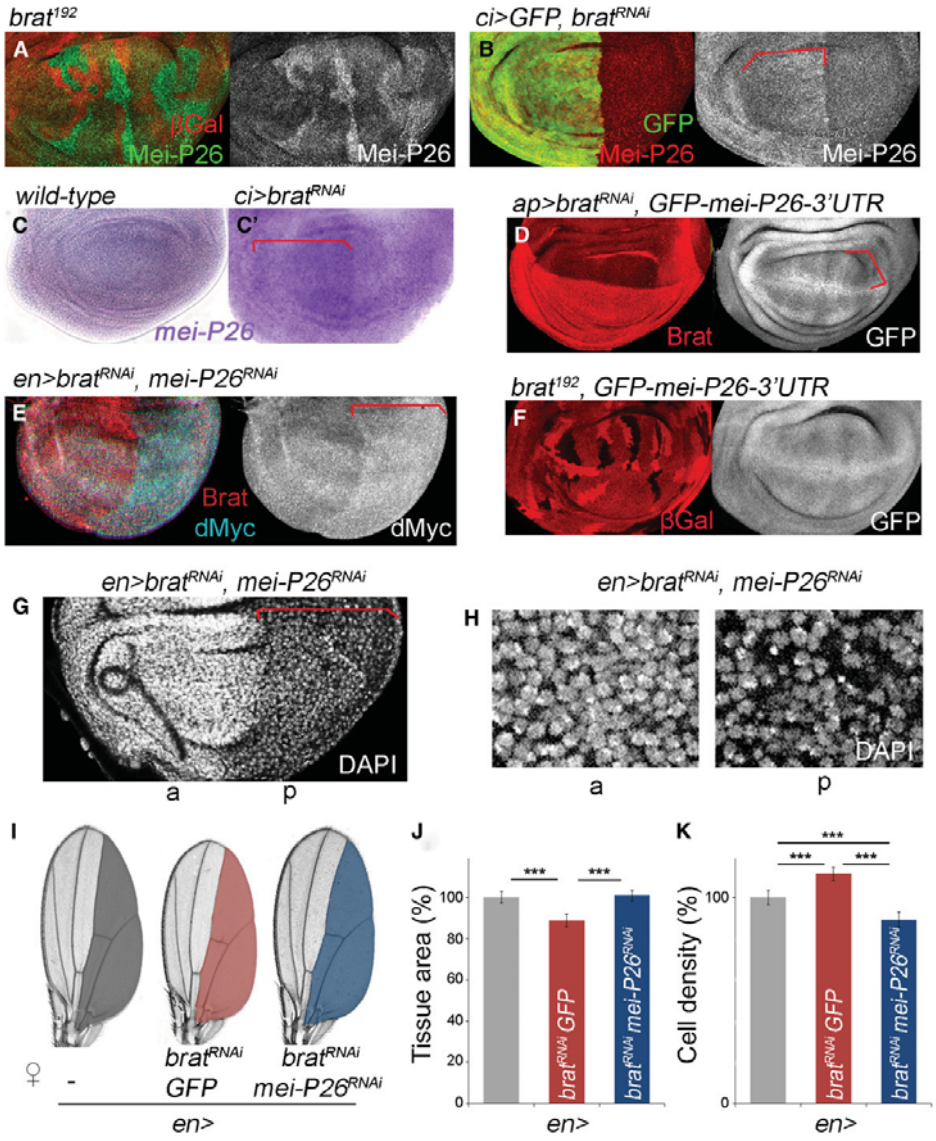

Figure 2 Mei-P26 upregulation limits dMyc protein levels and cell growth upon depletion of Brat in epithelial cells. (A) *brat*^{192} homozygous mutant clones, marked by the absence of βGal (in red) and stained for Mei-P26 protein (in green or white). (B) *brat*^{RNAi}-expressing cells labeled to visualize GFP in green (transgene expressed in the *ci* domain, red brackets) and Mei-P26 protein (in red or white). (C) *In situ* hybridization monitoring *mei-P26* mRNA (in purple) levels in wing primordia from wild-type larvae (C) or larvae with decreased *brat* expression in the *ci* domain (C′, red brackets). (D) Larval wing primordium expressing *brat*^{RNAi} in the *apterous* domain (red brackets), labeled to visualize Brat protein (in red) and a GFP-mei-P26-3′-UTR sensor (in white). (E) Larval wing primordium where *brat*^{RNAi} was coexpressed with *mei-P26*^{RNAi} under the control of the *en-Gal4* driver (red brackets) and labeled to visualize Brat (in red) and dMyc (in blue and white) proteins. (F) *brat*^{192} homozygous mutant clones marked by the absence of βGal (in red) carrying the GFP-mei-P26-3′-UTR sensor (in white). (G) Larval wing primordium expressing *brat*^{RNAi} and *mei-P26*^{RNAi}in the *engrailed* domain (red brackets), stained with DAPI (white) to monitor cell densities. (H) Higher magnification of the anterior and posterior compartments of the wing primordium shown in G. Note reduced cell density in the posterior compartment. Anterior (a) and posterior (p) compartments are labeled in G and H. (I) Cuticle preparations of female adult wings expressing the indicated transgenes in the *en* domain (highlighted in colors). (J and K) Histograms plotting tissue size (J) and cell density values (K), normalized as a percentage of control wing values, of the *en* domain expressing the indicated transgenes. In *en* > *brat*^{RNAi}, *GFP* adult wings, a significant reduction in tissue and cell size was observed in the posterior compartment when compared to control wings raised in the same conditions. Coexpression of *mei-P26*^{RNAi} significantly rescued tissue and cell size. Error bars represent standard deviation. ***$P < 0.001$. Number of wings analyzed per genotype, ≥10.

(Figure 3C). Instead, we observed a decrease in Mei-P26 levels in this condition (Figure 3C), consistent with the fact that Mei-P26 is normally expressed in differentiating neurons (Neumüller *et al.* 2008) and that neurons fail to differentiate in overgrowing *brat* mutant clones (as seen by the absence of cells positive for the neuronal marker Elav; Figure 3D).

Driving the expression of Mei-P26 in *brat* mutant clones was sufficient to significantly rescue the overgrowth phenotype (Figure 3, A′′ and B) and prevent dMyc up-regulation (Figure 3A′′) 72 and 96 hr after induction. However, neural progenitors still failed to differentiate, as reflected by the absence of Elav-positive neurons (Figure 3D′). Thus, Mei-P26 can also prevent the overgrowth of *brat* mutant cells in the neural lineage, most probably through the inhibition of dMyc rather than by driving cell differentiation. These results also illustrate that tumorous overgrowth can be uncoupled from differentiation in neural progenitors.

We propose that this tissue-specific regulation of Mei-P26 by Brat accounts for the opposite growth phenotypes observed in the neural lineage and in the wing epithelium. While in stem cell lineages the depletion of *brat* or *mei-P26* alone is sufficient to induce dMyc upregulation, the crosstalk between the two TRIM-NHL proteins in epithelial cells adds another layer of control to prevent an increase in dMyc levels and in cell and tissue size (Figure 3E).

Mei-P26 up-regulation maintains tissue homeostasis upon dMyc overexpression

Although dMyc is a cellular growth promoter, as shown by its ability to increase cell size when overexpressed (quantified as cell density in Figure 4A; Johnston *et al.* 1999), dMyc overexpression does not cause tissue overgrowth (Figure 4, B and C; Doumpas *et al.* 2013). Strikingly, we observed that dMyc overexpression in the wing primordium strongly upregulates Mei-P26 protein and mRNA levels (Figure 4, D and E). Could Mei-P26 also act as a brake in the context of dMyc gain of function?

Tissue overgrowth is prevented upon dMyc overexpression by the induction of apoptosis (De La Cova *et al.* 2004) through a Dp53-independent mechanism (Montero *et al.* 2008). Interestingly, the depletion of *mei-P26* was sufficient to strongly reduce the number of apoptotic cells in a dMyc-overexpressing tissue (Figure 4, F–H and see quantification in Figure 4I). Moreover, it further enhanced cell growth (Figure 4A) and led to increased tissue size (Figure 4, B and C) when compared to dMyc overexpression alone. These observations indicate that Mei-P26 upregulation contributes to maintaining tissue homeostasis upon dMyc overexpression in epithelial cells, by limiting dMyc growth potential and by mediating dMyc-induced apoptosis (Figure 4J).

Discussion

Our results unravel an unexpected tissue-specific growth-regulatory activity of the TRIM-NHL protein Brat. While *brat* loss of function gives rise to overgrowth, dMyc up-regulation, and tumor formation in the neural lineage (Bello *et al.* 2006; Betschinger *et al.* 2006; Lee *et al.* 2006), it causes the opposite phenotype in the proliferative wing epithelium by reducing cell and tissue size. Thus, Brat functions as a tumor suppressor in a context-dependent manner. In epithelial cells, like in neural progenitors, the depletion of *brat* leads to the post-transcriptional derepression of *dMyc* through its *3′UTR*. It also triggers the up-regulation of Mei-P26, which in turn targets dMyc protein for degradation (Herranz *et al.* 2010). In the neural lineage, *brat* loss of function does not result in increased Mei-P26 levels. However, Mei-P26 overexpression significantly rescues the overgrowth of *brat* mutant clones in the brain. This tumor suppressor activity is most likely due to the capacity of Mei-P26 to prevent the up-regulation of dMyc in these cells. Driving Mei-P26 expression in overgrowing *brat* mutant clones in the brain does not induce neuronal differentiation, although Mei-P26 overexpression has been shown to trigger premature neuronal differentiation in otherwise wild-type brains (Neumüller *et al.* 2008). Thus, the ability of Mei-P26 to promote neuronal differentiation appears to depend on the presence of functional Brat.

The oncogene Myc has been extensively studied in mammals for its role in normal conditions and in tumorigenesis (Eilers and Eisenman 2008). In normal cells, an increase in Myc levels promotes growth but concomitantly activates safety mechanisms—such as apoptosis or increased dependency on nutrients—that maintain tissue homeostasis. Hence, the tumorigenic potential of Myc overexpression requires additional mutations that disable these mechanisms. In line with this, we and others have observed that dMyc overexpression in the wing primordium of *Drosophila* promotes cell growth but does not cause tissue overgrowth. These findings suggest that epithelial cells also activate such safety mechanisms. Here we show that dMyc overexpression triggers a strong up-regulation of Mei-P26, thereby establishing a feedback mechanism between the two factors. Increased Mei-P26 levels limit dMyc growth potential and mediate dMyc-induced apoptosis. The activation of Mei-P26 by dMyc provides a new mechanism that contributes to tissue homeostasis in dMyc-overexpressing epithelial cells.

We observed that the capacity of overexpressed dMyc to drive tissue growth in the absence of Mei-P26 was still limited, opening the possibility that other homeostatic mechanisms limiting dMyc activity might be at play in epithelial cells. A feedback mechanism between dMyc and Yorkie, the *Drosophila* homolog of the Hippo pathway transducer, has also been proposed to regulate tissue size (Neto-Silva *et al.* 2010). dMyc overexpression reduces the levels of Yorkie, a potent inducer of tissue growth and inhibitor of apoptosis. Thus, both Mei-P26 up-regulation and Yorkie down-regulation contribute to dMyc-induced apoptosis and limit dMyc potential to drive cell and tissue growth.

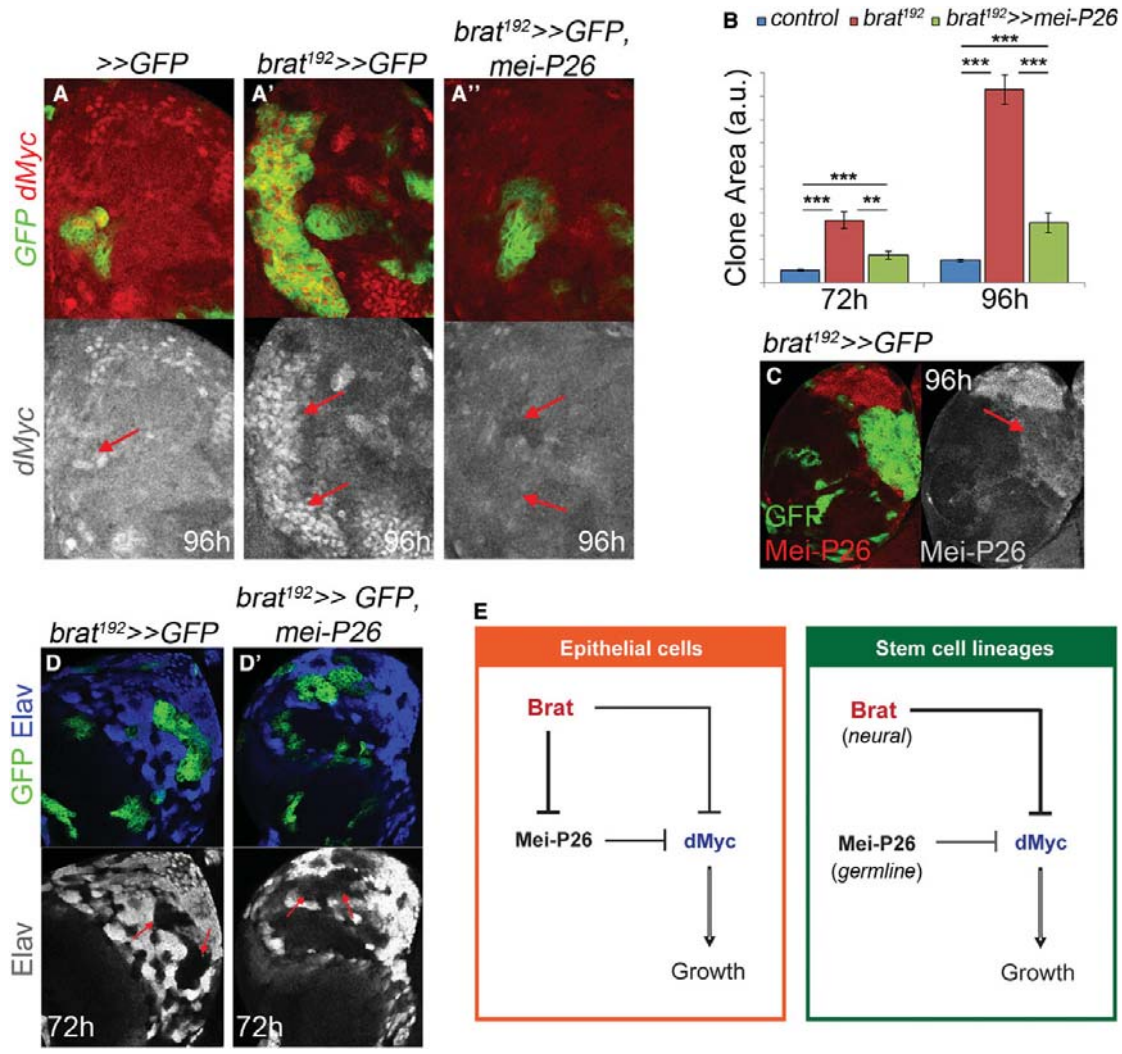

Figure 3 No crosstalk between Brat and Mei-P26 in the neural lineage. (A–A′′) Larval brains with wild-type (A), *brat*^{192} mutant clones (A′), and *brat*^{192} mutant clones coexpressing *mei-P26* (A′′) marked with GFP (in green), and labeled to visualize dMyc protein (in red or white). Brains were dissected 96 hr after induction. Note that dMyc was up-regulated in *brat*^{192} mutant clones (red arrows in A′) compared to wild-type clones (red arrow in A). This accumulation was lost when *mei-P26* was coexpressed in the clones (red arrows in A′′). (B) Quantification of clonal area, 72 and 96 hr after induction. Note that coexpression of *mei-P26* rescued the size of *brat*^{192} mutant clones. ***$P < 0.001$. (C) Larval brains with homozygous *brat*^{192} mutant clones marked with GFP and labeled to visualize Mei-P26 protein (in red or white). Mei-P26 was not up-regulated in overgrowing *brat* mutant clones (red arrow). Brains were dissected 96 hr after induction. (D–D′) Larval brains with *brat*^{192} mutant clones (D) and *brat*^{192} mutant clones coexpressing *mei-P26* (D′), marked by GFP expression and labeled to visualize the neuronal marker Elav (in blue or white). Brains were dissected 72 hr after induction. Note that the loss of differentiated cells in *brat*^{192} mutant clones was not rescued by *mei-P26* coexpression (red arrows). (E) Model explaining the tissue-specific outcomes of *brat* loss of function in terms of dMyc levels and tissue growth.

To date, Mei-P26 has been shown to negatively regulate tissue growth by degrading the dMyc protein (Herranz *et al.* 2010). Our results suggest that other molecular effectors are involved in this process. We observed that increased Mei-P26 levels are responsible for tissue and cell undergrowth upon depletion of Brat. However, dMyc protein levels remain unchanged in this condition, pointing to a dMyc-independent role of Mei-P26 in inhibiting cell growth. Furthermore, we show that Mei-P26 antagonizes dMyc-induced cell growth and mediates dMyc-induced apoptosis, thereby preventing tissue overgrowth upon dMyc overexpression in epithelial cells. The challenge is now to further

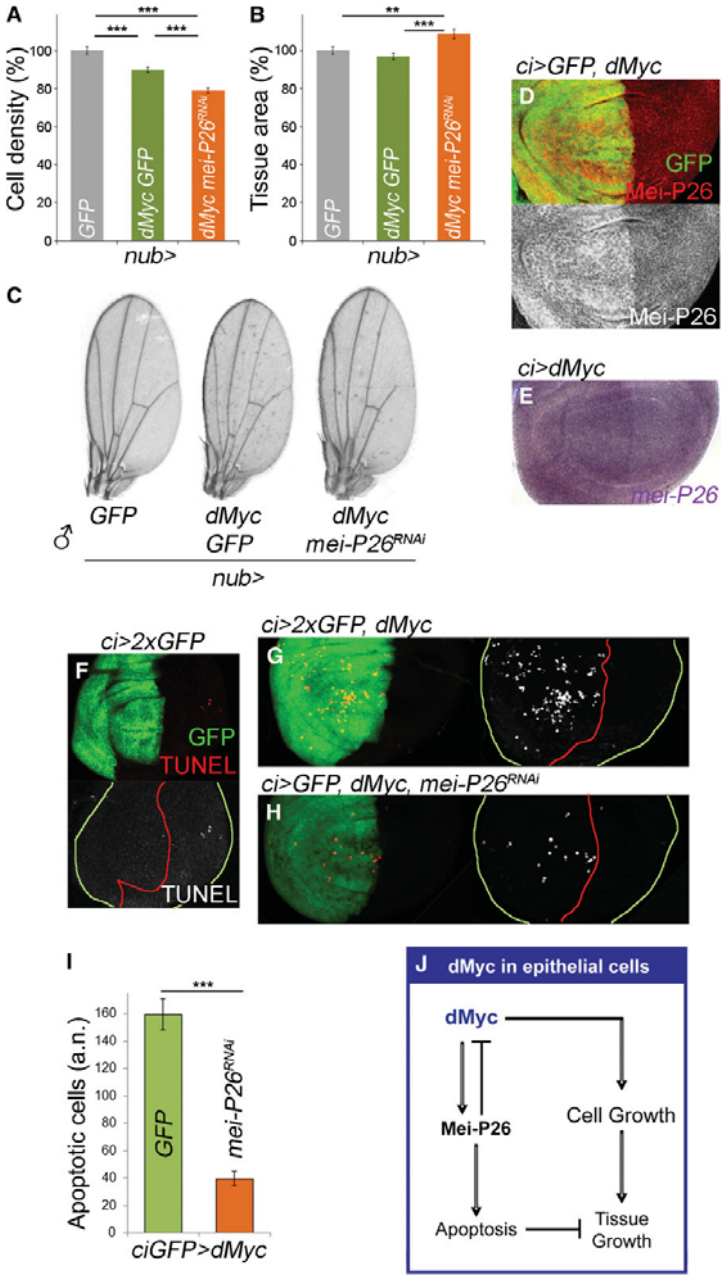

Figure 4 The up-regulation of Mei-P26 maintains tissue homeostasis upon dMyc overexpression. (A and B) Histograms plotting cell density (A) and tissue size (B) values of the *nubbin* domain expressing the different transgenes, normalized as a percentage of control GFP-expressing wings. In *nub* > *dMyc*, *GFP* adult wings, no significant change in tissue size was observed when compared to control wings raised in the same conditions (B). However, in this condition the cells were significantly larger (A). Coexpression of *mei-P26*^{RNAi} gave rise to significantly larger wings when compared to GFP-expressing wings and to wings overexpressing *dMyc* and *GFP* (B). Concerning cell size, the cells were larger when *mei-P26*^{RNAi} was coexpressed when compared to the GFP-expressing cells and to wings overexpressing *dMyc* alone (A). Errors bars represent standard deviation. $^{**}P < 0.01$ and $^{***}P < 0.001$. Number of wings analyzed per genotype, ≥10. (C) Cuticle preparations of male adult wings expressing GFP, expressing dMyc and GFP, or expressing GFP and *mei-P26*^{RNAi} in the *nubbin* domain. (D and E) Larval wing primordia from individuals in which dMyc and GFP (green, D) or dMyc alone (E) were overexpressed in the *ci* domain, and labeled to visualize Mei-P26 protein (in red or white, D) and *mei-P26* mRNA (in purple, E). (F–H) Larval wing primordia from individuals in which GFP (F), dMyc and GFP (G), or dMyc, GFP and *mei-P26*^{RNAi} (H), were expressed in the *ci* domain. Wing primordia were labeled to visualize GFP (in green) and apoptotic cells by TUNEL (in red or white). Note that the number of UAS-transgenes was similar in G and H. (I) Histogram plotting the number of apoptotic nuclei (a.n.) per anterior compartment of wing discs expressing the indicated transgenes under the control of the *ci-Gal4* driver. (J) Model explaining the epithelial-specific response to dMyc overexpression.

characterize the mechanisms by which Mei-P26 regulates cell growth and apoptosis and thus provide greater insight into the homeostasis of epithelial tissues.

In conclusion, the use of the wing epithelium as a model system has allowed us to analyze the participation of Brat, Mei-P26, and dMyc in growth control. Surprisingly, we have observed that *brat* loss of function and dMyc overexpression have a negative impact on growth in this tissue. In both cases, we have identified the up-regulation of Mei-P26 to be responsible for the tissue-specific growth alteration. A previous study also identified Mei-P26 as a target of the miRNA machinery and showed that the depletion of the

miRNA machinery in the wing disc causes undergrowth as a result of increased Mei-P26 levels (Herranz *et al.* 2010). The observation that Mei-P26 mediates the response to perturbations opens up the possibility that modulations of Mei-P26 levels serve to maintain the homeostasis of epithelial tissues.

Mutations leading to the overexpression of an oncogene constitute the starting point of tumorigenesis. Yet, abnormal cell proliferation and tissue growth also activate well-described tumor suppressor mechanisms preventing neoplastic growth, such as oncogene-induced cell death (Lowe *et al.* 2004). The formation of a malignant tumor therefore requires additional mutations that disable these tumor suppressor mechanisms. Different types of tumors display different oncogenic signatures, which are suggestive of tumor-specific therapies (Ciriello *et al.* 2013). The sensitivity to a given oncogene therefore varies from one tissue to another and may depend on the activation—or not—of tissue-specific tumor suppressive mechanisms. Our study illustrates how the interplay between oncogenes and tumor suppressors can mediate tissue-specific responses to genetic alterations in terms of growth and apoptosis.

Acknowledgments

We thank S. Cohen, G. Morata, P. Lasko, the Bloomington Stock Center, the Developmental Studies Hybridoma Bank, Cappel, and the Vienna *Drosophila* RNAi Center for flies and reagents; T. Yates for text editing; L. Barrio and C. Recasens for helpful comments on the manuscript; and H. Herranz for his contribution to the initial steps of this project. A.F. was funded by a PhD fellowship from the Fundação para a Ciência e a Tecnologia and L.B. was funded by a PhD fellowship from "la Caixa" Foundation. M.M. is an Institució Catalana de Recerca i Estudis Avançats research professor and this work was funded by BFU2010-21123, CSD2007-00008, and 2005 SGR 00118 grants.

Literature Cited

Arama, E., D. Dickman, and Z. Kimchie, A. Shearn, and Z. Lev, 2000 Mutations in the beta-propeller domain of the Drosophila brain tumor (brat) protein induce neoplasm in the larval brain. Oncogene 19: 3706–3716.

Bello, B., H. Reichert, and F. Hirth, 2006 The brain tumor gene negatively regulates neural progenitor cell proliferation in the larval central brain of Drosophila. Development 133: 2639–2648.

Betschinger, J., K. Mechtler, and J. A. Knoblich, 2006 Asymmetric segregation of the tumor suppressor brat regulates self-renewal in Drosophila neural stem cells. Cell 124: 1241–1253.

Bowman, S. K., V. Rolland, J. Betschinger, K. A. Kinsey, G. Emery *et al.*, 2008 The tumor suppressors Brat and Numb regulate transit-amplifying neuroblast lineages in Drosophila. Dev. Cell 14: 535–546.

Brennecke, J., D. R. Hipfner, A. Stark, R. B. Russell, and S. M. Cohen, 2003 bantam encodes a developmentally regulated microRNA that controls cell proliferation and regulates the proapoptotic gene hid in Drosophila. Cell 113: 25–36.

Ciriello, G., M. L. Miller, B. A. Aksoy, Y. Senbabaoglu, N. Schultz *et al.*, 2013 Emerging landscape of oncogenic signatures across human cancers. Nat. Genet. 45: 1127–1133.

Cohen, S. M., 1993 Imaginal disc development, pp. 747–841 in *Drosophila Development*, edited by A. Martinez-Arias, and M. Bate. Cold Spring Harbor Laboratory Press, Cold Spring Harbor, NY.

Dang, C. V., 2012 MYC on the path to cancer. Cell 149: 22–35.

De la Cova, C., M. Abril, P. Bellosta, P. Gallant, and L. A. Johnston, 2004 Drosophila myc regulates organ size by inducing cell competition. Cell 117: 107–116.

Doumpas, N., M. Ruiz-Romero, E. Blanco, B. Edgar, and M. Corominas *et al.*, 2013 Brk regulates wing disc growth in part via repression of Myc expression. EMBO Rep. 14: 261–268.

Eilers, M., and R. N. Eisenman, 2008 Myc's broad reach. Genes Dev. 22: 2755–2766.

Frank, D. J., B. A. Edgar, and M. B. Roth, 2002 The Drosophila melanogaster gene brain tumor negatively regulates cell growth and ribosomal RNA synthesis. Development 129: 399–407.

Gallant, P., 2013 Myc Function in Drosophila. Cold Spring Harb. Perspect. Med. 3: a014324.

Grewal, S. S., L. Li, A. Orian, R. N. Eisenman, and B. A. Edgar, 2005 Myc-dependent regulation of ribosomal RNA synthesis during Drosophila development. Nat. Cell Biol. 7: 295–302.

Hammell, C. M., I. Lubin, P. R. Boag, T. K. Blackwell, and V. Ambros, 2009 nhl-2 Modulates microRNA activity in Caenorhabditis elegans. Cell 136: 926–938.

Harris, R. E., M. Pargett, C. Sutcliffe, D. Umulis, and H. L. Ashe, 2011 Brat promotes stem cell differentiation via control of a bistable switch that restricts BMP signaling. Dev. Cell 20: 72–83.

Herranz, H., L. Perez, F. A. Martin, and M. Milan, 2008 A Wingless and Notch double-repression mechanism regulates G1-S transition in the Drosophila wing. EMBO J. 27: 1633–1645.

Herranz, H., X. Hong, L. Perez, A. Ferreira, D. Olivieri *et al.*, 2010 The miRNA machinery targets Mei-P26 and regulates Myc protein levels in the Drosophila wing. EMBO J. 29: 1688–1698.

Johnston, L. A., D. A. Prober, B. A. Edgar, R. N. Eisenman, and P. Gallant, 1999 Drosophila myc regulates cellular growth during development. Cell 98: 779–790.

Kohlmaier, A., and B. A. Edgar, 2008 Proliferative control in Drosophila stem cells. Curr. Opin. Cell Biol. 20: 699–706.

Lee, C.-Y., B. D. Wilkinson, S. E. Siegrist, R. P. Wharton, and C. Q. Doe, 2006 Brat is a Miranda cargo protein that promotes neuronal differentiation and inhibits neuroblast self-renewal. Dev. Cell 10: 441–449.

Li, Y., J. Z. Maines, O. Y. Tastan, D. M. McKearin, and M. Buszczak, 2012 Mei-P26 regulates the maintenance of ovarian germline stem cells by promoting BMP signaling. Development 139: 1547–1556.

Liu, N., H. Han, and P. Lasko, 2009 Vasa promotes Drosophila germline stem cell differentiation by activating mei-P26 translation by directly interacting with a (U)-rich motif in its 3′ UTR. Genes Dev. 23: 2742–2752.

Liu, Y., R. Raheja, N. Yeh, and D. Ciznadija, 2014 TRIM3, a tumor suppressor linked to regulation of p21(Waf1/Cip1). Oncogene 33: 308–315.

Loedige, I., and W. Filipowicz, 2009 TRIM-NHL proteins take on miRNA regulation. Cell 136: 818–820.

Loedige, I., D. Gaidatzis, R. Sack, G. Meister, and W. Filipowicz, 2013 The mammalian TRIM-NHL protein TRIM71/LIN-41 is a repressor of mRNA function. Nucleic Acids Res. 41: 518–532.

Lowe, S. W., E. Cepero, and G. Evan, 2004 Intrinsic tumour suppression. Nature 432: 307–315.

Meroni, G., and G. Diez-Roux, 2005 TRIM/RBCC, a novel class of "single protein RING finger" E3 ubiquitin ligases. BioEssays 27: 1147–1157.

Montero, L., N. Müller, and P. Gallant, 2008 Induction of apoptosis by Drosophila Myc. Genesis 46: 104–111.

Neto-Silva, R. M., S. de Beco, and L. A. Johnston, 2010 Evidence for a growth stabilizing regulatory feedback mechanism between Myc and Yorkie, the Drosophila homolog of Yap. Dev. Cell 19: 507–520.

Neumüller, R. A., J. Betschinger, A. Fischer, N. Bushati, I. Poernbacher *et al.*, 2008 Mei-P26 regulates microRNAs and cell growth in the Drosophila ovarian stem cell lineage. Nature 454: 241–245.

Page, S. L., K. S. McKim, B. Deneen, T. L. Van Hook, and R. S. Hawley, 2000 Genetic studies of mei-P26 reveal a link between the processes that control germ cell proliferation in both sexes and those that control meiotic exchange in Drosophila. Genetics 155: 1757–1772.

Schwamborn, J. C., E. Berezikov, and J. A. Knoblich, 2009 The TRIM-NHL protein TRIM32 activates microRNAs and prevents self-renewal in mouse neural progenitors. Cell 136: 913–925.

Slack, F. J., and G. Ruvkun, 1998 A novel repeat domain that is often associated with RING finger and B-box motifs. Trends Biochem. Sci. 23: 474–475.

Sonoda, J., and R. P. Wharton, 2001 Drosophila brain tumor is a translational repressor. Genes Dev. 15: 762–773.

Vita, M., and M. Henriksson, 2006 The Myc oncoprotein as a therapeutic target for human cancer. Semin. Cancer Biol. 16: 318–330.

Communicating editor: I. Hariharan

GENETICS

Supporting Information
http://www.genetics.org/lookup/suppl/doi:10.1534/genetics.114.167502/-/DC1

Mei-P26 Mediates Tissue-Specific Responses to the Brat Tumor Suppressor and the dMyc Proto-Oncogene in *Drosophila*

Ana Ferreira, Laura Boulan, Lidia Perez, and Marco Milán

DOI: 10.1534/genetics.114.167502

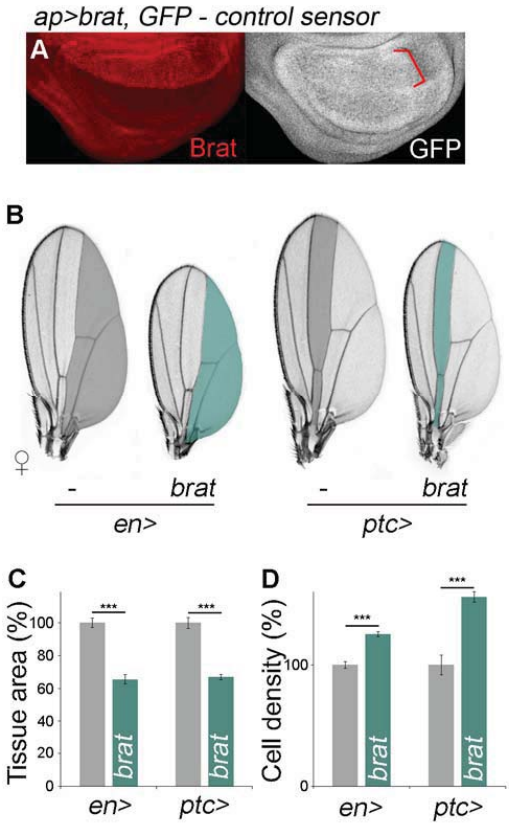

Figure S1 *brat* overexpression represses dMyc at the post-transcriptional level.

(A) Larval wing primordium overexpressing *brat* in the *apterous* domain (red brackets) stained for Brat protein (in red), and carrying a GFP-control sensor (in white).

(B) Cuticle preparations of female adult wings expressing either the *Gal4* driver alone or *UAS-brat* in the *en* or *patched* (*ptc*) domains (highlighted in gray and green in controls and experiments, respectively).

(C,D) Histograms plotting tissue size (C) and cell density values (D) of the *en* and *ptc* domains expressing the transgene, normalized as a percentage of control wings. Overexpression of *brat* induced a significant reduction in tissue and cell size in the corresponding domains compared to control wings raised in the same conditions. Errors bars represent standard deviation. ***p<0.001. Number of wings analyzed per genotype≥10.

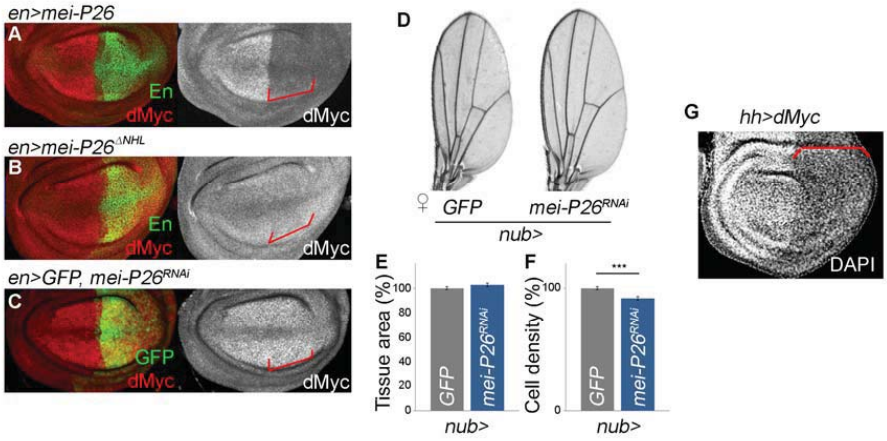

Figure S2 Regulation of dMyc by Mei-P26 and endogenous Mei-P26 activity.

(A-C) Larval wing primordia overexpressing *mei-P26* (A), a form of *mei-P26* that lacks the NHL domain (B), or expressing a dsRNA against *mei-P26* (C) in the *en* domain (red brackets) labeled to visualize En or GFP (in green) and dMyc (in red or white) proteins.

(D) Cuticle preparations of female adult wings expressing GFP or *mei-P26^{RNAi}* in the *nubbin* domain.

(E,F) Histograms plotting tissue size (E) and cell density (F), normalized as a percentage of control GFP-expressing wings, of the *nubbin* domain expressing *mei-P26^{RNAi}*. No significant change in tissue size was observed when compared to control wings raised in the same conditions. However, in this condition the cells were significantly larger. Errors bars represent standard deviation. ***p<0.001. Number of wings analyzed per genotype≥10.

(G) Larval wing primordium overexpressing *dMyc* in the *hh* domain (red brackets), stained for DAPI (white) to visualize nuclear densities as a proxy to cell densities.

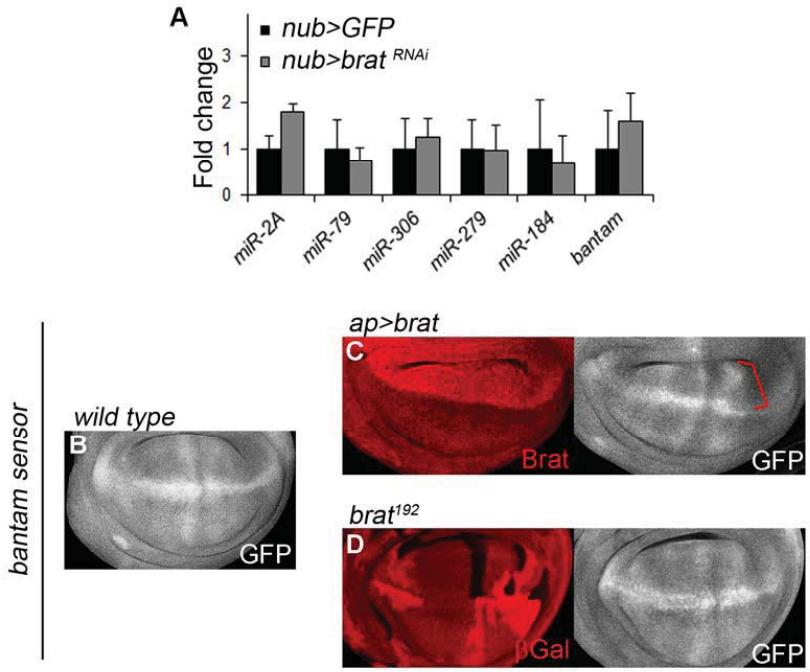

Figure S3 Brat does not modulate microRNAs.

(A) Levels of six mature microRNAs in *nub>brat*^{RNAi} (gray bars) compared with *nub>GFP* (black bars) wing imaginal discs, measured by qRT-PCR. No significant changes were observed.

(B-D) Larval wing primordia carrying the *bantam* sensor (in white) in wild-type conditions (B), in cells overexpressing *brat* in the *apterous* domain (C, red brackets) stained for Brat protein (in red), or in *brat*^{192} homozygous mutant clones marked by the absence of βGal (D, in red).

File S1

Supporting Material and Methods

Quantification of miRNA expression levels

Ten wing discs from *nub-gal4; UAS-GFP* and *nub-gal4; UAS-brat*^{RNAi} larvae at the wandering stage were dissected, and the notum domain was cut and removed. Total RNA was extracted using the TRIzol Reagent (Life Technologies). Biological triplicates were performed for each genotype. Mature miRNAs were amplified from 20 ng total RNA samples from the respective genotypes using TaqMan microRNA assays (Applied Biosystems). Relative expression levels were obtained by quantitative PCR, using a TaqMan Universal PCR Mastermix (Applied Biosystems). U27 was used as a reference gene for data normalization.